

**ANÁLISE DO COMPORTAMENTO DE RADIER  
ESTAQUEADOS COM ESTACA DEFEITUOSA  
CARREGADOS HORIZONTALMENTE EM  
SOLO TROPICAL**

**FRANCISCO JAVIER ALVA GARCIA**

**TESE DE DOUTORADO**

**DEPARTAMENTO DE ENGENHARIA CIVIL E  
AMBIENTAL**



**FACULDADE DE TECNOLOGIA  
UNIVERSIDADE DE BRASÍLIA**

**UNIVERSIDADE DE BRASÍLIA**  
**FACULDADE DE TECNOLOGIA**  
**DEPARTAMENTO DE ENGENHARIA CIVIL E AMBIENTAL**

**ANÁLISE DO COMPORTAMENTO DE RADIER  
ESTAQUEADOS COM ESTACA DEFEITUOSA  
CARREGADOS HORIZONTALMENTE EM  
SOLO TROPICAL**

**FRANCISCO JAVIER ALVA GARCIA**

**ORIENTADOR: RENATO PINTO DA CUNHA Ph.D.**  
**CO-ORIENTADOR: PAULO JOSÉ ROCHA DE  
ALBUQUERQUE D.Sc.**

**TESE DE DOUTORADO**

**PUBLICAÇÃO: G.TD-135/17**

**BRASÍLIA / DF: JUNHO / 2017**

**UNIVERSITY OF BRASÍLIA**  
**FACULTY OF TECHNOLOGY AND ENVIRONMENTAL**  
**ENGINEERING DEPARTMENT**

**ANALYSIS OF THE BEHAVIOR OF PILED  
RAFTS WITH AND WITHOUT DEFECTIVE  
PILE HORIZONTALLY LOADED IN TROPICAL  
SOIL**

**FRANCISCO JAVIER ALVA GARCIA**

**SUPERVISOR: RENATO PINTO DA CUNHA Ph.D.**  
**CO-SUPERVISOR: PAULO JOSÉ ROCHA DE**  
**ALBUQUERQUE D.Sc.**

**DOCTORAL THESIS IN GEOTECHNICAL ENGINEERING**

**PUBLICATION: G.TD-135/17**

**BRASÍLIA / DF: JUNE 2017**

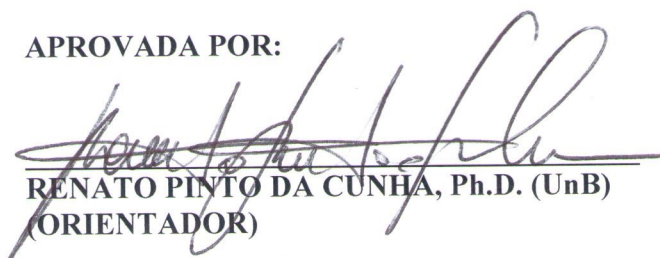
**DEPARTAMENTO DE ENGENHARIA CIVIL E AMBIENTAL**

**ANÁLISE DO COMPORTAMENTO DE RADIER  
ESTAQUEADOS COM ESTACA DEFEITUOSA  
CARREGADOS HORIZONTALMENTE EM SOLO TROPICAL**

**FRANCISCO JAVIER ALVA GARCIA**

TESE DE DOUTORADO SUBMETIDA AO DEPARTAMENTO DE ENGENHARIA CIVIL E AMBIENTAL DA UNIVERSIDADE DE BRASÍLIA COMO PARTE DOS REQUISITOS NECESSÁRIOS PARA A OBTENÇÃO DO GRAU DE DOUTOR.


APROVADA POR:

  
RENATO PINTO DA CUNHA, Ph.D. (UnB)  
(ORIENTADOR)

  
MARCIO MUNIZ DE FARIAS, D.Sc. (UnB)  
(EXAMINADOR INTERNO)

  
MAURICIO MARTINES SALES D.Sc. (UFG)  
(EXAMINADOR EXTERNO)

  
ROBERTO QUENTAL COUTINHO D.Sc. (UFPE)  
(EXAMINADOR EXTERNO)

  
PAULO JOSÉ ROCHA DE ALBUQUERQUE D.Sc. (UNICAMP)  
(EXAMINADOR EXTERNO)

DATA: BRASÍLIA/DF, 28 DE JUNHO DE 2017

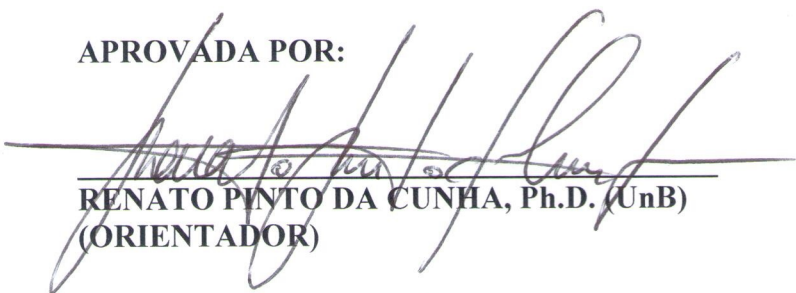
**DEPARTAMENTO DE ENGENHARIA CIVIL E AMBIENTAL**

**ANALYSIS OF THE BEHAVIOR OF PILED RAFTS WITH  
AND WITHOUT DEFECTIVE PILES HORIZONTALLY  
LOADED IN TROPICAL SOIL**

**FRANCISCO JAVIER ALVA GARCIA**

TESE DE DOUTORADO SUBMETIDA AO DEPARTAMENTO DE ENGENHARIA CIVIL E AMBIENTAL DA UNIVERSIDADE DE BRASÍLIA COMO PARTE DOS REQUISITOS NECESSÁRIOS PARA A OBTENÇÃO DO GRAU DE DOUTOR.

APROVADA POR:



---

RENATO PINTO DA CUNHA, Ph.D. (UnB)  
(ORIENTADOR)



---

MARCIO MUNIZ DE FARIAS, D.Sc. (UnB)  
(EXAMINADOR INTERNO)




---

MAURICIO MARTINES SALES D.Sc. (UFG)  
(EXAMINADOR EXTERNO)



---

ROBERTO QUENTAL COUTINHO D.Sc. (UFPE)  
(EXAMINADOR EXTERNO)



---

PAULO JOSÉ ROCHA DE ALBUQUERQUE D.Sc. (UNICAMP)  
(EXAMINADOR EXTERNO)

DATA: BRASÍLIA/DF, 28 DE JUNHO DE 2017

## FICHA CATALOGRÁFICA

ALVA, FRANCISCO JAVIER GARCIA

Análise do comportamento de radier estaqueados com estaca defeituosa carregados horizontalmente em solo tropical [Distrito Federal] 2017

xxiii, p., 169 mm (ENC/FT/UnB, Doutor, Geotecnia, 2017)

Tese de Doutorado - Universidade de Brasília.

Faculdade de Tecnologia. Departamento de Engenharia Civil e Ambiental

- |                                |   |
|--------------------------------|---|
| 1. Introduction                | 2. State of the art                         |
| 3. Numerical analysis of piles | 4. Materials and methods                    |
| 5. Results and discussion      | 6. Conclusions and future research projects |

I. ENC/FT/UnB

II. Título (série)

## REFERÊNCIA BIBLIOGRÁFICA

ALVA, F. G. (2017). Análise do comportamento de radier estaqueados com estaca defeituosa carregados horizontalmente em solo tropical. Tese de Doutorado, Publicação G.TD-135/17, Departamento de Engenharia Civil e Ambiental, Universidade de Brasília, D.F. 169p.

## CESSÃO DE DIREITOS

NOME DO AUTOR: Francisco Javier Alva García

TÍTULO DA TESE DE DOUTORADO: Análise do comportamento de radier estaqueados com estaca defeituosa carregados horizontalmente em solo tropical

GRAU: Doutor ANO: 2017

É concedida à Universidade de Brasília a permissão para reproduzir cópias desta tese de doutorado e para emprestar ou vender tais cópias somente para propósitos acadêmicos e científicos. O autor reserva outros direitos de publicação e nenhuma parte desta dissertação de mestrado pode ser reproduzida sem a autorização por escrito do autor.

---

**Francisco Javier Alva García**

fj\_alva@icloud.com

## **DEDICATION**

To my beloved parents Nati and Boni,  
thank you for being an example for me and especially for giving me the best possible  
inheritance: a solid education.

To my beloved sister María Aurora and my dear Martina,  
thank you for all the support you gave me during all this long time.

To my wife Sonia and our little Sebastião,  
thank you for changing my life.

# ACKNOWLEDGMENTS

To Professor Marcio Muniz,  
for the motivation gained through his lectures to study much more and for his advice concerning my research work, but especially for the support received personally from him at the end of my doctorate.

To Professor Carlos Recarey,  
for the interest, support and knowledge transmitted to me during the numerical works.

To Engineer José Luis Lara,  
for his support, trust and friendship, but especially for the opportunity to work on an engineering project that challenged me to search for greater knowledge, which led me to study my doctorate.

To Professor Luis Fernando Martins,  
for his friendship and wise advice.

To Professor Renato Pinto da Cunha,  
for his invitation to study at University of Brasilia.

To the staff Professors of the Geotechnical Postgraduate Program of this University.

To my friend Russ Paradice,  
for his great support and patience with the English review of this thesis.

To São Paulo Foundation (FAPESP) for the financial support;  
Process number 14/06611-4.

Especially to Brazil,  
for paying for my studies and training for four years, and for giving me the opportunity to become not only a better engineer, but also a better person.  
My expectations were exceeded! I will be forever grateful!



## RESUMO

Esta tese de doutorado tem por finalidade investigar a presença e o comportamento de radiers estaqueados, com e sem estacas defeituosas, carregados horizontalmente em solo tropical. Para tanto, foram estudados cinco modelos de sistemas de fundação para análise. O primeiro deles consiste num radier estaqueado de apenas uma estaca intacta. Já o segundo e o terceiro consistem num radier estaqueado com três estacas, com mesma geometria, dimensões e materiais. A única diferença entre o segundo e o terceiro modelo é que um deles possui uma estaca danificada. Também, o quarto e o quinto modelos possuem constituição similar: um radier estaqueado com quatro estacas, com mesma geometria, dimensões e materiais, mas com a diferença que num deles há uma estaca danificada.

Cabe informar que todos esses modelos foram construídos e testados sob carregamento vertical antes mesmo deste trabalho e fizeram parte do projeto de pesquisa Fapesp 2011/17959-3. Utilizaram, na época, uma broca helicoidal para construir esses sistemas de fundação, e que as estacas têm as dimensões de 5 metros de comprimento e 25 centímetros de diâmetro.

Como parte do trabalho de pesquisa, testes de carga horizontal em verdadeira grandeza foram realizados em cada um dos cinco sistemas, dos quais foi possível obter uma curva experimental  $p-y$  para cada um deles. Todo esse trabalho de campo foi feito no campo experimental da Faculdade de Engenharia Civil, Arquitetura e Urbanismo da Universidade de Campinas, SP. O perfil geotécnico da pesquisa lá do campo correspondeu a uma camada de argila limpa (que é porosa, coluvial, laterítica e colapsível), cobrindo uma camada de areia marrom com rochas alteradas.

Para avaliar a importância da presença de uma estaca danificada, cada uma das curvas obtidas experimentalmente foi analisada por meio do critério de falha para estudar o efeito da estaca danificada no sistema de fundação. Assim, a carga final e de trabalho para cada sistema de fundação foi determinada usando alguns métodos clássicos de extrapolação e um critério de deslocamento.

Posteriormente, baseado nos resultados dos testes de campo, foi possível modelar os cinco sistemas de fundação por meio do Método dos Elementos Finitos (MEF), usando o *software* comercial Abaqus, versão 14.4.

A simulação numérica foi bem correlacionada em cada um deles, em relação aos resultados experimentais obtidos a partir das provas de carga em verdadeira grandeza. Por isso, conclusões interessantes foram obtidas quanto aos procedimentos e metodologias envolvidos na análise não-linear numérica 3D, bem como em relação à presença de uma estaca defeituosa.

Além disso, a variação no módulo de reação com a profundidade do solo e o comportamento estrutural durante o fenômeno foi estudado para o radier estaqueado de apenas uma estaca intacta.

Finalmente, foi possível estudar a interação solo-estrutura para cada sistema de fundação. No que diz respeito às pontas e o radier, o comportamento em diferentes estágios de carga foi avaliado e, para os fustes das estacas de cada sistema de fundação, o comportamento deles foi estudado sob critérios de deslocamento.

## ABSTRACT

With the aim of investigating the impact of the presence and engagement of defective piles, a three-dimensional approach to analyzing laterally loaded intact and defective piled raft systems is presented. Five subsurface models are used in the analyses. The first one consists of piled raft with one intact pile. The second and third models consist of a piled raft system with three piles each; they have the same geometry, dimensions and materials, and the only difference between them is that one of them has a defective pile. The fourth and fifth models are a piled raft system with four piles, and like the three-pile systems, the only difference between them is also a defective pile.

It is important to emphasize that all the above-mentioned foundation systems were built and vertically loaded prior to this research work, as part of the research project: Fapesp 2011/17959-3. All piled raft systems involved bored piles drilled with helical auger to 5.0 m in depth and measuring 0.25 m in diameter.

As part of this research work, a full-scale lateral load test was performed on each of the aforementioned five models, and an experimental  $p$ - $y$  curve was obtained for each of them. All those measurement field works were executed at the *FEC* experimental site of the Campinas University, SP. The geotechnical profile of this research site consists of a silty clay layer, which is porous, colluvial, lateritic and collapsible, overlying a brown silty sand layer with altered rocks.

To evaluate the importance of the presence of a defective pile, each of the experimental curves obtained through some failure criteria were analyzed to study the effect of the defective pile in the foundation systems. Thus, the ultimate and works load for each foundation system were determined previously using some classical methods of extrapolation and a displacement criterion.

Later, based on the field test results, it was possible to model the five piled raft systems through the finite element method (FEM), using Abaqus commercial software, version 14.4.

A numerical simulation was well correlated in each one of them, with respect to the experimental results obtained from the respective full-scale load test. Interesting conclusions

have been drawn regarding the procedures and methodology involved in 3D numerical nonlinear analysis, as well as in relation to the presence of a defective pile.

Moreover, the variation in the subgrade reaction modulus with soil depth and the structural behavior during the phenomenon was studied only for the piled raft with one intact pile.

Finally, it was possible to study the interaction soil-structure for each foundation system. Concerning the tips and the raft, the behavior under different loading stages was evaluated, and only for the shaft of each pile of each system was the behavior studied under a displacement criterion set.

# INDEX

<b>DEDICATION .....</b>	<b>vi</b>
<b>ACKNOWLEDGMENTS .....</b>	<b>vii</b>
<b>RESUMO .....</b>	<b>viii</b>
<b>ABSTRACT .....</b>	<b>x</b>
<b>INDEX .....</b>	<b>xii</b>
<b>TABLE INDEX .....</b>	<b>xv</b>
<b>FIGURES INDEX .....</b>	<b>xvi</b>
<b>LIST OF ABBREVIATIONS AND SYMBOLS .....</b>	<b>xxii</b>
<b>1 INTRODUCTION .....</b>	<b>1</b>
1.1 JUSTIFICATION .....	3
1.2 GENERAL OBJECTIVE .....	5
1.3 SPECIFIC OBJECTIVES .....	5
1.4 SCOPE .....	6
<b>2 STATE OF THE ART .....</b>	<b>7</b>
2.1 OCCURRENCE OF LATERALLY LOADED PILES .....	7
2.2 NATURE OF SOIL RESPONSE .....	7
2.3 BEHAVIOR OF LATERALLY LOADED SINGLE PILES .....	10
2.3.1 WINKLER APPROACH .....	11
2.3.2 <i>p-y</i> METHOD OF ANALYSIS .....	13
2.3.3 ELASTICITY THEORY .....	16
2.3.4 FINITE ELEMENT METHOD (FEM) .....	16
2.4 BEHAVIOR OF A REINFORCED CONCRETE PILE .....	18
2.4.1 VARIATION IN BENDING STIFFNESS .....	18
2.4.2 EFFECT OF CRACKING ON THE RESPONSE OF A PILE TEST .....	19
2.4.3 AN INELASTIC CONSTITUTIVE MODEL FOR CONCRETE .....	20
2.5 DEFECTIVE PILES .....	22
2.5.1 NUMERICAL ANALYSIS OF DEFECTIVE PILES .....	24
2.6 INTERNATIONAL AND NATIONAL STUDIES ON PILED RAFTS UNDER LATERAL LOADING DURING THE LAST 15 YEARS .....	26
2.7 HORIZONTAL BEARING CAPACITY OF PILES IN A LATERITIC SOIL .....	34
<b>3 NUMERICAL ANALYSIS OF PILES .....</b>	<b>37</b>

3.1	CONSTITUTIVE METHODS FOR SOILS .....	37
3.2	ELASTICITY .....	38
3.2.1	PLANE STRAIN CONDITION .....	39
3.2.2	PLANE STRESS CONDITION .....	40
3.3	PLASTICITY .....	41
3.3.1	MOHR-COULOMB MODEL .....	42
3.3.2	CAM-CLAY MODIFIED MODEL .....	44
3.4	NUMERICAL MODELING .....	45
3.4.1	FINITE ELEMENT METHOD (FEM) .....	45
3.4.2	FINITE ELEMENT MODELING FOR LATERALLY LOADED PILES IN CLAY .....	46
3.4.3	PHYSICS OF LATERALLY LOADED PILE AND SOIL ANISOTROPY EFFECT .....	48
3.4.4	ABAQUS SOFTWARE 14.4 .....	51
3.4.5	NUMERICAL ANALYSIS FROM AN EXAMPLE IN THE LITERATURE .....	52
<b>4</b>	<b>MATERIALS AND METHODS .....</b>	<b>55</b>
4.1	EXPERIMENTAL RESEARCH SITE .....	55
4.2	EXPERIMENTAL PROGRAM AT RESEARCH SITE .....	59
4.2.1	HORIZONTAL LOADING TESTS .....	65
4.2.2	CONSTRUCTION OF DEFECTIVE PILES .....	67
4.3	EXPERIMENTAL RESULTS OF THE HORIZONTAL TESTING LOAD .....	68
4.3.1	ANALYSIS OF EXPERIMENTAL LOADING TEST RESULTS .....	69
4.3.2	BEHAVIOR PREDICTION .....	73
4.3.3	DEVELOPMENT OF GENERAL MODELING FRAMEWORK .....	75
4.3.4	PARAMETERS OF THE MATERIALS .....	83
4.3.5	NUMERICAL MODELING METHODOLOGY .....	91
<b>5</b>	<b>RESULTS AND DISCUSSION .....</b>	<b>95</b>
5.1	EVALUATION OF BACK ANALYSIS METHODOLOGY .....	95
5.2	NUMERICAL SUBGRADE REACTION MODULUS FOR <i>CC1</i> MODEL .....	102
5.3	NUMERICAL EVALUATION OF A DEFECTIVE PILE .....	105
5.4	STRUCTURAL BEHAVIOR OF THE <i>CC1</i> PILED RAFT SYSTEM .....	108
5.5	PREDICTION BEHAVIOR OF THE PILED RAFT GROUPS .....	112
5.6	EVALUATION OF THE INFLUENCE OF THE DEFECTIVE PILE ON THE FOUNDATION GROUP .....	114
5.6.1	<i>CC3</i> AND <i>CF3</i> PILED RAFT SYSTEMS .....	114
5.6.2	<i>CC4</i> AND <i>CF4</i> PILED RAFT SYSTEMS .....	119
5.6.3	PREDICTION STUDIES .....	122
5.7	GEOTECHNICAL BEHAVIOR OF THE PILED RAFT SYSTEMS .....	125
5.7.1	<i>UNIT BEARING PRESSURE AT PILE TIP</i> .....	125
5.7.2	<i>RAFT TILTING</i> .....	134

5.7.3	<i>INTERACTION BETWEEN THE PILE SHAFT AND THE GROUND</i> .....	137
<b>6</b>	<b>CONCLUSIONS AND FUTURE RESEARCH PROJECTS</b> .....	<b>154</b>
6.1	FUTURE RESEARCH PROJECTS .....	157
	<b>REFERENCES</b> .....	<b>158</b>
	<b>APPENDICES</b> .....	<b>162</b>
	MATLOCK AND REESE METHOD .....	163
	BROMS' METHOD .....	164
	EMPIRICAL PARAMETERS FROM <i>SPT</i> FIELD TEST.....	166

## TABLE INDEX

Table 2.1. Works on piled raft systems under lateral loading (last 15 years).....	26
Table 2.2. Classical methods of analysis .....	32
Table 4.1. Geotechnical parameters of the porous clay .....	57
Table 4.2. Load testing works performed at experimental site, Campinas University, SP. ....	61
Table 4.3. Results from the vertical loading tests.....	62
Table 4.4. Experimental measurements of each piled raft system.....	69
Table 4.5. The ultimate and work loads from the experimental loading test of all piled raft systems.....	71
Table 4.6. Failure analysis from the experimental loading test of all piled raft systems.....	72
Table 4.7. Soil dominium for the <i>CCI</i> piled raft system .....	79
Table 4.8. Detailed information of the modeling of the <i>CCI</i> piled raft system. ....	82
Table 4.9. Initial geotechnical parameters. ....	84
Table 4.10. Coefficients of variation of the soil parameters.....	84
Table 4.11. Final geotechnical parameters for each piled raft system analyzed.....	86
Table 4.12. Coefficients of variation of the concrete. (Garcia, 2015). ....	88
Table 4.13. Concrete parameters adopted for all piled raft systems numerically simulated. ...	88
Table 4.14. Coefficients of variation for steel material. ....	90
Table 4.15. Steel parameters adopted for numerically simulated piled raft systems.....	90
Table 4.16. General methodology for numerical simulations.....	93
Table 5.1. Numerical error.....	99
Table 5.2. Analysis of the control elements under the work load results .....	110
Table 6.1. Matlock and Reese method.....	164
Table 6.2. Broms' Method .....	165
Table 6.3. Results of the <i>SPT</i> field works.....	167
Table 6.4 Comparison of the modulus $n_h$ .....	168



## FIGURES INDEX

Figure 2.1. (a) Cylindrical pile under lateral load $Q_h$ . (b) Deflection $y_l$ . (c) Distribution of soil normal stress on element of pile. (d) & (e) distribution of stresses against a pile before and after lateral deflection respectively. ....	8
Figure 2.2. (a) Typical p-y curve; (b) Subgrade reaction modulus. Reese & Van Impe (2001).9	9
Figure 2.3. Behavior of a laterally loaded pile divided into segments (Norris & Ashour, 2001). ....	19
Figure 2.4. Uniaxial behavior of plain concrete. (Abaqus Theory Manual, 2008). ....	22
Figure 2.5. Some actual examples of damaged piles. (Freitas Neto, 2013). ....	24
Figure 2.6. Basic types of defective piles for numerical analysis. (Xu, 2000). ....	25
Figure 2.7. Pile under lateral loading. ....	30
Figure 2.8. Simplified geotechnical profile (Cunha, 2011). ....	35
Figure 3.1. Plane strain condition. (Helawany, 2007) ....	40
Figure 3.2. Plane stress condition. (Helawany, 2007) ....	41
Figure 3.3. Elastic-perfectly plastic assumption of Mohr-Coulomb model. (Helwany, 2007) 42	42
Figure 3.4. (a) The Mohr-Coulomb failure criterion, and (b) yield surface in principal stress space ( $c=0$ ). (Ti et al., 2009) ....	43
Figure 3.5. Consolidation curve in the void ratio versus mean effective stress (natural logarithm of $p'$ ) plane. (Helawany, 2007). ....	44
Figure 3.6. Stress path for: (1) a soil element behind the pile; (2) compression triaxial test with constant confined pressure; (3) a soil element in front of the pile. Note that $p$ and $q$ represent isotropic and deviatoric stresses respectively (Ahmadi and Ahmari, 2009). ....	49
Figure 3.7. Components in the numerical model. (Ahmadi and Ahmari, 2009). ....	50
Figure 3.8. Proposal problem, soil meshing and piled raft simulated through Abaqus software (Poulos and Davis, 1980). ....	53
Figure 3.9. (a) Piled raft with 15 piles. (b) Soil dominium. ....	54
Figure 3.10. Results of settlement calculated by different authors using different numerical tools. ....	54
Figure 4.1. Campinas City in Brazil, and layout at experimental site. ....	55
Figure 4.2. SPT chart and simplified geological profile from FEC-UNICAMP. ....	56
Figure 4.3. Location of field trials and sample collection ....	57
Figure 4.4. Geotechnical parameters of the porous clay. ....	57
Figure 4.5. Oedometer test results at 1 <sup>st</sup> and 2 <sup>nd</sup> meter depth (Gon, 2011). ....	58
Figure 4.6. Soil water characteristic curves at each meter depth (Gon, 2011). ....	59

Figure 4.7. Accumulated rain during the month of July, 2015. ....	60
Figure 4.8. Layout of the full-scale piled raft systems at experimental field. (July, 2015) .....	62
Figure 4.9. Layout at experimental field, Campinas University, SP. ....	63
Figure 4.10. Details of <i>CC1</i> piled raft system already built at the experimental field. ....	64
Figure 4.11. Details of the <i>CF1</i> piled raft system.....	64
Figure 4.12. Details of the <i>CC3</i> , <i>CF3</i> , <i>CC4</i> and <i>CF4</i> piled raft systems already built at the experimental field. ....	65
Figure 4.13. Sketch of the horizontal load test. ....	66
Figure 4.14. Horizontal load tests at full scale on the piled raft systems used in this research work. Experimental field at Campinas University, July, 2015. ....	66
Figure 4.15. (a) Making damage and placement of damaged region into the pile. (b) Hollow concrete cylinder. July 2012. (Freitas Neto, 2013). ....	67
Figure 4.16. Experimental results of the piled raft systems tested. (See appendix A). ....	68
Figure 4.17 Ultimate load for <i>CC1</i> piled raft system.....	69
Figure 4.18. Ultimate load for <i>CC3</i> and <i>CF3</i> piled raft systems. ....	70
Figure 4.19. Ultimate load for <i>CC4</i> and <i>CF4</i> piled raft systems. ....	70
Figure 4.20. Ultimate load defined for all piled raft systems. ....	71
Figure 4.21. Graphical analysis of all piled raft systems to define ultimate and work load.....	73
Figure 4.22. <i>CC1</i> prediction curve obtained by preliminary numerical ways. ....	74
Figure 4.23. <i>CC3</i> prediction curve obtained by preliminary numerical ways. ....	74
Figure 4.24. <i>CF4</i> prediction curve obtained by preliminary numerical ways. ....	75
Figure 4.25. Clear space around the rafts of each of the piled raft systems was provided to place the equipment and to carry out the full-scale horizontal loading tests. ....	78
Figure 4.26. Different geometries and mesh type for soil part of the <i>CC1</i> piled raft system...79	79
Figure 4.27. Components of the <i>CC1</i> piled raft system.....	80
Figure 4.28. Graphical results of the final geostatic stress state for the <i>CC1</i> model. Analysis included a total assembly of all component parts. ....	82
Figure 4.29. Simplified soil dominium composed of three layers used during the numerical simulations according to Table 4.9. ....	85
Figure 4.30. <i>CC1</i> and <i>CF1</i> concrete piled raft systems. ....	89
Figure 4.31. <i>CC3</i> , <i>CF3</i> , <i>CC4</i> and <i>CF4</i> concrete piled rafts systems. ....	89
Figure 4.32. Rebar placed inside <i>CC1</i> and <i>CF1</i> piled rafts. ....	91
Figure 4.33. Rebar placed inside <i>CC3</i> , <i>CF3</i> , <i>CC4</i> and <i>CF4</i> piled rafts.....	91

Figure 4.34. All different foundation systems simulated through Abaqus software. ....	92
Figure 5.1. Elastic analysis shows some different approximation tests.....	95
Figure 5.2. Elastic-plastic analysis shows some different approximation tests.....	96
Figure 5.3. Element type study shows some different approximation tests.....	96
Figure 5.4. Shape and size study shows some different approximation tests.....	97
Figure 5.5. Meshing density study shows different approximation tests.....	98
Figure 5.6. Mean absolute percentage error.....	99
Figure 5.7. Acceptable and reliable numerical results. ....	100
Figure 5.8. Graphical results of the horizontal displacements. <i>CC1</i> foundation system. ....	101
Figure 5.9. Contact between the pile shaft and the ground.....	103
Figure 5.10. The subgrade reaction modulus $K$ variation with soil depth. ....	103
Figure 5.11 The variation in the reaction modulus $n_h$ with soil depth. ....	104
Figure 5.12. Plotted numerical results of the <i>CC1</i> and <i>CF1</i> models. ....	105
Figure 5.13. Graphical results of horizontal displacements.....	106
Figure 5.14. Profile of the horizontal displacements under work loading.....	107
Figure 5.15. Piled rafts isolated at the final horizontal loading. Scale 15 times enhanced.....	107
Figure 5.16. Control elements assigned for the materials. Scale 5 times enhanced. ....	109
Figure 5.17. Numerical stress results of the control elements under working load.....	110
Figure 5.18. Capacity developed of the control elements under working load. ....	111
Figure 5.19. Engagement of each material under several lateral loading stages. ....	111
Figure 5.20. Behavior prediction of the <i>CC3</i> piled raft system from the <i>CC1</i> numerical Abaqus model. ....	112
Figure 5.21. Behavior prediction of the <i>CF4</i> piled raft system from the <i>CC1</i> numerical Abaqus model. ....	113
Figure 5.22. Plotted numerical results of the <i>CC3</i> intact model and <i>CF3</i> prediction study ...	115
Figure 5.23. Plotted numerical results of <i>CF3</i> defective model. ....	116
Figure 5.24. Piled rafts isolated at the final horizontal loading. Scale 15 times amplified. ...	117
Figure 5.25. Control finite elements in each piled raft according to Figure 5.24.....	117
Figure 5.26. Graphical horizontal displacement results. Amplified 3 times. ....	118
Figure 5.27. Graphical results of the horizontal displacements.....	119
Figure 5.28. Numerical results plotted for the <i>CC4</i> intact and <i>CF4</i> defective foundation systems.....	120
Figure 5.29. Numerical results plotted of the <i>CC4</i> intact model and <i>CC4</i> parametric study. ....	121

Figure 5.30. Graphical results of the horizontal displacements.....	121
Figure 5.31. Graphical results of the horizontal displacements.....	122
Figure 5.32. Sketch of the <i>CC3</i> and <i>CF3</i> foundation systems.....	126
Figure 5.33. Pile 1 of the <i>CC3</i> and <i>CF3</i> foundation systems. ....	126
Figure 5.34 Pile 2 of the <i>CC3</i> and <i>CF3</i> foundation systems .....	127
Figure 5.35. Pile 3 of the <i>CC3</i> and <i>CF3</i> foundation systems .....	127
Figure 5.36. Evaluation of the effect of a defective pile for the <i>CC3</i> and <i>CF3</i> piled rafts through normalized loading.....	129
Figure 5.37. Evaluation of the effect of a defective pile for the <i>CC3</i> and <i>CF3</i> piled rafts through loading values.....	129
Figure 5.38. Sketch of the <i>CC4</i> and <i>CF4</i> foundation systems.....	130
Figure 5.39. Pile 1 of the <i>CC4</i> and <i>CF4</i> foundation systems .....	131
Figure 5.40. Pile 2 of the <i>CC4</i> and <i>CF4</i> foundation systems .....	131
Figure 5.41. Pile 3 of the <i>CC4</i> and <i>CF4</i> foundation systems .....	132
Figure 5.42. Pile 4 of the <i>CC4</i> and <i>CF4</i> foundation systems .....	132
Figure 5.43. Evaluation of the effect of a defective pile for the <i>CC4</i> and <i>CF4</i> piled rafts through normalized loading.....	133
Figure 5.44. Evaluation of the effect of a defective pile for the <i>CC4</i> and <i>CF4</i> piled rafts through loading values.....	134
Figure 5.45. Sketch of the raft tilting.....	134
Figure 5.46. The raft tilting of the <i>CC3</i> and <i>CF3</i> foundation systems. ....	135
Figure 5.47. The raft tilting of the <i>CC4</i> and <i>CF4</i> foundation systems. ....	135
Figure 5.48. The raft tilting of the <i>CC3</i> and <i>CF3</i> foundation systems. ....	136
Figure 5.49. The raft tilting of the <i>CC4</i> and <i>CF4</i> foundation systems. ....	137
Figure 5.50. Sketch of the horizontal subgrade force transmitted by the pile shaft to the vertical borehole walls.....	138
Figure 5.51. The horizontal subgrade force transmitted by pile 1 to the borehole vertical walls in both the <i>CC3</i> and <i>CF3</i> foundation systems.....	139
Figure 5.52. The horizontal subgrade force transmitted by pile 2 to the borehole vertical walls in both the <i>CC3</i> and <i>CF3</i> foundation systems.....	139
Figure 5.53. The horizontal subgrade force transmitted by pile 3 to the borehole vertical walls in both the <i>CC3</i> and <i>CF3</i> foundation systems.....	140
Figure 5.54. The horizontal subgrade force transmitted by pile 1 to the borehole vertical walls in both the <i>CC4</i> and <i>CF4</i> foundation systems.....	141

Figure 5.55. The horizontal subgrade force transmitted by pile 2 to the borehole vertical walls in both the <i>CC4</i> and <i>CF4</i> foundation systems. ....	141
Figure 5.56. The horizontal subgrade force transmitted by pile 3 to the borehole vertical walls in both the <i>CC4</i> and <i>CF4</i> foundation systems. ....	142
Figure 5.57. The horizontal subgrade force transmitted by pile 4 to the borehole vertical walls in both the <i>CC4</i> and <i>CF4</i> foundation systems. ....	142
Figure 5.58. Sketch of the lateral shear forces transmitted by the pile shaft to the borehole vertical walls. ....	144
Figure 5.59. The lateral shear force transmitted by pile 1 to the front vertical wall in both the <i>CC3</i> and <i>CF3</i> foundation systems. ....	144
Figure 5.60. The lateral shear force transmitted by pile 1 to the back vertical wall in both the <i>CC3</i> and <i>CF3</i> foundation systems. ....	145
Figure 5.61. The lateral shear force transmitted by pile 2 to the front vertical wall in both the <i>CC3</i> and <i>CF3</i> foundation systems. ....	145
Figure 5.62. The lateral shear force transmitted by pile 2 to the back vertical wall in both the <i>CC3</i> and <i>CF3</i> foundation systems. ....	146
Figure 5.63. The lateral shear force transmitted by pile 3 to the front vertical wall in both the <i>CC3</i> and <i>CF3</i> foundation systems. ....	146
Figure 5.64. The lateral shear force transmitted by pile 3 to the back vertical wall in both the <i>CC3</i> and <i>CF3</i> foundation systems. ....	147
Figure 5.65. The lateral shear force transmitted by pile 1 to the front vertical wall in both the <i>CC4</i> and <i>CF4</i> foundation systems. ....	148
Figure 5.66. The lateral shear force transmitted by pile 1 to the back vertical wall in both the <i>CC4</i> and <i>CF4</i> foundation systems. ....	148
Figure 5.67. The lateral shear force transmitted by pile 2 to the front vertical wall in both the <i>CC4</i> and <i>CF4</i> foundation systems. ....	149
Figure 5.68. The lateral shear force transmitted by pile 2 to the back vertical wall in both the <i>CC4</i> and <i>CF4</i> foundation systems. ....	149
Figure 5.69. The lateral shear force transmitted by pile 3 to the front vertical wall in both the <i>CC4</i> and <i>CF4</i> foundation systems. ....	150
Figure 5.70. The lateral shear force transmitted by pile 3 to the back vertical wall in both the <i>CC4</i> and <i>CF4</i> foundation systems. ....	150
Figure 5.71. The lateral shear force transmitted by pile 4 to the front vertical wall in both the <i>CC4</i> and <i>CF4</i> foundation systems. ....	151
Figure 5.72. The lateral shear force transmitted by pile 4 to the back vertical wall in both the <i>CC4</i> and <i>CF4</i> foundation systems. ....	151

Figure 6.1. Variation in the reaction modulus subjected to the full-scale load test of the *CCI* piled raft system.....166

# LIST OF ABBREVIATIONS AND SYMBOLS

## ABBREVIATIONS

$C_c$	Coefficient of curvature
$C_u$	Coefficient of uniformity
$E_p I_p$	Bending stiffness or flexural rigidity
$E_c$	Modulus of elasticity of the concrete material
$E_s$	Modulus of elasticity of the soil
$E_p$	Elasticity modulus of the pile
$f_{ck}$	Strength of the concrete
$f_s$	Friction stress
$I_p$	Moment of inertia of the pile
$L_p$	Pile length
$l s f_{wl}$	lateral shear force acting under the work loading stage
$l s f_{maxwl}$	maximum lateral shear force developed under work loading stage
$M_o$	Moment at top of the pile
$n_h$	Reaction modulus
$P_i$	Internal vertical load transmitted from the pile tip to the ground
$P_{imax}$	Maximum internal vertical load transmitted to the ground
$P_{ult}$	Ultimate load
$q_{iwl}$	Horizontal subgrade force transmitted from both pile faces to the vertical walls of the borehole under work loading stage
$q_{imaxwl}$	Maximum horizontal subgrade force developed under work loading stage
$Q_H$	Horizontal or lateral load
$Q_v$	Axial load

## SYMBOLS

### Arabic letters

$B$	Raft width
$E$	Young's modulus

$G$	Shear modulus of the soil
$K$	Subgrade reaction modulus
$p$	Intensity of the horizontal load
$T$	Relative stiffness factor
$V$	Shear force
$y$	Deflection of the pile

### **Greek letters**

$\beta$	Betha method
$\sigma$	Normal stress
$\varepsilon$	Unit strain
$\mu$	Friction factor
$\phi$	Soil friction angle
$\phi_p$	Pile diameter
$\nu$	Poisson's ratio
$\Omega$	Dilatancy angle
$\tau$	Shear stress
$\psi_i$	Angle formed by the raft and the natural ground during the horizontal loading
$\psi_{max}$	Maximum angle formed by the raft and the natural ground at the end of the ultimate load applied



# 1 INTRODUCTION

The concept of raft foundations enhanced with deep foundation elements, typically piles and therefore the name “piled rafts”, has received considerable attention in recent years. The raft in this system has adequate bearing capacity and hence the main objective of introducing these pile elements is to control or minimize the average and or differential displacements of the piled raft system, rather than to carry the major portion of the loads.

According to Katzenbach & Schmitt (2004), the term raft just means the shape of the foundation system, as only the pile elements receive and transmit all the loads from the superstructure, and the raft just plays the structural role of tying all the piles. When there is contact between the raft and soil, then all the elements together are called a piled raft, regardless of the size of the raft and the number of piles.

According to Janda et al. (2009), the term piled raft refers to a foundation system where the raft, the piles and the adjacent soil interact with each other to support vertical and horizontal loads as well as overturn forces from the superstructure.

This combination (raft and piles) is a new type of foundation. It was introduced because of the benefit obtained by having the raft and the well-located piles working together, resulting in a geotechnical and structural improvement of the foundation system when it is subjected to heavy loads and/or low soil resistance; in addition, it has economic benefits, better performance and shorter construction time.

The majority of cities in Brazil and indeed throughout the world are subjected to structural changes, as there is great demand for offices, buildings, apartment complexes and other buildings, but in small spaces; this situation results in the need to build tall and slender structures.

According to Patil et al. (2013), the piled raft system has emerged as a good alternative to the foundation-type system used for tall buildings. However, predicting their behavior is one of the greatest challenges in relation to soil-superstructure interaction. The difficulty in analyzing these challenges is due to the use of simplified calculation methods that do not model the real problem in an appropriate way.

Consequently, a major design question is how to design the piles optimally to control the displacements. To address this question, much attention has been given to the development of analytical models for piled rafts (Randolph & Wroth, 1979). This development has subsequently resulted in numerous parametric studies that have investigated the influence of system geometry and soil conditions on the performance of piled rafts (Poulos, 2001).

Two different design approaches have also evolved to address this question (Randolph, 2003). The first focuses mainly on reducing the average displacements, while the second focuses on reducing the differential displacements. Obviously, there are cases where both average and differential displacements are among the main concerns.

Also, laboratory and field tests on piled rafts and pile groups (a system where the raft has no contact with the soil) have been conducted and provided useful insights into the behavior of piled rafts and pile groups. Case histories, in which extensive field measurements were made, have also been reported in the literature (Freitas, 2013). As a result, some aspects of the field behavior of piled rafts have been determined.

At the present time, there are a great number of methods to design piled raft systems, and they generally fall into simplified and rigorous methods. One of the more commonly used tools to model the real behavior of the piled raft system is the powerful finite element method, and there are already a large number of tall buildings in the world that were designed using this analysis tool, for example the Burj Khalifa Tower, the world's tallest artificial structure.

The deep foundation system provides great advantages, both constructive and economic as already mentioned above, but at the same time it involves a lot of unknowns during the design stage, because the real behavior of the soil (stress and strain state within the soil mass) under loads from the superstructure is not known with certainty.

During the construction stage, the concrete piles can be placed into the ground using driven piles or bored piles. The driven piles are the oldest type of deep foundation in existence and are installed using some form of hammer to drive them into previously unexcavated soil. By contrast, the bored pile is a non-displacement form of foundation that is cast *in situ* using drilling equipment for all types of soil.

By choosing either of the two previously-mentioned piles types for installation, a certain level of damage will appear; in the case of the thru driven pile, the constant pounding on the pile cap could produce fissuring on the concrete, whereas for the bored pile, some discontinuities could be produced during construction due to a lack of supervisory control, both in terms of materials quality and constructive process, among other aspects. These problems are becoming more frequent and are not taken into account during the design of the foundation system.

In addition to the unknowns of interaction between the raft, piles and soil, usually considered by any calculation method, there is another variable that should be added, which is the damage in the piles themselves due to the previously mentioned reasons.

Experimental studies on piled raft systems in real scale taking into account defective piles are not common; therefore, this paper should be of major interest since it analyzes piled raft foundation systems under lateral loads on three different concrete piled raft structures, which were built especially for some research projects, including this one. Static horizontal load tests were performed in accordance with local and international standards, on several piled raft systems composed of one, three and four piles, measuring 0.25 m in diameter and 5.0 m in length.

Numerical analyses of the experimental results were performed using some computational tools such as Abaqus 6.14.4 software, in order to simulate and evaluate the 3D behavior of the foundations, as well as the conduct of the defective piles working together.

It is important to emphasize that this research could not have been conducted without the joint research work of both the University of Campinas, SP. and the Geotechnical Postgraduate Program at the University of Brasilia, D.F., as well as the financial support provided by the São Paulo Foundation (FAPESP) and process number 14/06611-4.

## **1.1 JUSTIFICATION**

The behavioral dynamics of laterally loaded piles is complex because several factors are acting at the same time. The non-linearity in the mechanical behavior of elements such as soil,

pile, interface between them, and non-linear system response also represent a major geotechnical problem linked to soil-structure interaction in the deep foundation area.

For the calculation and design of laterally loaded piles, several analytical methods based on simplified assumptions, in many cases far removed from the real response of the system, have been proposed. The deficiencies present in conventional analysis include: consideration of the foundation soil as an elastic but not continuous base (Winkler's model), the behavior of linear-elastic materials instead of non-linear elastic-plastic, overlapping effects instead of soil-structure interaction analysis, and 2D numerical analysis instead of 3D modeling, among others.

In the bibliographical review provided herein, there are few papers with respect to certain specific aspects of the piled raft subjected to lateral loads with the presence of piles with a structural defect, or the superposition's effect of nearby excavations such as tunnels, subways, basements, etc. on this sort of deep foundation system.

Consequently, there is a real need for a greater amount of experimental data for verification of the calculation methodologies that use different criteria and model soil actions, as well as the soil-piles interaction and the effect of ground contact between the soil and the raft.

The use of load testing has shown great promise in the evaluation of laterally loaded piles, and therefore it is necessary to explore this subject more deeply through more experimental full-scale piled raft systems and compare them with an extensive numerical simulation of the problem.

Finally, this sort of full-scale testing should consider, through parametric studies, different loading combinations, varying the geometry of the piles and setting several configurations and distributions, in order to study in depth the contribution of the raft when it has contact with the soil, and to study the phenomenon under different subsoil conditions.

It is believed that the development of this project will contribute significantly to areas linked to the behavior of foundations, which undoubtedly require additional technical information and research related to topics that are difficult to find in the literature.

## **1.2 GENERAL OBJECTIVE**

Understand the behavior of laterally loaded piled raft systems, with and without the presence of defective piles.

## **1.3 SPECIFIC OBJECTIVES**

- To study the behavior of soil-pile interaction through full-scale static horizontal load testing.
- To establish a specific numerical analysis methodology to simulate the soil-pile interaction through 3D modeling software based on the finite element method (FEM).
- To compute the bearing capacity through 3D finite element models, comparing the final results with those obtained at the experimental site.
- To obtain the influence from geotechnical parameters involved in the behavior of laterally loaded piles, determining the influence of each variable and evaluating which of the constitutive models chosen to represent the soil behavior has a better performance.
- To consider the concrete damaged plasticity model, trying to represent the plasticity performance of the concrete, taking into account the stiffness of the degraded material with increasing load on piles.
- To attain parametric analysis of piled raft systems loaded horizontally with the presence of defective piles through numerical analysis, so that it will be possible to include some models that cannot be effectively tested at the experimental field.
- To study the influence of the damage on the behavior of the piled rafts foundation systems, when comparing the intact and defective foundation systems.

## **1.4 SCOPE**

It is hoped that the technical-scientific findings of this research work, will contribute to a better understanding of the behavior of this sort of deep pile foundation system, submitted to horizontal loading with presence of defective piles; more specifically, it is hoped that this research will provide additional support, knowledge and some experience in the matter to the scientific and technical community, as well as provide new paths to create more efficient design projects, and possibly improve the current construction methods used for such piled raft structures.

No doubt this research will be of major interest to those in the national and international geotechnical community that deal with engineering foundations under critical (defective piles) conditions.

## 2 STATE OF THE ART

### 2.1 OCCURRENCE OF LATERALLY LOADED PILES

With regard to actual use, laterally loaded piles may be termed active or passive. An active pile has loading applied principally at its top in supporting a superstructure, such as a bridge. A passive pile has loading applied principally along its length due to earth pressure, such as for piles in a moving slope, or for a secant pile wall. These active piles must sustain lateral loading from storm-driven waves and wind. With the advent of offshore structures, the design of such piles was of primary concern and promoted a number of full-scale field test. The design of the piles for an offshore platform presents interesting problems in soil-structure interaction.

Other examples of active piles are found in the design of foundations for bridges, high-rise structures, overhead signs, and piers for ships. Active piles must be designed for mooring dolphins, breasting dolphins, and pile groups that protect bridge foundations against ship impact.

### 2.2 NATURE OF SOIL RESPONSE

The main soil parameter in the design of a pile under lateral loading is a reaction modulus  $n_h$  [ $FL^{-3}$ ], defined as the resistance from the soil  $\sigma_y$  [ $FL^{-2}$ ] at a point along the pile divided by the deflection of the pile  $y$  [ $L$ ] at that point. The reaction modulus is a function both of depth below the ground surface  $z$  and the deflection of the pile  $y$ , thus:

$$n_h = \frac{\sigma_y}{y} \quad (2.1)$$

The sketch in Figure 2.1-a shows a cylindrical pile under lateral load  $Q_h$  with a thin slice of soil shown at the depth  $z_l$ , whereas Figure 2.1-b&c depict the same situation below the ground line. The uniform distribution of stresses normal to the wall of the pile in Figure 2.1-d is correct for the case of a pile that has been installed without bending. If the pile were caused to deflect a distance  $y_l$  (exaggerated in the sketch for clarity), the distribution of the stresses would be similar to that shown in Figure 2.1-e. The stresses will have decreased on the back side (active zone) of the pile and increased on the front side (passive zone). Some of

the stresses will have both a normal and shearing component.

Integration of the stresses  $\sigma_y$  will result in the quantity  $p$  (intensity of the load  $Q_h$  acting on the unit length of the pile), which acts in the opposite direction to  $y$ . The dimensions of  $p$  are load per unit length along the pile  $[FL^{-1}]$ . Multiplying the equation 2.1 by the diameter of the pile  $\phi_p$  results in:

$$\sigma_y \cdot \phi_p = n_h \cdot \phi_p \cdot y \tag{2.2}$$

Thus:

$$p = -K \cdot y \tag{2.3}$$

where:  $K [FL^{-2}]$  is known as subgrade reaction modulus. It is important to note that the deflection of the pile is equal to horizontal displacement of the soil ( $y = \delta$ ).

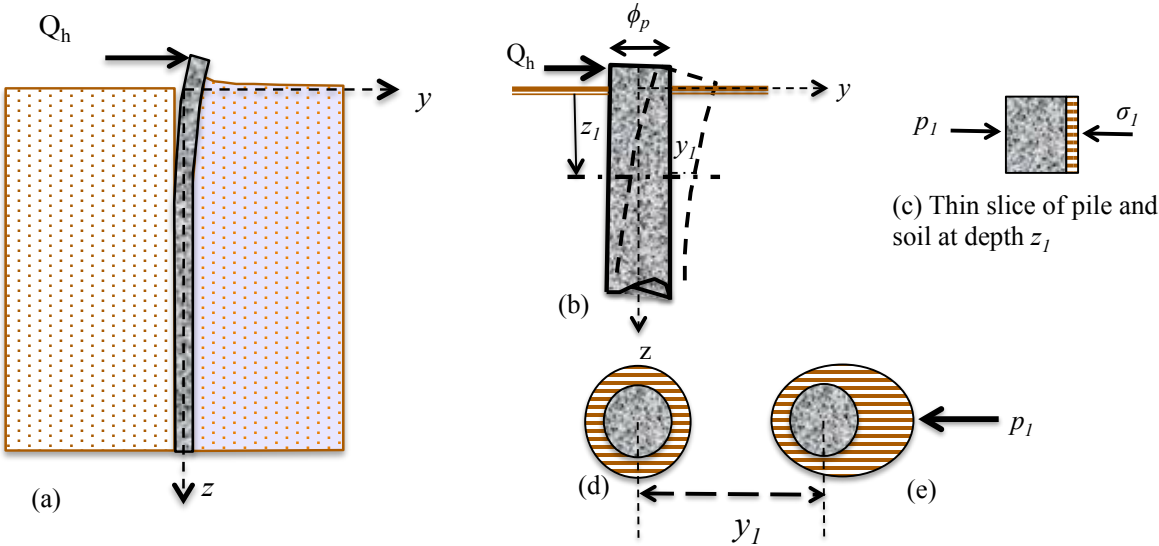


Figure 2.1. (a) Cylindrical pile under lateral load  $Q_h$ . (b) Deflection  $y_I$ . (c) Distribution of soil normal stress on element of pile. (d) & (e) distribution of stresses against a pile before and after lateral deflection respectively.

A typical  $p$ - $y$  curve is shown in Figure 2.2-a, where  $K$  represents the slope of the trace to a  $p$ - $y$  curve. The curve is one member of a family of curves that shows the intensity of the horizontal load  $Q_h$  acting on the pile, as a function of depth  $z$ . The curve in Figure 2.2-b depicts the value  $K$  that is constant for small deflections for a particular depth, but decreases with increased deflection. While  $K$  will vary with the properties of the particular soil, the term does not uniquely represent a soil property. Rather,  $K$  is a simple parameter for convenient



use in computations. For a particular practical solution, the term is modified point by point along the length of the pile as iteration occurs. The iteration leads to compatibility between pile deflection and soil resistance, according to the nonlinear  $p$ - $y$  curves that have been selected.

The portion of the curve in Figure 2.2-a from point  $a$  to point  $b$  shows that the values of  $p$  are increasing at a decreasing rate with increasing deflection  $y$ . This behavior undoubtedly is reflecting the nonlinear portion of the in situ stress-strain curve. Many suggestions have been made for predicting the  $a$ - $b$  portion of a  $p$ - $y$  curve but there is no widely accepted analytical procedure. Rather, that part of the curve is empirical and based on results of full-scale tests of piles in a variety of soils with both monotonic and cyclic loading.

The straight line, horizontal portion of the  $p$ - $y$  curve in Figure 2.2-a implies that the in situ soil is behaving plastically with no loss of shear strength with increasing strain. With that assumption, analytical models can be used to compute the ultimate load  $p_{ult}$  as a function of pile dimensions and soil properties.

A more direct approach to formulating  $p$ - $y$  curves would be to consider the response of the soil, rather than the pile. The nonlinear stress-strain characteristics of the soil must be modeled, taking into account large strains. Properties must be selected for the various layers of soil around the pile. In addition, nonlinear geometry must be considered, particularly near the ground surface, where gaps in cohesive soils will occur behind a pile and upward bulging in front. For cohesionless soils, there will be settlement of the ground surface due to densification, especially under repeated loading.

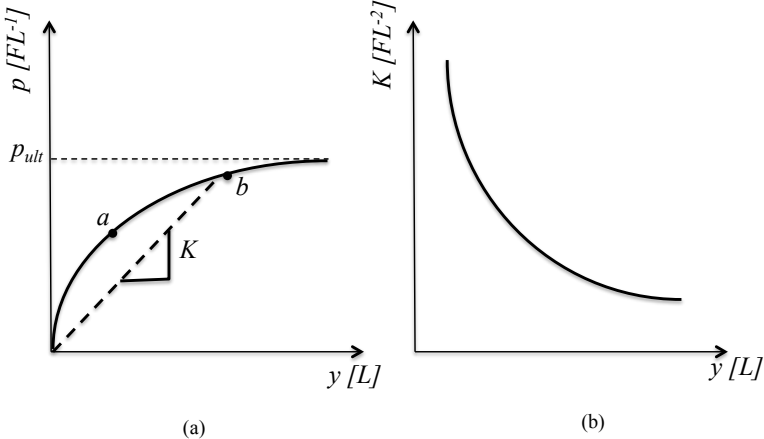


Figure 2.2. (a) Typical  $p$ - $y$  curve; (b) Subgrade reaction modulus. Reese & Van Impe (2001).

## 2.3 BEHAVIOR OF LATERALLY LOADED SINGLE PILES

The pile head may move horizontally over an appreciable distance before rotation or failure of the pile occurs, to such an extent that the movement of the structure supported by the pile or pile group exceeds tolerable limits. Thus even though working load is obtained by dividing the estimated ultimate pile load by a suitable safety factor, it is still necessary to determine the deflection of the pile and ensure that the permissible deflection is not exceeded. The following methods are extensively employed in estimating the pile deflections under later loads (Reese & Van Impe, 2001):

- Modulus of subgrade reaction  $K$  approach in which the continuous nature of the soil medium is ignored and the pile reaction at a point is simply related to the deflection at that point.
- The elastic approach, which assumes the soil to be an ideal elastic continuum.

The modulus of subgrade reaction  $K$  is relatively simple and has been used in practice for a long time. This method can incorporate factors such as nonlinearity and variation of subgrade reaction with depth. It can also account for various soil layers.

Three criteria must be satisfied in the design of pile foundations subjected to lateral forces and moments:

1. The soil should not be stressed beyond its ultimate capacity
2. Deflections should be within acceptable limits
3. The structural integrity of the foundation system must be assured

The first criteria can be addressed during design using ultimate resistance theories such as those of Broms (1964a) or Hansen (1961). The second and third criteria apply to deflections and stresses that occur at working loads. The behavior of piles under working load conditions has been the focus of numerous studies over the past 40 to 50 years. A brief review of the most widely recognized analytical techniques is provided in this section. Many of these techniques can be modified to predict the behavior of closely spaced piles, or pile groups. Modifications for group response are often in the form of empirically or theoretically derived factors that are applied, in various ways, to account for group interaction effects. Analytical

methods for predicting lateral deflections, rotations and stresses in single piles can be grouped under the following four headings:

- Winkler approach
- $p$ - $y$  method
- Elasticity theory
- Finite element method

These techniques provide a framework for the development of analytical techniques that can be used to evaluate the response of piles in closely spaced groups

### 2.3.1 WINKLER APPROACH

The Winkler approach, also called the subgrade reaction theory, is the oldest method for predicting pile deflections and bending moments. The approach uses Winkler's modulus of subgrade reaction concept  $K$  to model the soil as a series of unconnected linear springs with a stiffness  $E_s$  expressed in units of force per length squared ( $FL^{-2}$ ).  $E_s$  is the modulus of soil reaction (or soil modulus); from equation (2.3) it can be written as:

$$E_s = \frac{-P}{y} \quad (2.4)$$

The negative sign indicates the direction of soil reaction is opposite to the direction of the pile deflection. It is possible to express the modulus of horizontal subgrade reaction  $E_s$ , as a function of the reaction modulus  $n_h$  in units of force per unit volume; from the equation (2.2) the relationship between  $E_s$  and  $n_h$  can be expressed as:

$$E_s = n_h \cdot \phi_p \quad (2.5)$$

$E_s$  is a more fundamental soil property because it is not dependent on pile size. The behavior of a single pile can be analyzed using the equation of an elastic beam supported on an elastic foundation, which is represented by the 4<sup>th</sup> order differential beam bending equation:

$$E_p I_p \cdot \frac{d^4 y}{dx^4} + E_s \cdot y = 0 \quad (2.6)$$

Where:

$E_p$  - is the modulus of elasticity of the pile;  $I_p$  is the moment of inertia of the pile section  
 $E_p I_p$  - bending stiffness or flexural rigidity;  $y$  - is the lateral deflection of the pile at point  $z$  along the length of the pile.

Solutions to equation (2.6) have been obtained by making simplified assumptions regarding the variation in  $E_s$  (or  $n_h$ ) with depth, and are generally expressed as follows:

$$y = e^{\beta z} \cdot (A \cdot \cos \beta z + B \cdot \sin \beta z) - e^{-\beta z} \cdot (C \cdot \cos \beta z + D \cdot \sin \beta z) \quad (2.7)$$

Where:  $A, B, C$  and  $D$  – are constants of integration and:

$$\beta = \sqrt[4]{\frac{K}{4 \cdot E_p \cdot I_p}} \quad (2.8)$$

Where:  $\beta$  – Constant [ $L^{-1}$ ]

The most common assumption is that  $E_s$  is constant with depth for clays and  $E_s$  varies linearly with depth for sands. Poulos & Davis (1980) provide tables and charts that can be used to determine pile deflections, slopes, and moments as a function of depth and non-dimensional coefficients for a constant value of  $E_s$  with depth.

The soil modulus for sand and normally consolidated clay is often assumed to vary linearly with depth  $z$ , as follows:

$$E_s = n_h \cdot z \quad (2.9)$$

For this linear variation in  $E_s$  with depth, Matlock & Reese (1962) and Poulos & Davis (1980) present non-dimensional coefficients that can be used to calculate pile deflections, rotations, and bending moments for various pile-head boundary conditions. Other authors present other formulations for the variation of  $E_s$  with depth, such as step functions, hyperbolic functions, and exponential functions.

The subgrade reaction method is widely employed in practice because it has a long history of use, and because it is relatively straightforward to apply using available chart and tabulated solutions, particularly for a constant or linear variation in  $E_s$  with depth. Despite its frequent use, the method is often criticized because of its theoretical shortcomings and limitations. The primary shortcomings are:

1. The modulus of subgrade reaction is not a unique property of the soil, but depends intrinsically on pile characteristics and the magnitude of deflection.
2. The method is semi-empirical in nature.

3. Axial load effects are ignored.
4. The soil model used in the technique is discontinuous.

That is, the linearly elastic Winkler springs behave independently and thus displacements at a point are not influenced by displacements or stresses at other points along the pile.

Modifications to the original subgrade reaction approach have been proposed to account for some of these shortcomings. One of these modifications attempts to convert the Winkler model to a continuous model by coupling the springs using an inter-spring shear layer component. This model also accounts for the contribution of edge shear along the pile boundaries. The model has not gained widespread acceptance because of difficulties associated with obtaining soil parameters necessary to develop coefficients for use in the model. Several authors have argued in favor of the subgrade reaction approach using finite difference techniques to solve the beam bending equation with nonlinear load versus deflection curves to model the soil (Reese & Van Impe, 2001). Their approach is known as the  $p$ - $y$  method of analysis. This method has gained popularity in recent years with the availability of powerful personal computers and commercial software such as COM624 (1993) and LPILE Plus3.0 (1997).

### **2.3.2 $p$ - $y$ METHOD OF ANALYSIS**

The  $p$ - $y$  approach for analyzing the response of laterally loaded piles is essentially a modification or “evolutionary refinement” of the basic Winkler model, where  $p$  is the intensity of the load  $Q_h$  acting on the unit length of the pile, and  $y$  is the pile deflection. The soil is represented by a series of nonlinear  $p$ - $y$  curves that vary with depth and soil type. The method is semi-empirical in nature because the shape of the  $p$ - $y$  curves is determined from field load tests. (Reese, 1977) has developed a number of empirical or “default” curves for typical soil types based on the results of field measurements on fully instrumented piles. The most widely used analytical expression for  $p$ - $y$  curves is the cubic parabola, represented by the following equation:

$$\frac{P}{P_{ult}} = 0.5 \cdot \left[ \frac{y}{y_{50}} \right]^{\frac{1}{3}} \quad (2.10)$$

Where:

$P_{ult}$  - ultimate soil resistance per unit length of pile;  $y_{50}$  - the deflection at one-half the ultimate soil resistance.

To convert from strains measured in laboratory triaxial tests to pile deflections, the following relationship is used for  $y_{50}$ :

$$y_{50} = A \cdot \varepsilon_{50} \cdot \phi_p \quad (2.11)$$

Where:  $\varepsilon_{50}$  - strain at  $\frac{1}{2}$  the maximum principal stress difference determined in a laboratory triaxial test;  $\phi_p$  - pile diameter;  $A$  – constant that varies from 0.35 to 3.0

The deflections, rotations, and bending moments in the pile are calculated by solving the beam bending equation using finite difference or finite element numerical techniques. The pile is divided into a number of small increments and analyzed using  $p$ - $y$  curves to represent the soil resistance.

In this representation, the axial load in the pile,  $Q_v$ , is implicitly assumed constant with depth, to simplify the computations. This assumption does not adversely affect the analysis because  $Q_v$  has very little effect on the deflection and bending moment. Furthermore, the maximum bending moment is generally only a relatively short distance below the groundline, or pile cap, where the value of  $Q_v$  is undiminished (Reese, 1977). Four additional equations are necessary to balance the number of equations and the number of unknowns in the finite difference formulation. Boundary conditions, two at the pile top and two at its bottom, represent these four equations. At the bottom of the pile, one boundary condition is obtained by assuming a value of zero moment, or:

$$E_p I_p \cdot \frac{d^2 y}{dz^2} = 0 \quad (2.12)$$

The second boundary condition at the pile bottom involves specifying the shear of the pile using the following expression at  $z = L$ :

$$E_p I_p \cdot \frac{d^3 y}{dz^3} + Q_v \frac{dy}{dx} = V \quad (2.13)$$

Where:  $V$  - shear force, which is usually set equal to zero for long piles.

The two boundary conditions at the top of the pile depend on the shear, moment, rotation, and displacement circumstances at the pile top. These are generalized into the following four categories:

1. Pile not restrained against rotation. This is divided into subcategories (a) “flagpole” and (b) free-head conditions.
2. Vertical load applied eccentrically at the ground surface (moment loading condition).
3. Pile head extends into a superstructure or is partially restrained against rotation (partially restrained condition).
4. Pile head rotation is known, usually assumed = 0 (fixed-head condition).

The method is an improvement over the subgrade reaction approach because it accounts for the nonlinear behavior of most soils without the numerical limitations inherent in the subgrade reaction approach. However, the method has some limitations, as described below:

- a. The  $p$ - $y$  curves are independent of one another. Therefore, the continuous nature of soil along the length of the pile is not explicitly modeled.
- b. Suitable  $p$ - $y$  curves are required. Obtaining the appropriate  $p$ - $y$  curve is analogous to obtaining the appropriate value of  $E_s$ ; one must either perform full-scale instrumented lateral load tests or adapt the existing available standard curves (default curves) for use in untested conditions. These default curves are limited to the soil types in which they were developed; they are not universal.
- c. A computer is required to perform the analysis.

Mokwa & Duncan (2001) present a means of adjusting the shape of the  $p$ - $y$  curve to model the behavior of soils that have both cohesion and friction using Hansen (1961)  $f$ - $c$  ultimate theory. In situ tests such as the dilatometer, cone, penetrometer and pressuremeter ones have also been used by several authors to develop  $p$ - $y$  curves.

### **2.3.3 ELASTICITY THEORY**

Several methods may be employed to estimate Young's modulus for soil for use in theoretical solutions, including the following (Poulos & Davis 1980):

- 1.- Laboratory tests in which the stress path of typical soil elements along the pile are simulated.
- 2.- Plate-bearing tests, preferably on vertical plates, at various depths.
- 3.- Pressuremeter tests.
- 4.- The use of full-scale loading tests to back-figure the modulus.
- 5.- Empirical correlations with other properties.

Full-scale loading tests are probably the most satisfactory means of determining the soil modulus, since such factors as the effects of installation and pile-soil separation are taken into account automatically and reflected in the back-figured moduli. There appears to be two possible means of interpreting pile-load results:

- 1.- To use the ground line deflection at the working load to back-figure a secant value of soil modulus, which may be used with the elastic theory to predict deflections at the working load (ignoring the effects of local yield and soil pile separation).
- 2.- To use the linear portion of the load-deflection curve to back-figure a tangent value of soil modulus, which may then be used with the theory (including the effects of local yield) to predict the load-deflection curve to failure.

The latter procedure would appear to be preferable, as a more relevant value of the pile-flexibility factor may be obtained. However, in some cases, the use of the first procedure may be more expedient if piles similar to the test pile are to be used in the foundation, and the use of a secant modulus with purely elastic theory should give results of adequate accuracy at normal working loads.

### **2.3.4 FINITE ELEMENT METHOD (FEM)**

Pile foundation systems are often used in weaker soil to transfer superstructure loads to underlying ground, aiming to increase the bearing capacity or lessen the settlement of infrastructures. However, the load transfer mechanism and failure mode of pile foundations



are very complex and not fully understood yet. There are no general equations to predict the bearing capacity and settlement for single pile or pile group systems under different working conditions. Studies on this problem using field or laboratory tests are ongoing (Zhan et al., 2012).

Recently, due to the rapid development of computing technology, numerical analysis methods involving finite element method (FEM) have been widely used for the following purposes: to understand the bearing capacity behavior of the piles, especially for piles under combined loading conditions, such as axial, torsion, and lateral loads; to assess the capability of considering the nonlinear behavior of structure and soil; and to determine the potential to model soil-pile-structure interactions (Lee et al., 2002; Rajagopal and Karthigeyan, 2008).

A complete three-dimensional analysis of a piled raft foundation system can be carried out by finite element analysis or by use of the commercially available computer programs that have appropriate numerical methods available for piled raft analysis (Katzenbach et al., 1998). The components of a structure supported by a piled raft include the superstructure, the raft that is supported by the piles, and the soil mass around the pile shaft and below the pile tip.

The interactions between two or more of these elements increase the degree of difficulty in obtaining a solution. A closed form solution is often difficult to obtain and the designer may have to employ numerical techniques. Some problems still remain, however, in relation to the modeling of the pile-soil interfaces, and whether interface elements should be used. If they are required, then approximations are usually involved in the assignment of joint stiffness properties. Such analyses are therefore more suited to obtaining benchmark solutions against which to compare simpler analysis methods, rather than as routine design tools.

Time-dependent results can be obtained and more intricate conditions such as battered piles, slopes, excavations, tie-backs, and construction sequences can be modeled. The method can be used with a variety of soil stress-strain relationships, and is suitable for analyzing pile group behavior. Performing three-dimensional finite element analyses requires considerable engineering time for generating input and interpreting results. For this reason, the finite element method has predominately been used for research on pile foundation system behavior, but rarely for design.

In the particular case of piles under horizontal loading, an appropriate solution with the FEM requires three-dimensional modeling, for various reasons including: transverse loading and subsequent deformation at the pile head causes the system to lose its symmetry around the pile center, the response of the upper soils (at and near the ground surface) has a dominant effect on pile behavior, the constitution of the soil is not the same (the pile could cross several layers), the elastic properties of soils vary with depth, etc.

A solution with the FEM must start with the consecutive modeling of the in situ soil, then the influence of the installation on the piles must be modeled, and finally the modeling must address the influence of the various kinds of loading and loading directions, geometry, dimensions, soil properties, etc.

## **2.4 BEHAVIOR OF A REINFORCED CONCRETE PILE**

### **2.4.1 VARIATION IN BENDING STIFFNESS**

The flexural behavior of a structural element such as a beam, column, or pile subjected to bending is dependent on its bending stiffness  $EI$  (also named flexural rigidity). The value of  $EI$  is found from the product of the modulus of elasticity of the material of which it is made, and the moment of inertia of the cross section around the axis of bending. The value of  $EI$  is essentially constant for the level of loading to which a structural-steel member is subjected, but both  $E$  and  $I$  vary as the stress conditions change for a reinforced-concrete member. The  $EI$  value of a reinforced-concrete pile is assumed to be constant for simplicity in the analysis.

Behavior of piles under lateral loading is basically influenced by the properties of both the soil and pile (pile material and shape). The nonlinear modeling of pile material, whether it is steel and/or concrete, should be employed in order to predict the value of the lateral load and the realistic associated bending moment and pile deflection especially at large values of pile-head deflection and the onset of pile material failure. It is known that the variation in the bending stiffness  $EI$  of a laterally loaded pile is a function of the bending moment distribution along the pile (moment-curvature relationship) as seen in Figure 2.3.

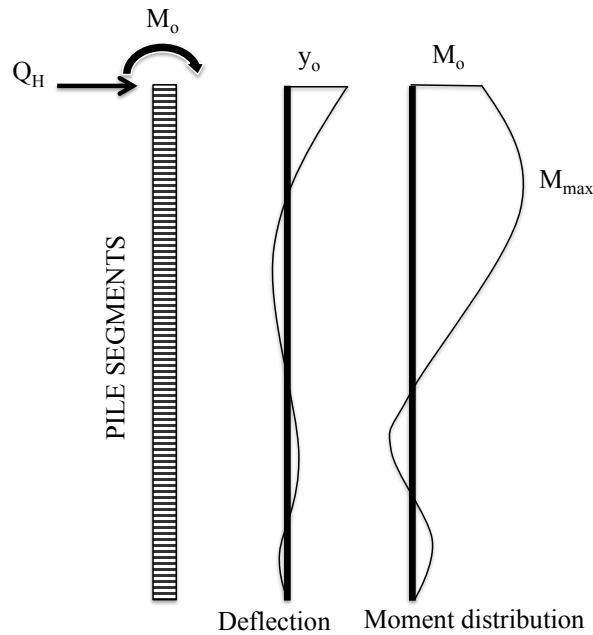


Figure 2.3. Behavior of a laterally loaded pile divided into segments (Norris & Ashour, 2001).

Consequently, some of the pile cross sections which are subjected to high bending moment experience a reduction in bending stiffness and softer interaction with the surrounding soil. Such behavior is observed with drilled shafts and steel piles at advanced levels of loading and has an impact on the lateral response and capacity of the loaded pile. The pile bending stiffness along the deflected pile changes with the level of loading, the moment-curvature relationship of the pile material, and the soil reaction which affects the pattern of pile deflection. Therefore, the equilibrium among the distributions of pile deflection, bending moment, bending stiffness, and soil reaction along the pile should be maintained.

## 2.4.2 EFFECT OF CRACKING ON THE RESPONSE OF A PILE TEST

Capacity-based structure design, still used in many cases, limits the soil-structure interaction mechanism to the determination of the bearing capacity of a pile group. However, in many cases the criterion for the design of piles to resist lateral loads is not the ultimate lateral capacity but the deflection of the piles (Poulos and Davis 1980; Comodromos and Pitilakis 2005).

As was mentioned in the previous section, many procedures exist for estimating the response of single piles and pile groups under lateral loading, ranging from application of

empirical relationships and simple closed-form solutions to sophisticated non-linear numerical procedures. On the basis of the experience gained from the research studies performed over recent decades, empirical relationships were proposed to estimate the reduction factors with respect to the stiffness of a group due to the interaction between the piles.

Specific values for these factors have been proposed by the Canadian Geotechnical Society (1992), Naval Facilities Engineering Command (1982), Randolph (1981), Wakai et al. (1999), Peterson and Rollins (1996), McVay et al. (1998), and Comodromos and Pitolakis (2005).

Most of the above-mentioned methods disregard the effect of cracking on the response of reinforced concrete piles. In many cases, where the response of a pile group under lateral loading is significant to the design process and high precision is required, a full-scale test may contribute to the elimination of practically all the uncertainties arising from these topics. More specifically, a profound back-analysis of a pile test may provide appropriate design values for soil and pile strength and deformation parameters.

### **2.4.3 AN INELASTIC CONSTITUTIVE MODEL FOR CONCRETE**

The behavior of the concrete material under compression loading is complex, due to its non-linearity behavior caused by the micro-cracking (even present without loading); however, what is even more complex is its behavior under compression loading, due to the macro-cracking and the fragility of the components when the aggregates are separated.

Another important characteristic of concrete is its low tensile strength, particularly at low-confining pressures, which results in tensile cracking at a very low stress compared with compressive stresses. The tensile cracking reduces the stiffness of concrete structural components. Therefore, the use of continuum damage mechanics is necessary to accurately model the degradation in the mechanical properties of concrete.

Plasticity theory has also been used for the concrete material, developing some plastification functions, criteria of rupture and plastic flow, suitable for this type of material (Abaqus Theory Manual, 2010).

One of the best constitutive models in recent times to simulate the behavior of the concrete might be the concrete damage plasticity model, the theoretical bases of which were developed by Lubliner, Oliver, Oñate and Oller (1989).

The concrete damaged plasticity model is based on the assumption of scalar (isotropic) damage and is designed for applications in which the concrete is subjected to arbitrary loading conditions, including cyclic loading. The model takes into consideration the degradation of the elastic stiffness induced by plastic straining both in tension and compression (Abaqus Theory Manual, 2010).

The model is defined by a set of curves obtained from uniaxial compression and traction laboratory tests and by the use of damage factors, or even by other considerations (Sümer & Aktaş, 2015).

When concrete is loaded in compression, it initially exhibits elastic response. As the stress is increased, some non-recoverable (inelastic) straining occurs, and the response of the material softens. An ultimate stress is reached, after which the material softens until it can no longer carry any stress. If the load is removed at some point after inelastic straining has occurred, the unloading response is softer than the initial elastic response: this effect is ignored in the model. When a uniaxial specimen is loaded into tension, it responds elastically until, at a stress that is typically 7-10% of the ultimate compressive stress, cracks form so quickly that it is very difficult to observe the actual behavior. The uniaxial response of a specimen is shown in Figure 2.4.

This phenomenon affects the geometrical features of the section and breaks the strains compatibility between the steel and concrete. It is important to clarify that with this constitutive model it is possible to simulate the plastic behavior of the concrete material under static load, and in this research work it is not representing the degradation of stiffness of materials through damage factors, since that only applies when there is cyclic loading.

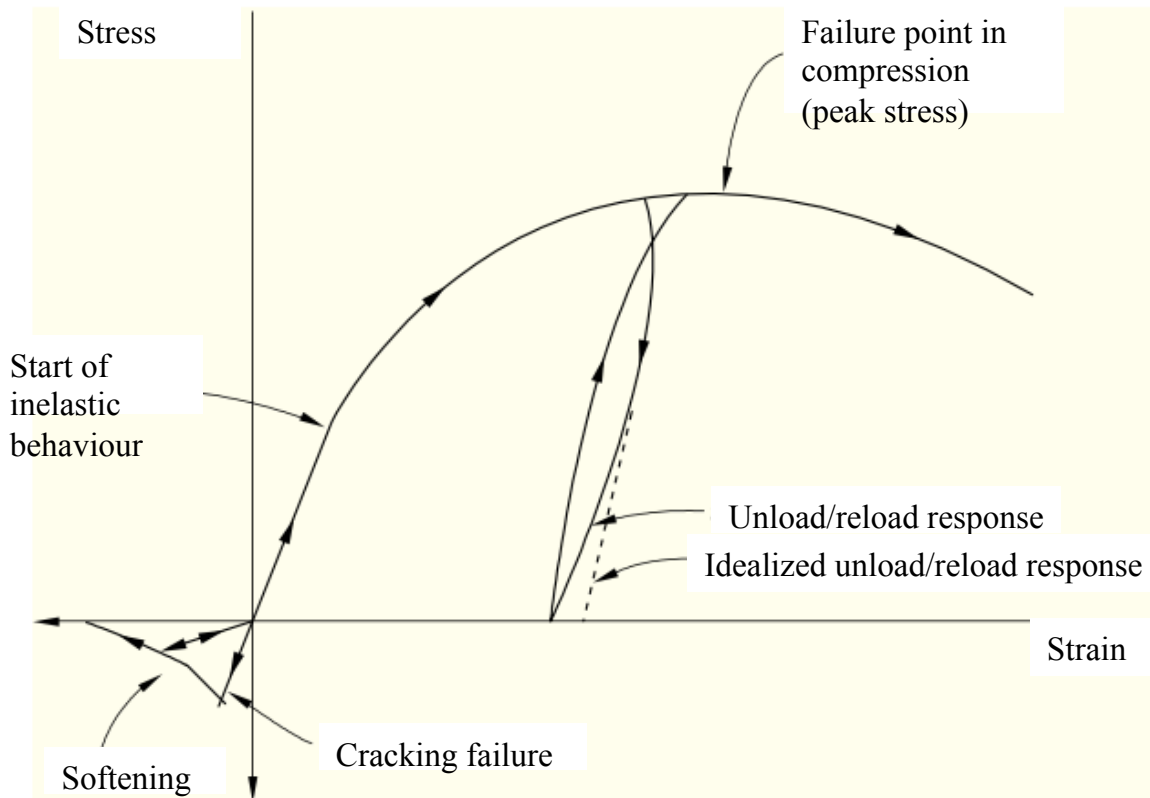


Figure 2.4. Uniaxial behavior of plain concrete. (Abaqus Theory Manual, 2008).

## 2.5 DEFECTIVE PILES

Defects in piles may be introduced during the construction of both driven and cast-in situ-piles. Techniques have been developed for assessing the nature, location and extent of a defect in a pile, including low-strain integrity testing, and high-strain dynamic pile testing (Poulos, 1999). Integrity tests can be carried out on all working piles. Existing integrity test techniques, however, are not able to detect every defect that may exist in a pile, so a risk of missing one or a few defective piles still exists.

Pile defects can affect structural safety; thus, it is necessary to analyze the behavior of pile groups with defects. Some researchers, such as Xu (2000), have paid attention to the problem of interactions among defective piles.

The general behavioral characteristics of a group with piles containing geotechnical defects are similar to those with structural defects. The ability of the group to redistribute loads from defective piles to integral piles results in a less severe reduction in axial stiffness than is the case for a single defective pile. However, the presence of defective piles will

generally lead to the development of lateral deflection and rotation of the group, and induces additional bending moments in the piles.

A defect may have different effects on pile groups in different soil profiles. For a vertically loaded bored pile socketed into rocks, the toe resistance plays an important role if the pile is not very long. If the pile toe is not founded on the design rock level or there is a serious strength reduction in the pile shaft, the effect of this defective pile on pile group behavior will be significant (Kong & Zhang, 2004).

There appear to be no well-established procedures for assessing the likely effect of the defects on pile performance, other than by a load test. In many cases in the past, it has been assumed that the defective pile will not carry any load and an additional pile or piles have been installed within the group to compensate for the defective pile. Such a procedure is both costly and time-consuming, and it is therefore of some interest to examine whether such remedial works are indeed justified, or whether the group containing the defective pile (or piles) can still function satisfactorily.

The imperfections were divided into geological and construction types and the sources of these imperfections were summarized in:

- Natural geological sources
- Inadequate ground investigation
- Construction problems

One or more piles of a group may have very different behavior as a consequence of an individual problem or a combination thereof. If this anomalous pile behavior is very different from the other piles, it is called a defective pile. This fact leads to an unexpected pile group performance in terms of settlement and/or bearing capacity. “Lack of time” is probably the greatest problem of foundation designers in dealing with pile groups containing a defective pile. Foundation problems are always unexpected, although some of them could be predicted with a better geotechnical approach.

A pile with lesser length is a common situation with many kinds of piles (driven piles, flight auger piles, bored piles, and others). The main reasons for this could be:

- The presence of a high resistant layer
- Presence of bounders
- Sloping bedding planes
- Inexperience during the pile installation process

The second source of defective piles, i.e., a lower stiffness, can be the consequence of:

- Inadequate construction control
- Pile material property, especially in cast-in-place concrete piles; shaft and/or base resistance being reduced due to the construction operations.

Figure 2.5 shows some actual cases under different situations of damaged concrete piles.



Figure 2.5. Some actual examples of damaged piles. (Freitas Neto, 2013).

### 2.5.1 NUMERICAL ANALYSIS OF DEFECTIVE PILES

It is a not uncommon experience to encounter defects in various types of piles. The usual types of defects in concrete piles are necking, honey-combing and the presence of a soft base. There is a need to understand the behavior of defective piles so as to design effective remedial measures for the foundation systems.

For single piles, the presence of defects leads to a reduction in pile head stiffness, and the possibility of reduced load capacity. If failure of the pile occurs because of a structural defect, there is a sudden and dramatic increase in settlement. With geotechnical defects, the apparent loss of load capacity is characterized by a more gradual increase in settlement with



increasing load (Xu, 2000). Figure 2.6 displays the defects on piles.

In an elastic analysis, the key parameters of a sound pile are assumed to be: pile Young’s modulus  $E_p$ , soil Young’s modulus  $E_s$ , base Young’s modulus  $E_b$ , diameter  $\phi_p$ , cross sectional area  $A_p$  and length  $L_p$  of the pile.

For convenience in the numerical analysis, the pile defects are represented by simple idealization. Necking is idealized via reduction in the value of the local diameter of a pile. The parameters of necking are the diameter  $\phi_d$ , length  $L_d$ , area  $A_d$ , and depth  $z_d$  of the necked zone.

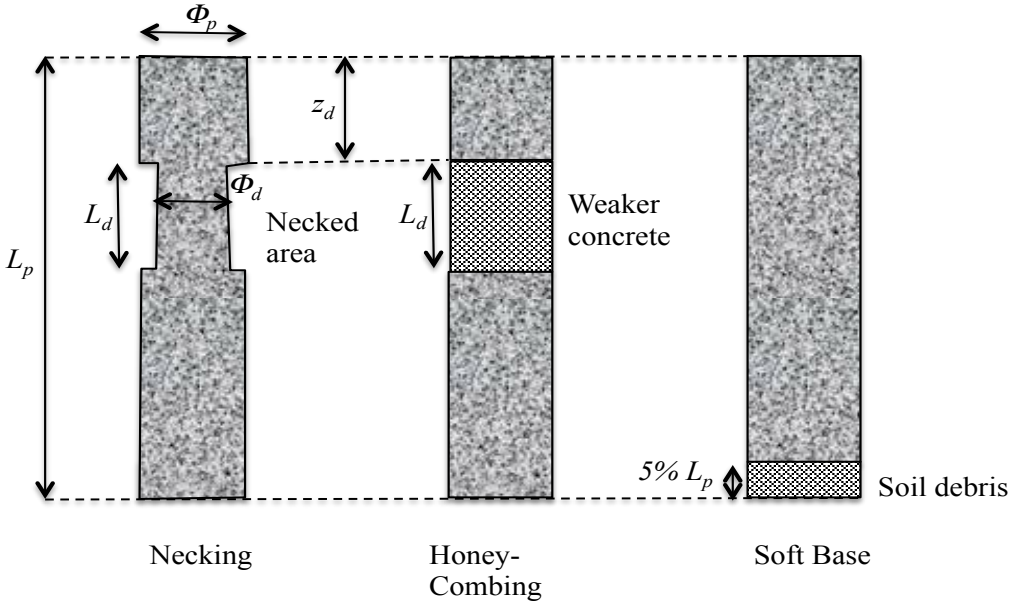


Figure 2.6. Basic types of defective piles for numerical analysis. (Xu, 2000).

Honey-combing is idealized via reduction in the value of the Young’s modulus pile over the defective zone  $E_{pd}$ , length  $L_d$  and depth  $z_d$ .

Soft base is idealized via reduced Young’s modulus at the pile base  $E_{bd}$ , with 5% of the pile length at pile tip being assumed to be softened.

With regard to Brazil, several numerical works have studied this subject by incorporating a damaged region into the piles in a particular way, as in the case of Cordeiro (2007). This research work involved analyzing different piled raft systems composed of three, four and six concrete piles that were subjected to vertical loading. Some of the concrete piles

were defective in that their elasticity modulus was reduced between 30% and 80%, and their length also, but by less than 10 m, both features compared to those assigned to the intact piles.

Another numerical work that also analyzes defective piles was carried out by Freitas Neto (2013). In this research work, some defective piled raft systems with one, three and four piles were subjected to vertical loading; a damaged region was specially built and placed in only one pile of each of those structures, with geometrical and elastic properties less than those assigned to the intact pile region.

In fact, it should be emphasized that the present research is based on the aforementioned research work done by Freitas Neto, 2013.

## 2.6 INTERNATIONAL AND NATIONAL STUDIES ON PILED RAFTS UNDER LATERAL LOADING DURING THE LAST 15 YEARS

During the literature review, national and international theses and studies dealing with piled rafts under lateral loading were searched for. A summary of these works conducted over the past 15 years is shown below in Table 2.1

Table 2.1. Works on piled raft systems under lateral loading (last 15 years).

AUTHOR	TOPIC	TYPE OF WORK	REMARKS
Zhang (2000)	Finite layer method for analysis of piled draft foundations	Analysis of the behavior of piles, rafts and piled draft foundations, subjected to lateral and vertical loads as well as moments	Calculation method with little discussion on the geotechnical area
Xu (2000)	General analysis of pile foundations and application to defective piles	3-D elastic numerical analysis for multiple pile groups, under axial and lateral loading, and moment and torsional forces as well.	Calculation method using a FORTRAN computer program called GEPAN; little discussion on the geotechnical area
Lima (2001)	Evaluation of design methodologies for horizontally loaded piles embedded on collapsible porous clay	Experimental analysis for evaluation of horizontal load vs. deflection behavior	Broms' and Sousa & Coutinho methods were used to get horizontal load vs. deflection curves
Mokwa & Duncan (2001)	Experimental evaluation of lateral-load resistance of pile caps	Thirty-one tests were conducted to evaluate the lateral-load resistance of pile caps	Response comparison between pile groups with caps fully embedded and with soil removed around the caps

Gonçalves et al. (2001)	Horizontal load tests on auger piles in collapsible soil of Londrina	Horizontal tests were performed in natural and pre-wetted conditions. Study of the influence of soil collapsibility in the reduction of pile bearing capacity.	Load test produced curves of horizontal coefficient subgrade reaction vs. horizontal displacement. Flexural rigidity with concrete cracking was taken into account.
Miranda Jr. (2006)	Horizontally loaded piles in collapsible soils of the interior of the state of São Paulo, under natural humidity, improved and pre-flooded soil conditions	Horizontal tests were performed in natural, improved and pre-wetted conditions. Study of the influence of the reaction modulus $n_h$ .	Values obtained for reaction modulus as from horizontal load vs. displacement experimental curves for different types of piles.
Zammataro (2007)	Behavior of isolated bored piles and continuous flight auger, under horizontal forces.	Static horizontal loading tests in a stratified clay	Values obtained for reaction modulus for a chosen interval from curves horizontal load vs. displacement curves.
Russo & Viggiani (2008)	Piles under horizontal load: an overview	Behavior of piles under lateral loading, by full-scale and centrifuge tests	Simple procedure to evaluate the maximum bending moment in the pile shaft is presented and assessed.
Abagnara (2009)	Modeling and analysis of piles under horizontal loads	Numerical analysis of behavior of pile groups under vertical and horizontal loading	Soil is treated as elastic continuous, using non-linear analysis. Computer program NAPHOL
Comodromos et al. (2009)	Effect of cracking on the response of piles tested under horizontal loading	Experimental full-scale pile load test.	3-D non-linear analysis that accounts for cracking is presented. Numerical simulation was performed using the finite difference code FLAC 3D 2005.
Basu et al. (2009)	A continuum-based model for analysis of laterally loaded piles in layered soils	Analysis to calculate the response of laterally loaded piles in multilayered elastic media. Differential equations for the pile deflections in different soil layers are obtained using the principle of minimum potential energy.	The method produces results with accuracy comparable with that of a three-dimensional finite element analysis but requires much less computation time.
Chandrasekaran et al. (2010)	Group interaction effects on laterally loaded piles in clay	Tests were carried out on model pile groups embedded in soft clay.	Effect of pile spacing, number of piles, embedment length, and configuration on pile group interaction were investigated
Ribeiro (2010)	Numerical behavior of deep foundations subjected to lateral loading	Loading capacity used in electrical energy transmission towers and poles with horizontal loading	3D numerical simulations, using Abaqus software
Almeida et al.	Horizontal bearing	Horizontal loading tests are	Two prediction methods were

(2011)	capacity of piles in a lateritic soil	compared with methods which predict the horizontal bearing capacity of piles using in situ measurements of soil behavior.	evaluated using $p$ - $y$ curves computed from DMT results.
Kim et al. (2011)	Wedge failure analysis of soil resistance on laterally loaded piles in clay	Study of pile-soil systems subjected to lateral loads in clay soil was conducted by using experimental tests and a lateral load-transfer approach.	Wedge failure model developed by considering 3-D combination forces and a new hyperbolic $p$ - $y$ criterion.
Nath et al. (2011)	Study of lateral resistance of pile cap using finite element analysis	Parametric study of pile-soil-cap interaction under lateral loads is performed on a single pile and different pile groups.	Analytical study of pile cap resistance under lateral load using finite element analysis.
Papadopoulou & Comodromos (2012)	Response evaluation of horizontally loaded pile groups in clayey soils	Behavior of laterally loaded pile groups with a rigid head was analyzed, and the response of a pile group to that of a single pile was correlated	Numerical modeling with FLAC 3D 3.10
Kassouf (2012)	Analysis of static load test in the open caisson, subjected to horizontal stress in unsaturated diabasic soil of Campinas.	Horizontal tests were performed in natural, improved and pre-wetted conditions. Study of the influence of the reaction modulus $n_h$ .	The analyses were based on the experimental load vs displacements results, measured to the caisson head and the caisson shaft in depth.
Gomes (2013)	Static lateral loading tests on continuous flight auger bored piles and metallic driven steel piles in cohesionless soil	Bored piles and metallic H-section were tested at the same site, which consisted of compacted superficial fill of pure sand with different relative densities.	Horizontal coefficient of sub-grade reaction was determined from the results of the loading tests and compared with values determined by SPT tests.
González (2014)	Numerical study of pile behavior under lateral loading	Study of soil-structure interaction of a deep single pile using constitutive models for soil and pile	Numerical method using (FEM) Abaqus software, considering concrete damage plasticity model for the pile concrete.
Abreu (2014)	Experimental evaluation of the behavior of laterally loaded pile groups embedded in tropical collapsible soil in Brasilia D.F.	Experimental and numerical analysis on pile groups under lateral loading	The equivalent pile method was used to represent the pile group obtaining load vs. deflection through the commercial software LPILE Plus 5.0.
Bergan et al. (2015)	Numerical experiments on the response to lateral loading in piles in improved ground	A ground improvement technique dealing with cemented-soil is presented, studying numerically the behavior of piles subjected to lateral forces.	Correlation between numerical model and loading tests. Abaqus software (FEM) was used.
Christan &	Study of soil-pile	Study of a vertical reinforced	Comparison of the values

Kuster (2015)	interaction under horizontal loading	concrete pile, subjected to horizontal load and moment, partially buried in a cohesive soil.	obtained by SAP2000 software and the classical differential equation method for maximum horizontal displacements and bending moments
Miranda, M. (2016)	Analysis of the behavior of the small diameter bored pile subjected to horizontal loading in unsaturated soil	Evaluation of the behavior a small diameter pile subjected to horizontal static load test. Two full-scale tests were carried out under natural and flooded soil conditions.	Horizontal coefficient of sub-grade reaction was determined from the results of the loading tests and compared with values determined by Plaxis 3D software. Some p-y numerical curves were obtained as from the measured displacement along the pile through an inclinometer.

According to what was reviewed and is shown in the table above, it is possible to say that a few research works addressed the topic of foundation groups subjected to lateral loading by studying the soil-structure interaction based on a full-scale test load. Only in some of them were experimental measurements carried out, followed by numerical simulations of those experimental works. This is very important because the experimental works allow comparing and calibrating with the numerical analysis.

On the other hand in this list of works shown above, there is a shortage of information from studies on the behavior of piles or group piles including defective piles. In fact, those types of studies were only numerically considered not experimentally performed.

There are several studies that carried out numerical simulations using different commercial software packages; some of them even developed their own programming codes to simulate the corresponding geotechnical problem, but none of them proposes a general methodology to follow that addresses the numerical simulation. This point is very important to highlight, because there are a lot of papers and theses based on carrying out several numerical simulations that mention the software used and show and discuss the final results, but very often no explanation is given about the methodology applied to find the successful numerical model developed.

In general terms, no information regarding geotechnical and structural issues were found, such as the engagement of each material (soil, concrete and steel) when subjected to lateral loading and their overall interaction, and the importance of the presence of a defective pile(s) in the groups. There is not only a lack of information about the overall behavior of

piled raft groups, but also about the individual behavior of the raft, the tips and the shaft of each pile.

Finally, very little information was found concerning parametric studies of hypothetical situations that could arise in the engineering foundations of piled raft systems, such as behavioral differences between the intact and defective foundation systems.

### *Technical knowledge of the problem*

The analysis of deep foundations under lateral loading is a rather complex three-dimensional problem, even more so than under axially loading, because the properties of the materials that compose the foundation system, such as the soil, concrete and steel, have different behavior under bending or flexion.

In general the analysis of piles subjected to horizontal loading is approached in two ways, the first is the analysis of the bearing capacity of the soil-pile system, and the second is the horizontal bending of the pile. With regard to use in practice, laterally loaded piles may be termed active or passive. An active pile has loading applied principally at its top in supporting a superstructure, whereas a passive pile has loading applied principally along its length due to earth pressure.

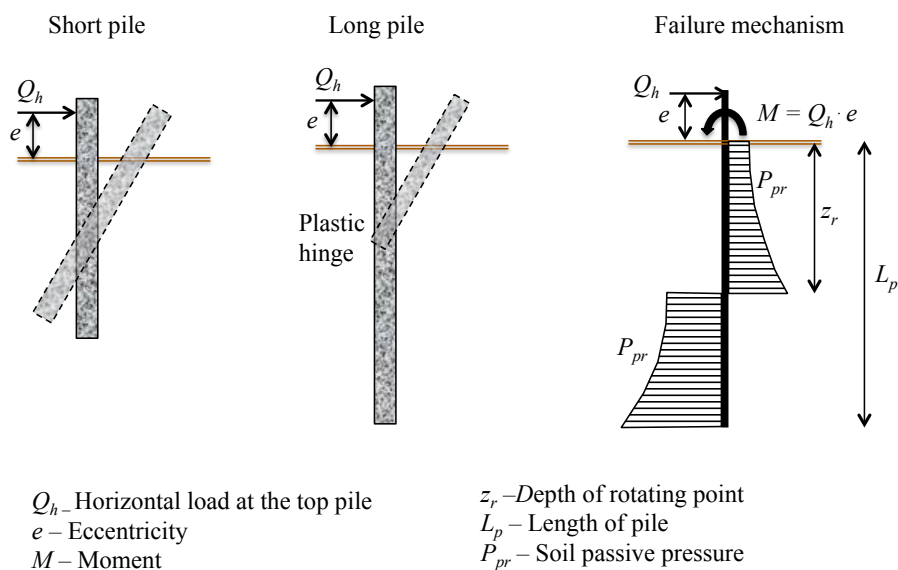


Figure 2.7. Pile under lateral loading.

Solving for the response of a deep foundation under lateral loading is one type of soil-structure interaction problem, since it involves the interaction forces between the soil surrounding the pile and the shaft and tip of the pile. Besides that, the soil reaction at any point along the shaft of the pile is a function of the deflection at that point (causing a horizontal displacement in the soil), which in turn is dependent on the soil resistance itself.

According to Qin (2010), the behavior of the phenomenon depends directly on the length of the pile. Short piles (or rigid piles) are those in which the lateral capacity is wholly dependent on the soil resistance, while long piles (or flexible piles) are those whose lateral capacity is primarily dependent on the yield moment of the pile itself. See Figure 2.7.

### *Theoretical and practical analysis of the problem*

As regards the works to obtain the geotechnical parameters, lateral pile analyses require use of subgrade reaction modulus  $K$  or lateral elasticity soil modulus  $E_s$ . The soil parameters may be determined from the laboratory triaxial test on undisturbed samples. However, laboratory triaxial test parameters are not very reliable for driven piles and bored piles (drilled shafts) since the soil in the vicinity of the pile undergoes extensive remolding, a change in water content, and usually an increase in density (or particle packing). Since the changes are highly indeterminate there is no way to duplicate them in any current laboratory test with any confidence. Thus, if laboratory tests are used, they are on the original in situ undisturbed samples, with experience used to extrapolate these data to obtain the design parameters. For these reasons the SPT (standard penetration test) is widely used.

On the other hand, with regard to the calculation works, several classical methods are used to analyze the lateral capacity of pile foundations in soil as shown in Table 2.2. All of them use the concept of soil reaction modulus under lateral loading, and present some limitations, mainly in the fact they admit a linear relationship between the soil reaction and the corresponding displacement.

Table 2.2. Classical methods of analysis

Method	Acting forces and conditions	Modulus of soil reaction $E_s$	Remarks
Matlock & Reese (1961)	Horizontal force $Q_h$ and moment $M_o$ on the end at ground level.	Linear variation with depth: $K = n_h z$  Long pile length $\frac{L}{T} > 4$ $T = \sqrt[5]{\frac{E_p I_p}{n_h}}$	The effects of loading and moment are considered separately and later overlapping  $y = y_p + y_m$
Navdocks (U.S. NAVY) (1962)	Horizontal force $Q_h$ and moment $M_o$ on ground level. Considers three conditions:  1. Pile with free head  2. Pile with fixed head on the ground level  3. Pile with fixed head above the ground level	Linear variation with depth: $K = n_h z$  $T = \sqrt[5]{\frac{E_p I_p}{n_h}}$	Method is valid for sands and clays normally consolidated. Might be applied to overconsolidated clays using a modification of $K$
Broms	Considers piles fixed or free to rotate at the head.  - Lateral deflections of piles at ground level at working loads  - Ultimate lateral resistance of piles under lateral loads	Linear variation with depth: $K = n_h z$  Considers modulus subgrade horizontal reaction  $T = \sqrt[5]{\frac{E_p I_p}{n_h}}$  $R = \sqrt[4]{\frac{E_p I_p}{E_s}}$	Provides solutions for both short rigid and long flexible piles installed in cohesive and cohesionless soils respectively.  Criterion for:  - short rigid pile $\frac{L}{T} \text{ or } \frac{L}{R} \leq 2$  - long flexible pile $\frac{L}{T} \geq 4 \text{ or } \frac{L}{R} \geq 3.5$
Davisson & Robinson (1965)	Pile with free head, partial buried length and a length over ground level. Acting horizontal force $P_h$ , moment $M_o$ and vertical force $P_v$ on the head.	Considers two cases of $E_s$ :  1. No variation with depth: $E_s = \text{constant}$	Studies overconsolidated cohesive soils (case 1) and sands, limes and normally consolidated clays (case 2)  The effects of horizontal and vertical loading and moment are considered separately.



		$R = \sqrt[4]{\frac{E_p I_p}{E_s}}$ <p>2. Linear variation with depth:</p> $E_s = K_h z$ $T = \sqrt[5]{\frac{E_p I_p}{K_h}}$	
Werner (1970)	Acting horizontal force $P_h$ and moment $M_o$ separately on the end at ground level.	<p>Uses 5 different diagrams of <math>E_s</math> varying with depth <math>z</math>, so that they include within its boundaries, practical values of <math>E_s</math>.</p> <p>Defines a unique modulus of soil reaction varying with depth:</p> $\beta = \sqrt[4]{\frac{4E_p I_p}{K_L}}$ <p><math>K_L</math> at <math>z=L</math> (tip pile)</p> <p>varying between linear and constant with <math>z</math>.</p>	<p>Considers four cases for the tip of the pile:</p> <ol style="list-style-type: none"> <li>1. Free. Acting <math>P_h</math> on the top of the pile</li> <li>2. Free. Acting <math>M_o</math> on the top of the pile</li> <li>3. Fixed. Acting <math>P_h</math> on the top of the pile (rock embedment)</li> <li>4. Fixed. Acting <math>M_o</math> on the top of the pile (rock embedment)</li> </ol> <p>Considers a parabolic varying as intermediate between linear and constant with <math>z</math>.</p>
Davisson (1970)	Horizontal force $P_h$ and moment $M_o$ on the end at ground level.	<p>Linear variation with depth or non-linear:</p> <p><math>E_s = \text{constant}</math> (overconsolidated clays)</p> <p><math>E_s = n_h z</math> (sands)</p> <p>Considers an embedding factor</p> $F = \frac{M_o}{P_h T}$	<p>Studies cohesive soils and cohesionless soils.</p> <p>The solutions are dimensionless.</p>

All these methods are widely used to study the problem of a single pile under lateral loading, and they have provided acceptable results in practical engineering. However, they have some theoretical shortcomings since they do not take into account, among other factors,

a layered soil system, load application time, cohesive-frictional soils, and intensity and variation in loading.

Therefore, based on this summary, the most suitable option currently available to study a deep foundation system under horizontal forces is the employment of some of the numerical methods, through the use of software tools installed in powerful computers.

## **2.7 HORIZONTAL BEARING CAPACITY OF PILES IN A LATERITIC SOIL**

In Brazil, pile foundations are generally installed using a mechanical auger and are commonly used in foundations and retaining structures. However, many of these piles were designed for horizontal loading using empirical models that do not adequately consider the resistance properties and compressibility of the residual soils in the region. These residual soils are often lateritic and can be collapsible. The use of inadequate equations has led to over-dimensioned projects and thus excessive building costs and the unnecessary use of natural resources (Almeida et al., 2011).

Laterite is a soil and rock type rich in iron and aluminum, and is commonly considered to have formed in hot and wet tropical areas. Nearly all laterites are of rusty-red coloration, because of high iron oxide content. They develop by intensive and long-lasting weathering of the underlying similar rock. Tropical weathering (laterization) is a long chemical process which produces a wide variety of thickness, chemical compositions and mineralogical formations in lateritic soils. The largest area of laterites is located between the tropics of Cancer and Capricorn.

According to the Committee on Tropical Soils of ISSMFE (1982), tropical soils are those that present peculiarities as a result of originating in regions where hot and humid weather conditions are predominant. In Brazil, according to Guimarães (2002), tropical soils are divided into two large groups: lateritic soils and saprolite soils.

The experimental works of this thesis were developed in Campinas, SP. This region is constituted by lateritic soils, which are difficult to be saturated; thus, they have some particular features such as high porosity and suction, as well as a certain rigidity in their

natural conditions, but when they are wet the collapsibility phenomenon may occur. The collapse consists of immediate excessive settlement under external loading, due basically to the sudden decrease of suction values. Figure 2.8 shows a typical geotechnical profile of Brazil.

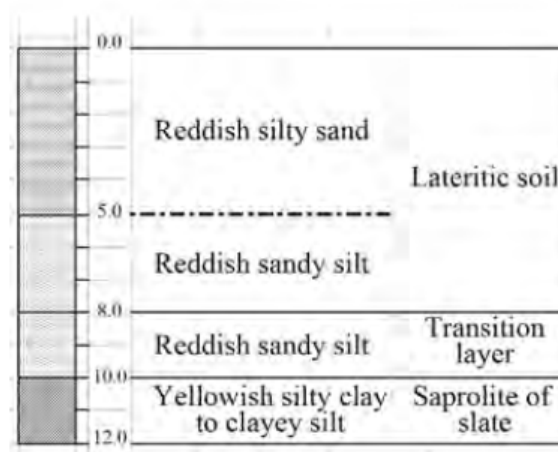


Figure 2.8. Simplified geotechnical profile (Cunha, 2011).

The lateritic soil contributes to deteriorating the bearing capacity of the piles embedded in this type of soil. Studies indicate that lateralization of clays, very common in tropical soils, is responsible for over-dimensioned foundation projects through the use of classical theory in the literature.

According to Almeida et al. (2011), the lateritic clays could have higher rigidity properties than other non-lateritic ones, even though they have similar resistance values to the standard SPT sampler. Thus, the results from classical prediction methods for bearing capacity of foundations in this type of clay prove to be conservative when compared with the actual results.

In general, for the calculations of bearing capacity in foundations, the phenomenon of collapsibility is usually not taken into account; consequently, they can behave satisfactorily for some time, but they may abruptly suffer additional stresses due to the sudden appearance of a water source that increases soil moisture, such as sewage, rainwater infiltration, or a rise in the water table, etc.

Classical methods for predicting the bearing capacity of foundations with collapsibility are not the most suitable, since they do not consider the reduction in the bearing capacity of the foundations when the natural ground experiences wet changes causing the collapse.

The “Associação Brasileira de Normas Técnicas” NBR 6122 (2010) prescribes that, in the case of foundations resting on porous and unsaturated soils, porosity and soil collapsibility should be analyzed under inundated conditions, as those features indicate the presence of collapsible soils; therefore, shallow foundations should be avoided in such soils.

Foundation structures built in this type of soil may undergo a large-scale collapse, which can occur at any stage of their work life, because they were built beyond the admissible foundation settlements; it's also possible that this could cause some damage to neighboring buildings.

Relating to the lateral loading on piles embedded in lateritic soil, several studies have shown that the soil depth influenced by the phenomenon is between 3 to 5 times the diameter of the pile, which means the lateral loading happens at a shallow depth; however, the greatest wet changes also occur around this depth (especially by inundated conditions). As a result, foundation projects must take great care with this type of loading on foundation structures embedded in this type of soil.

## **3 NUMERICAL ANALYSIS OF PILES**

### **3.1 CONSTITUTIVE METHODS FOR SOILS**

Soil is a complicated material that behaves non-linearly and often shows anisotropic and time dependent behavior when subjected to stresses. Generally, soil behaves differently in primary loading, unloading and reloading. It exhibits non-linear behavior well below failure condition with stress dependent stiffness. Soil undergoes plastic deformation and is inconsistent in dilatancy. Soil also experiences small strain stiffness at very low strains and upon stress reversal. This general behavior may not have been accounted for in the simple elastic-perfectly plastic Mohr-Coulomb model, although the model does offer advantages which makes it a favorable option as a soil model.

Brinkgreve (2005) discussed in more detail the five basic aspects of soil behavior. Briefly, the first aspect concerns the influence of water on soil behavior as a result of effective stresses and pore pressures. The second aspect covers the factors which influence soil stiffness, such as the stress level, stress path (loading and unloading), strain level, soil density, soil permeability, consolidation ratio and the directional-dependent stiffness (stiffness anisotropy) of the soil. The third aspect centers on the irreversible deformation as a result of loading. The fourth aspect is related to soil strength that is usually expressed in terms of shear strength. Since soil is a frictional material, the shear strength depends on the confining effective stress level. And finally the fifth aspect relates to the time dependency of soil behavior. Soil stiffness and strength are influenced by time. Even when loading conditions remain unchanged, time can play an important role in the mechanical behavior of soil. Other aspects of soil behavior that should be considered include factors such as compaction, dilatancy and memory of pre-consolidation stress.

In addition to soil behavior, its failure in a three-dimensional state of stress is extremely complicated. Numerous criteria have been devised to explain the condition for failure of a material under such a loading state. Among these three-, four-, and five-parameter models, the Mohr-Coulomb model is a two-parameter model with criterion of shear failure and can also be a three-parameter model with criterion of shear failure with a small tension cut-off (Ti et al., 2009).

There are a large number of models that have been recommended in recent years to represent the stress-strain and failure behavior of soils. All these models have advantages and limitations, which largely depend on their application. Alternatively, (Ti et al., 2009) provided three basic criteria for model evaluation. The first criterion is theoretical evaluation of the models with respect to the basic principles of continuum mechanics to ascertain their consistency with the theoretical requirements of continuity, stability and uniqueness.

The second criterion is the experimental evaluation of the models with respect to their suitability to fit experimental data from a variety of available tests and the ease of the determination of the material parameters from standard test data.

The final criterion is numerical and computational evaluation of the models with respect to the ease with which they can be implemented in computer calculations.

In general, the criterion for soil model evaluation should always be a balance between the requirements from the continuum mechanics aspect, the requirements of realistic representation of soil behavior from the laboratory testing aspect (also the convenience of parameters derivation), and the simplicity in computational application.

A few basic and practical soil constitutive models such as Hooke's law, Mohr-Coulomb, Drucker-Prager, Duncan-Chang or Hyperbolic (model), (Modified) Cam Clay, Plaxis Soft Soil (Creep) and Plaxis Hardening Soil Model were discussed and summarized by Brinkgreve (2005) according to the model's advantages and limitation. Application of each model was stated briefly in addition to selection of soil parameters from correlation and laboratory testing for application in finite element models. In this research work only the Hooke and Mohr-Coulomb models are described, due to the fact they were used in all numerical modeling analyses.

## **3.2 ELASTICITY**

The theory of elasticity is used to calculate the elastic strains that occur prior to yielding in an elasto-plastic material. The generalized Hooke's law will be applied to the uniaxial stress condition (one-dimensional), the plane strain condition (two-dimensional), and the plane stress condition (also two-dimensional). Hooke's law is not appropriate for soils

because soils are neither linear elastic nor isotropic. Nevertheless, sometimes we idealize soils as being linear elastic and isotropic materials—only then can we use Hooke’s law to estimate the elastic strains associated with applied stresses within a soil mass.

The simplest form of linear elasticity is the isotropic case. Being isotropic means that the elastic modulus, such as  $E$  and  $\nu$ , are orientation independent. This means, for example, that  $E_{11}$ ,  $E_{22}$ , and  $E_{33}$  are identical and they are all equal to  $E$  (Young’s modulus). The stress–strain relationship of the linear elastic isotropic case is given by equation (3.1), known as the generalized Hooke’s law. The elastic properties are defined completely by Young’s modulus,  $E$ , and Poisson’s ratio  $\nu$ . Recall that Hooke’s law for the one-dimensional (uniaxial) stress condition is:

$$\sigma = E \cdot \varepsilon \tag{3.1}$$

The equation (3.1) has the same general form as:

$$\begin{Bmatrix} \varepsilon_{11} \\ \varepsilon_{22} \\ \varepsilon_{33} \\ \varepsilon_{12} \\ \varepsilon_{13} \\ \varepsilon_{23} \end{Bmatrix} = \begin{bmatrix} 1/E & -\nu/E & -\nu/E & 0 & 0 & 0 \\ -\nu/E & 1/E & -\nu/E & 0 & 0 & 0 \\ -\nu/E & -\nu/E & 1/E & 0 & 0 & 0 \\ 0 & 0 & 0 & 1/(2 \cdot G) & 0 & 0 \\ 0 & 0 & 0 & 0 & 1/(2 \cdot G) & 0 \\ 0 & 0 & 0 & 0 & 0 & 1/(2 \cdot G) \end{bmatrix} \begin{Bmatrix} \sigma_{11} \\ \sigma_{22} \\ \sigma_{33} \\ \tau_{12} \\ \tau_{13} \\ \tau_{23} \end{Bmatrix} \tag{3.2}$$

Where  $G$  is the shear modulus, and can be expressed in terms of  $E$  and  $\nu$  as

$$G = \frac{E}{2 \cdot (1 + \nu)} \tag{3.3}$$

**3.2.1 PLANE STRAIN CONDITION**

The plane strain assumption is frequently used in geotechnical analysis of soil structures that are very long in one dimension while having a uniform cross section with finite dimensions. Figure 3.1 illustrates a soil embankment that is long in the  $z$ -direction while having a uniform cross section with finite dimensions in the  $x$ - $y$  plane. In this case we can

assume a plane strain condition in which the strains along the z-axis are assumed to be null (i.e.  $\epsilon_{33} = \epsilon_{13} = \epsilon_{23} = 0$ ). The seemingly three-dimensional embankment problem reduces to a two-dimensional plane problem in which the cross of the embankment, in the x-y plane, is assumed to represent the entire embankment. Substituting  $\epsilon_{33} = \epsilon_{13} = \epsilon_{23} = 0$  into equation (3.2) we get:

$$\begin{Bmatrix} \epsilon_{11} \\ \epsilon_{22} \\ \epsilon_{12} \end{Bmatrix} = \frac{1+\nu}{E} \begin{bmatrix} 1-\nu & \nu & 0 \\ \nu & 1-\nu & 0 \\ 0 & 0 & 1 \end{bmatrix} \begin{Bmatrix} \sigma_{11} \\ \sigma_{22} \\ \tau_{12} \end{Bmatrix} \quad (3.4)$$

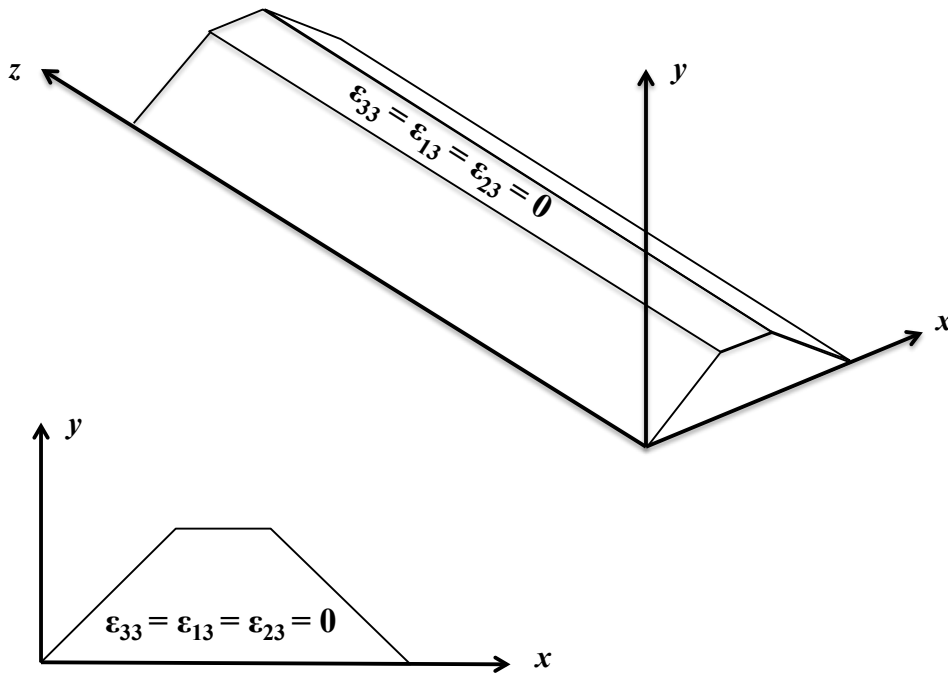


Figure 3.1. Plane strain condition. (Helawany, 2007)

### 3.2.2 PLANE STRESS CONDITION

In the plane stress condition the stresses in the z-direction are assumed negligible (i.e.  $\sigma_{33} = \tau_{13} = \tau_{23} = 0$ ); see Figure 3.2. Substituting these stresses into equation (3.2) we have:

$$\begin{Bmatrix} \sigma_{11} \\ \sigma_{22} \\ \tau_{12} \end{Bmatrix} = \frac{E}{1-\nu^2} \begin{bmatrix} 1 & \nu & 0 \\ \nu & 1 & 0 \\ 0 & 0 & 1-\nu \end{bmatrix} \begin{Bmatrix} \epsilon_{11} \\ \epsilon_{22} \\ \epsilon_{12} \end{Bmatrix} \quad (3.5)$$



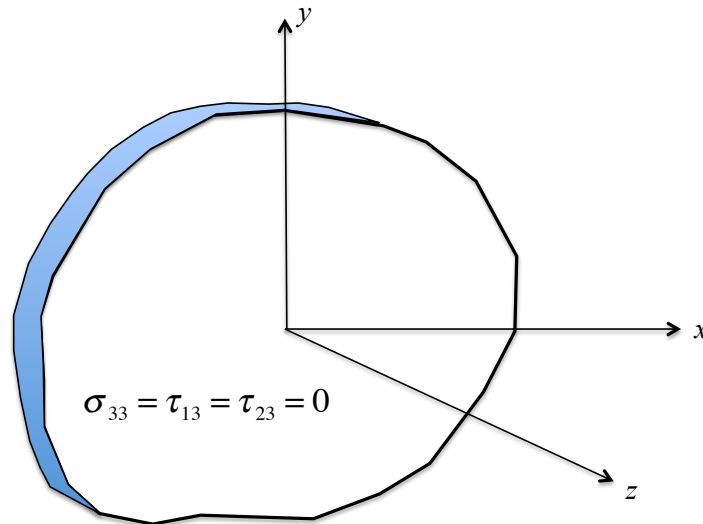


Figure 3.2. Plane stress condition. (Helwany, 2007)

### 3.3 PLASTICITY

When an elastic material is subjected to load, it sustains elastic strains. Elastic strains are reversible in the sense that the elastic material will spring back to its undeformed condition if the load is removed. On the other hand, if a plastic material is subjected to a load, it sustains elastic and plastic strains. If the load is removed, the material will sustain permanent plastic (irreversible) strains, whereas the elastic strains are recovered. Hooke's law, which is based on elasticity theory, is sufficient (in most cases) to estimate the elastic strains. To estimate the plastic strains, one needs to use plasticity theory (Helwany, 2007).

Plasticity theory was originally developed to predict the behavior of metals subjected to loads exceeding their elastic limits. Similar models were developed later to calculate the irreversible strains in concrete, soils, and polymers. Three plasticity models are presented for soils that are frequently used in geotechnical engineering applications. It is customary in plasticity theory to decompose strains into elastic and plastic parts. A plasticity model includes three basic rules:

- A yield criterion that predicts whether the material should respond elastically or plastically due to a loading increment.
- A strain hardening rule that controls the shape of the stress–strain response during plastic straining.

- A plastic flow rule that determines the direction of the plastic strain increment caused by a stress increment.

### 3.3.1 MOHR-COULOMB MODEL

The Mohr-Coulomb model as shown in Figure 3.3 is an elastic-perfectly plastic model often used to model soil behavior in general and serves as a first-order model. In general stress state, the model of stress-strain behaves linearly in the elastic range, with two defining parameters from Hooke's law as Young's modulus  $E$  and Poisson's ratio  $\nu$ . There are two parameters that define the failure criterion as the friction angle  $\phi$  and cohesion  $c$ , and also a parameter to describe the flow rule as dilatancy angle  $\Omega$ , which comes from the use of non-associated flow rule which is used to model a realistic irreversible change in volume due to shearing.

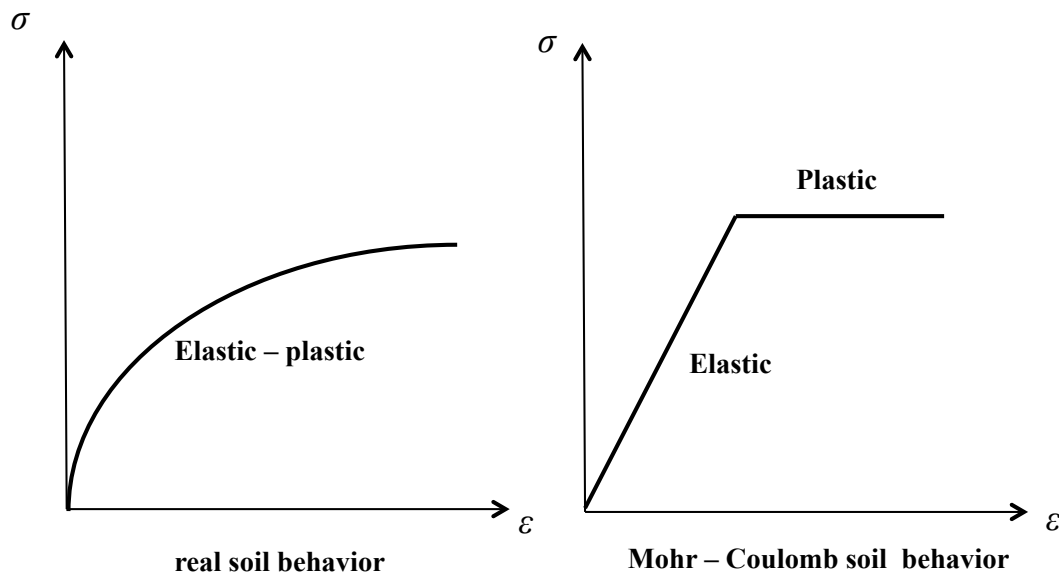


Figure 3.3. Elastic-perfectly plastic assumption of Mohr-Coulomb model. (Helwany, 2007)

In the conventional plastic theory, the flow rule is used as the evolution law for plastic strain rates. If the plastic potential function is the same as the yield function, the flow rule is called the associated flow rule and if it is different, it is called the non-associated flow rule. In soil mechanics, an associated flow rule has been used to model the behavior in the region where negative dilatancy is significant, for example, the Cam clay model for normally consolidated clay. However, non-associated flow rule is frequently used to describe the behavior of sands with both negative and positive dilatancy.

The Mohr-Coulomb model is a simple and applicable three-dimensional stress space model (see Figure 3.4), with only two strength parameters to describe the plastic behavior. Regarding its strength behavior, this model performs better. Researchers have indicated by means of true-triaxial tests that stress combinations causing failure in real soil samples agree quite well with the hexagonal shape of the failure contour (Goldscheider, 1984). This model can be used to analyze the stability of dams, slopes, embankments and shallow foundations.

Although failure behavior is generally well captured in drained conditions, the effective stress path that is followed in undrained materials may deviate significantly from observations. It is preferable to use undrained shear parameters in an undrained analysis, with friction angle set equal to zero. The stiffness (hence also deformation) behavior before reaching the local shear is poorly modeled. For perfect plasticity, the model does not include strain hardening or softening effect of the soil.

The simplification of the Mohr-Coulomb model where the hexagonal shape of the failure cone was replaced by a simple cone was known as the Drucker-Prager model (Obrzud, 2010). Generally, it shares the same advantages and limitations with the Mohr-Coulomb model but the latter model was preferred over this model.

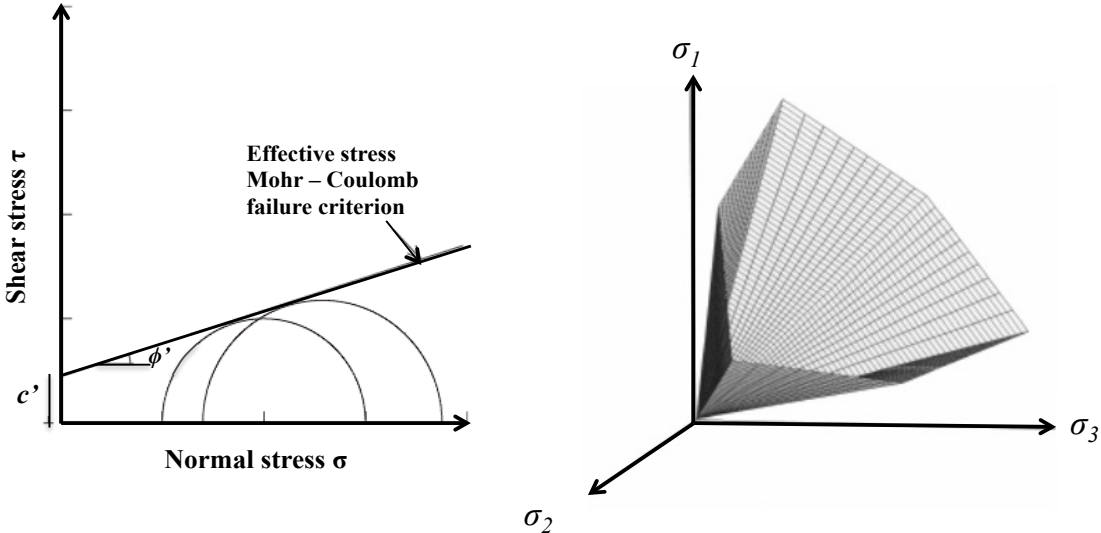


Figure 3.4. (a) The Mohr-Coulomb failure criterion, and (b) yield surface in principal stress space ( $c=0$ ). (Ti et al., 2009)

### 3.3.2 CAM-CLAY MODIFIED MODEL

Long before the maximum stress has been reached, some irreversible straining has occurred as evidenced by the fact that reloading leaves a residual strain. Soil might be referred to as a strain hardening material since the onset of plastic yielding is not synonymous with the maximum stress. A few researchers have investigated the possibility of modeling soil as a strain hardening material, and this has been one of the major thrusts of the soil mechanics group at Cambridge University for the past thirty years (Roscoe, 1970). Roscoe et al (1963a) utilized the strain hardening theory of plasticity to formulate a complete stress-strain model for normally consolidated or lightly over-consolidated clay in a triaxial test known as the Cam-Clay model (Schofield and Wroth, 1968). Burland (1965) suggested a modified version of the Cam-Clay model, which was subsequently extended to a general three-dimensional stress state by Roscoe and Burland (1968).

The Modified Cam-Clay is an elastic-plastic strain hardening model where the non-linear behavior is modeled by means of hardening plasticity. The model is based on Critical State theory and the basic assumption that there is a logarithmic relationship between the mean effective stress,  $p'$  and the void ratio,  $e$ . Virgin compression and recompression lines are linear in the  $e - \ln p'$  space, which is most realistic for near-normally consolidated clays (see Figure 3.5). Only linear elastic behavior is modeled before yielding and may result in unreasonable values of  $\nu$  due to log-linear compression lines.

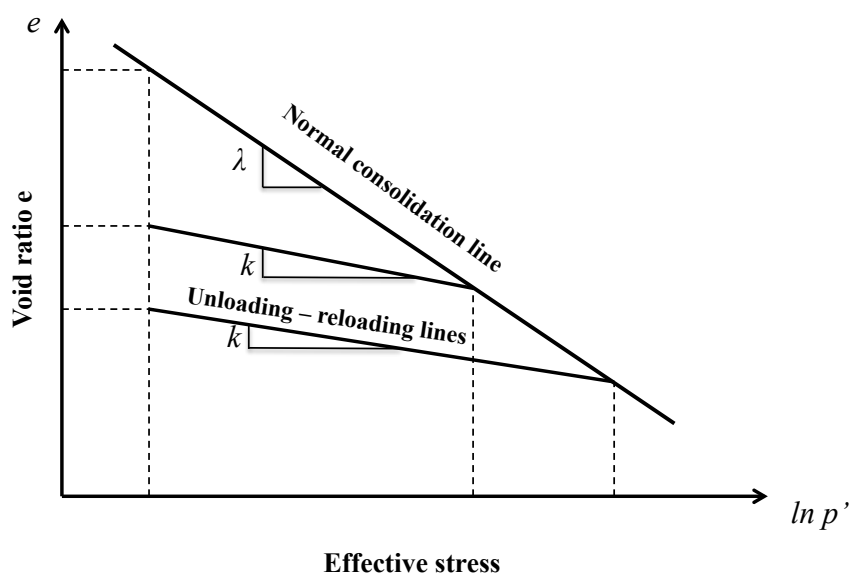


Figure 3.5. Consolidation curve in the void ratio versus mean effective stress (natural logarithm of  $p'$ ) plane. (Helawany, 2007).

This model is more suitable for describing deformation than failure especially for normally consolidated soft soils. The model also performs best in applications involving loading conditions such as an embankment or foundation. It involves several parameters, i.e. the isotropic logarithmic compression index,  $\lambda$ , the swelling index,  $\kappa$ , Poisson's ratio for unloading and reloading,  $\nu_{ur}$ , friction constant,  $M$ , pre-consolidation stress,  $p_c$  and the initial void ratio,  $e_o$ . Shear strength can only be modeled using the effective friction constant. In the case of primary undrained deviatoric loading of soft soils, the model predicts better undrained shear strength compared to the Mohr-Coulomb model.

In addition to achieving better agreement between predicted and observed soil behavior, a large number of modifications have been proposed to the standard Cam-Clay models over the last two decades. Despite some successes in modifying the standard Cam-Clay in the 1980s, Yu (1995, 1998) identified the limitations of this model. The yield surfaces adopted in many critical state models significantly overestimate failure stresses on the 'dry side'. These models assumed an associated flow rule and therefore were unable to predict an important feature of behavior that is commonly observed in undrained tests on loose sand and normally consolidated undisturbed clays, and that is a peak in the deviatoric stress before the critical state is approached. The critical state had been much less successful for modeling granular materials due to its inability to predict observed softening and dilatancy of dense sands and the undrained response of very loose sands. The above limitations were confirmed by Gens and Potts (1987), who also noted that the materials modeled by critical state models appeared to be mostly limited to saturated clays and silts, and the stiff over-consolidated clays did not appear to be generally modeled with critical state formulations.

## **3.4 NUMERICAL MODELING**

### **3.4.1 FINITE ELEMENT METHOD (FEM)**

A complete three-dimensional analysis of a piled raft foundation system can be carried out by finite element analysis (Katzenbach et al., 1998) or by use of commercially available computer programs that have appropriate numerical methods available for piled raft analysis. The components of a structure supported by a piled raft include the superstructure, the raft that is supported by the piles, and the soil mass around the pile shaft and below the pile tip. The interactions between two or more of these elements increase the degree of difficulty in

obtaining a solution. A closed form solution is often difficult to obtain and the designer may have to employ numerical techniques. Some problems still remain, however, in relation to the modeling of the pile-soil interfaces, and whether interface elements should be used. If they are required, then approximations are usually involved in the assignment of joint stiffness properties. Such analyses are therefore more suited to obtaining benchmark solutions against which to compare simpler analysis methods, rather than as routine design tools.

Outstanding features of this powerful method include: the ability to apply any combination of axial, torsion, and lateral loads; the capability of considering the nonlinear behavior of structure and soil; and the potential to model soil-pile-structure interactions. Time-dependent results can be obtained and more intricate conditions such as battered piles, slopes, excavations, tie-backs, and construction sequences can be modeled. The method can be used with a variety of soil stress-strain relationships, and is suitable for analyzing pile group behavior. Performing three-dimensional finite element analyses requires considerable engineering time for generating input and interpreting results. For this reason, the finite element method has predominately been used for research on pile group behavior, but rarely for design.

### **3.4.2 FINITE ELEMENT MODELING FOR LATERALLY LOADED PILES IN CLAY**

There are two general approaches to analyzing laterally loaded piles: simplified methods and continuum-based methods (Ahmadi, and Ahmari, 2009).

Simplified methods principally use the theory of a beam on an elastic foundation. The so-called '*p*-*y* curve method' is one such conventional and semi-empirical method. The assumption of soil non-linear behavior may be an advantage for the *p*-*y* curve method, but the simulation of three-dimensional (3D) pile-soil interaction by a one-dimensional spring element is a disadvantage of this method.

There are two main continuum-based approaches for analyzing laterally loaded piles. The first approach suggests that the soil around the pile be treated as an elastic continuum. These solutions are based on Mindlin's solution for a point load in an elastic half-space using superposition. In this approach the appropriate elastic properties may be obtained by back-

analyzing experimental results, and hence most continuum-based methods need experimental information for calibration of the required parameters. The major deficiency of these elastic solutions is that they assume a constant elastic modulus throughout the model, whereas in practice the soil close to the pile shows a lower stiffness than the soil located further away. This is because the soil close to the pile undergoes higher strains, and so its stiffness decreases.

The second continuum-based approach applies non-linear numerical methods to model the soil–pile interaction. Because of the computational difficulties of 3-D modeling, two-dimensional models have been used in many studies. Some researchers have demonstrated a 3-D finite-element analysis of laterally loaded piles in clay by using standard von Mises constitutive law. Although they showed good trends in the results of numerical analyses, they did not provide sufficient field data for verification purposes. Comparison of soil ultimate pressures predicted from finite-element analyses with experimental observations shows that the finite-element analyses provide a stiffer response of the pile. It is argued that the lack of agreement between the predicted values of soil ultimate pressure and field measurements is probably due to the geotechnical limitations in the total stress approach and the constitutive model used in the finite-element model. It is also argued that the elastic-perfectly plastic von Mises constitutive law cannot capture the stress path correctly.

Brown and Shie (1990) obtained finite-element analysis results that were not in good agreement with the  $p$ – $y$  curve results. Compared with the results obtained from  $p$ – $y$  curves, their finite-element analyses predicted more resistance of the soil near the ground surface. They attributed the discrepancy to the following:

- The shear strength values measured by unconfined and unconsolidated-undrained (UU) triaxial tests provide a simple representation of the shear stress in the soil at failure. The loading path near the ground level resembles a triaxial extension test, and not a compression test.
- The simple von Mises constitutive model probably does not represent the undrained loading in saturated clay in a fundamental way; in reality the mobilized shear strength is influenced by the loading path.

The total stress approach implies that the undrained shear strength  $C_u$  is independent of the stress path taken to induce shear failure. This means that two stress paths, one for the triaxial extension test and the other for the triaxial compression test, will lead to the same shear strength values if the von Mises model is used as the yield criterion. Near the ground surface, the soil experiences a stress path similar to that in the triaxial extension test. In this test the vertical stress is kept constant while the horizontal stress gradually increases. By contrast, in the triaxial compression test, the vertical stress increases while the horizontal stress remains constant. In other words, in the triaxial extension test the confining stress is increased, whereas it is kept constant in the compression test.

Obviously, the difference in soil behavior in these two tests is due to the difference in the direction of application of stresses, which induce different stress paths. The difference in soil behavior arising from applying stresses in different directions and along accordingly different stress paths is attributed to its anisotropy effect. The anisotropy effect means differing soil reactions depending on the direction of application of stresses in this research work. The measured shear strength values do not reflect features such as fissures and cracks.

To compensate for this in over-consolidated clays, Wu et al. (1998) proposed a reduction in the shear strength depending on the soil over-consolidation ratio and testing method.

### **3.4.3 PHYSICS OF LATERALLY LOADED PILE AND SOIL ANISOTROPY EFFECT**

When a pile is loaded laterally, two principal phenomena occur between the pile and the soil: a gap is opened behind the pile, and slip occurs between the pile and the soil in front and to the side. The stress paths for the soil in front of the pile and behind it are different. Similarly, they are different near the surface of the ground and at depth. A soil element behind the pile undergoes a stress path similar to that experienced in a triaxial compression test. For this case, the stress state may be simulated by a triaxial compression test in which the confined stress decreases while the vertical stress is constant, since a small volume of the soil behind the pile experiences lateral stress release, and does not contribute significantly to the equilibrium.



The pile response under lateral load is influenced by the soil at shallow depths in front of the pile. The soil at this location behaves in extension mode, and therefore this extension effect is changing the soil strength. Figure 3.6 shows three different stress paths: (1) for the soil behind the pile, (2) for a triaxial compression test with constant confining pressure, and (3) for the soil in front of the pile.

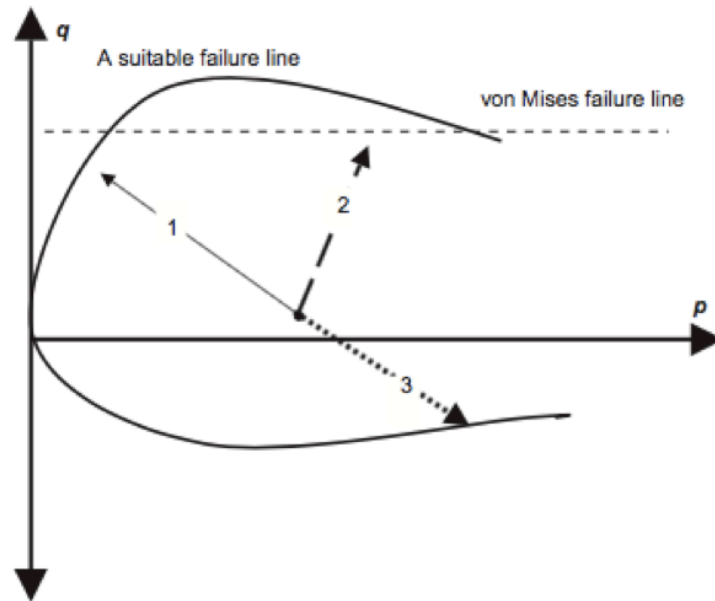


Figure 3.6. Stress path for: (1) a soil element behind the pile; (2) compression triaxial test with constant confined pressure; (3) a soil element in front of the pile. Note that  $p$  and  $q$  represent isotropic and deviatoric stresses respectively (Ahmadi and Ahmari, 2009).

Since the properties of the soil in front of a pile play a much larger role in the lateral behavior of the pile, only the strength anisotropy in this zone should be considered in the finite-element modeling. Path 3 in the same Figure 3.6 schematically shows the stress path in this zone. The corresponding strength value for this stress path is obtained by a back-calculation procedure. In addition to the soil anisotropy effect, the soil structure may be another effective factor in the laterally loaded pile response.

Wu et al. (1998) proposed using reduced shear strength in overconsolidated clays, because the secondary structure (including cracks, fissures, etc.) significantly affects the pile response. For instance, a 30% reduction in shear strength value was proposed for triaxial UU tests in overconsolidated clays. To account for both anisotropy and testing method, a reduction in shear strength of more than 30% may be needed.

## Constitutive model

The analyses performed in this research work are meant to model groups of laterally loaded piles in clay. The finite-element procedure consists of modeling pile, soil domain, and pile–soil interface (see Figure 3.7); each is represented in the model by a different constitutive law. An interface element is introduced to simulate pile–soil interaction.

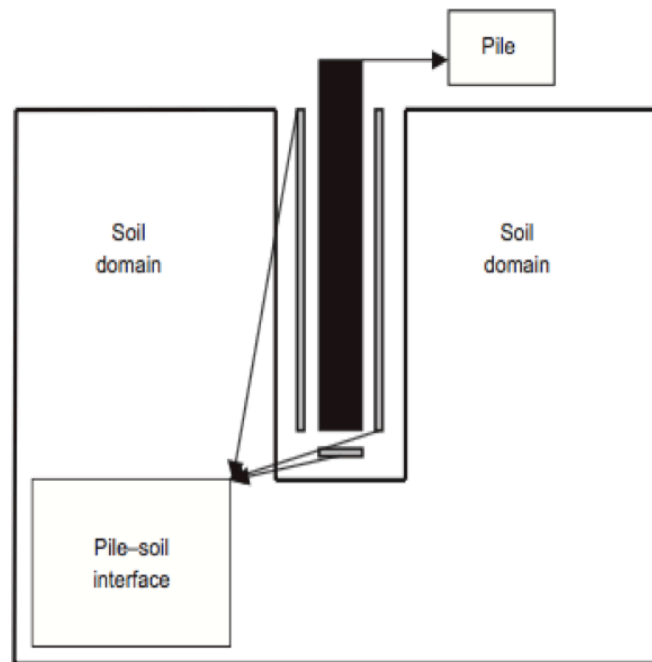


Figure 3.7. Components in the numerical model. (Ahmadi and Ahmari, 2009).

## Soil Domain

The lateral elastic modulus is determined by a trial-and-error procedure with the assumption of soil elastic behavior. The trial analyses are performed until the resulting numerical pile-head load–deflection curve converges with the initial portion of the field-measured curve.

## Pile-soil interaction

Pile–soil contact is modeled for sliding beside and in front of the pile, and gapping behind. Pile–soil contact behavior depends on the drainage conditions. The interface behavior is modeled using the Mohr–Coulomb elastic-plastic model. The input parameters are the

elastic modulus of the soil  $E_s$ , Poisson's ratio, and pile–soil adhesion. Pile–soil adhesion is obtained by the  $\beta$ -method. This method is a well-known in evaluating the axial bearing capacity of pile in clay, and is described by Helwany (2007).

## Pile

The reinforced concrete pile is modeled with steel and concrete materials; for both materials, elastic-plastic behavior is assumed. All parameters required during the numerical performance for both materials can be accurately specified, based on recommended values in various codes. Interaction between these materials is not considered in this paper, since the steel is embedded into the concrete without relative displacements between them.

### **3.4.4 ABAQUS SOFTWARE 14.4**

The numerical analysis of the piled raft system will be carried out using the Finite Element Method (FEM) software package ABAQUS 14.4. This software is being widely used in different branches of engineering. ABAQUS is a suite of powerful engineering simulation programs, based on the finite element method, which can be used for everything from simple linear analysis to more challenging nonlinear simulations. It has an extensive list of material models that can simulate the behavior of most typical engineering materials including metals, rubbers, polymers, composites, reinforced concrete, and geotechnical materials such as rock and soils.

ABAQUS can be used to study more than just structural problems. It can simulate problems in such diverse areas as heat transfer, mass diffusion, thermal management of electronic components, acoustics, soil mechanics, and piezoelectric analysis. (ABAQUS Manual, 2010).

A complete ABAQUS analysis usually consists of three distinct stages:

- Pre-processing
- Simulation
- Post-processing

### Preprocessing (ABAQUS/CAE)

In this stage, we must define the model of the physical problem and create an ABAQUS input file. The model is usually created graphically by using ABAQUS/CAE or another preprocessor, although the ABAQUS input file can also be created directly using a text editor. (ABAQUS Manual, 2014).

### Simulation (ABAQUS/Standard or ABAQUS/Explicit)

The simulation, which normally runs as a background process, is the stage in which ABAQUS/Standard or ABAQUS/Explicit solves the numerical problem defined in the model. Examples of output from stress analysis include displacements and stresses, and are stored in binary files ready for post-processing. Depending on the complexity of the problem being analyzed and the power of the computer being used, it may take anywhere from seconds to days to complete an analysis run (ABAQUS Manual, 2014).

### Post-processing (ABAQUS/CAE)

We can evaluate the results once the simulation has been completed and displacements, stresses or other fundamental variables have been calculated. The evaluation is generally done interactively using the visualization module of ABAQUS/CAE or another postprocessor. The visualization mode, which reads the neutral binary output database file, has a variety of options for displaying the results, including color, contour plots, animations, deformed shape plots, and X-Y plots. (ABAQUS Manual, 2014).

## **3.4.5 NUMERICAL ANALYSIS FROM AN EXAMPLE IN THE LITERATURE**

In order to become familiar with the use of Abaqus software, a real case found in the literature involving a concrete piled raft under vertical loading was chosen for simulating the behavior of deep foundations.

The main objective was to test Abaqus software using some constitutive models, along with other tools such as meshing and integration techniques, types of elements, etc., and

afterwards compare these numerical models with some results obtained by other authors using real loading tests.

The piled raft consisting of 15 piles shown in Figure 3.8 was addressed by Poulos (1997), and the results obtained were compared with those of other authors who used different numerical tools.

The problem consists of a concrete piled raft subjected to vertical loading, with 15 piles of 0.50 m in diameter and 10.0 m in length each; the axial loads are  $P_1 = 1.0$  MN and  $P_2 = 2.0$  MN respectively. Geometrical layout and materials information are displayed in Figure 3.8.

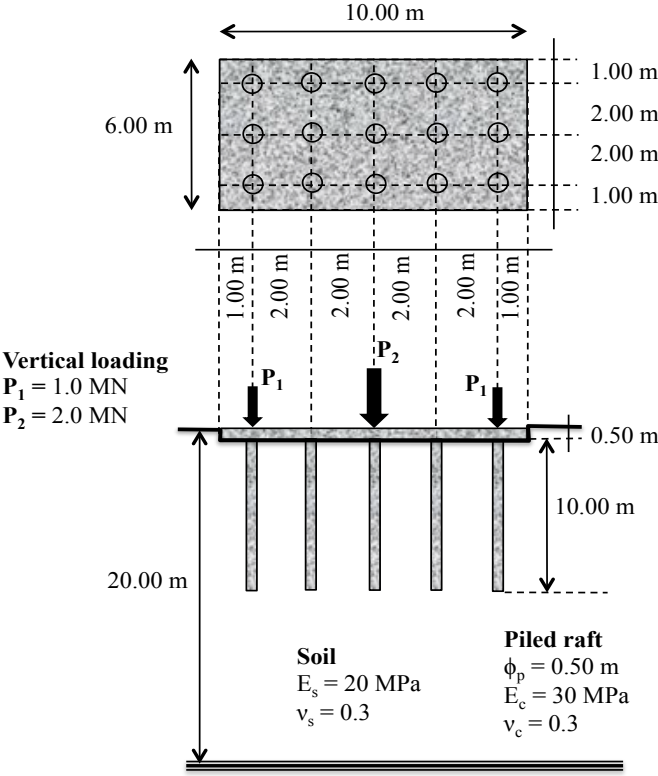


Figure 3.8. Proposal problem, soil meshing and piled raft simulated through Abaqus software (Poulos and Davis, 1980).

The simulated model consists of three parts: homogeneous soil, raft and fifteen piles. There is no existing interaction between the piles and the raft; the soil dominium was 2 times the length of the piles in vertical direction “z” (20.0 m), and three times the wider dimension in horizontal direction “x” and “y” (30.0 m).

The elements used for the meshing of the whole model were of the hexahedral C3D8R type (continuous, three dimensional, eight nodes and reduced integration).

The total number of nodes in the whole model was 193,311; the total number of elements was 174,299 and the running time to get results was around 27 hrs.

This problem was solved using only elastic analyses considering for the soil  $E_s = 20$  MPa and  $\nu_s = 0.3$ . Parts of the piled raft modeled with Abaqus software are displayed in Figure 3.9. The shear stress around the piles produced by the interaction between the concrete pile and the soil was calculated by the beta method  $\beta$  (Helwany, 2007); the value obtained was 14.7 kPa.

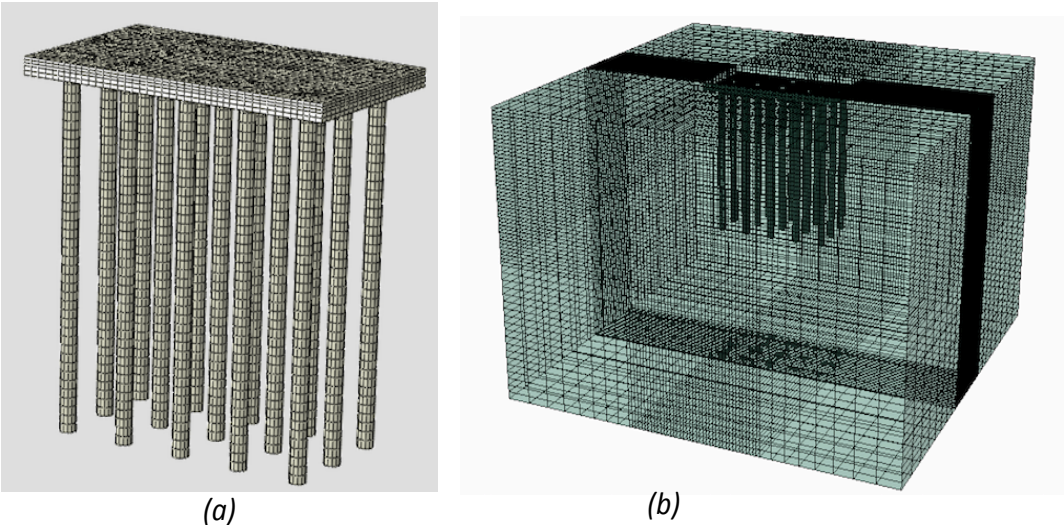


Figure 3.9. (a) Piled raft with 15 piles. (b) Soil dominium.

The numerical results computed by different authors are displayed in Figure 3.10. Finally, the settlement of 23.2 mm evaluated by means of Abaqus Software is consistent with the findings of most of the authors.

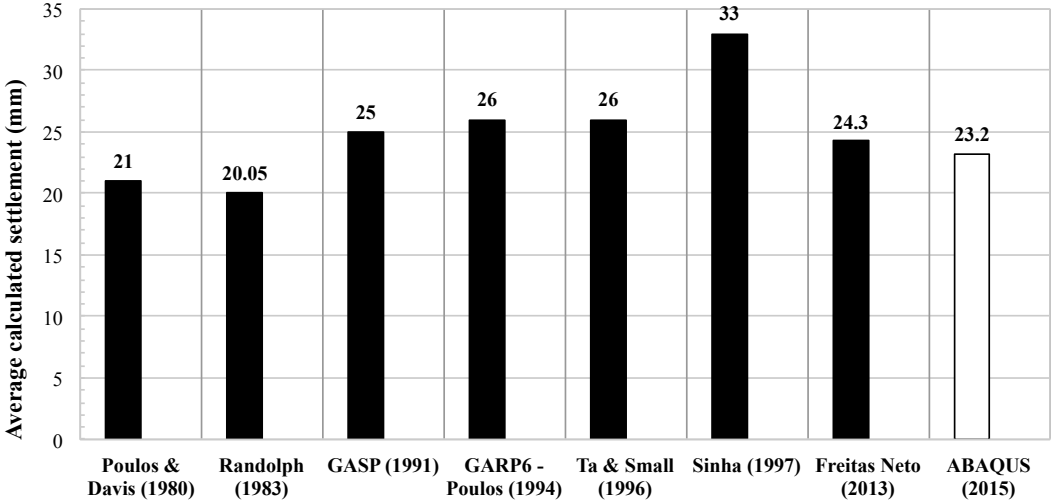


Figure 3.10. Results of settlement calculated by different authors using different numerical tools.

## 4 MATERIALS AND METHODS

### 4.1 EXPERIMENTAL RESEARCH SITE

The City of Campinas is located in the northwest region of São Paulo State, 100 km away from São Paulo City. The University of Campinas (UNICAMP) is located north of Campinas City in a neighborhood called Barão Geraldo. All site works were done at the experimental research site of the Faculty of Engineering and Architecture (FEC) within the University Campus. Figure 4.1 shows the location.

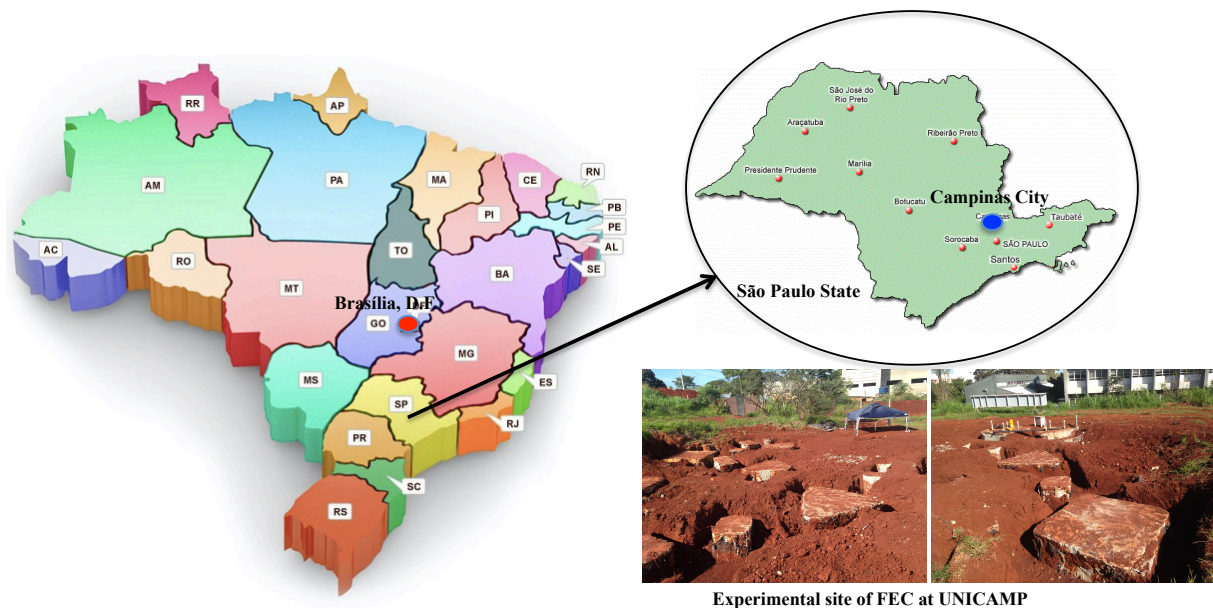


Figure 4.1. Campinas City in Brazil, and layout at experimental site.

The Campinas region is formed by a flood plain, where alluvial sediments are found in the river formations such as that of the Rio Claro and Serra Geral, which consist of unconsolidated sediments (sand and clay) and basic intrusive rocks of fractured Diabase, and such fractures may or may not be filled with clay materials. In addition to these formations, the geological framework of the Campinas region is constituted by materials of the Itararé group (diamictite, varvite and sandstone), as well as by sill and dike formation (mylonite), and the granitic Morungaba, Jaguariúna and Caipira complex.

The Barão Geraldo region, where UNICAMP is located, consists of basic intrusive rocks of the Serra Geral formation (Diabase), from the São Bento group. The soils of the region can be classified as purple latosols according to pedology classification.

Mineralogically, they are made of quartz, ilmenite, magnetite, kaolinite, gibbsite, iron oxides and hydroxides, with thickness ranging from to 5 to 30 m (Scallet, 2011).

The geotechnical profile of the FEC-UNICAMP research site (600 m<sup>2</sup> area) consists of a silty clay layer, which is porous, colluvial, lateritic and collapsible, overlying a brown silty sand layer with altered rocks. Figure 4.2 shows this profile based on the Terzaghi and Peck (1948) SPT classification.

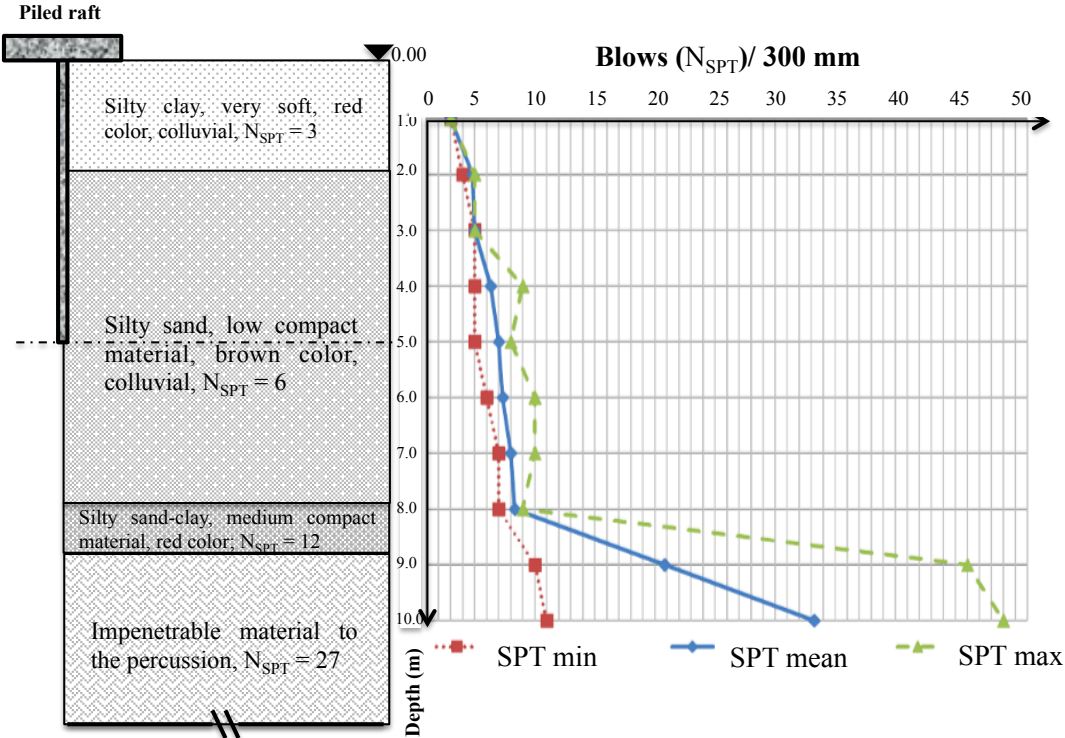


Figure 4.2. SPT chart and simplified geological profile from FEC-UNICAMP.

Field test results have been obtained for this experimental site using a comprehensive program, which included SPT with energy measurement, CPT-M mechanical test and CPT-E electric test (Rodriguez, 2013); see Figure 4.3.

Also, laboratory results from physical characterization, consolidation, triaxial compression (type CU), permeability, normal Proctor compaction and suction tests were obtained (Gon, 2011). The major geotechnical parameters of this soil are displayed in Table 4.1 and Figure 4.4.



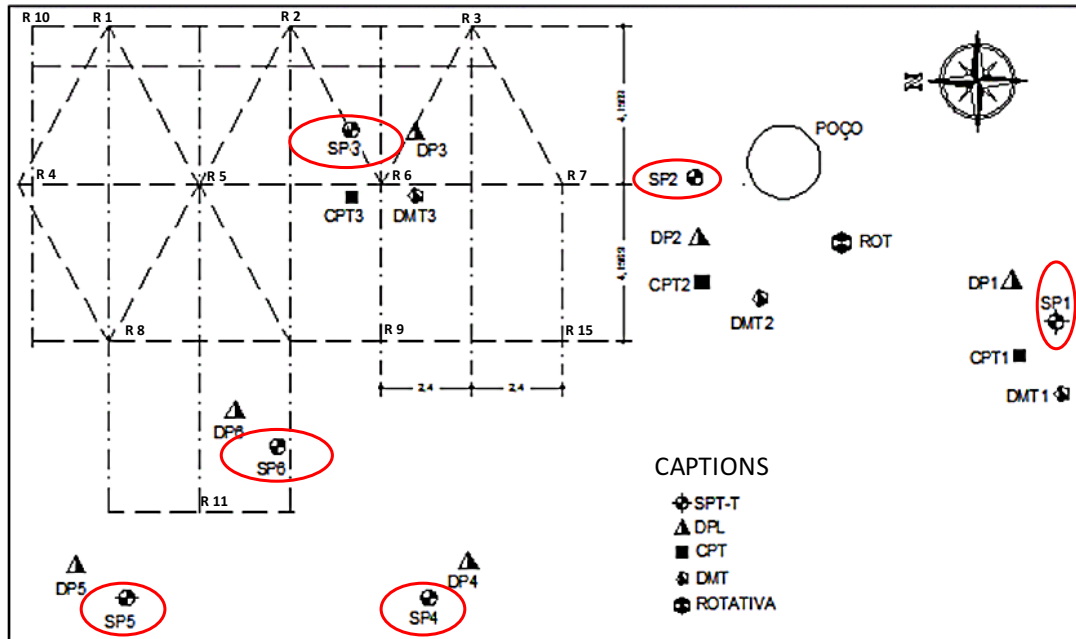


Figure 4.3. Location of field trials and sample collection

Table 4.1. Geotechnical parameters of the porous clay

LABORATORY TESTING RESULTS OF THE POROUS CLAY (FREITAS NETO, 2013)						
Depth (m)	USCS	$\gamma_{nat}$ (kN/m <sup>3</sup> )	w (%)	$E_s$ (Mpa)	c (kPa)	$\phi$ (°)
1.00	MH	14.10	28.30	13.79	7.40	22.00
2.00	ML	14.20	27.90	11.43	7.85	21.00
3.00	ML	14.00	28.00	8.50	11.60	22.00
4.00	ML	14.40	25.50	11.49	5.75	23.00
5.00	ML	15.50	26.20	9.86	24.00	21.00
6.00	ML	15.30	26.10	19.95	42.40	22.00
7.00	ML	15.40	28.30	10.93	41.93	22.00
8.00	MH	15.20	32.30	11.01	26.40	22.00

USCS - Unified soil classification system: MH – Silty with high compressibility; ML – Silty with low compressibility;  $\gamma_{nat}$  - Natural unit weight; w – Moisture content;  $E_s$  – Undrained elastic modulus; c – Undrained cohesion;  $\phi$  – Undrained friction angle.

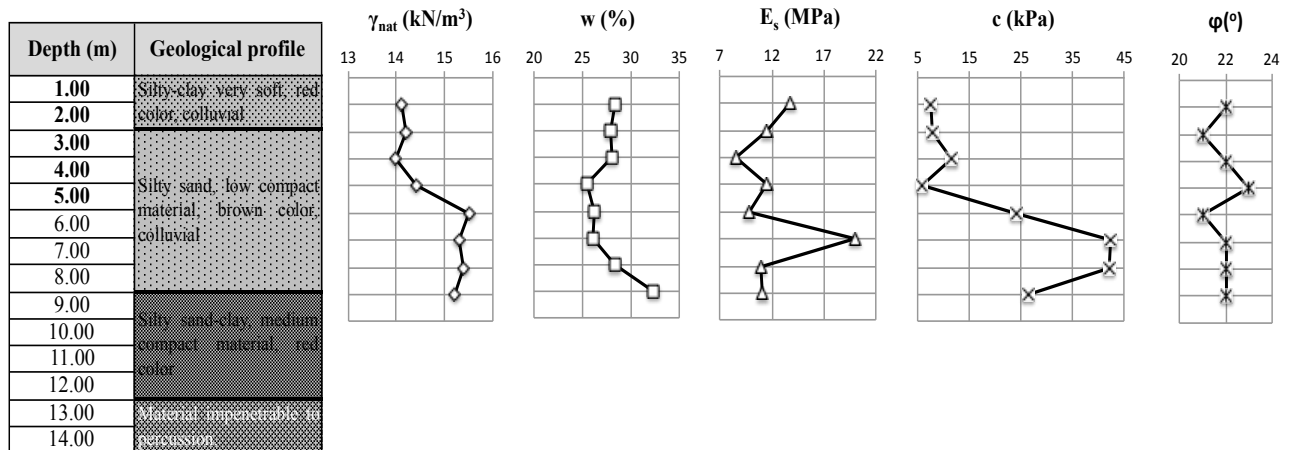


Figure 4.4. Geotechnical parameters of the porous clay.

The consolidation tests enabled obtaining the collapsibility potential of the experimental site from 1.0 m until 8.0 m depth; the results of each of the deep underground methodologies classify it as collapsible soil. All these samples were collected every meter below the soil surface. Figure 4.5 displays those results from the oedometer test (unidimensional consolidation) only at shallow depth. The moistening-induced deformations (collapse deformations) were measured under stresses of 100 kPa, 200 kPa and 400 kPa.

Also, those curves showed considerable evidence of volumetric variation under the inundated soil condition (sudden change in the void ratio normalized); it means that the effect of a change in the natural moisture of the soil is very considerable, causing large deformations in the soil.

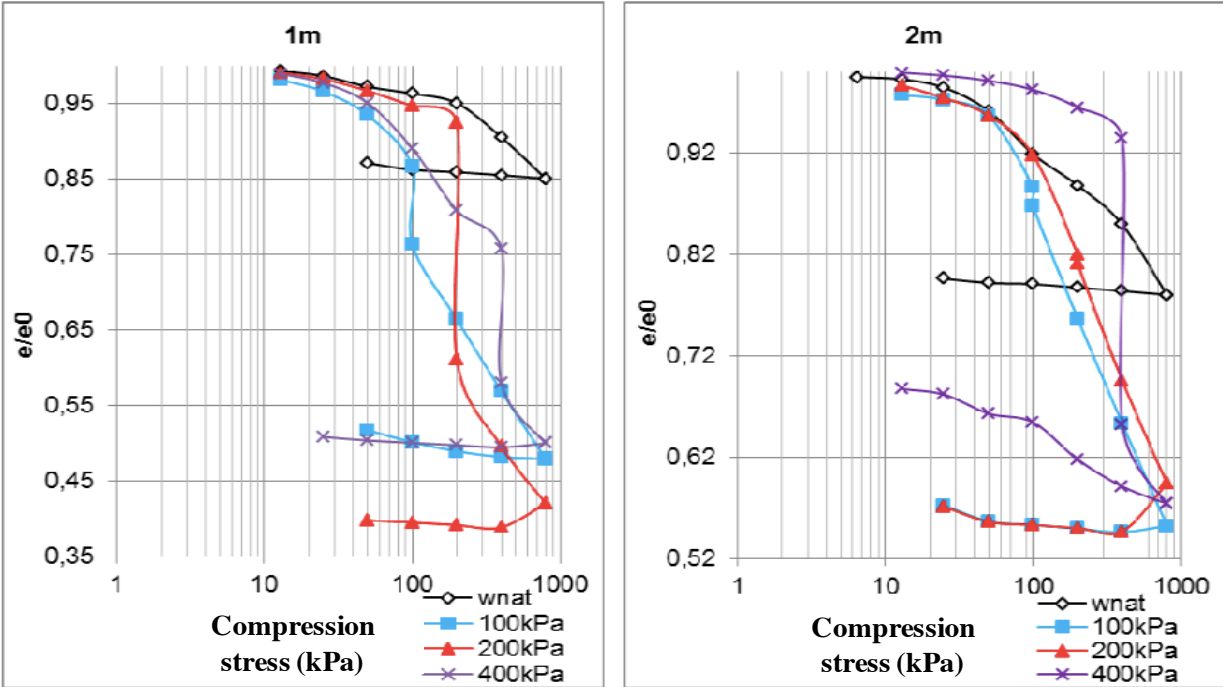


Figure 4.5. Oedometer test results at 1<sup>st</sup> and 2<sup>nd</sup> meter depth (Gon, 2011).

Finally, some soil-water characteristic curves (or water retention curves) corresponding to the first three meters depth are shown in Figure 4.6; it can be seen in each one of them that due to the approximately 12% increase in moisture content, the suction drops by up to 1000 times at the first meter depth. Thus, the shear strength of the soil can vary drastically in its bearing capacity. Some research works indicate that bored piles in collapsible soil, can lose up to 50% of their bearing capacity (Freitas Neto, 2013).

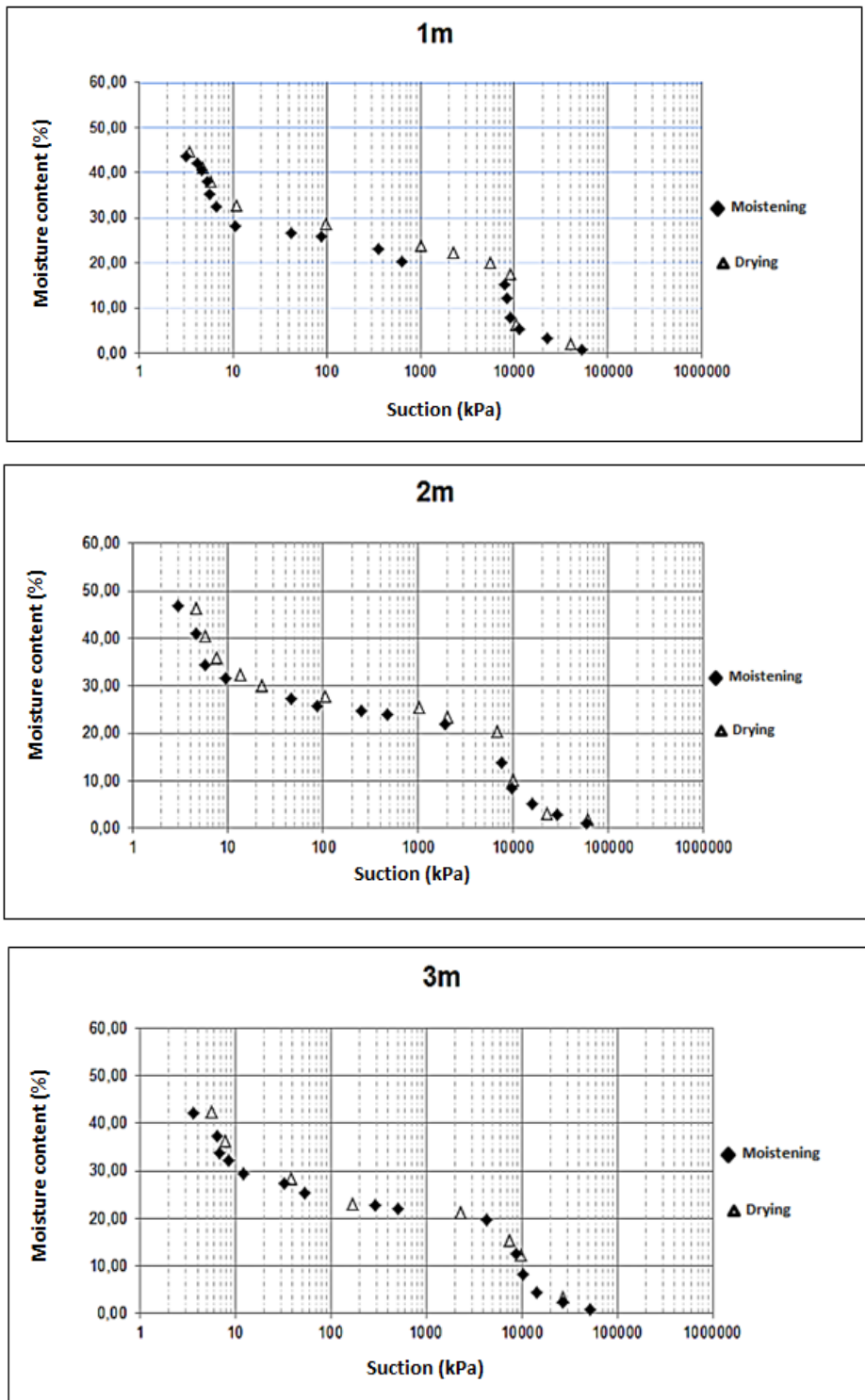


Figure 4.6. Soil water characteristic curves at each meter depth (Gon, 2011).

## 4.2 EXPERIMENTAL PROGRAM AT RESEARCH SITE

A total of thirteen horizontal load tests were carried out and are summarized in Table 4.2. The tested piled rafts consisted of different geometry, a distinct diameter pile, and

different pile and soil moisture conditions. The strength of the concrete used during construction was  $f_{ck} = 20,0$  MPa; in addition, CA50-type steel of 10 mm in diameter for the rods and steel stirrups (helical type) and of 6.5 mm in diameter for reinforcement of the structures were used.

All piled raft systems involved bored piles drilled with helical auger to 5.0 m in depth, installation of reinforcing steel within holes, concreting of the piles, digging up until the bottom level of the raft, placement of reinforcing steel and concreting of the raft. The spacing between piles in all systems was five diameters equal to 1.25 m.

With respect to the inclinometry measurement tests, the inclinometer case was an aluminum tube of 10.0 cm in diameter and 5.0 m in length. One such case was placed in the center of each pile during construction of some piled raft systems.

Special note should be made of the weather conditions during the experimental works, because any variation in the soil's natural moisture can produce sudden change in its behavior, mainly due to the presence of collapsible soils (see section 2.7). The rainy days during the month of July, 2015 are shown in Figure 4.7. Data obtained from Instituto Nacional de Meteorologia, at Sorocoba, SP station.

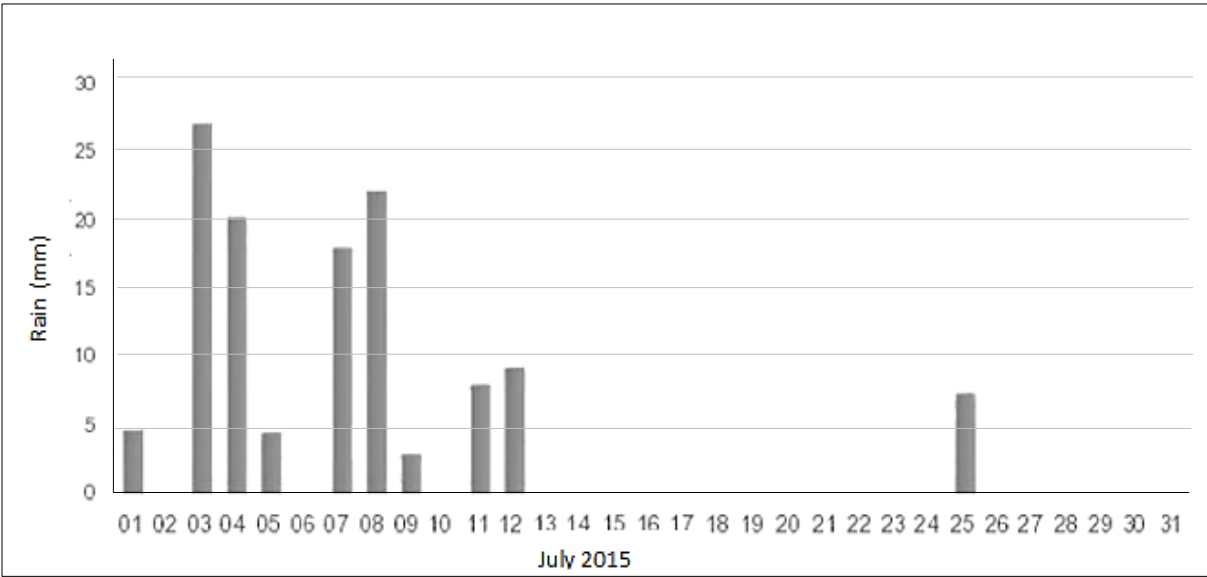


Figure 4.7. Accumulated rain during the month of July, 2015.

Table 4.2. Load testing works performed at experimental site, Campinas University, SP.

TEST	DATA (JULY, 2015)	SYSTEM	P I L E		LOADING TEST TYPE	SOIL CONDITIONS
			Length $L$ (m)	Diameter $\Phi$ (m)		
1	14	SC2	5,0	0,25	Horizontal slow	Natural moisture
2	15	SC1	5,0	0,25	Horizontal slow	Natural moisture
3	16	CC2	5,0	0,25	Horizontal slow	Natural moisture
4	17	SC3	5,0	0,25	Horizontal slow	Natural moisture
5	18	CC1	5,0	0,25	Horizontal slow	Natural moisture
6	20	CF4	5,0	0,25	Horizontal slow	Natural moisture
7	21	CF3	5,0	0,25	Horizontal slow	Natural moisture
8	23	RD2	5,0	0,30	Horizontal slow	Natural moisture
9	24	RD3	5,0	0,30	Horizontal slow	Natural moisture
10	27	RD3	5,0	0,30	Horizontal fast	Inundated
11	28	RD2	5,0	0,30	Horizontal fast	Inundated
12	29	CC3	5,0	0,25	Horizontal slow	Natural moisture
13	March 2017	CC4	5,0	0,25	Horizontal slow	Natural moisture

Caption:

- *SC2 - 2 intact piles, structure tested previously under vertical loading; no ground contact.*
- *SC1 - Intact pile, structure tested previously under vertical loading, no ground contact.*
- *CC2 - 2 intact piles, structure tested previously under vertical loading, ground contact.*
- *SC3 - 3 intact piles, structure tested previously under vertical loading, no ground contact.*
- ***CC1 - 1 intact pile, structure tested previously under vertical loading, ground contact.***
- ***CF4 - 3 intact piles and one defective pile, structure tested previously under vertical loading, ground contact.***
- ***CF3 - 2 intact piles and one defective pile, structure tested previously under vertical loading, ground contact.***
- *RD2 - 3 intact piles, structure never tested, inclinometer measurements in each pile, ground contact.*
- *RD3 - 4 intact piles, structure never tested, inclinometer measurements in each pile, ground contact.*
- ***CC3 - 3 intact piles, structure tested previously under vertical loading, ground contact.***
- ***CC4 - 4 intact piles, structure tested previously under vertical loading, ground contact.***

The “meaning” of *structure tested previously under vertical loading* (bold letters) refers to earlier experimental works on these structures, and the ground contact refers to the fact that there was contact between the raft and the soil surface.

All of those vertical loading tests were performed for the DSc thesis of Freitas Neto (2013) and Garcia (2015); Table 4.3 displays the experimental results.

Table 4.3. Results from the vertical loading tests.

EXPERIMENTAL VERTICAL LOADING			
FOUNDATION SYSTEM	DISPLACEMENT (mm)	ULTIMATE LOAD (kN)	AUTHOR
CC1	45.09	208.00	Garcia, 2015
CC3	52.02	490.00	
CC4	40.14	700.00	
CF1	100.00	131.00	Freitas Neto, 2013
CF3	54.65	420.00	
CF4	50.00	625.00	

It needs to be emphasized that only the five load testing experiments highlighted in shaded rows within Table 4.2, namely *CC1*, *CC3*, *CF3*, *CC4* and *CF4*, were used in this research thesis.

Figure 4.8 shows the layout at the experimental field of these piled raft systems. They are also indicated by circles in Figure 4.9.

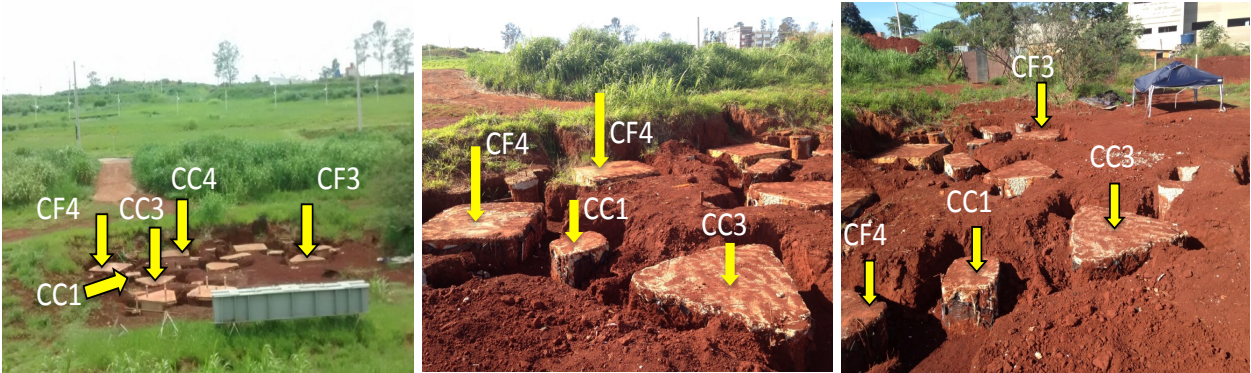


Figure 4.8. Layout of the full-scale piled raft systems at experimental field. (July, 2015)

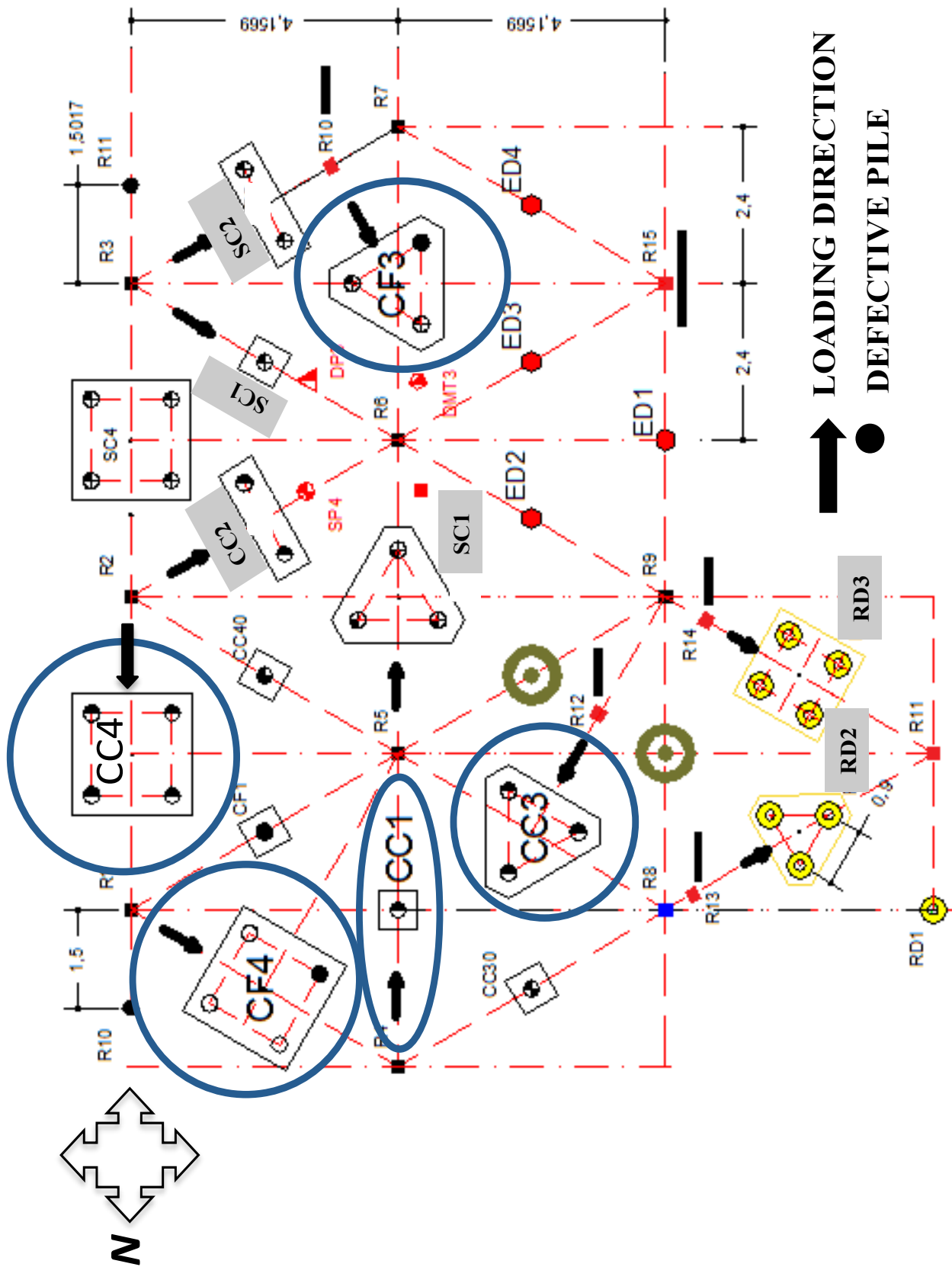


Figure 4.9. Layout at experimental field, Campinas University, SP.

Figure 4.10, Figure 4.11, and Figure 4.12 show in detail the geometry, dimensions and other general information about all the aforementioned piled raft systems.

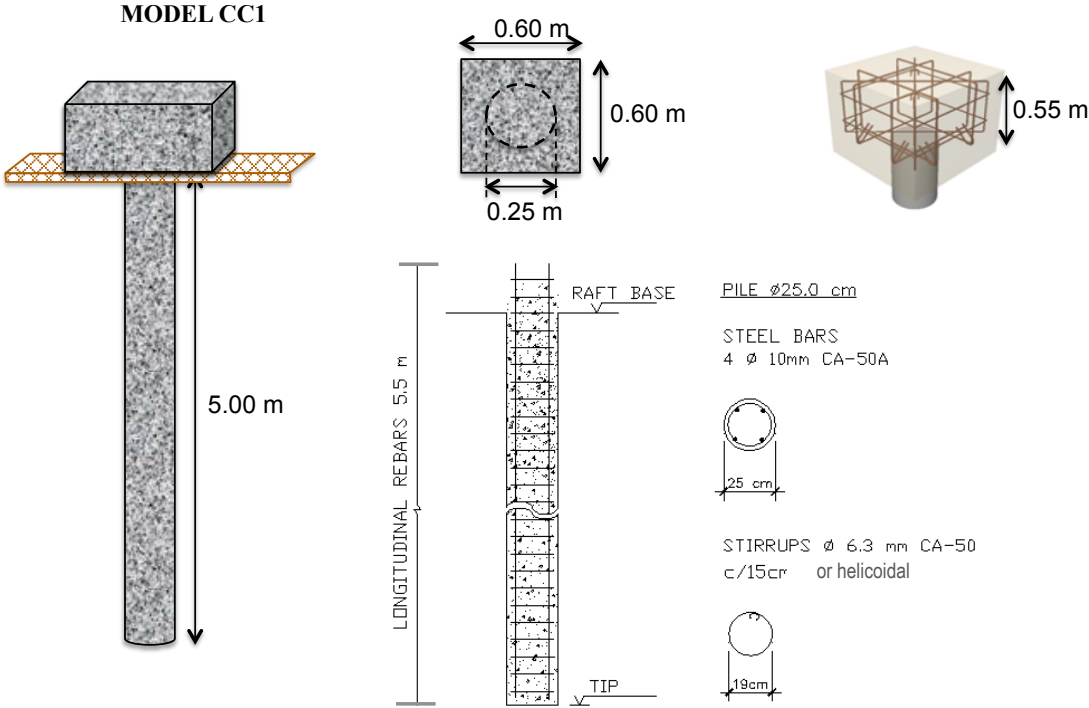


Figure 4.10. Details of *CC1* piled raft system already built at the experimental field.

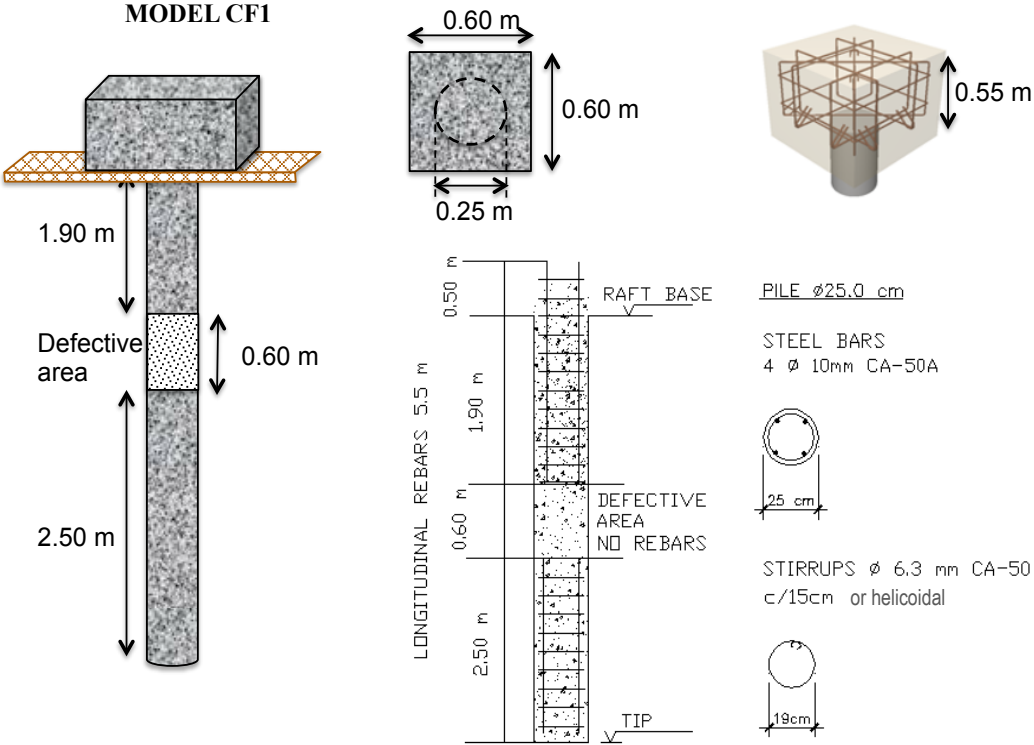


Figure 4.11. Details of the *CF1* piled raft system.



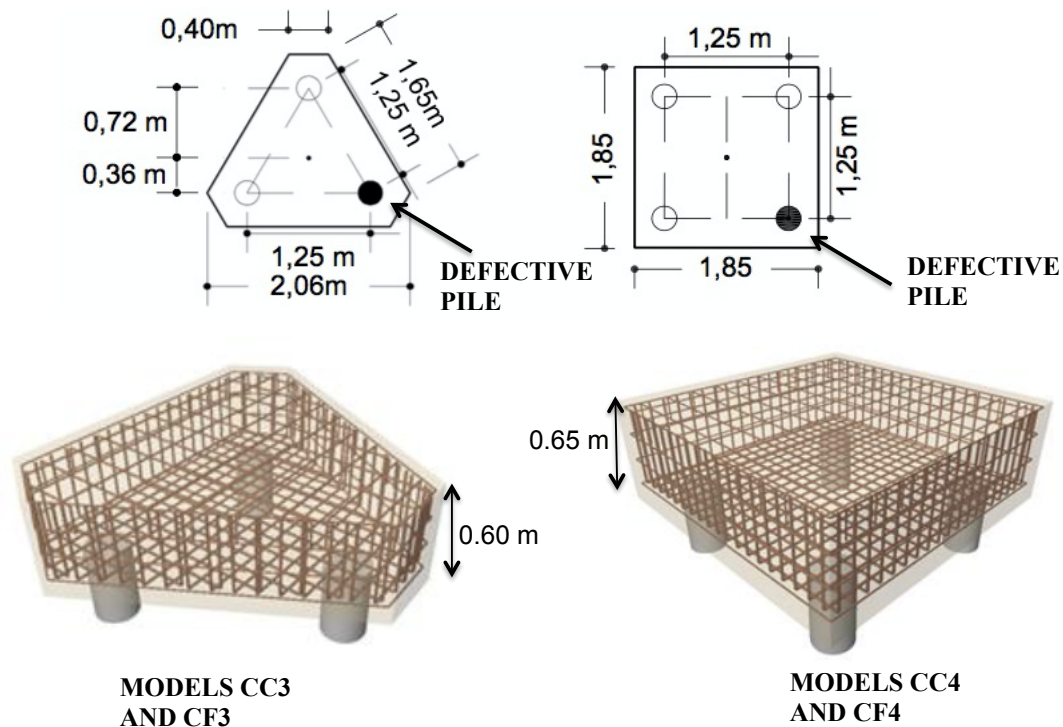


Figure 4.12. Details of the *CC3*, *CF3*, *CC4* and *CF4* piled raft systems already built at the experimental field.

It is important to mention several specific details about the *CF1* and *CC4* piled raft systems presented in this research thesis:

- The *CF1* system no longer exists at the experimental field because it was exhumed for verification in previous works (Freitas Neto, 2013). However, this foundation system was studied by prediction behavior analysis, given the importance of its behavior.
- The defective pile used in the *CF1* system and depicted in Figure 4.11 is the same type adopted for the *CF3* and *CF4* systems.
- The *CC4* full-scale loading test was carried out by Kassouf (2017) (doctoral thesis in progress), after the experimental research period of the present thesis had been completed.

#### 4.2.1 HORIZONTAL LOADING TESTS

The field horizontal loadings were performed in accordance with the recommendations of Brazilian testing standard NBR12131 (ABNT 2010). Eleven slow and two fast tests were executed, all until failure. A 200 kN precision load cell monitored the applied force on one

lateral face of the raft, and four 0.01mm precision dial gauges measured the horizontal displacements and tilt of the raft. A concrete pile of 0.60 m in diameter and 9.0 m in length embedded into the soil was used to react against the loads imposed by a 200-kN hydraulic jack.

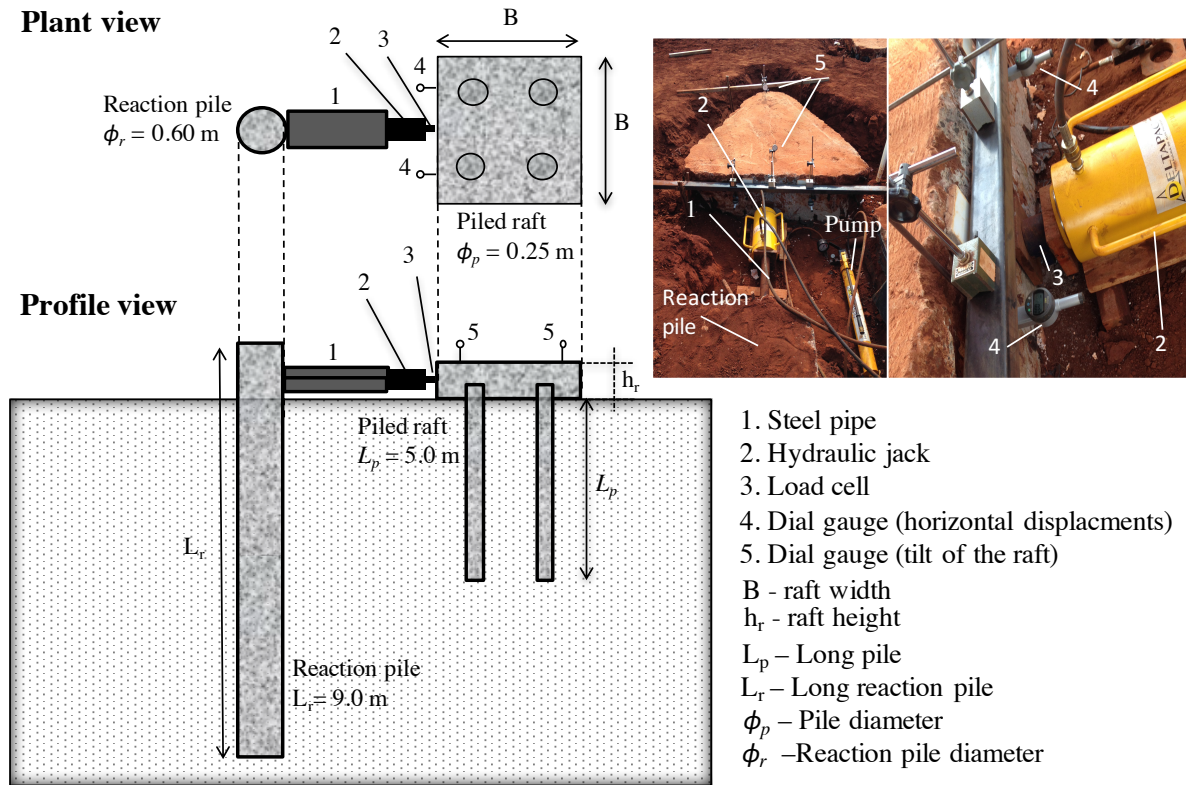


Figure 4.13. Sketch of the horizontal load test.

Figure 4.13 shows a sketch with general details of the horizontal load test, support elements and tools used during the field works. Figure 4.14 shows full-scale tests of some of the aforementioned piled raft systems.

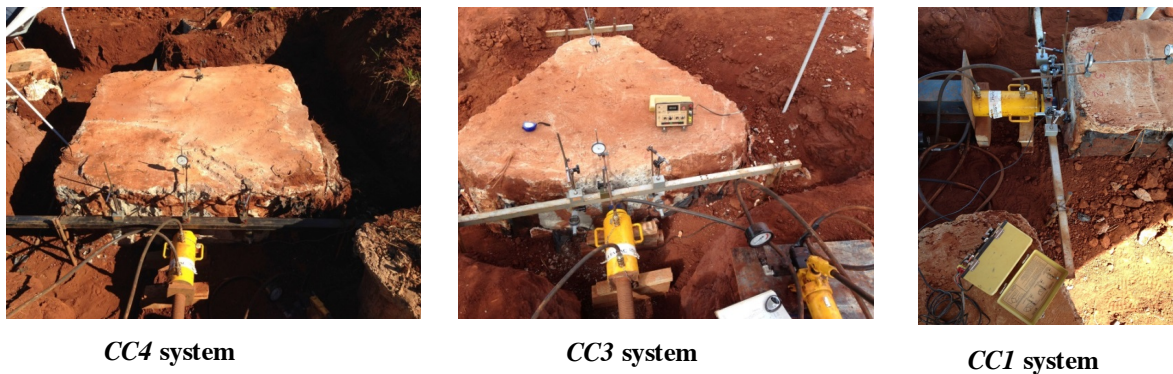


Figure 4.14. Horizontal load tests at full scale on the piled raft systems used in this research work. Experimental field at Campinas University, July, 2015.

## 4.2.2 CONSTRUCTION OF DEFECTIVE PILES

The damage to the defective piles consisted of creating a region of lower structural resistance in the pile, equal to half the previous ultimate vertical load of the pile, and whose position was between 1.90 and 2.50 m in depth (0.60 m damage length) without any steel reinforcement in this region. The *CF3* and *CF4* piled raft systems have been built with all these characteristics in the defective pile; Figure 4.11 displays these geometric details. For the construction of the damaged region, a cylindrical metallic cast of 0.25 m in external diameter, 0.245 m in internal diameter (almost equal to the diameter of the pile), and 0.60 m in height was used; a PVC pipe of 0.195 m in external diameter was placed in the center of the cylindrical metallic cast. The void created between the internal diameter of the cylinder cast and the external diameter of the PVC pipe was 0.025 m in thickness and 0.60 m in height.

The material used to fill this void was a “poor” concrete whose compressive strength was calculated through several resistance compression tests, in order to be sure that element would break during vertical load testing (Freitas Neto, 2013). Figure 4.15 shows some details of the damaged area during manufacture and placement on reinforcing steel. The equivalent diameter for the damaged region in the pile is 0.215 m and corresponds to the “necking” case shown in Figure 2.6. According to the author responsible for this work, the final geotechnical parameters for use during the numerical modeling process will be an equivalent diameter of 0.19 m just for the defective section, with Young’s modulus of 5.9 GPa.

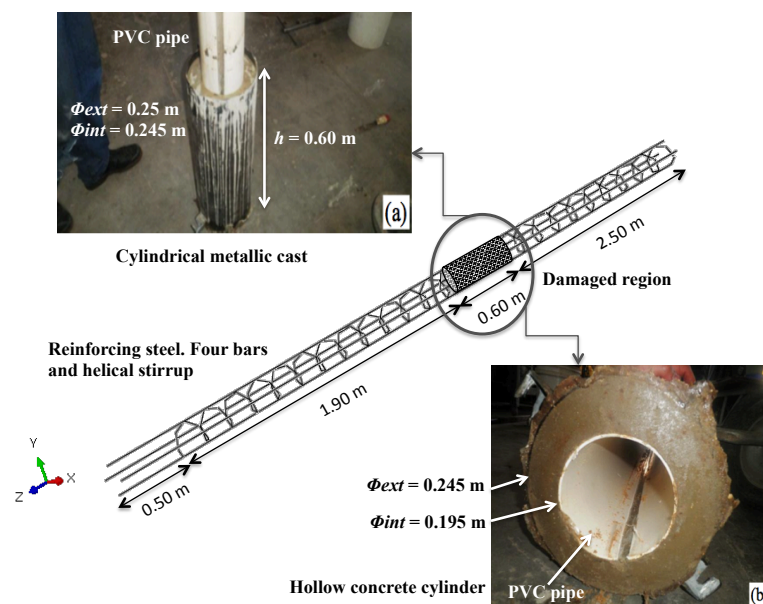


Figure 4.15. (a) Making damage and placement of damaged region into the pile. (b) Hollow concrete cylinder. July 2012. (Freitas Neto, 2013).

### 4.3 EXPERIMENTAL RESULTS OF THE HORIZONTAL TESTING LOAD

The experimental horizontal loading versus displacement curves of some of the testing loads, highlighted in Table 4.2, are presented next. The cases presented in this chapter are the most relevant to this research. As a preliminary step, the results of those five highlighted experimental loading tests were plotted, and an interesting comparison among them was made in order to understand the behavior of the tested structures.

Figure 4.16 shows the experimental curves obtained for the *CC1*, *CC3*, *CF3*, *CC4* and *CF4* systems, where it is possible to observe the rigidity effect of each of them, due to the number of piles, geometry, dimensions, etc.; the comparison between the *CC3* and *CF3* systems as well as the *CC4* and *CF4* ones will be focused on in the next section, since only those systems with the same features, such as geometry, size, materials, pile number, etc., were experimentally compared, in order to evaluate the actual presence of a damaged pile.

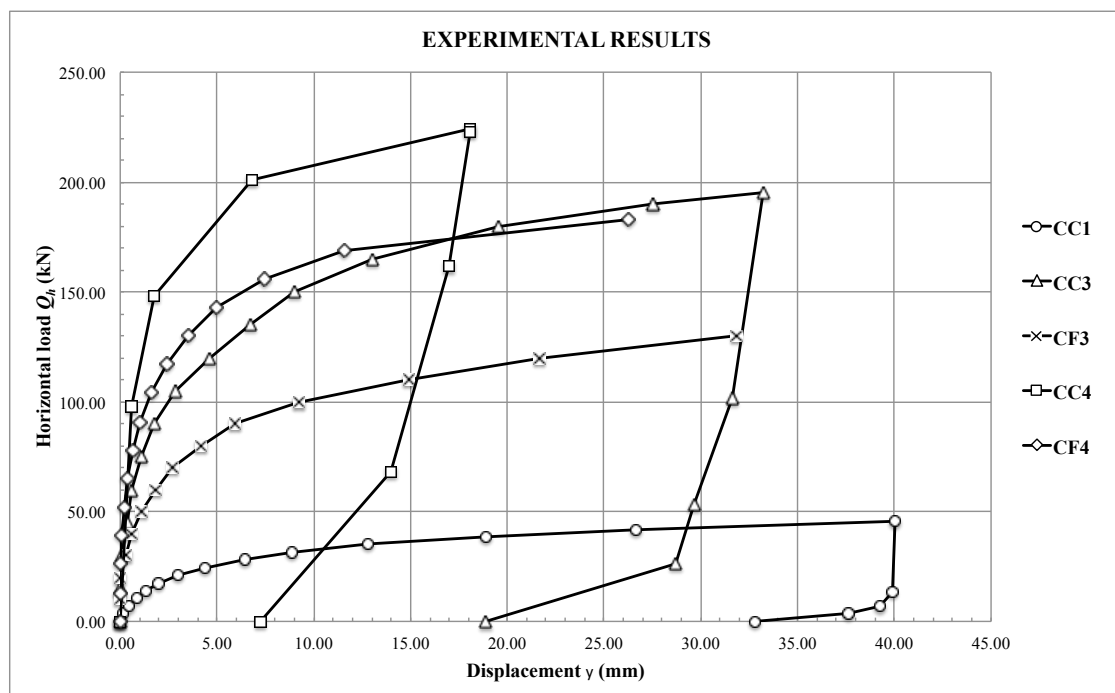


Figure 4.16. Experimental results of the piled raft systems tested. (See appendix A).

It is important to mention that during the full-scale unloading test of the *CF4* and *CC3* systems, it was difficult to control the hydraulic jack, and although some data were recorded, it was decided to disregard them and therefore they were not plotted. Table 4.4 displays the

maximum horizontal displacement and the ultimate horizontal loading according to the figure above. The appendices section of this thesis includes the experimental data measured.

Table 4.4. Experimental measurements of each piled raft system.

EXPERIMENTAL MEASUREMENTS SUMMARY		
FOUNDATION SYSTEM	DISPLACEMENT (mm)	ULTIMATE LOAD (kN)
CC1	40.04	45.50
CC3	33.22	195.00
CF3	31.86	130.00
CC4	18.07	224.00
CF4	26.30	183.00

### 4.3.1 ANALYSIS OF EXPERIMENTAL LOADING TEST RESULTS

Based on the experimental results, some computations are performed to determine the ultimate load for the *CC1*, *CC3*, *CF3*, *CC4* and *CF4* piled raft systems using some classical methods of extrapolation. Although those methods were developed to estimate the ultimate vertical loading, they were also used in the same way to estimate the ultimate horizontal loading.

Figure 4.17 shows the average value of all methods used here to obtain the representative ultimate load values of the *CC1* foundation system, resulting in 44.65 kN.

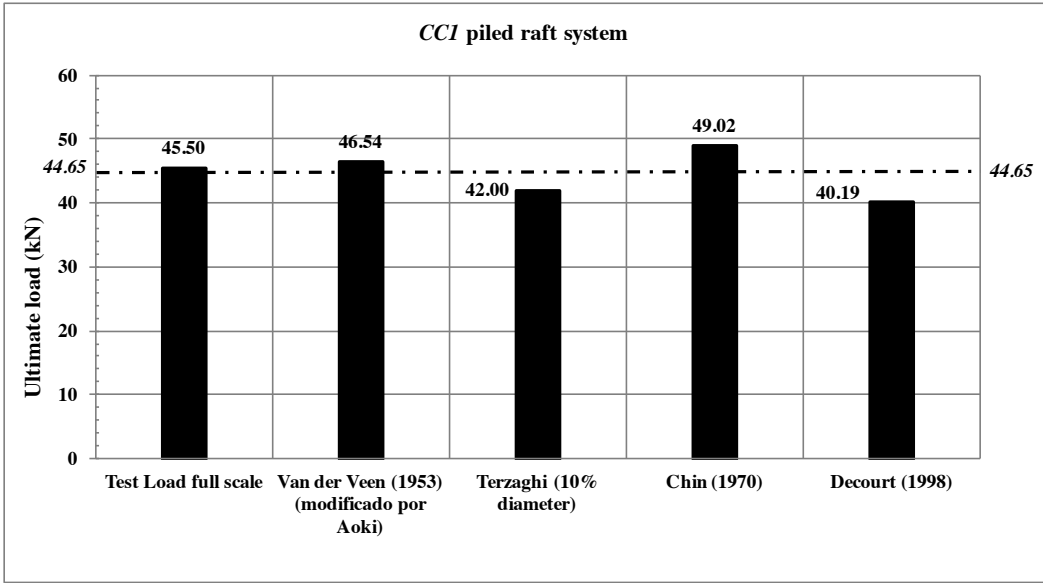


Figure 4.17 Ultimate load for *CC1* piled raft system.

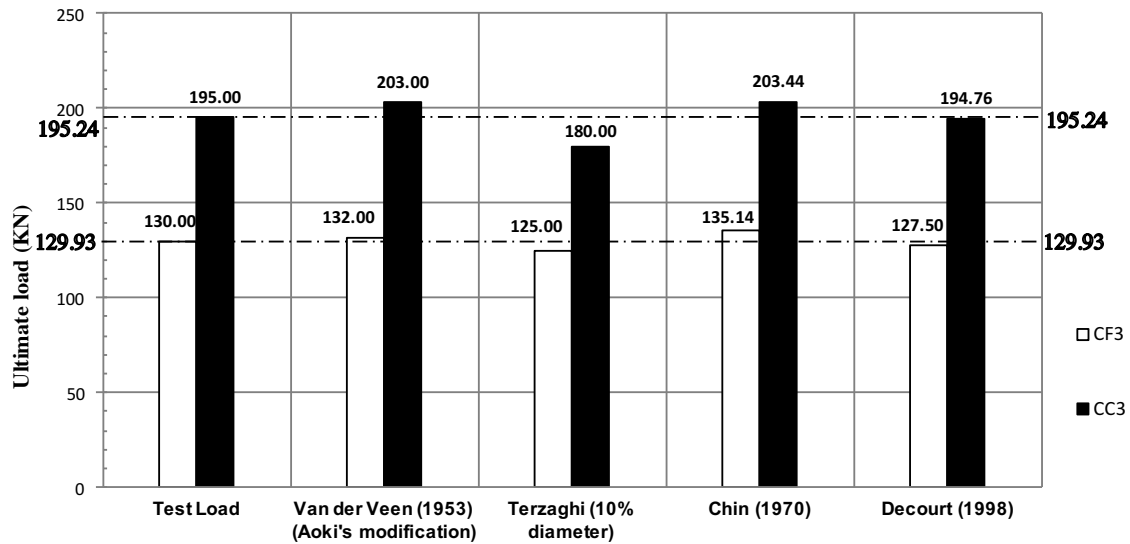


Figure 4.18. Ultimate load for *CC3* and *CF3* piled raft systems.

Figure 4.18 clearly shows the difference in the ultimate load between the *CF3* defective and *CC3* intact systems. The average value of all methods is used here to obtain the representative ultimate load values of each system, resulting in 195.24 kN for *CC3* and 129.93 kN for *CF3*.

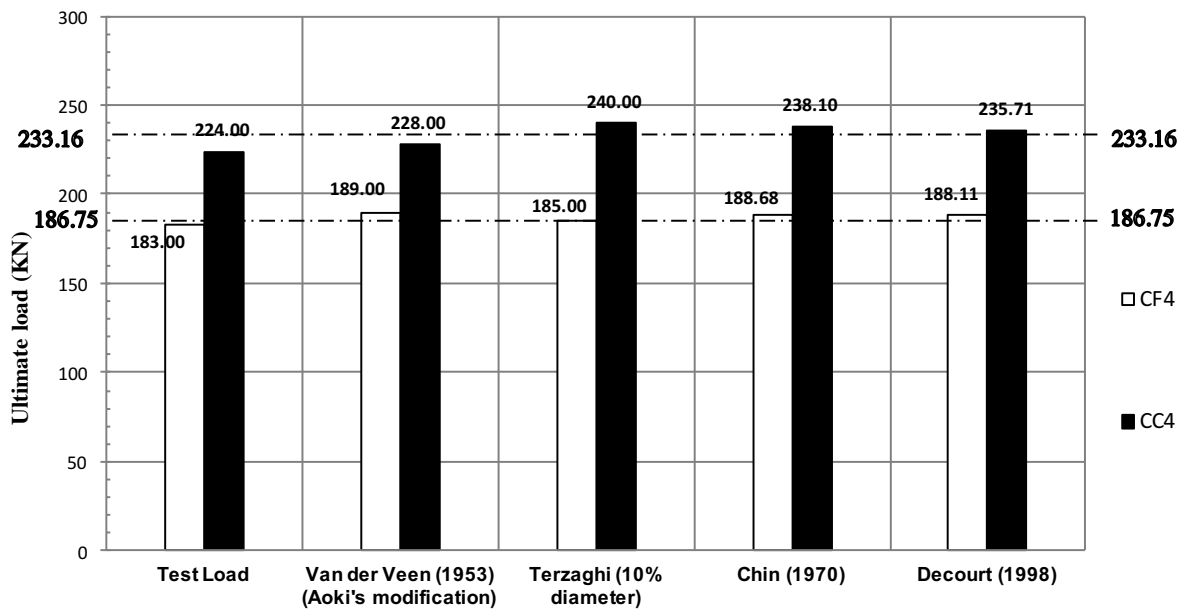


Figure 4.19. Ultimate load for *CC4* and *CF4* piled raft systems.

Figure 4.19 also clearly shows the difference in the ultimate load between the *CF4* defective and *CC4* intact systems. The average value of all methods is used here to obtain the

representative ultimate load values of each system, resulting in 233.16 kN for *CC4* and 186.75 kN for *CF4*.

In order to establish a failure criterion to study the effect of a defective pile in those foundations, the initial plan was to use those representative ultimate loads divided by 2.0 (safety factor) and thus obtain the corresponding work loads for each of them; Figure 4.20 shows the ultimate defined loads as from some classical methods of extrapolation. Table 4.5 shows the ultimate defined loads as from some classical methods of extrapolation. Table 4.5 shows the ultimate load and work load set under this selected criterion.

Table 4.5. The ultimate and work loads from the experimental loading test of all piled raft systems.

Selected Criterion	Horizontal load $Q_h$ (kN)				
	CC1	CC3	CF3	CC4	CF4
Ultimate load (average from methods of extrapolation)	44.65	195.24	129.93	233.16	186.75
Work load (1/2 ultimate load)	22.33	97.62	64.97	116.58	93.38

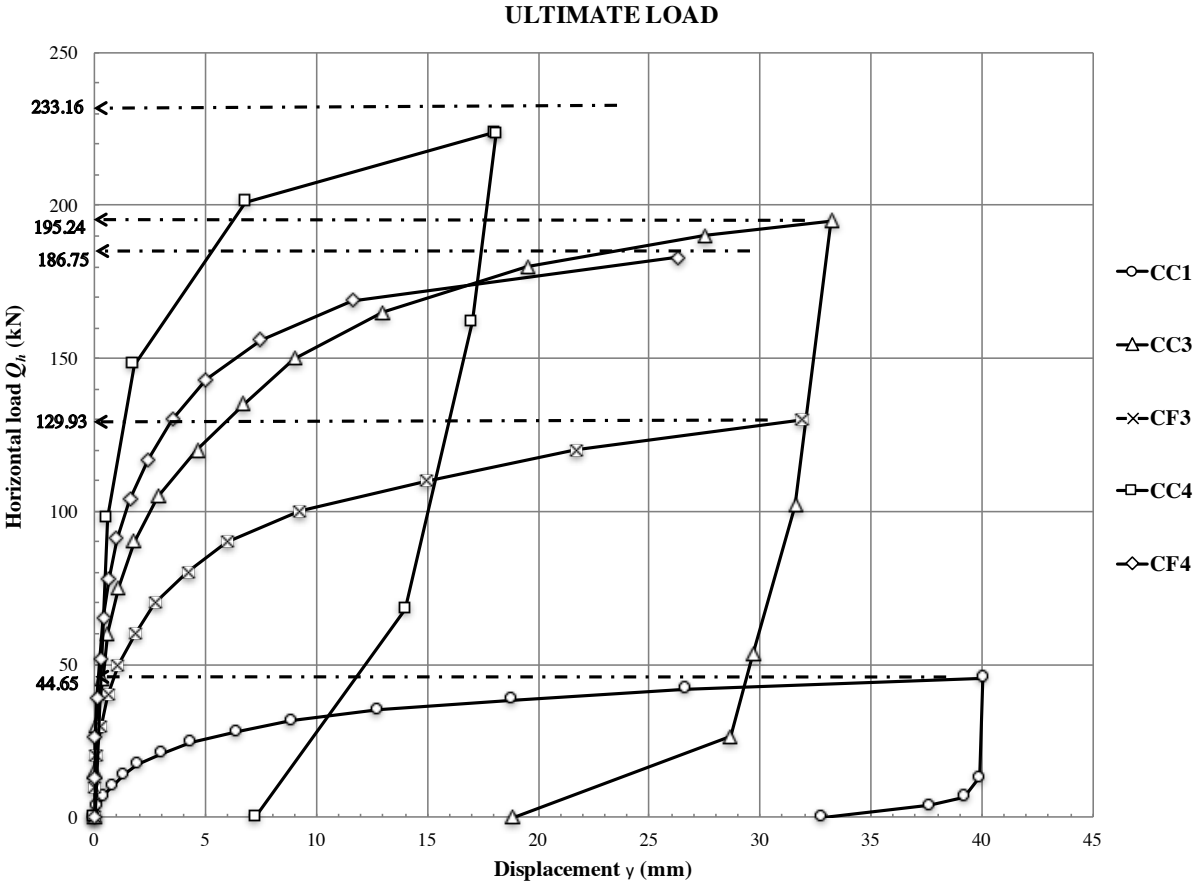


Figure 4.20. Ultimate load defined for all piled raft systems.

Terzaghi's failure displacement was another criterion selected to study the experimental behavior of the systems by comparing their plotted experimental curves (see Figure 4.16); it was thus possible to study all foundation systems tested under a single displacement. A graphical analysis comparing the piled raft systems, which were geometrically equal (some of them) and established under the same soil conditions, was conducted to study the effect of a defective pile when it is present in the foundation systems.

To find out the ultimate load according to Terzaghi, a displacement of 10% of the pile diameter (25 mm) was used, and it shows as a vertical long dashed line in Figure 4.21. This vertical line extends until touching all experimental curves; from those intersection points, horizontal lines extend until touching the vertical axis (horizontal load  $Q_h$ ), thereby indicating the ultimate load values for each of the piled raft systems. Then the admissible or allowable displacement is located on the horizontal axis, parallel to the same vertical dashed line; a half value of the ultimate displacement equal to 12.5 mm (5%) was considered, and it is shown as a vertical dashed-dotted line. Following the same procedure as described above, the work loads were also determined. The results obtained by this graphical analysis are shown in Table 4.6.

Table 4.6. Failure analysis from the experimental loading test of all piled raft systems

Selected criterion	Displacement (mm)	Horizontal load $Q_h$ (kN)				
		CC1	CC3	CF3	CC4	CF4
10% of pile diameter	25.00	40.00	188.00	122.00	233.00	180.00
Allowable displacement (5% of pile diameter)	12.50	35.00	162.00	105.00	212.00	170.00
Safety factor (S.F)	2.00	1.14	1.16	1.16	1.10	1.06

It is important to mention that although the vertical line crossing the horizontal load at 25 mm does not touch the *CC4* experimental curve (Figure 4.21), then the average ultimate load calculated from the extrapolation methods was used; see Table 4.5.

Finally, through the use of two different failure criteria, it has been shown that the presence of a defective pile in one of the piled raft systems causes a considerable change in behavior that deserves further study.



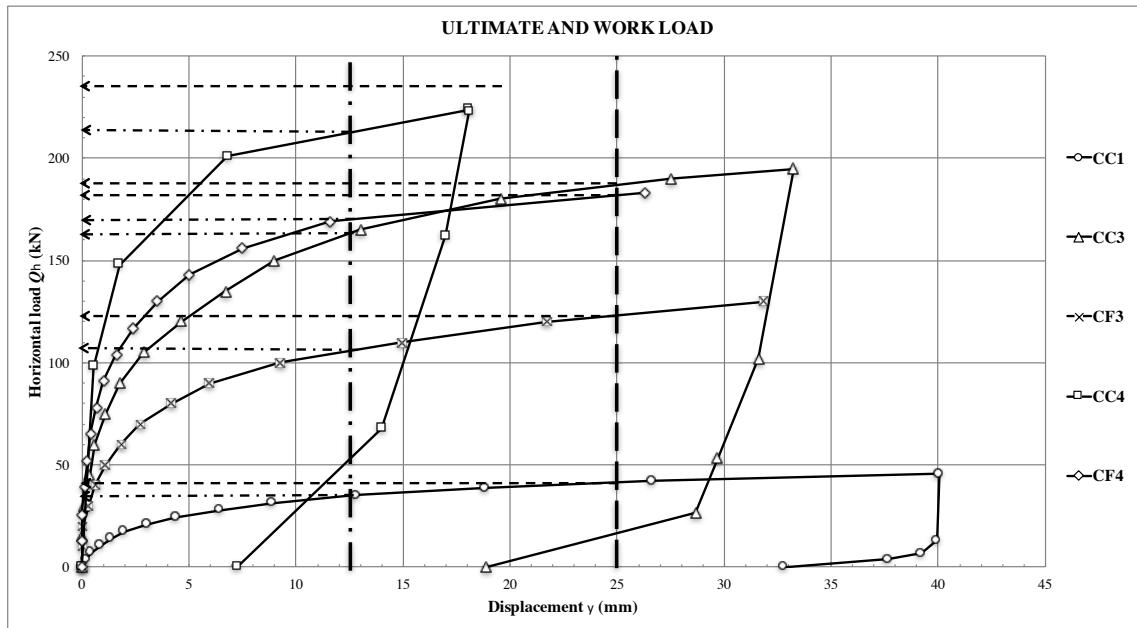


Figure 4.21. Graphical analysis of all piled raft systems to define ultimate and work load.

### 4.3.2 BEHAVIOR PREDICTION

Through the use of Abaqus software and the geotechnical parameters shown in Table 4.1, it was possible to make a preliminary simulation for the *CC1*, *CC3* and *CF4* foundation systems and later to compare those findings with the experimental results. The main reason for carrying out those simulations was to obtain a prediction of behavior prior to executing the full-scale load testing, setting an initial modeling framework and getting an idea about the processing time of each one of them. It is important to mention that some arbitrary horizontal loads were assigned in each one of the foundations systems as initial input data based on their vertical loadings full-scale tests (50% of the maximum vertical load developed).

Later, those arbitrary values were replaced with the maximum horizontal load value developed during the experimental works in each one of them, and hence used as input data to run Abaqus software again. Figure 4.22, Figure 4.23 and Figure 4.24 show the prediction results. The main features set in the numerical prediction modelling were the following:

- The linear elastic and elasto-plastic Mohr-Coulomb constitutive models were used for simulating the soil; the geotechnical parameters used are shown in Table 4.1.
- Reinforced concrete parameters rather than those of plane concrete were considered (the rebar was not considered as part in Abaqus models).

- Plasticity behavior was not considered for the concrete material, only elastic behavior.
- Only the C3D8R-type a linear hexahedral element for the soil meshing, and the C3D6-type linear wedge element for the piles and raft meshing.
- The type of numerical analysis used was only the Static General method, in accordance with Abaqus software.

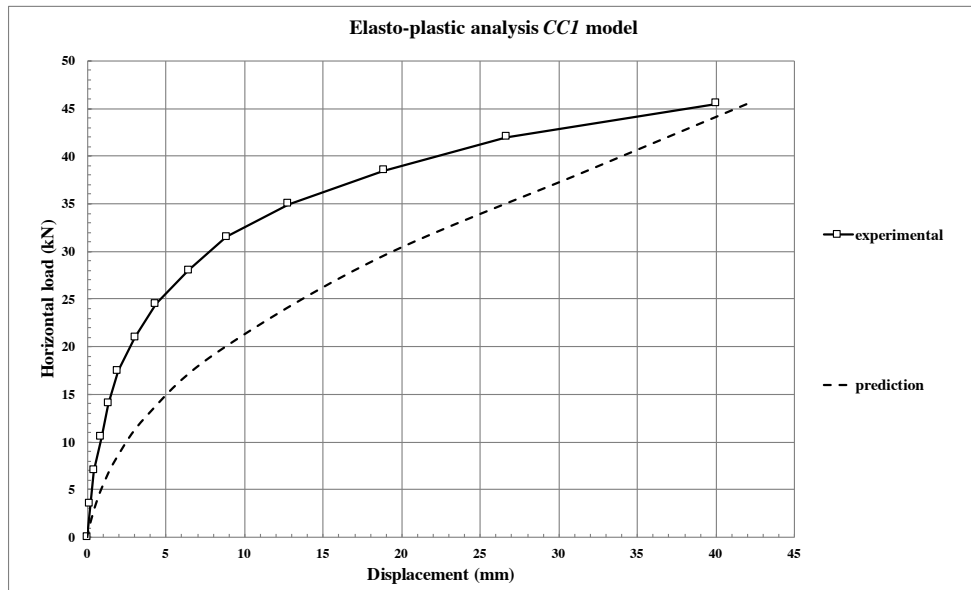


Figure 4.22. *CC1* prediction curve obtained by preliminary numerical ways.

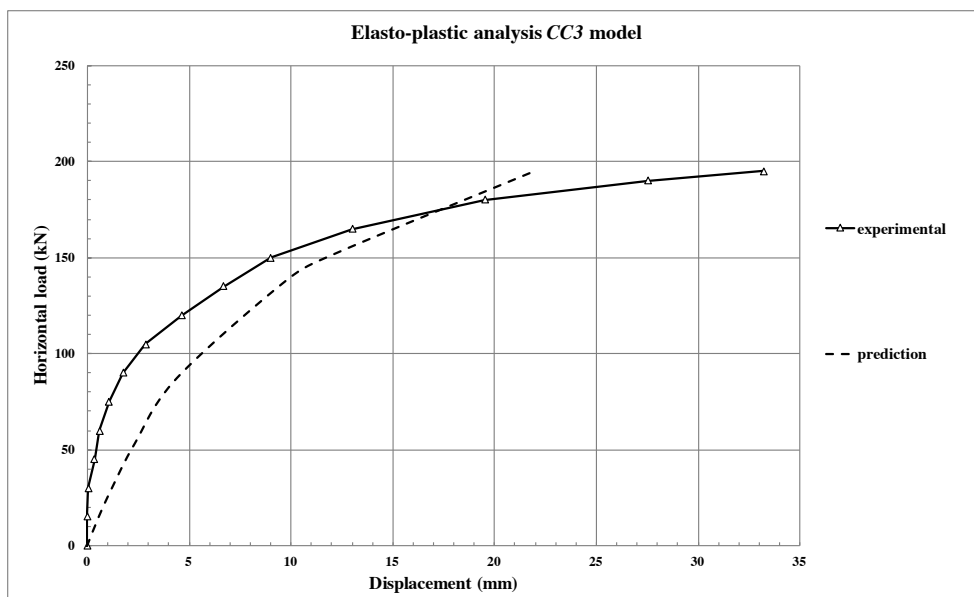


Figure 4.23. *CC3* prediction curve obtained by preliminary numerical ways.

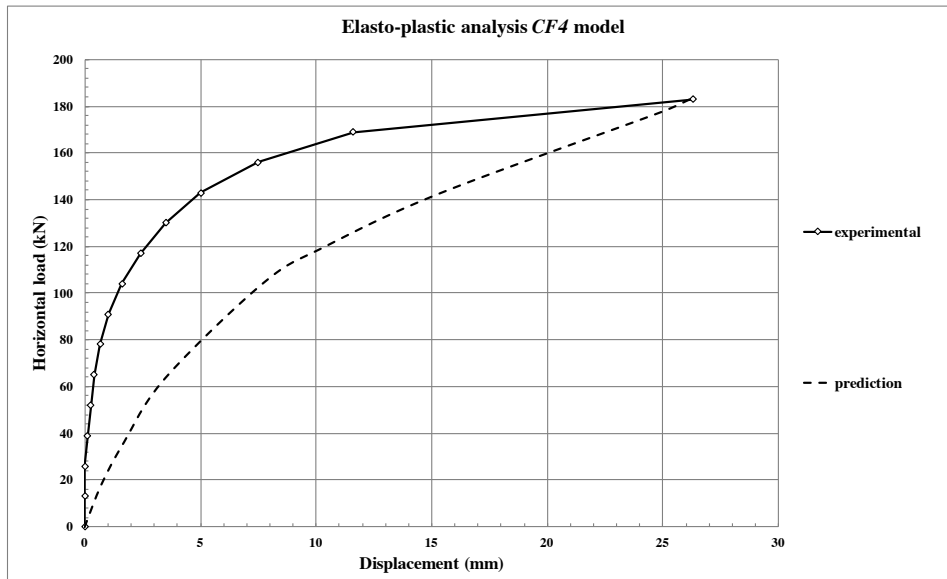


Figure 4.24. *CF4* prediction curve obtained by preliminary numerical ways.

Finally, those preliminary results obtained do not display satisfactory performance compared to the actual behavior observed in the field. Therefore, it will be necessary to make another adjustment to improve those numerical simulations.

### 4.3.3 DEVELOPMENT OF GENERAL MODELING FRAMEWORK

One main focus of this study is to develop a modeling framework representing the behavior of the piled raft systems. Abaqus 14.4 Standard Software was used for the finite element modeling (FEM) in this research work. This FEM package includes a large variety of material models and elements including facilities necessary for this particular subject of pile behavior under lateral loads. Some details and features of this software were already mentioned in chapter 3 section 3.4.4.

All numerical models are composed of four parts: soil dominium, concrete raft, concrete pile, and steel reinforcement. There are several important issues involving these materials and the constitutive models that simulate their behavior, as well as in relation to types, geometry and meshing, convergence and boundary conditions, analysis steps, etc. How these issues (modeling techniques) were handled is described in this section.

An overall piece of knowledge acquired regarding these issues is that the model must be rich enough to be able to capture the important phenomena, but it should not be more

complex than necessary since this would only increase the computer time needed. Afterward, in order to be able to verify the quality of the models, numerical results must be compared to experimental results; those data results and the charts obtained from them will be presented in Chapter 5.

### *Constitutive models*

#### *Concrete*

To simulate the plastic behavior of this material, the concrete damage plasticity constitutive model was employed (included in the Abaqus software library). It requires several values; for elastic behavior, the modulus of the concrete  $E_c$  and Poisson's ratio  $\nu$  are required. For plastic behavior five parameters are required, as well as from a concrete resistance laboratory test, the compressive behavior (yield stress, inelastic strain) and tensile behavior (yield stress, displacement).

From the compression strength of the concrete  $f_{ck}$ , the modulus of elasticity of the concrete  $E_c$  was obtained according to NBR 6118. A couple of strength–strain curves (compression and traction laboratory test results) correspond to this modulus, and those values together with five plastic parameters made up the input data representing the plasticity behavior of the concrete.

The five plastic parameters required are the dilation angle, the flow potential eccentricity, the ratio of initial equibiaxial compressive yield stress to initial uniaxial compressive yield stress, the ratio of the second stress invariant on the tensile meridian to that on the compressive meridian and the viscosity parameter that defines visco-plastic regularization. The values for defining the concrete plasticity behavior were set to  $15^\circ$ , and all the rest zero (González, 2014).

The interaction between the raft and the pile (or piles), depending on the analyzed foundation system, was neglected, setting as tie type between the contacts of both parts according to Abaqus Software.

### *Steel reinforcement*

The constitutive model used to simulate the steel reinforcement was the classical metal elastic-perfectly plastic model. The input data for the steel model includes elastic modulus, the Poisson's ratio and the yield stress. With respect to the interface between the concrete material and the steel material, a perfect bond between them was assumed in this work, setting as embedded region according to Abaqus Software.

### *Soil*

One of the main considerations for this material was to represent the soil dominium by the first three layers and discard all the rest, according to the laboratory report shown previously in Table 4.1. This decision was based on the fact that the horizontal loading has a depth influence between 3 to 5 times the diameter of the pile (Reese & Van Impe, 2001), resulting in a depth influence of around 1.25 m. The geologic profile displayed in Figure 4.2 gives a clear overall idea of the position of all piled raft systems embedded in the natural underground.

It is important to mention that part of the soil surrounding the raft was removed in order to be able to carry out the full-scale horizontal loading tests, so that the thickness of the excavation was equal to the raft of each of the piled raft systems tested, and wide enough to place all the necessary equipment and be able to correctly perform the works (see Figure 4.25). Therefore, the thickness of the soil profile was modified and taken into account to define the thickness of each layer that represents the soil dominium of the soil during the numerical simulations. Detailed information about this modified soil profile will be provided in the next section.

With regard to the constitutive model used to simulate soil behavior, the elasto-plastic Mohr-Coulomb model was selected. The input data were the elastic modulus of soil, Poisson's ratio, cohesion resistance, friction angle, and dilatancy angle (in all numerical analyses this last parameter was considered null).

With respect to the interface between the pile shaft and the surrounding soil, the  $\beta$  method was considered. This method can be used for both cohesive and cohesionless soils.

The method is based on effective stress analysis, and is suited for short and long-term analysis of pile load capacity (Helwany, 2007).

The contact between the pile tip and soil was considered to be a hard contact according to the software. With regard to the contact between the raft base and the ground surface, a tangential behavior was considered, using a frictional coefficient of 0.15 without shear stress limit (González, 2014).

### *Model geometry and element types*

3D simulations were performed to get an accurate approximation of the overall behavior, such as failure mode and other soil-structure interaction details. In the component parts of the model, such as steel bars and stirrups, pile and raft concrete, the geometry was totally defined.

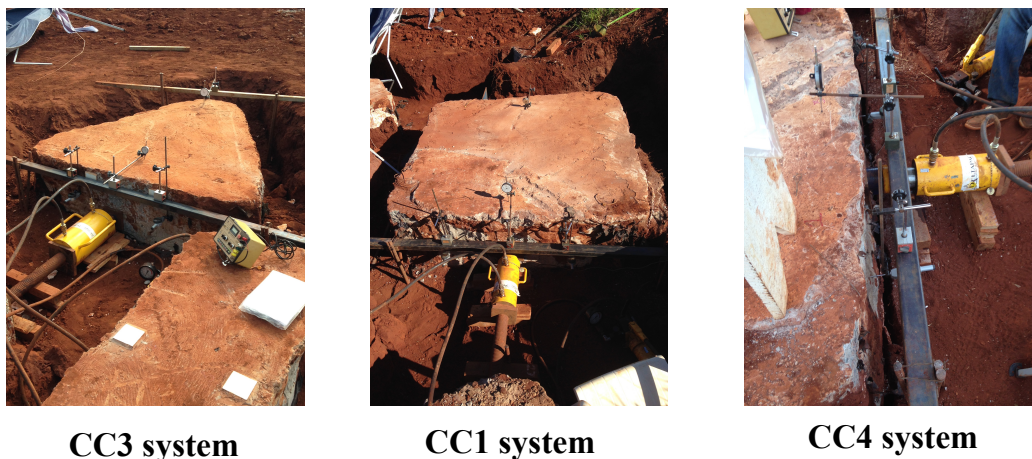


Figure 4.25. Clear space around the rafts of each of the piled raft systems was provided to place the equipment and to carry out the full-scale horizontal loading tests.

Since the soil does not have a defined geometry (size and shape), it was necessary to assume different geometries, such as a square prism and cylindrical shape (see Figure 4.26), considering as preliminary dimensions the following proportions displayed in Table 4.7.

These preliminary size proportions should be large enough to not interfere with the modeled phenomenon yet small enough to avoid high computational costs. The preliminary graphical results gave an idea about the best size and shape of this part (displacements close to zero at the edges of the domain).

Table 4.7. Soil dominium for the *CCI* piled raft system

Geometry	Dimensions
Square prism	Width = 10; times $B$ ; Height = $2 L_p$
Cylindrical	Diameter = 20 times $\phi_p$ Height = $2 L_p$

$B$  – width of the square raft;  $L_p$  - pile length;  $\phi_p$  - pile diameter

Otherwise, to model the piled raft systems, different 3D types of elements were used for the concrete, reinforcement steel, and the soil. Therefore, to obtain a good numerical approximation, it was necessary to carry out a sensitivity study varying the types of elements recommended by the Abaqus Manual and other works indicated in the literature.

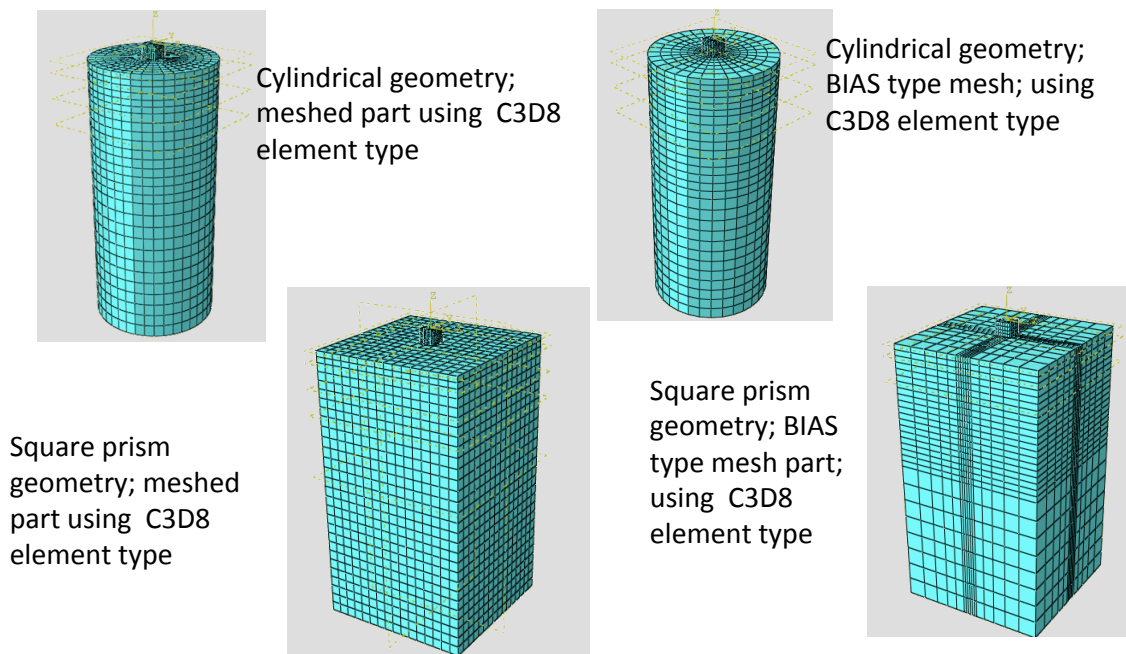


Figure 4.26. Different geometries and mesh type for soil part of the *CCI* piled raft system.

Figure 4.27 displays the different meshed part components of the *CCI* foundation system, using different 3D elements as follows: C3D6 (continuum element, third dimension, six nodes); C3D8 (continuum element, third dimension, eight nodes) and T3D2 (Truss element, third dimension, two nodes).

### *Mesh and convergence issues*

Preliminary results obtained with a rather coarse mesh showed that it was fairly difficult to obtain convergence and the results were not acceptable. The results obtained from a fine

mesh were more accurate. Even a finer mesh gave almost the same result as the previous mesh but more time was needed for computations. Therefore, a moderately fine mesh was chosen in this study based on a sensitivity study varying the element types for each material. The solution time with this mesh is approximately 1.0 hr (*CCI model*), using an Intel Core i5 2.53 GHz processor.

When performing a non-linear analysis, convergence difficulties may occur; one solution applied in this study was to use small enough time increments to ensure that the analysis will follow the load-displacement curve, which improved the convergence.

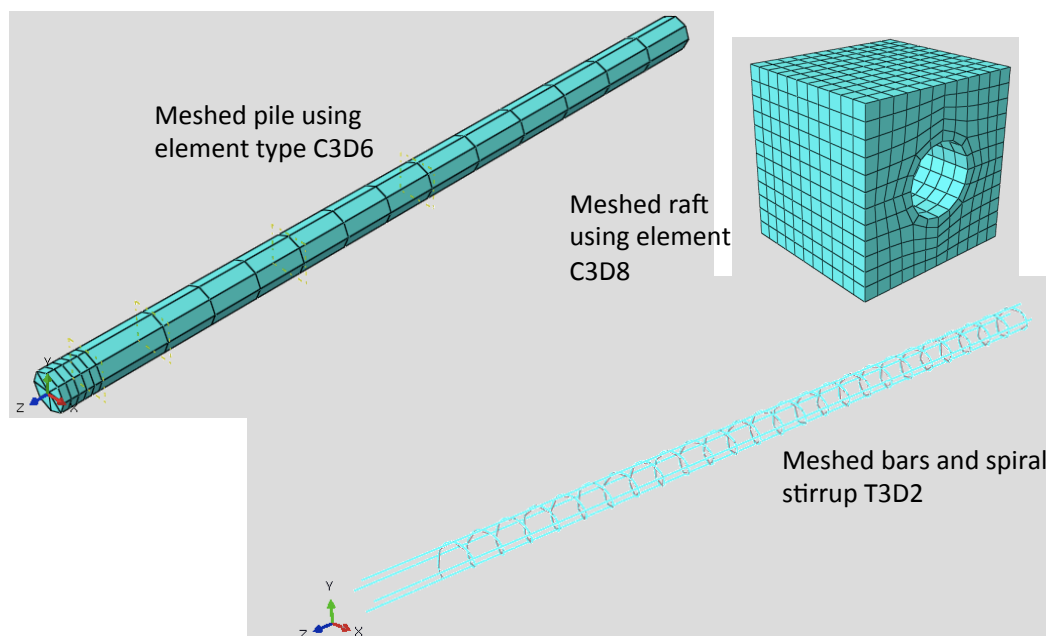


Figure 4.27. Components of the *CCI* piled raft system.

### *Boundary conditions*

Boundary conditions specify values of displacement and rotation constants at appropriate nodes, located in positions where they do not interfere with the simulated phenomenon (soil dominium large enough). In all cases herein studied, only the vertical displacement ( $z$  axis direction) was allowed in the external faces of the dominium; in all other directions the displacements and rotations were null, while at the base of the model in all directions ( $x,y,z$ ), the displacements and rotations were restricted to zero.



## *Analysis steps*

All simulated models in this research work were analyzed according to the following order:

- Step 1 – Geostatic stress state; an initial predefined stress state of the soil, equal to the geostatic stress state (compression stress) calculated by hand, was specified, and an opposite sign was set; that is, the soil traction stress state was set as input data and, therefore, a vertical displacement state was also induced. Then the software calculated the self-weight of the whole model (total assembly of all parts), resulting numerically in a compression stress state similar to that calculated by hand, so that the vertical displacements at the end of this step were very close to zero due to the equilibrium of the vertical displacements of traction and compression (see Figure 4.28). A static general analysis method was considered in this step.
- Step 2 –Incremental loading; a unit load was applied in a location corresponding to the experimental test, located at the center of one lateral face, at half the height of the raft in the positive direction  $y$  (see Figure 4.13). The type of analysis used in this step was the Static General method, as a requirement to avoid numerical convergence problems before using the Static Riks analysis method, in step number three.
- Step 3 – Horizontal “real” loading; the horizontal experimental load was applied in the same location described in the previous step. The Static Riks analysis was used because it is best suited to problems where there is an unstable buckling or collapse; it uses an arc-length method to determine the response of the loaded structure, where there are significant changes in the structure of stiffness. The Static Riks method uses the load magnitude as an additional unknown; it solves simultaneously for loads and displacements. Therefore, another quantity must be used to measure the progress of the solution (Abaqus Manual, 2014).

Based on the general modeling framework described in previous paragraphs, more detailed information about the foundation systems are presented as a summary (See Table 4.8). The initial considerations column in that table refers to initial modeling features, and the

final considerations column refers to the final definitive features used to obtain satisfactory numerical results.

To determine those indicated final considerations, the *CCI* foundation system model had to be run as many times as was necessary to get better numerical approximations every time, modifying in each run the parameters of the materials, changing the undefined geometry, trying different element types, varying the mesh density, and testing the numerical integration, among other changes.

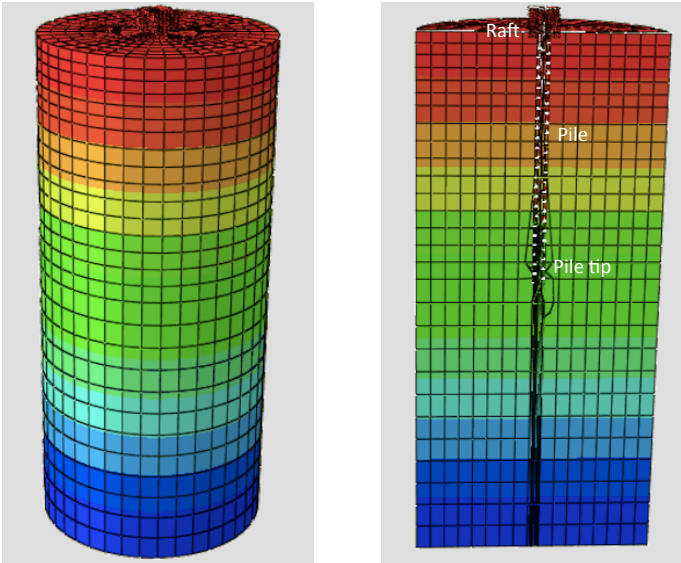


Figure 4.28. Graphical results of the final geostatic stress state for the *CCI* model. Analysis included a total assembly of all component parts.

Table 4.8. Detailed information of the modeling of the *CCI* piled raft system.

NUMERICAL MODELING SOFTWARE ABAQUS 14.4		
CONSTITUTIVE MODELS OF BEHAVIOR		
MATERIALS	INITIAL CONSIDERATIONS	FINAL CONSIDERATIONS
Soil	Geostatic Elastic Model Plastic Models: Mohr – Coulomb, Drucker – Prager modified and Cam–Clay modified	Geostatic Linear elastic behavior Mohr – Coulomb plastic behavior
Concrete	Self weight Elastic behavior	Self weight Elastic behavior Plastic behavior
Steel	Self weight Elastic behavior	Self weight Elastic behavior Plastic behavior

GEOMETRY AND SIZE OF THE PARTS		
PART	INITIAL CONSIDERATIONS	FINAL CONSIDERATIONS
Soil	Square prism geometry Width = 10 times $B$ Height = 2 times $L_p$	Cylindrical geometry Diameter = 20 times $\Phi_p$ Height = 2 times $L_p$
Raft, pile and rebars	Defined dimensions (full scale)	Defined dimensions (full scale)

INTERACTION AMONG THE PARTS		
PART	INITIAL CONSIDERATIONS	FINAL CONSIDERATIONS
Pile - soil	Tangential behavior (around the shaft) Normal Behavior (Pile tip)	Tangential behavior (around the shaft) Normal Behavior (Pile tip)
Raft - soil	Tangential behavior	Tangential behavior
Pile - raft	Perfect bond (no shear tension)	Perfect bond (no shear tension)
Pile - rebars	Perfect bond (no shear tension)	Perfect bond (no shear tension)
Raft - rebars	Perfect bond (no shear tension)	Perfect bond (no shear tension)

ELEMENT FINITE TYPE AND NUMERICAL INTEGRATION		
PART	INITIAL CONSIDERATIONS	FINAL CONSIDERATIONS
Soil (3D)	C3D8R, C3D4 (linear and quadratic integration)	C3D8R (linear)
Pile (3D)	C3D6, C3D8 (linear and quadratic integration)	C3D6 (linear)
Raft (3D)	C3D6, C3D8R (linear and quadratic integration)	C3D8R (linear)
Rebars (3D)	T3D2 (linear integration)	T3D2 (linear)

MESHING DENSITY		
PART	INITIAL CONSIDERATIONS	FINAL CONSIDERATIONS
Soil	A rather coarse mesh	A moderately fine mesh
Raft		A moderately fine mesh
Pile		A fine mesh
Rebars		A fine mesh

#### 4.3.4 PARAMETERS OF THE MATERIALS

This section presents the values of the required parameters of each material used during the numerical simulations. In all materials, the initial values were known from both at field and laboratory results (see section 4.3.2); therefore, it was possible to obtain a preliminary behavior of the foundation system. However, no single numerical result obtained was satisfactory when compared with the experimental test results; therefore, it was necessary to adjust partially or even completely those initial parameters and to make other considerations (see Table 4.8).

The variation or change rate of the initial parameters was carried out in relation to the coefficient of variation ( $C.V.$ ) or standard deviation value ( $s$ ) of each of the materials used for modeling; some of those data were supplied in previous studies related to this research work, and all missing data were obtained from the literature.

The initial and final parameters used during the numerical analysis of each material will be discussed separately below.

### *Soil material*

In accordance with the reasons discussed in the previous sections concerning the surrounding soil being removed and the depth of influence when lateral loading occurs, a simplified soil dominium composed of only three layers of different thickness was adopted; all reported parameters corresponding to the top two layers were kept (Table 4.1), and the third new layer was represented by the mean values from the 3<sup>rd</sup>, 4<sup>th</sup> and 5<sup>th</sup> original layers, for all parameters. That is why the shaded rows displayed in that table are of special interest, because all shafts of the piles cross over a thickness of 5.0 m, and all tips of the piles reach 5.0 m deep. The initial geotechnical parameters and the simplified soil dominium are presented in Table 4.9.

The coefficients of variation of each required geotechnical parameter are shown in Table 4.10. Figure 4.29 shows the different simplified soil dominium used for each piled raft system during the numerical simulations.

Table 4.9. Initial geotechnical parameters.

<b>INITIAL GEOTECHNICAL PARAMETERS USED DURING THE NUMERICAL SIMULATIONS</b>								
<b>Layer</b>	<b>Thickness (m)</b>	<b>Depth (m)</b>	<b><math>\gamma_{nat}</math> (kN/m<sup>3</sup>)</b>	<b><math>k_o</math></b>	<b><math>E_s</math> (Mpa)</b>	<b><math>\nu</math></b>	<b><math>c</math> (kPa)</b>	<b><math>\phi</math> (°)</b>
1	0.45	0.45	14.10	0.40	13.79	0.30	7.40	22.00
2	1.00	1.45	14.20	0.40	11.43	0.30	7.85	21.00
3	10.55	12.00	14.75	0.40	10.00	0.30	13.80	22.00

$\gamma_{nat}$  - Natural unit weight;  $k_o$  – Lateral stress ratio at rest;  $E_s$  – Undrained elastic soil modulus;  $\nu$  – Poisson’s ratio;  
 $c$  – Undrained cohesion;  $\phi$  – Undrained friction angle.

Table 4.10. Coefficients of variation of the soil parameters.

<b>SOIL</b>	
<b>Parameter</b>	<b>C.V. %</b>
<b><math>\gamma_{nat}</math> (kN/m<sup>3</sup>)</b>	2 - 8
<b><math>E_s</math> (Mpa)</b>	50
<b><math>c</math> (kPa)</b>	20 - 80
<b><math>\phi</math> (°)</b>	4 - 20

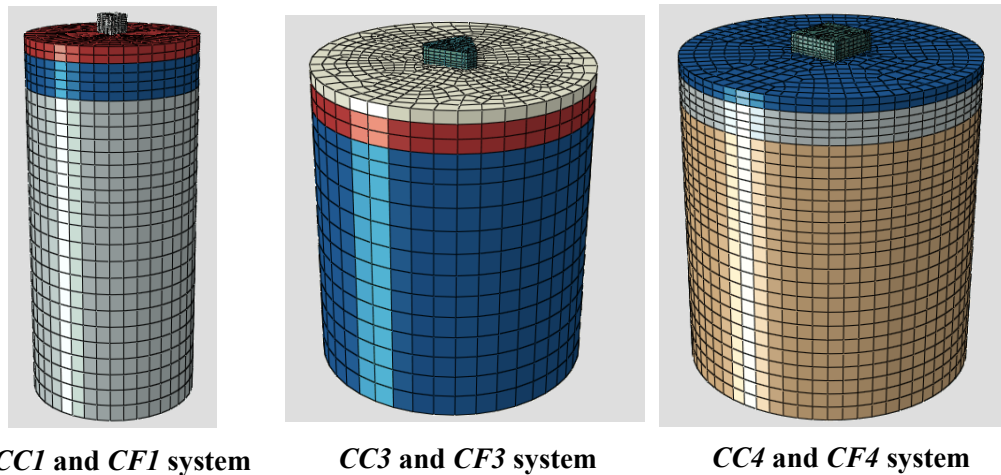


Figure 4.29. Simplified soil dominium composed of three layers used during the numerical simulations according to Table 4.9.

The final geotechnical parameters for this material are presented for each piled raft system numerically analyzed in Table 4.11; all those parameters were found by slowly adjusting the coefficients of variation mentioned before and respecting their range.

The first foundation system numerically analyzed was the *CC1* for being the “simplest model” (according to its total number of finite elements). The final geotechnical parameters were increased by 20%, 35%, and 6% for  $E_s$ ,  $c$  and  $\phi$  respectively, with respect to the initial geotechnical values (Table 4.9).

As a base line, and by analyzing Figure 4.16 (comparison of load-displacement experimental curves), it can be seen that the low stiffness of the *CC1* piled raft system is remarkable compared with all the other depicted systems; this difference is due to the number of piles, the geometry of those systems and the layout that they have at the experimental field.

It is important to remember that the stiffness modulus depends on the geometry of the system and the elastic soil modulus  $E_s$ . It was learned during the numerical simulation work that the geotechnical parameters, such as the elasticity soil modulus  $E_s$  and the cohesion  $c$ , had a great influence on the numerical behavior, whereas the friction angle  $\phi$  had a little less.

Other important aspects to highlight are that the natural soil structure was remolded during construction of the piled raft systems (drilled shafts), and subsequently by the previous vertical loading (full-scale tests) in the same piled raft systems here studied (Freitas Neto

2013), and that the initial geotechnical parameters used did not take into account the anisotropy of the soil. Therefore, the real alteration suffered by the soil under those imposed conditions and their current stress state at the experimental field are unknown.

Table 4.11. Final geotechnical parameters for each piled raft system analyzed.

*CC1 and CF1 foundation systems*

FINAL SOIL PARAMETERS FOR THE CC1 AND CF1 PILED RAFT SYSTEM								
Layer	Thickness (m)	$\gamma_{nat}$ (kN/m <sup>3</sup> )	$k_o$	(1.2) $E_s$ (Mpa)	$\nu$	(1.35) $c$ (kPa)	(1.06) $\phi$ (°)	$f_s$ (kPa)
1	0.45	14.10	0.40	16.55	0.30	10.00	23.32	2.73
2	1.00	14.20	0.40	13.72	0.30	10.60	22.26	3.78
3	10.55	14.75	0.40	12.00	0.30	18.63	23.32	12.41

*CC3 foundation system*

FINAL SOIL PARAMETERS FOR THE CC3 PILED RAFT SYSTEM								
Layer	Thickness (m)	$\gamma_{nat}$ (kN/m <sup>3</sup> )	$k_o$	(3.6) $E_s$ (Mpa)	$\nu$	$c$ (kPa)	$\phi$ (°)	$f_s$ (kPa)
1	0.45	14.10	0.40	49.64	0.30	7.40	22.00	2.56
2	1.00	14.20	0.40	41.15	0.30	7.85	21.00	3.54
3	10.55	14.75	0.40	36.00	0.30	13.80	22.00	11.63

*CF3 foundation system*

FINAL SOIL PARAMETERS FOR THE CF3 PILED RAFT SYSTEM								
Layer	Thickness (m)	$\gamma_{nat}$ (kN/m <sup>3</sup> )	$k_o$	(3.6) $E_s$ (Mpa)	$\nu$	(0.7) $c$ (kPa)	(0.92) $\phi$ (°)	$f_s$ (kPa)
1	0.45	14.10	0.40	49.64	0.30	5.18	20.24	2.34
2	1.00	14.20	0.40	41.15	0.30	5.50	19.32	6.47
3	10.55	14.75	0.40	36.00	0.30	9.66	20.24	10.08

*CC4 foundation system*

FINAL SOIL PARAMETERS FOR THE CC4 PILED RAFT SYSTEM								
Layer	Thickness (m)	$\gamma_{nat}$ (kN/m <sup>3</sup> )	$k_o$	(8.0) $E_s$ (Mpa)	$\nu$	(1.2) $c$ (kPa)	(1.2) $\phi$ (°)	$f_s$ (kPa)
1	0.45	14.10	0.40	110.32	0.30	8.88	26.40	3.15
2	1.00	14.20	0.40	91.44	0.30	9.42	25.20	8.69
3	10.55	14.75	0.40	80.00	0.30	16.56	26.40	13.57

*CF4 foundation system*

FINAL SOIL PARAMETERS FOR THE CF4 PILED RAFT SYSTEM								
Layer	Thickness (m)	$\gamma_{nat}$ (kN/m <sup>3</sup> )	$k_o$	(5.0) $E_s$ (Mpa)	$\nu$	(0.9) $c$ (kPa)	(0.9) $\phi$ (°)	$f_s$ (kPa)
1	0.45	14.10	0.40	68.95	0.30	6.66	19.80	2.28
2	1.00	14.20	0.40	57.15	0.30	7.07	18.90	6.32
3	10.55	14.75	0.40	50.00	0.30	12.42	19.80	9.84

$\gamma_{nat}$  - Natural unit weight;  $k_o$  - Lateral stress ratio at rest;  $E_s$  - Undrained elastic modulus of the soil;  $\nu$  - Poisson's ratio  $c$  - Undrained cohesion;  $\phi$  - Undrained friction angle.

It should be noted that all experimental curves depicted (Figure 4.16) intrinsically show those effects, among others, so it was necessary to increase this parameter  $E_s$  slowly until approaching the experimental results for the elastic behavior. The same justification was considered for the other  $c$  and  $\phi$  parameters as well for the plastic behavior.

In the case of the *CC3* foundation system, the elasticity soil modulus was 3.6 times greater than the initial parameter, and the cohesion and friction angle original values were kept (see Table 4.11). Here it was not possible to respect the variation rate mentioned in Table 4.10 for this particular parameter, due mainly to ignorance of the real conditions of the soil dominium after the construction and vertical loading works described previously.

By contrast, for the *CF3* foundation system, the same  $E_s$  used for the *CC3* foundation system was kept and the cohesion and friction angle were decreased by 30% and 8% respectively, with respect to the initial parameters shown in Table 4.9.

For the *CC4* an 8-fold increase was used for the elasticity soil modulus along with an increase of 20% for the cohesion and friction angle, with respect to the initial parameters (see Table 4.11). Finally, for the *CF4* system a 5-fold increase was used for the elasticity soil modulus along with decreases of 10% for the cohesion and friction angle, with respect to the initial parameters, also shown in Table 4.11.

According to all tables previously displayed, it should be noted that from the final geotechnical parameters for the *CCI* foundation system, it was possible through parametrical study to numerically simulate the behavior of the *CFI* foundation system (no lateral loading test was carried out on this system); this type of study will be explained in chapter 5.

Finally, the last column in all tables above shows the friction stress value ( $f_s$ ), used as an interface parameter between the soil and the shaft of the pile. The friction stress  $f_s$  between the pile and the surrounding soil can be calculated by multiplying the friction factor  $\mu$  by the horizontal effective stress  $\sigma'_h$ :

$$f_s = \mu \cdot \sigma'_h \quad (4.1)$$

But

$$\sigma'_h = k_o \cdot \sigma'_v \quad (4.2)$$

where:  $\sigma'_v$  is the vertical effective stress at the center of the soil layer, and  $k_o$  is the lateral stress ratio at rest. Therefore:

$$f_s = \mu \cdot k_o \cdot \sigma'_v = \beta \cdot \sigma'_v \quad (4.3)$$

In clays, the value  $\mu$  can be estimated with the following expression (Burland, 1973):

$$\mu = \tan \frac{2}{3} \phi' \quad (4.4)$$

For sands, values ranging from 0.15 and 0.35 are suggested (McClelland, 1974).

### Concrete material

With regard to this material, and by following the same logic applied to the soil material, some initial parameters were taken (see section 4.2) and preliminary numerical approximations obtained; thereafter it was necessary to change some values, respecting the range of variation of the coefficients (see Table 4.12); some of these parameters and coefficients were reported in previous studies conducted on these same foundation systems (Freitas, 2013, and Garcia, 2015).

Table 4.12. Coefficients of variation of the concrete. (Garcia, 2015).

<b>CONCRETE</b>	
<b>Parameter</b>	<b>C.V. %</b>
$f_{ck}$ (MPa)	17
$E_c$ (MPa)	13

Table 4.13 displays the concrete components, the raft and the intact and defective piles, as well as the initial and definitive parameters used during the numerical simulations.

Table 4.13. Concrete parameters adopted for all piled raft systems numerically simulated.

<b>Concrete Parameters</b>						
<b>Part</b>	$\gamma_c$ (kN/m <sup>3</sup> )	$f_{ck}$ (MPa)	$E_c$ (GPa) <i>initial</i>	(1.1) $E_c$ (GPa) <i>final</i>	$\nu$	<b>Plasticity behavior (MPa)</b>
Raft	21.58	36.70	45.00	49.50	0.20	-----
Integer pile	21.58	36.70	45.00	49.50	0.20	40.00
Defective pile	21.58	20.00	5.90	---	0.20	2.00

$\gamma_c$  - Unit weight;  $f_{ck}$  - Stress compression;  $E_c$  - Elasticity modulus;  $\nu$  - Poisson's ratio

Starting from the strength compression concrete  $f_{ck}$ , the elasticity modulus concrete  $E_c$  calculated through the NBR 6118 was obtained. Only this parameter had to be modified,



resulting in a 10% increase over the initial value. Moreover, the plasticity behavior input data (traction and compression) were obtained for a resistance of 40.0 and 2.0 MPa as indicated in Table 4.13, and the values were taken from the concrete manufacturer specifications.

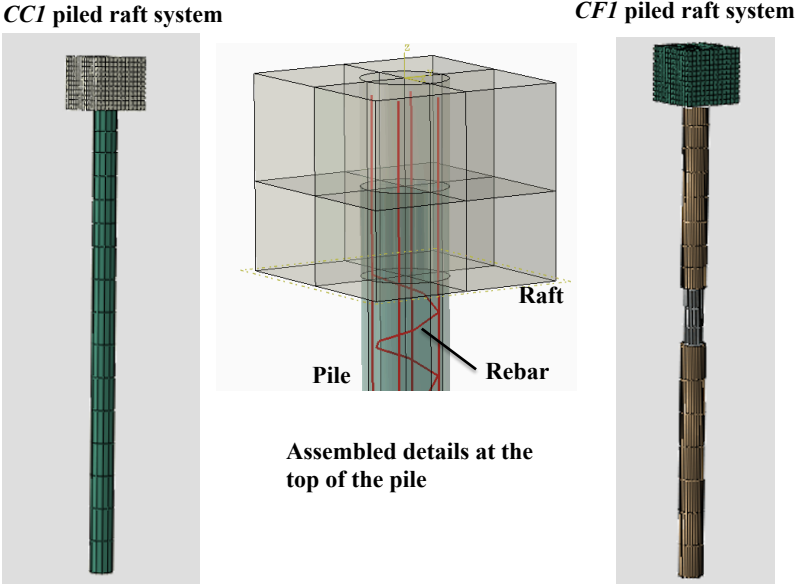


Figure 4.30. CC1 and CF1 concrete piled raft systems.

According to the experiences acquired during the numerical simulations, it was observed that this material does not change its behavior too much when increasing  $E_c$ . Figure 4.30 and Figure 4.31 display the piled raft part modeled in Abaqus software for each of the foundation systems.

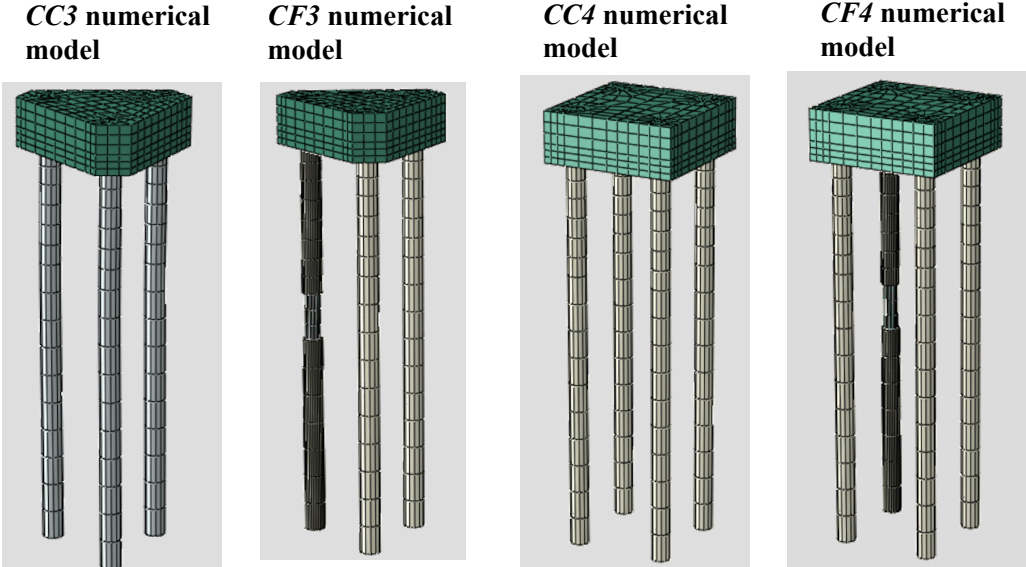


Figure 4.31. CC3, CF3, CC4 and CF4 concrete piled rafts systems.

### Steel material

With regard to this material, and following the same path taken with the other two materials considered, some initial parameters were taken (see section 4.2) and preliminary numerical approximations obtained; afterwards it was necessary to change some values, keeping the range of the coefficients of variation (see Table 4.14); all these coefficient values were found in CA-50 steel manufacturer specifications.

Table 4.14. Coefficients of variation for steel material.

<b>STEEL</b>	
<b>Parameter</b>	<b>C.V. %</b>
$f_{yk}$ (MPa)	5 - 10
$E_{steel}$ (GPa)	10
<b>Yield stress</b> (MPa)	$(0.1 - 1.0) E_{steel}$

Table 4.15 displays the steel components, rods and stirrups, as well as the initial and definitive parameters used during the numerical simulations. The only parameter modified to get a good numerical approximation was the yield stress within a very small variation range (0.23% – 0.28%) \*  $E_{steel}$ , with its value depending on the piled raft system numerically simulated.

Table 4.15. Steel parameters adopted for numerically simulated piled raft systems.

<b>Steel Parameters</b>							
<b>Rebars</b>	$\gamma_c$ (kN/m <sup>3</sup> )	$E_{steel}$ (Gpa)	$\nu$	$F_{yk}$ (Mpa)	<b>Yield Stress (Mpa)</b> [0.28 (%) * $E_{steel}$ ]	$\phi_r$ (mm)	<b>Transversal area (m<sup>2</sup>)</b>
Rods	77.01	231.00	0.30	500.00	646.80	10.00	7.85E-05
Stirrups	77.01	231.00	0.30	500.00	646.80	6.30	3.12E-05

The experience acquired during the numerical simulations was that this material had the lowest behavioral variations when compared to the other two materials. Figure 4.32 and Figure 4.33 display the piled raft part modeled in Abaqus software for each of the foundation systems.

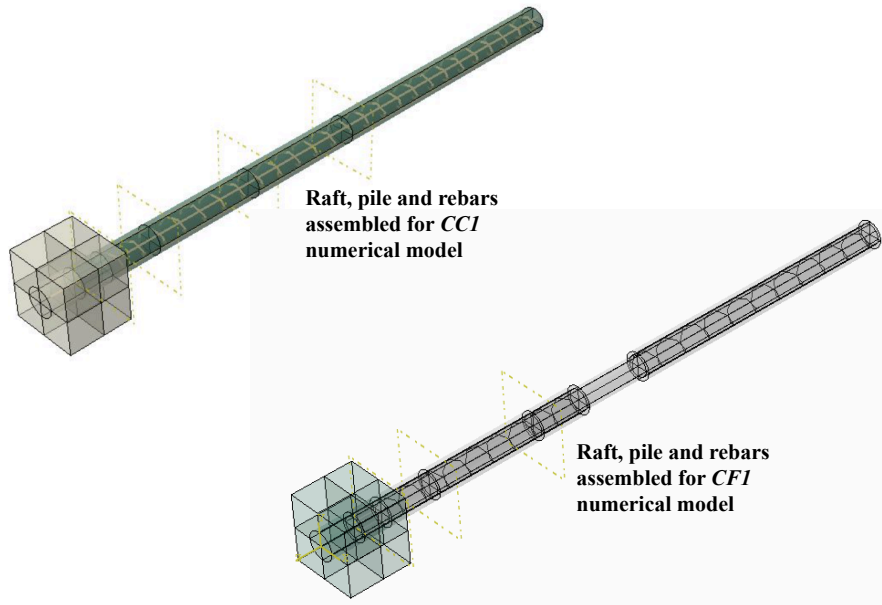


Figure 4.32. Rebar placed inside *CC1* and *CF1* piled rafts.

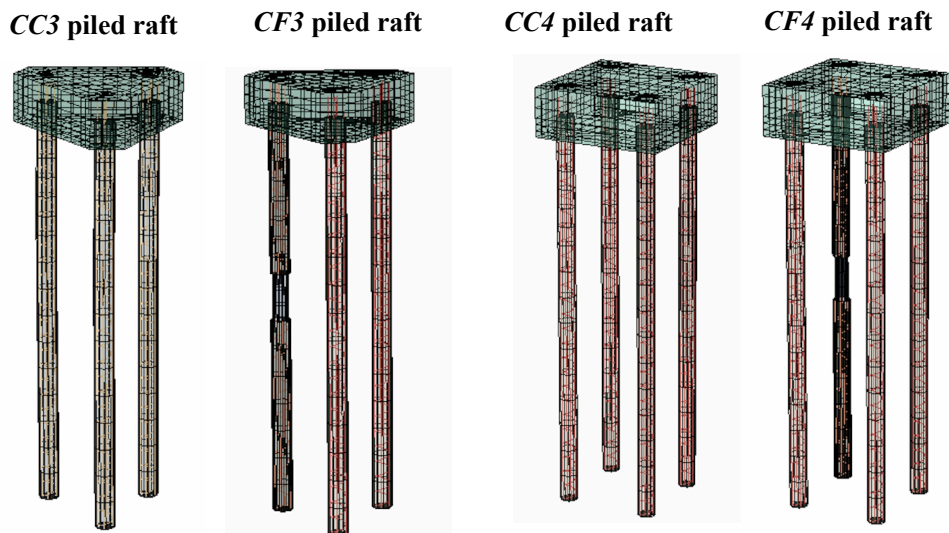


Figure 4.33. Rebar placed inside *CC3*, *CF3*, *CC4* and *CF4* piled rafts.

### 4.3.5 NUMERICAL MODELING METHODOLOGY

This section presents a step-by-step general methodology for numerical modeling, which was established on the basis of experiences learned during numerical works carried out for the *CC1* piled raft model in this study.

**Error! Reference source not found.** Table 4.16 displays that methodology followed during the modeling for that foundation system. Some additional comments in relation to this table are presented immediately below:

- Stages I to IV could be named the “*hard analysis*” because in each one of them it is necessary to pay attention to a lot of small details to get the software to run properly and obtain logical results, and thus be able to move on to the next stage.
- Stages V to VIII could be named the “*fine analysis*” because only a few details and more accurate results are being handled; some of these stages do not need to be followed in this strict order and it is possible to use some of them at the same time. It will depend on the skills of the user.
- After obtaining an acceptable, reliable and satisfactory numerical model, parametric studies may be carried out.
- All users should consider two very important but basic factors not previously mentioned: perseverance and patience. Both will be necessary.

Table 4.16. General methodology for numerical simulations.

STAGE	NUMERICAL SIMULATION METHODOLOGY	ANNOTATIONS
<b>Preliminary</b>	Understand the model that will be simulated numerically; clarify the role of each of the parts that make it up, as well as the interaction between them. This will help to simplify the simulation of the model. The choice of numerical software to be used will depend on the constitutive models of the materials it contains, different types of finite elements, meshing algorithms and numerical integration, among other factors.	It is recommended to read the libraries of the software itself, and get information about its capacity and limitations.

<b>HARD ANALYSIS</b>	STAGE	NUMERICAL SIMULATION METHODOLOGY	ANNOTATIONS
	<b>I</b>	Draw all parts of the model, those that have a defined geometry and size, and those that should assume an initial domain size and shape; then set initial parameters of each material involved in the phenomenon to be simulated. Assign to the model an initial coarse mesh and some recommended finite elements for each material. Review the software manual and study which are the most suitable depending on the phenomenon to be modeled.	Find out the coefficients of variation of all materials involved in the model.

	<b>II</b>	Run the geostatic analysis of the complete assembled model, that is, evaluate the self-weight including all parts that compose the model. It is necessary to have previously an idea beforehand about the geostatic stress state.	Run the model until getting good approximations (experimental results were obtained previously)
	<b>III</b>	Run an elastic analysis of the complete assembled model, keeping or varying the elastic parameters, trying to respect their corresponding coefficients of variation as much as possible. Compare the numerical results with the experimental ones in the elastic stretch.	
	<b>IV</b>	Run an elastic-plastic analysis of the complete assembled model, keeping or varying only the plastic parameters, trying to respect their corresponding coefficients of variation as much as possible. Compare the numerical results with the experimental ones in the overall stretch.	

FINE ANALYSIS	STAGE	NUMERICAL SIMULATION METHODOLOGY	ANNOTATIONS
	<b>V</b>	Choose and try different types of finite elements recommended for each material (study of the type of element).	Run the model until getting accurate or at least satisfactory results
	<b>VI</b>	Choose and try different types of numerical integration. It might be reduced, linear, and quadratic, and will depend on the finite element type chosen.	Run the model until getting good approximations (experimental results were obtained previously)
	<b>VII</b>	Choose and try different sizes and shapes for the non-defined parts (study of the type and size of the part).	
	<b>VIII</b>	Try different mesh sizes such as medium, fine and very fine (density study of mesh). Take into account the computational cost. The optimal mesh density will be the one that provides accurate results, when compared to the experimental results of the phenomenon, in the shortest time possible.	

STAGE	NUMERICAL SIMULATION METHODOLOGY	ANNOTATIONS
<b>IX</b>	An acceptable and reliable fitted numerical model has the smallest error rate between numerical and experimental results.	Acceptable numerical model
<b>X</b>	Parametrical studies. Starting from the acceptable numerical model it is possible to represent other hypothetical cases, by only changing the geometry of the parts, as well as the magnitude, position and direction of the loading.	Impossible to compare results



# 5 RESULTS AND DISCUSSION

As a summary of all works carried out for each foundation system, both experimental and those derived from numerical modeling, this section presents the most relevant aspects of this research work, the comparisons between the experimental measurements versus numerical simulation for each piled raft, and some parametric studies from some of those systems.

Next, in relation to only the *CCI* piled raft system, and based on the numerical methodology explained in **Error! Reference source not found.** (see chapter 4), the results from each stage until getting satisfactory results are presented, followed by the acceptable numerical model.

## 5.1 EVALUATION OF BACK ANALYSIS METHODOLOGY

After obtaining a satisfactory geostatic performance of the model (stage II of the numerical methodology), several numerical runs were conducted during the elastic analyses ( $T_{i\_elastic}$  up to  $T_{n\_elastic}$ ), beginning by setting initial values of the elastic parameters and then plotting the numerical results; thereafter, it was necessary to vary them (initial values) bit by bit, until obtaining good approximations or even satisfactory results (see Figure 5.1).

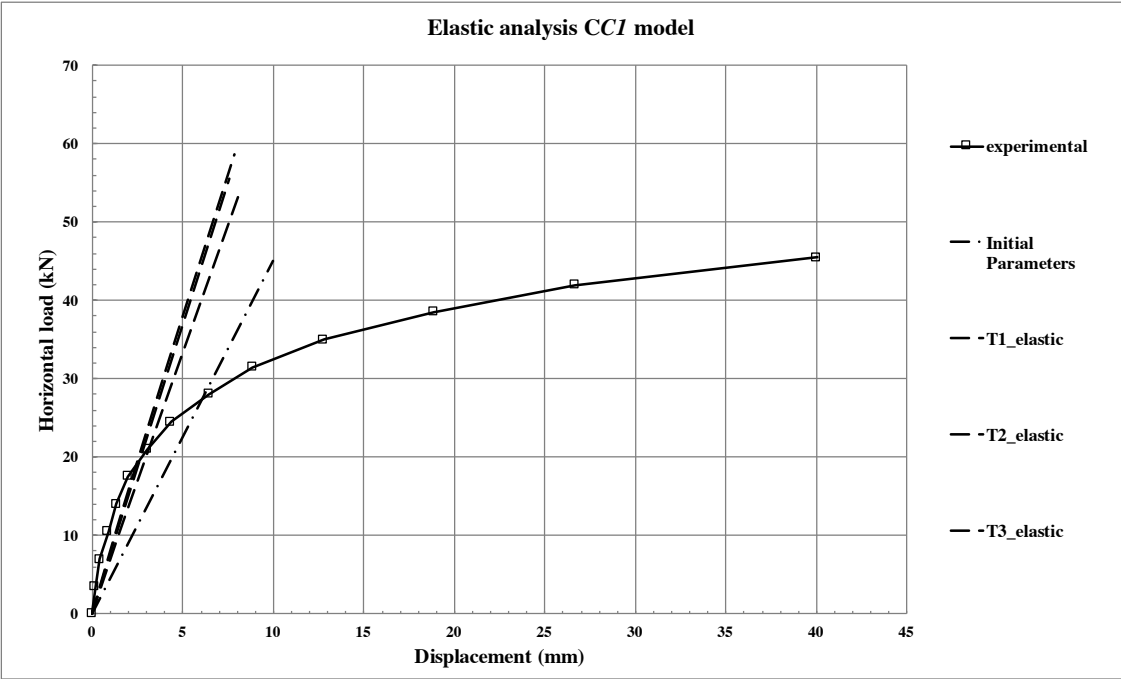


Figure 5.1. Elastic analysis shows some different approximation tests.

In the same way as for the elastic analysis, several numerical runs were conducted during the elastic-plastic analyses ( $T_{1\_elast-plast}$  up to  $T_{n\_elast-plast}$ ), varying the parameters bit by bit and then plotting the numerical results every time, until getting good approximations (see Figure 5.2).

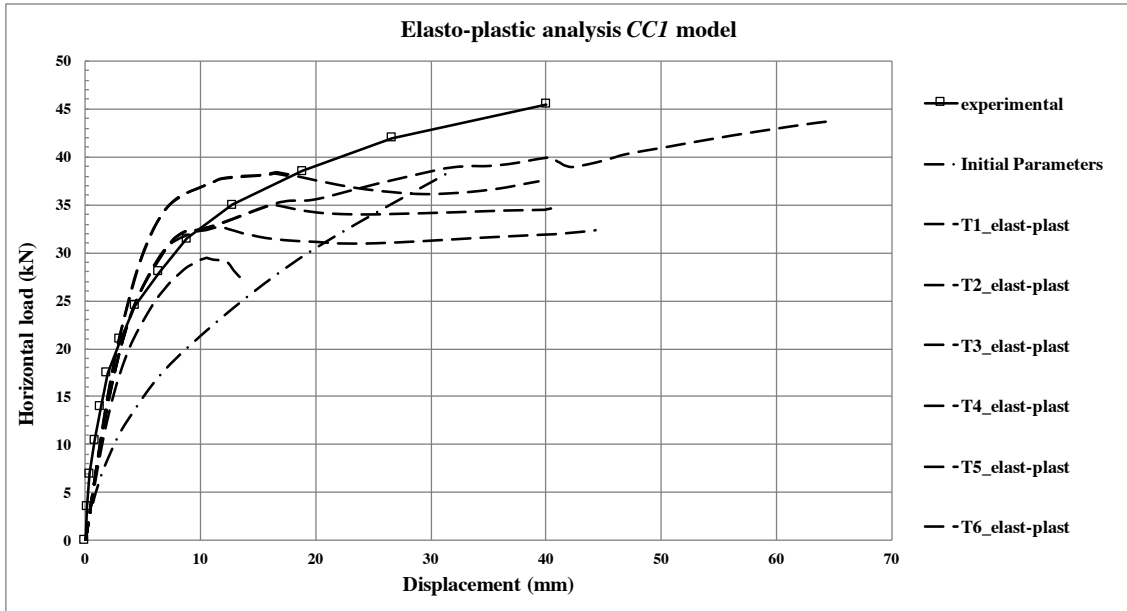


Figure 5.2. Elastic-plastic analysis shows some different approximation tests.

Afterwards, an element type study was performed (see Table 4.8), obtaining different numerical curves with respect to the experimental curve; many numerical attempts were carried out, testing and making different element combinations in each material and in each numerical run (type\_1 up to type\_n). See Figure 5.3.

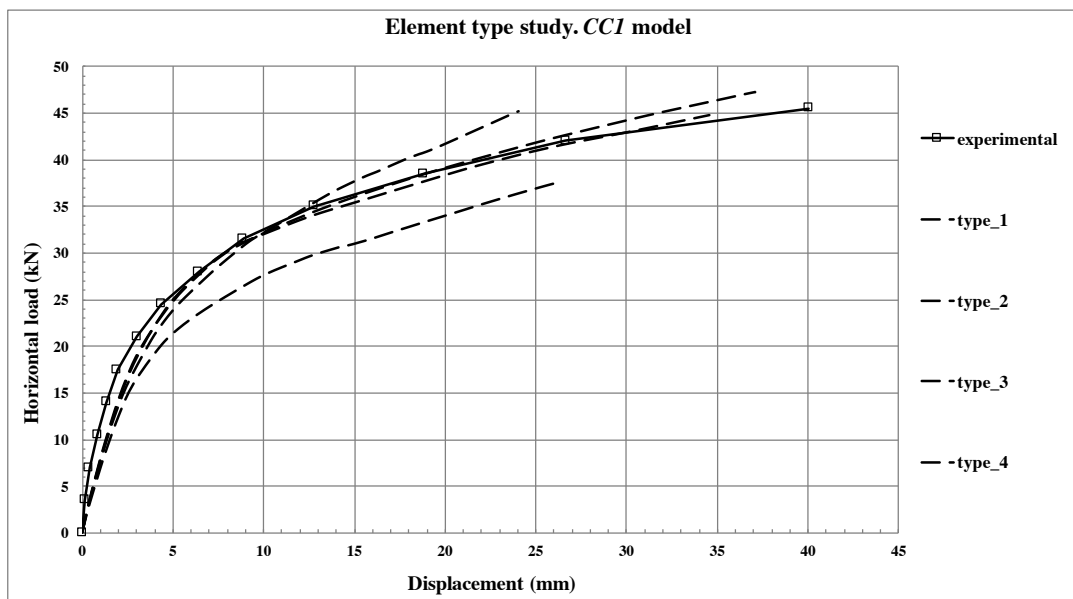




Figure 5.3. Element type study shows some different approximation tests.

Then a shape and size study was done, changing these features only in the non-defined geometry part of the model (soil), as was shown in Figure 4.26; it was possible to make some combinations with the element type study, and then plot the numerical curves obtained with respect to the experimental curve ( $T_1$  up to  $T_n$ ). Figure 5.4 displays those numerical approximations.

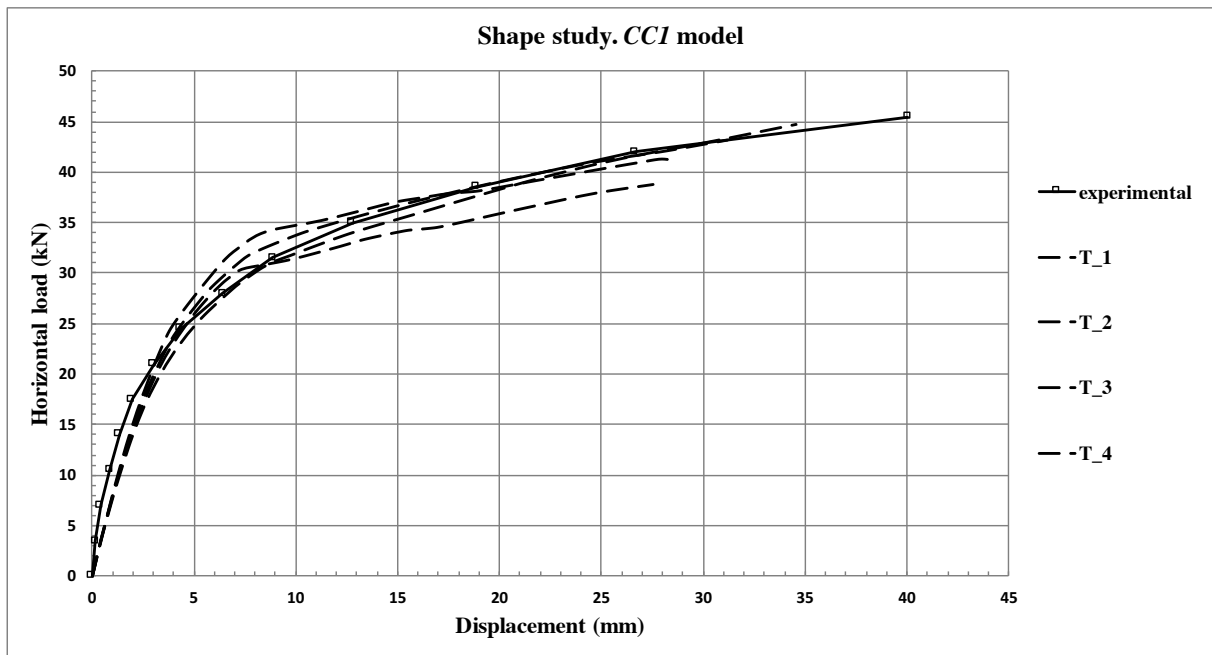


Figure 5.4. Shape and size study shows some different approximation tests.

According to the general methodology, one of the final stages is the meshing density study (stage VIII); prior to this stage, the best type element for each material, type of numerical integration, size and geometry of the non-defined parts, and a good meshing algorithm were already established; as a result, all that remains now is to vary the size of the elements and to find out accurate results (best fitting) in the shortest time possible.

During those previous studies, stages V to VII, it was observed that the most influential part in the overall behavior of the model was the soil, so this meshing density study was focused on it.

Several soil parts were tried with different mesh openings, such as 50, 45, 40, 35, 30 and 25 cm, then the numerical results were plotted for each numerical run, and displayed in Figure 5.5.

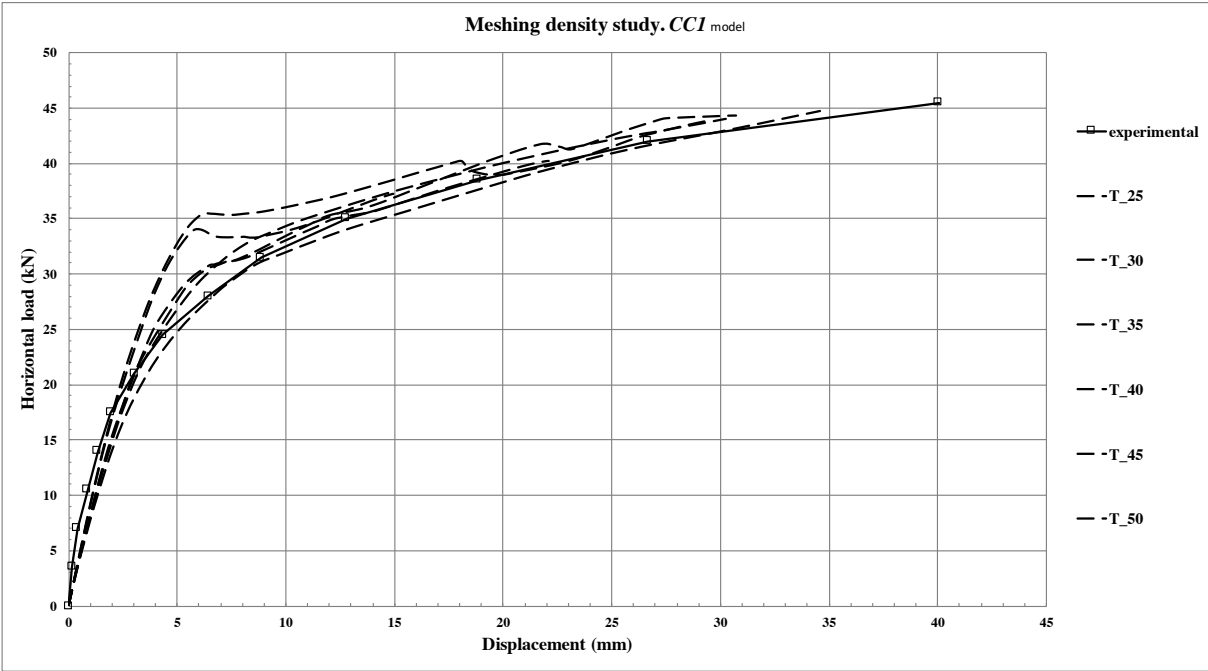


Figure 5.5. Meshing density study shows different approximation tests.

It can be seen in the plotted results in the chart above that there are several curves that approximate to the experimental curve, so it was necessary to choose the best fitted curve.

To evaluate the forecast accuracy, the percentage error was introduced, given by:

$$error(\%) = 100 \cdot \frac{|y_i - \hat{y}_i|}{y_i} \tag{5.1}$$

$y_i$  – denotes the  $i_{th}$  observation;  $\hat{y}_i$  – denotes a forecast of  $y_i$ .

A point-by-point comparison can be made between the experimental and numerical curves, meaning that the experimental and numerical displacement values were obtained from the same horizontal load. For example, under the 28 kN load, the experimental displacement is 6.44 mm, and for each mesh opening there is a corresponding specific calculated displacement. This value was chosen because it is at this horizontal load in the chart above that the other curves are the most points away from the experimental curve.

Therefore, using that experimental displacement value of 6.44 mm as reference, the horizontal displacement under the same horizontal loading was calculated for each test with a different mesh opening. The values obtained are shown in Table 5.1.

Table 5.1. Numerical error.

MESH OPENING	TOTAL FINITE ELEMENTS	EXPERIMENTAL LOAD (kN)	EXPERIMENTAL DISPLACEMENT (mm)	NUMERICAL DISPLACEMENT (mm)	ERROR (%)
50 cm	6,911	28.00	6.44	3.70	42.55
45 cm	7,823	28.00	6.44	4.00	37.89
40 cm	10,403	28.00	6.44	5.47	15.06
35 cm	13,375	28.00	6.44	5.27	18.17
30 cm	15,191	28.00	6.44	5.53	14.13
<b>25 cm</b>	<b>20,539</b>	<b>28.00</b>	<b>6.44</b>	<b>6.60</b>	<b>2.48</b>

Also, the analysis for the 20 cm mesh opening was carried out; however, it was not possible to run the model because when the shape factor between the finite elements loses the width – height proportion, then problems of numerical convergence arise.

Figure 5.6 shows graphically the variation in percentage error according to the mesh opening.

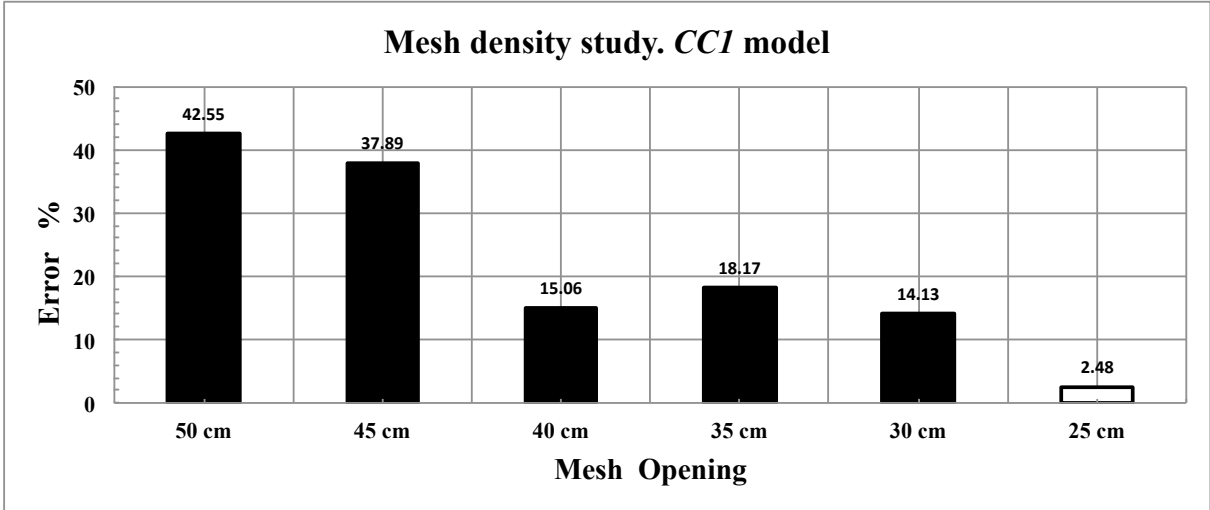


Figure 5.6. Mean absolute percentage error.

Based on the previous study, the mesh chosen to analyze the *CCI* model had an opening of 25 cm, total finite elements of 20,539 (complete assembled model), and a percentage error equal to 2.48%. The software ran for approximately 1 hr and 25 min. Finally, after complying

with the proposed general methodology, an acceptable and reliable numerical model was generated and is displayed in Figure 5.7.

However, the definitive *CCI* piled raft numerical model had 13,743 total finite elements, since the graphical results obtained showed that the influenced soil depth due to lateral loading was between 3 to 5 times the diameter of the pile, which means the lateral loading happens at a shallow depth between 0.75 and 1.25 m deep.

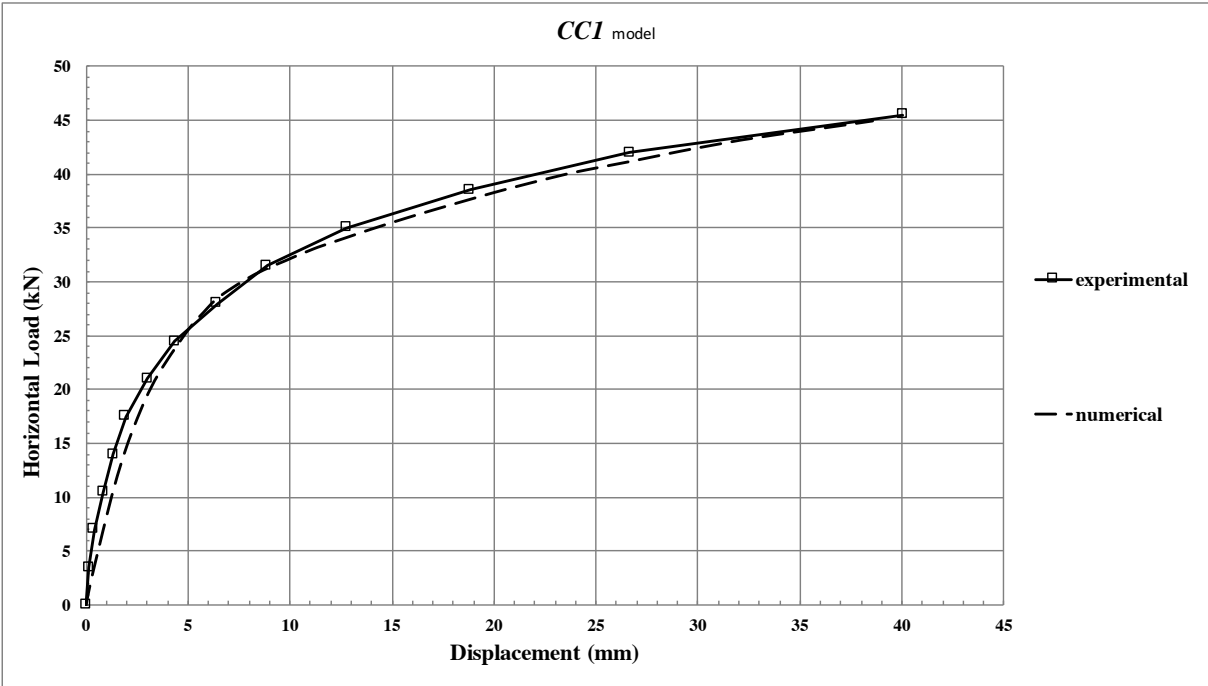


Figure 5.7. Acceptable and reliable numerical results.

In other words, it was not necessary to refine the mesh in the whole soil dominium; indeed, the mesh was carefully refined only in the first two layers until 1.45 m deep, and less refined between 1.45 m deep and the pile tip, located 5.0 m deep; from the pile tip until 12.0 m deep the mesh was significantly finer, always being mindful of the proportions of shape (width – height) of the finite element used, so as not to have numerical convergence problems.

Carrying out the procedures described above resulted in a reduction in the number of elements to analyze in the complete assembled model, and a saving of time in the numerical analysis but obtaining the same numerical and graphical results as the model that used more

finite elements. This is exactly what the preliminary stage refers to in the general methodology, being aware of the role of each part of the model.

Figure 5.8 shows the graphical results of the horizontal displacements in the same direction as the horizontal loading. It is possible to observe the formation of a failure wedge in the front area of the pile (passive zone), and it was possible to evaluate the angle that was formed with respect to the ground surface, which was very close to  $\theta = 45 + \frac{\phi}{2}$ , which is the angle of the failure plane according to Mohr-Coulomb criteria.

It should be noted that a gaping hole was formed between the pile and the back soil (active area). It should also be highlighted that this powerful Abaqus software feature allows graphically showing a separation between the parts (soil and pile), in spite of the fact that finite elements theory is based on continuum medium.

**CCI piled raft system**

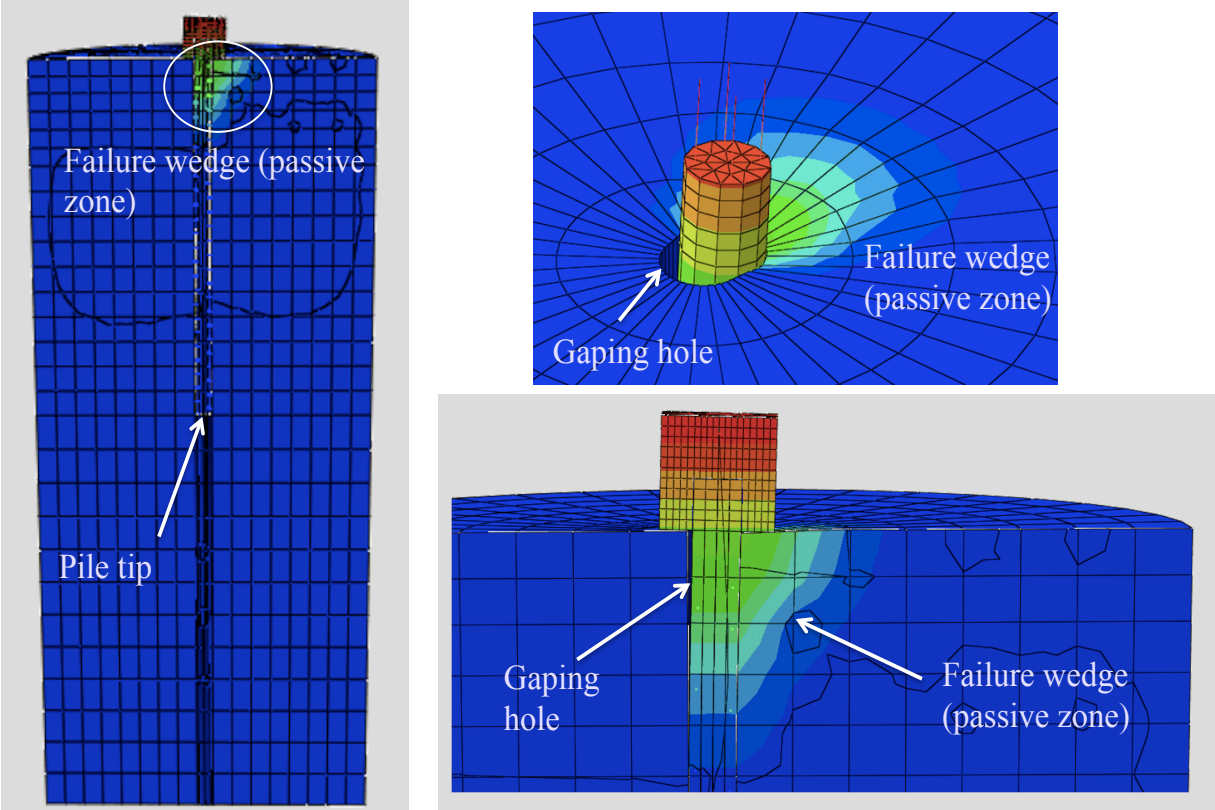


Figure 5.8. Graphical results of the horizontal displacements. CCI foundation system.

## *Discussion*

The *CCI* piled raft Abaqus model was the basis for carrying out all numerical works here studied, and it also served to establish a numerical methodology to model all the other foundation systems, through all experiences acquired during the numerical simulations of them. One of the most relevant aspects learned during the numerical works was the choice of the parameters of each one of the materials. The soil's parameters had the largest influence on the behavior of the foundation system simulated, especially the elasticity soil modulus  $E_s$  and the cohesion  $c$ ; the concrete and steel material had much less influence, but not much less importance.

It is very important to mention that from the laboratory soil parameters all numerical analyses were achieved as first attempts. This is because, firstly, better numerical approximations were obtained as preliminary results than by using the field trial parameters (back analysis), and secondly, because they were employed successfully in other numerical works previous to this research thesis.

Also, it was very important to understand the behavior of each one of the materials components separately, including their coefficients of variations, because the range of variations allowed by the material itself helps to significantly decrease some numeric convergence problems and to obtain logical results.

However, it is fundamental to take into account that the behavior of the system occurs as a result of all the materials working together at the same time, which is why the soil – structure interaction turned out to be very complicated to model.

## **5.2 NUMERICAL SUBGRADE REACTION MODULUS FOR *CCI* MODEL**

As from the numerical results of the *CCI* foundation system, it was possible to calculate the variation in the subgrade reaction modulus  $K$  with soil depth. Based on the element finite mesh for soil dominium (see Figure 4.29 and Figure 5.8), at each node along the borehole front wall (see Figure 5.9), the horizontal displacement  $y$  and the subgrade force  $p$  transmitted by the contact of the pile during the horizontal loading were calculated.

Thus, through the equation (2.3)  $p = K y$ , the  $K$  modulus variation with soil depth was obtained, and is shown in Figure 5.10. Also, the  $K$ -SPT modulus was obtained through SPT field tests and calculated in section Appendix B (see Table 6.3).

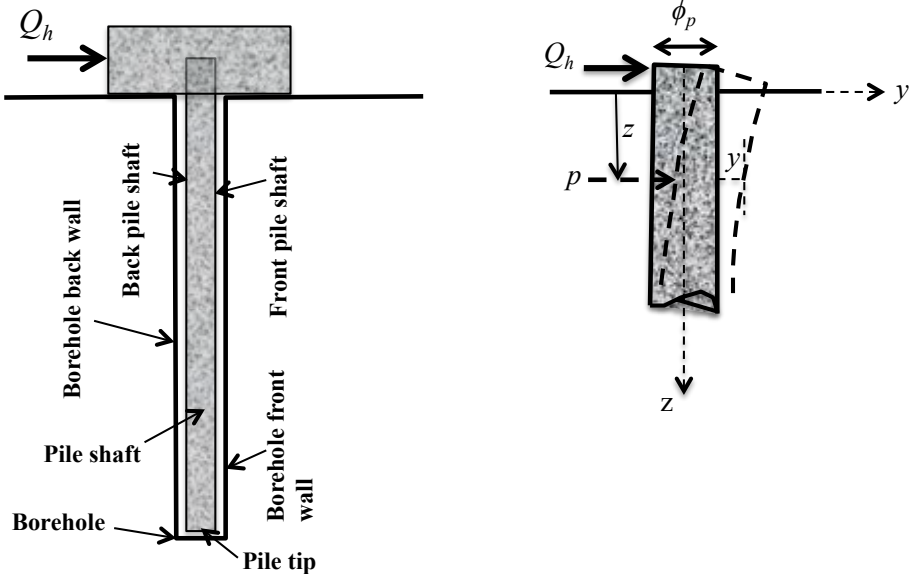


Figure 5.9. Contact between the pile shaft and the ground.

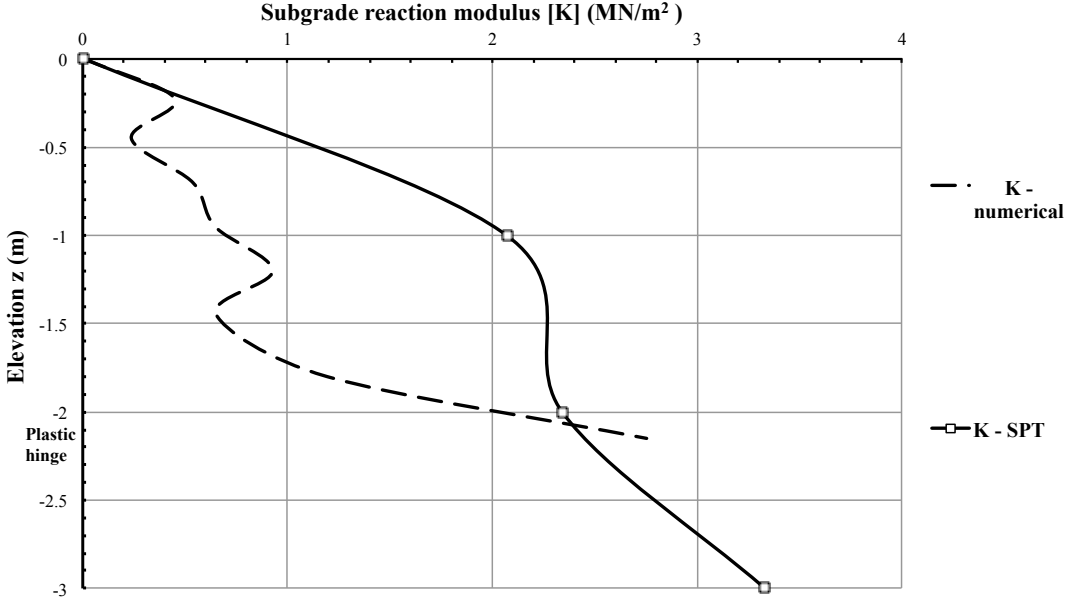


Figure 5.10. The subgrade reaction modulus  $K$  variation with soil depth.

With respect to the subgrade reaction modulus  $n_h$ , it was calculated through different equations, firstly using the equation (2.2) where  $K = n_h \phi_p$  and it is shown in Figure 5.11 as  $n_h$  diameter (numerical) curve. Secondly, it was calculated through the equation (2.9) where

$K=n_h z$ , and is shown in the same figure as  $n_h$  Winkler (numerical) curve. Finally, the curve  $n_h$  SPT refers to the same parameter calculated in section 4.4.4 and explained in Table 6.3.

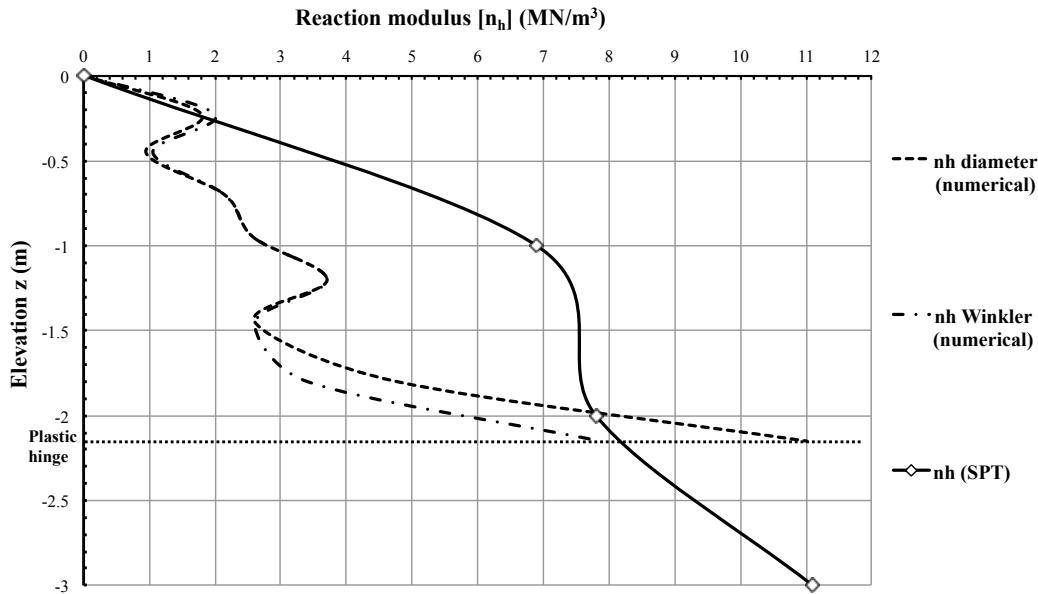


Figure 5.11 The variation in the reaction modulus  $n_h$  with soil depth.

### Discussion

It is possible to affirm that the reaction modulus  $n_h$  obtained by field tests did not represent with the required approximations the current stress state of the soil after the drilling work and later construction of each one of the piled rafts. The current stress state of the soil changed a lot after all these remolded conditions, and was really unknown.

Therefore, it was not successful to estimate the elasticity modulus of the soil  $E_s$  using both experimental and theoretical parameters  $K$  and  $n_h$  (see Table 6.4), and in turn use it as the initial geotechnical parameter during the numerical analysis. In fact, the final geotechnical parameter  $E_s$  used during the numerical simulation for the *CCI* foundation system was totally different (see Table 4.11).

Finally, the of  $K$  and  $n_h$  obtained from the numerical analysis, as shown in Figure 5.10 and Figure 5.11, gave an overall idea about the variation in those parameters with soil depth. It is thus feasible to think that those results are correct, because the numerical model represents the experimental results with acceptable accuracy (see Figure 5.7).



### 5.3 NUMERICAL EVALUATION OF A DEFECTIVE PILE

First, it was necessary to carry out the numerical analysis of the *CFI* defective foundation system from the numerical *CCI* intact model, and it was possible through prediction analysis to model it. This kind of study consists of describing, analyzing and examining the different relationships among several parameters and different geometrical conditions; for this case only the geometry in the defective area of the pile and some of the parameters of the concrete material designated for that specific area were altered.

Figure 5.12 displays both the numerical and the experimental curve of the *CCI* intact system as reference, as well as the parametric defective study for the *CFI* system. This chart shows a significant behavior difference between the numerical intact system and numerical defective system, which shows a loss of bending stiffness and lower load capacity, due to geometrical reduction in the defective area, and also because lower parameters, both elastic and plastic, were assigned in that specific area.

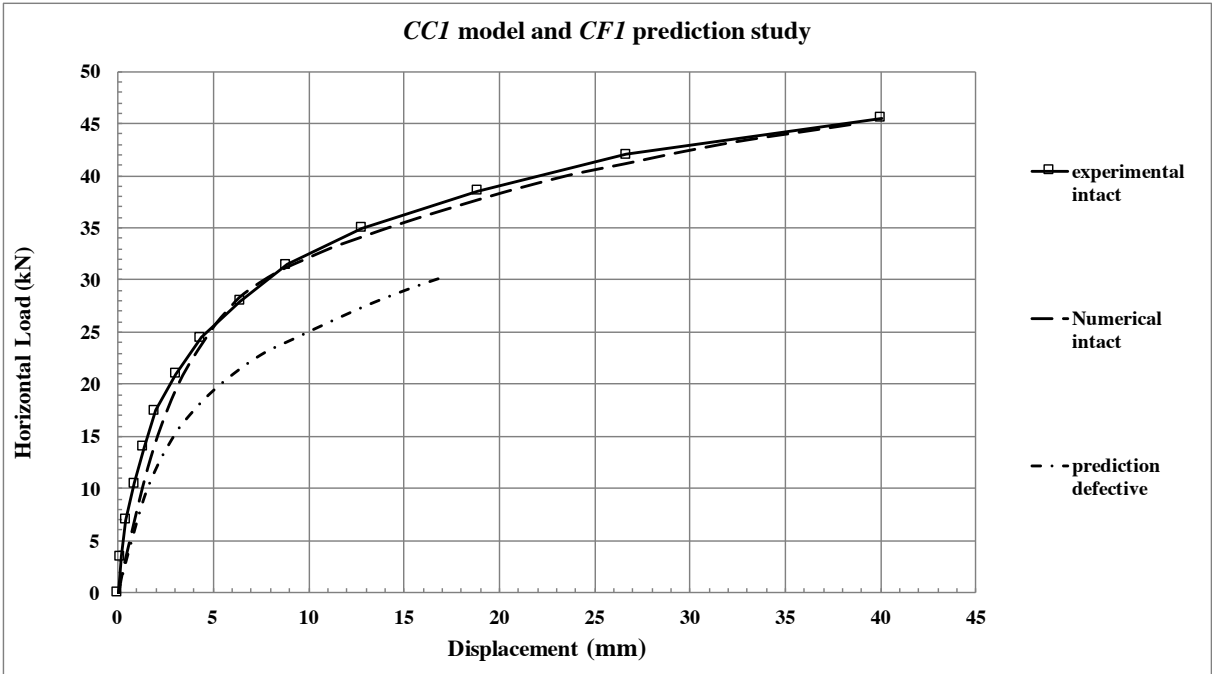


Figure 5.12. Plotted numerical results of the *CCI* and *CFI* models.

Some behaviors similar to those found in the *CCI* intact foundation system are observed at shallow depth, such as failure wedge formation, a gaping hole, etc. (see Figure 5.13.),

which occur during the horizontal displacements, and were already commented on in the previous section.

### ***CFI* piled raft system**

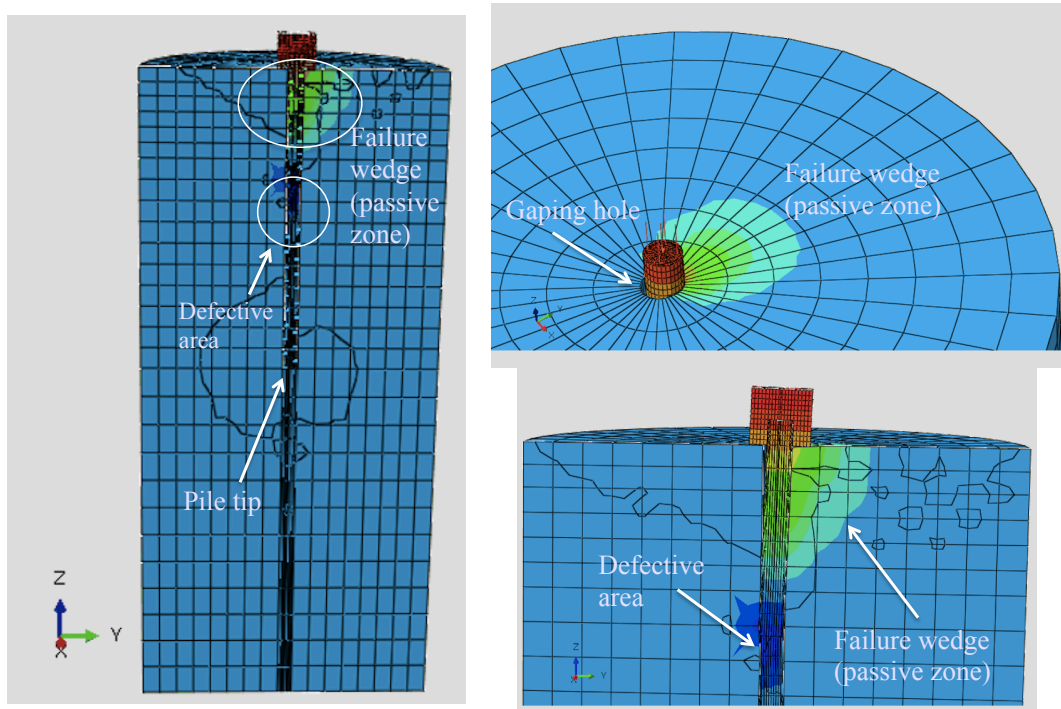


Figure 5.13. Graphical results of horizontal displacements.

Based on those numerical studies (*CCI* numerical model and *CFI* prediction model), it was decided to evaluate the damage performance through their behavior, because the damage on the pile is the only difference between them; the different behavior due to the presence of a defective pile experienced by the *CFI* foundation system was observed clearly in the plotted curve (see Figure 5.12).

Figure 5.14 displays the horizontal displacements computed for every meter of depth at the same work load of lateral loading (22.33 kN) according to Table 4.5. It is observed that at the depth of the damage, located between 1.90 and 2.5 m deep (indicated by shaded strip), a plastic hinge was formed for the *CCI* system, whereas for the *CFI* system it was also formed but shallower than for the intact system. Regarding the pile tip, the displacements calculated were almost null, in the -0.20 and -2.29 mm range; the negative sign means that there is a passive stress zone caused by the pile pushing the soil, but the stress state formed is so short that it was not shown by the graphical results.

As reference, the same figure also shows the soil thickness influenced by the lateral loading at the top of the pile (top shaded strip), between 0.0 and 1.60 and 0.0 and 2.40 m deep, delimited by the plastic hinges; this thickness is also shown graphically in Figure 5.8 and Figure 5.13 results as failure wedge.

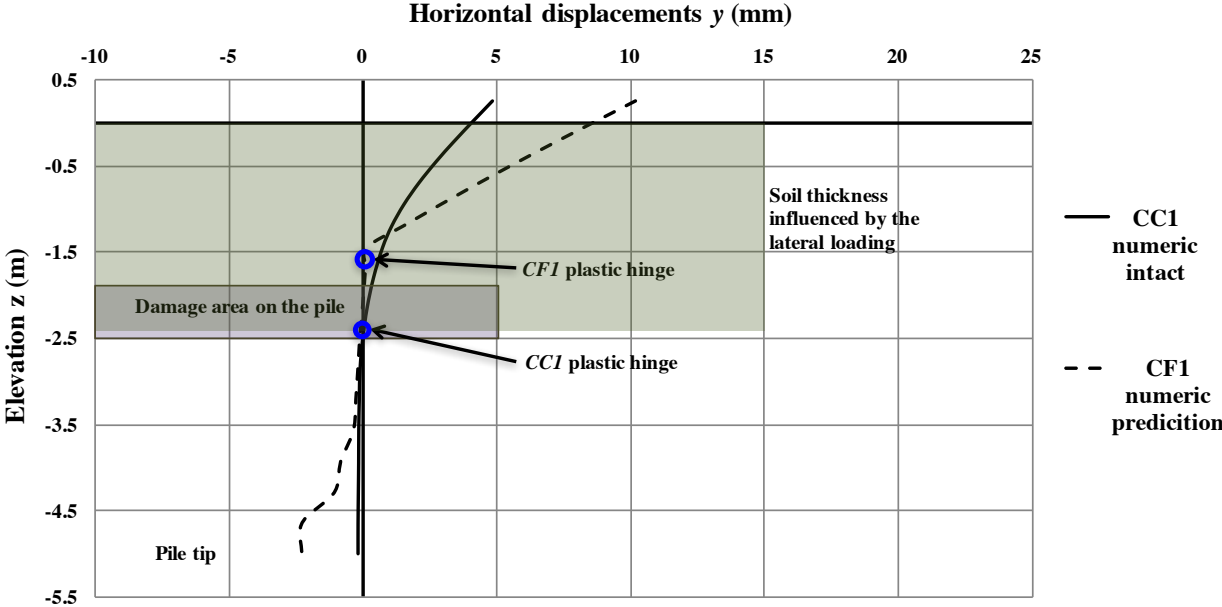


Figure 5.14. Profile of the horizontal displacements under work loading.

Therefore, the damage area (or zone of weakness) located at that depth did not represent the main factor that affected behavior, because the displacements in both cases are almost equal (practically null), and did not develop the state of failure in the control element of the concrete displayed in Figure 5.15.

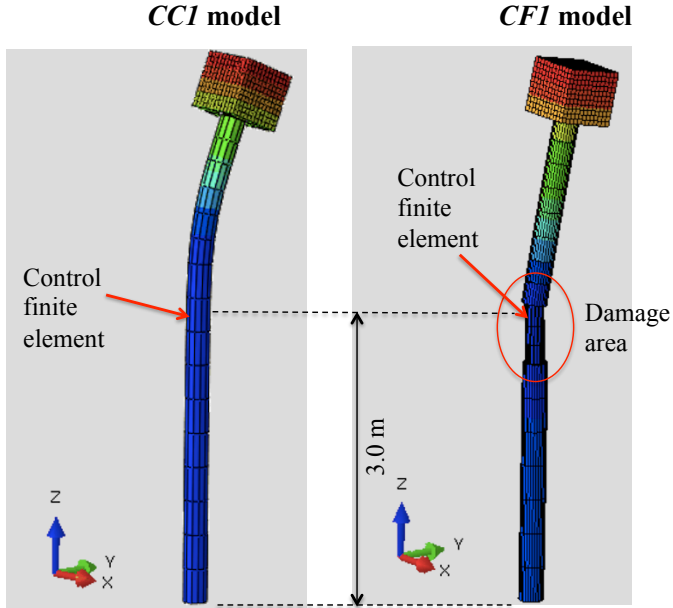


Figure 5.15. Piled rafts isolated at the final horizontal loading. Scale 15 times enhanced.

However, it was possible to affirm from a global point of view that it is the loss of rigidity stiffness in the pile that caused the different behavior, due to the reduction in the transversal area  $A$ , the decrease in the modulus of elasticity of the concrete material  $E_c$ , and the low plasticity parameters assigned to the defective area.

It can also be deduced that if the damage area were moved towards the top of the plastic hinge, it would probably cause the pile to break due to the new weakness zone position.

### *Discussion*

It was possible through a parametric study to simulate the possible behavior of a piled raft with the presence of a damaged section in the pile. The decreased cross-area of the pile and the specific elasto-plastic parameters assigned to the damaged concrete section were the only two changes made in the defective pile and considered by the Abaqus models. Indeed, these modeling changes from an intact to a defective pile were applied to all cases here simulated.

The numerical results plotted for both systems showed that the defective pile section had a great impact on their behavior. Nonetheless, it was important to realize that the damage itself (or weakness area), located at 2.0 m depth, was almost not mobilized when it was analyzed locally; it was proved because under the horizontal intensity load at that same depth, the horizontal displacements and the lower stress performance in the selected control elements were almost zero; see Figure 5.14.

By contrast, globally the defective area as part of the piled raft was important, as it had an impact on the behavior of the system, mainly because of the loss of bending stiffness in the concrete structure.

## **5.4 STRUCTURAL BEHAVIOR OF THE CCI PILED RAFT SYSTEM**

It is possible to realize that the materials used, such as the soil, concrete and steel, have different physical characteristics, as well as laboratory parameters and constitutive models that represent them; however, they worked together and for the same time under the same

phenomenon. Consequently, based on the numerical results obtained, one has to wonder what the contribution is of each of the materials since they are all interacting together.

This section presents the contribution of each material separately, through the analysis of control elements in each of the materials in order to find out the behavior of each of them under different lateral loadings. The selection of those elements was due to the position where each of them experienced the largest stresses according to their work direction; hence, stress-strain behavior was analyzed in all of them in an attempt to evaluate their performance. Figure 5.16 displays those control elements chosen.

First, it was interesting to study the behavior only under the set work load for the *CCI* foundation system, resulting in a load of 35 kN and displacement of 12.5 mm (see Table 4.6). Under this load, different stresses of each control element were developed (stress developed); those stresses were then compared with the maximum stress developed by each control element under the ultimate load (40 kN), resulting in the capacity developed for each control element. Table 5.2 shows the results from the numerical analysis of each control element only under the work load.

It should be noted that the maximum stress values developed under the ultimate load (see Table 5.2) were less those indicated as the maximum resistance to develop for each material to obtain an acceptable numerical *CCI* modeling (see Table 4.11, Table 4.13, and Table 4.15 in previous section 4.3.4); which is logical because the ultimate 40 kN load is less than the maximum numerical 45.5 kN simulated load (see Figure 5.7).

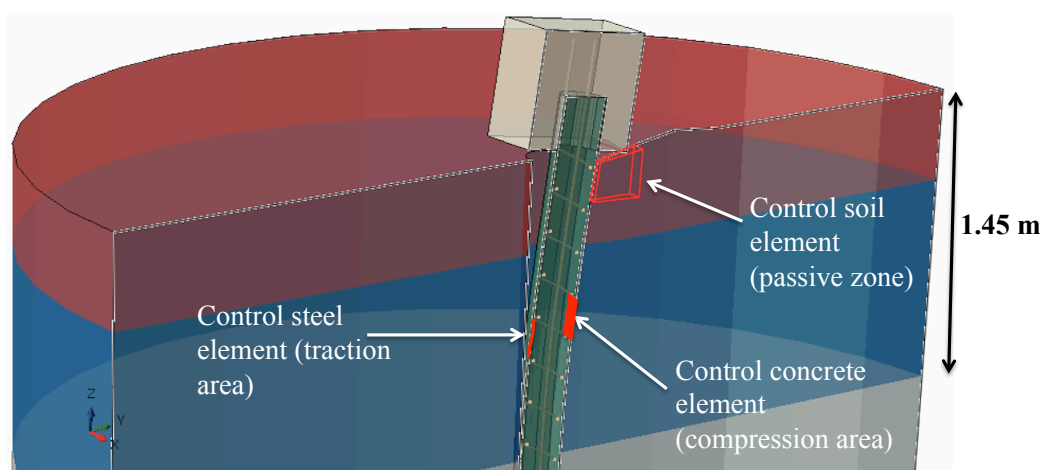


Figure 5.16. Control elements assigned for the materials. Scale 5 times enhanced.

According to Abaqus software, the positive sign represents traction and the negative one compression stress.

Table 5.2. Analysis of the control elements under the work load results

MATERIAL	MAXIMUM STRESS DEVELOPED (MPa)	STRESS DEVELOPED (MPa)	CAPACITY DEVELOPED %
soil	-0.160	-0.137	85.38%
concrete	-21.27	-13.91	65.37%
steel	460.88	242.17	52.54%

Using these values, the following charts show the maximum stress developed to each material and the stress developed under that defined work load (Figure 5.17 and Figure 5.18).

Figure 5.17 clearly shows the poor stress of the soil that can develop (resistance contribution), compared to the other two materials engaged; the steel showed that it has the greatest resistance, but it is not the material that takes most of the stress generated by the external lateral loading under the assumed working load.

According to Figure 5.18, when the soil had already contributed with 85.38% of its maximum capacity, the steel had only contributed 52.54%, and the concrete just slightly more with 65.37%. Thus, it is possible to realize that in this piled raft foundation system analyzed under the work load, the concrete and steel component materials did not show relevant engagement compared with the soil. Incidentally, these materials are the most expensive ones used in creating the foundation system.

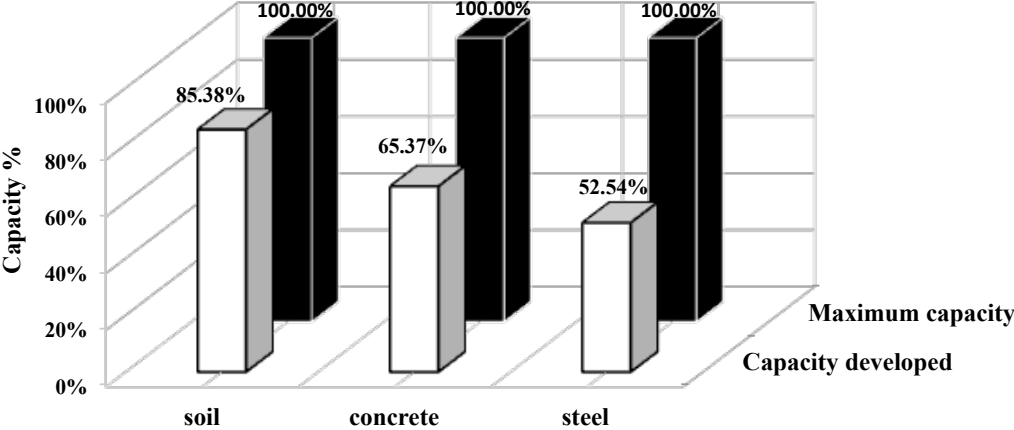


Figure 5.17. Numerical stress results of the control elements under working load.

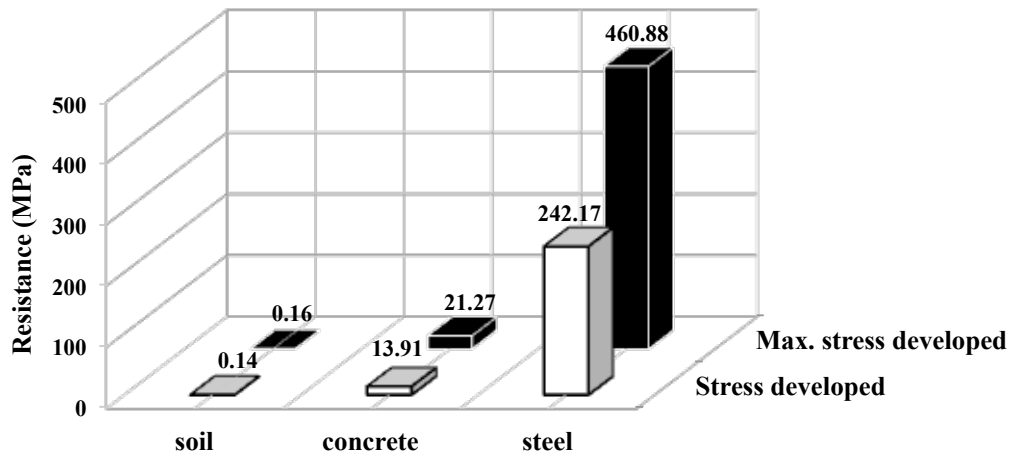


Figure 5.18. Capacity developed of the control elements under working load.

It is interesting to observe how each of the materials behave as the lateral loading increases; therefore, a general analysis of the behavior of the control elements under several loading stages was performed until reaching the 100% ultimate loading; such loading stages were set as a percentage of the ultimate load. Figure 5.19 displays the progress of each material under different loading stages, and it is possible to observe that the soil had a constant progress while the steel shows the most disproportional participation.

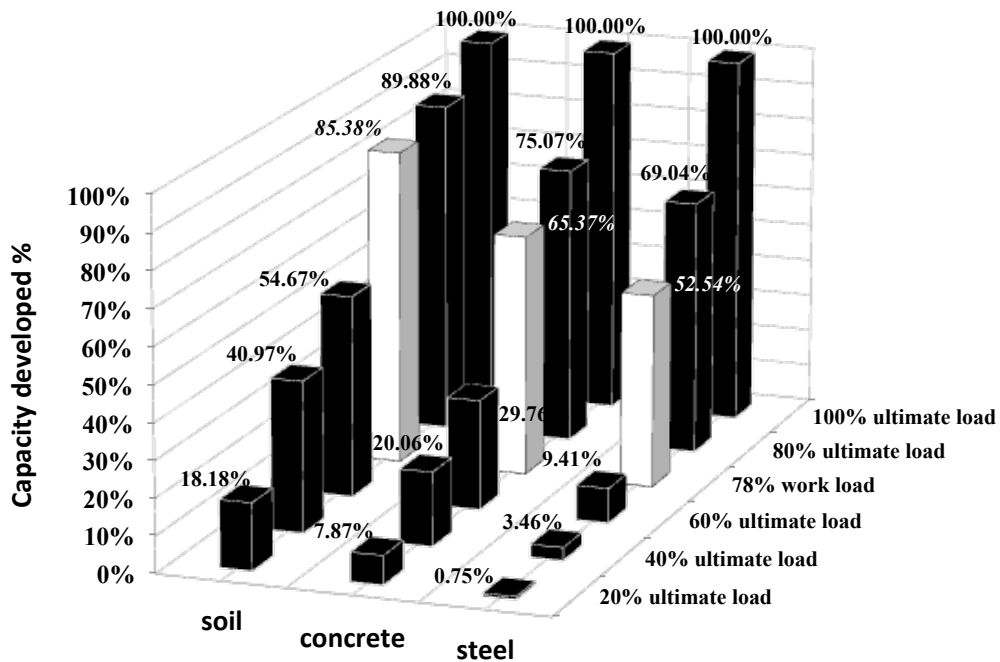


Figure 5.19. Engagement of each material under several lateral loading stages.

It is noteworthy that when 78% of the total lateral loading was applied (work load), the soil developed almost all its capacity, while the concrete and steel developed less than 50% of theirs. This analysis perspective generates new ideas, opens up some new paths about how piled rafts should be projected under lateral loadings, and stimulates creating thinking about how to build more efficient structures.

## 5.5 PREDICTION BEHAVIOR OF THE PILED RAFT GROUPS

Based on the *CC1* and *CF1* Abaqus models, and keeping all the same parameters of the three materials used on them (see Table 4.11, Table 4.13 and Table 4.15), it was possible to predict the behavior for the *CC3* and *CF4* piled rafts, increasing the number of intact piles and the soil dominium diameter, and also adding just one defective pile in the *CF4* Abaqus model. The results are shown in Figure 5.20 and Figure 5.21.

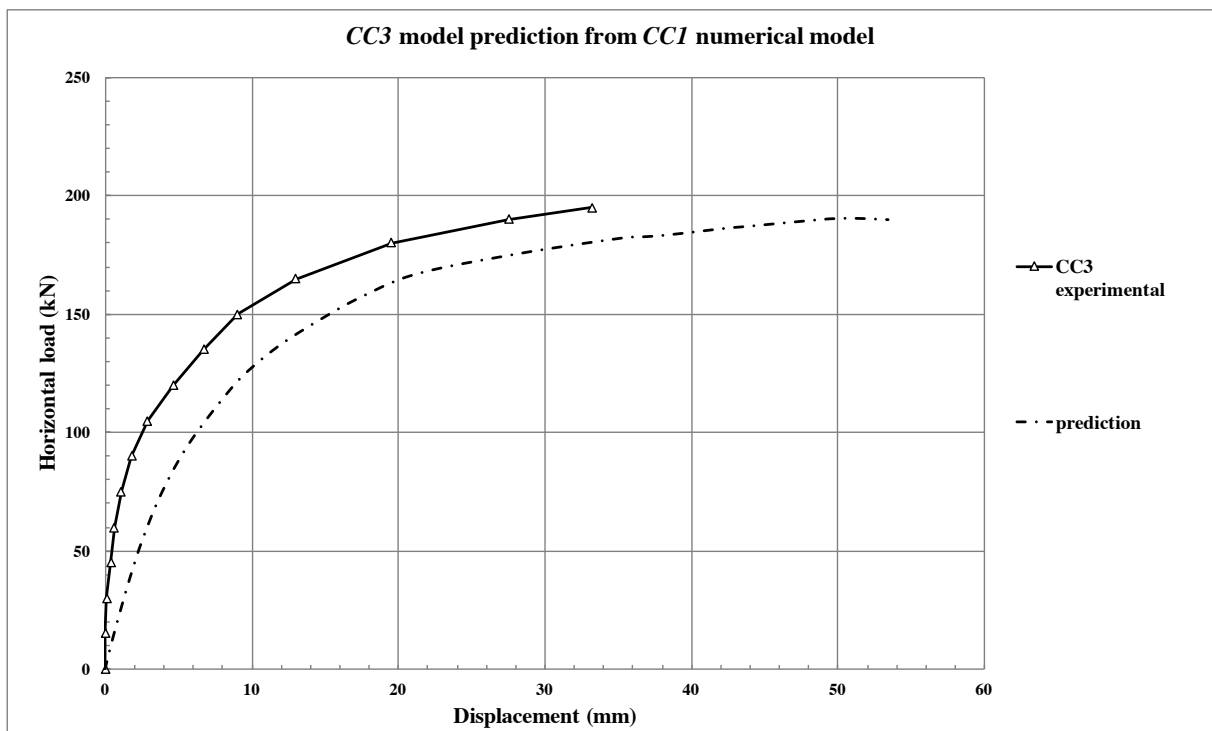


Figure 5.20. Behavior prediction of the *CC3* piled raft system from the *CC1* numerical Abaqus model.

It is very clear in both figures that the prediction curve does not fit with respect the experimental curves in each one. In fact, both prediction curves are missing stiffness in the elastic range and they display greater displacement than the experimental curves in the plastic



range. Even for the *CF4* foundation system, the prediction curve displays greater bearing capacity than the experimental one.

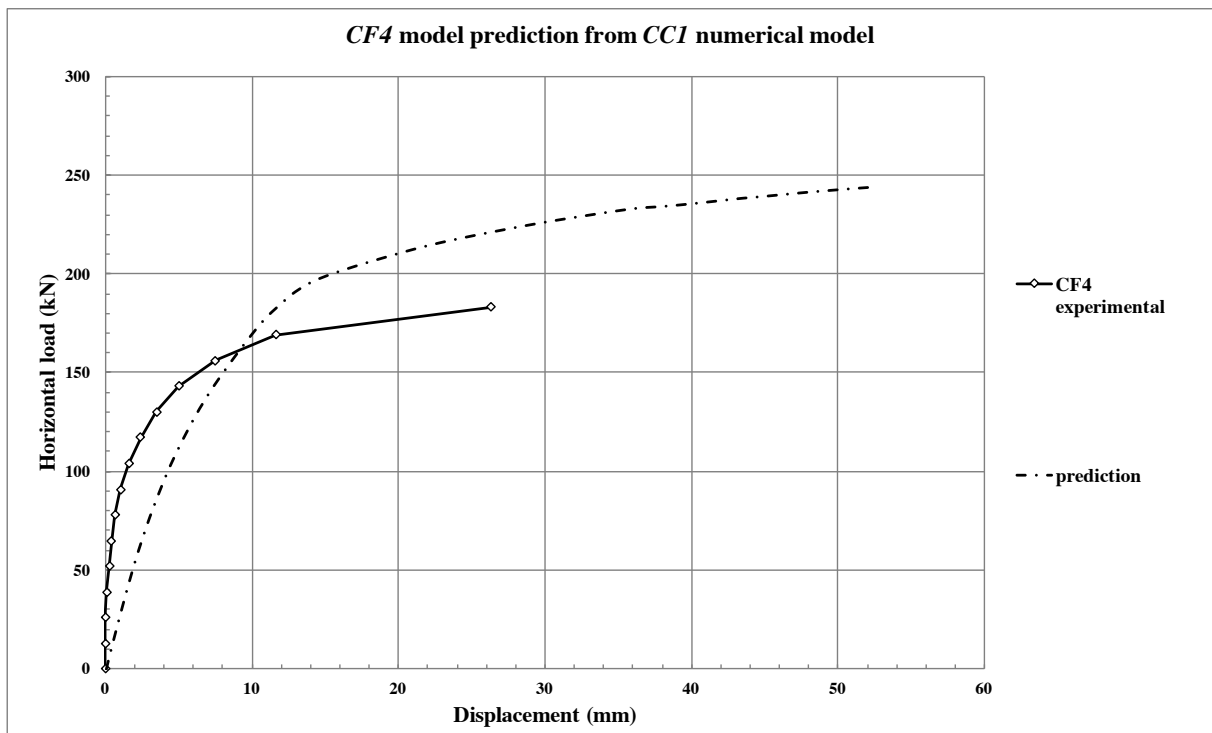


Figure 5.21. Behavior prediction of the *CF4* piled raft system from the *CCI* numerical Abaqus model.

### Discussion

All materials that make up the *CCI* piled raft system and that work at the same time under lateral loading were separately analyzed; by observing the behavior of the most critical control elements under the horizontal load, it was found that the engagement of the materials was totally disproportionate. For the analysis case under work loading, the concrete and the steel showed poor performance, despite being the most expensive materials in the piled raft system.

Form another point of view, the same assigned control elements were analyzed under different stages of lateral loading. Those analyses showed that the three material components of the foundation system performed differently at different times; specifically, at the beginning of the phenomenon the soil material took the lateral loading, constantly increasing its resistance, and the concrete and the steel materials took over almost at the end of the lateral loading.

Therefore, attention needs to be paid to improving the efficiency of each material, but especially the concrete and the steel, so that piled raft systems can perform as well as possible when they are submitted to lateral loading, in both a technical (quantity and position of the components) and economic (saving money on materials) manner.

Finally, with respect to the behavior prediction based on the *CCI* and *CFI* Abaqus models for some piled raft groups studied experimentally, reliable numerical results were not obtained. Therefore, it will be necessary to make modifications to the Abaqus models until obtaining better numerical results.

## **5.6 EVALUATION OF THE INFLUENCE OF THE DEFECTIVE PILE ON THE FOUNDATION GROUP**

The same general methodology for numerical simulations (see **Error! Reference source not found.**) learned during the numerical analysis for the *CCI* piled raft was also applied to obtain the numerical results for the *CC3*, *CF3*, *CC4* and *CF4* foundation systems.

### **5.6.1 CC3 AND CF3 PILED RAFT SYSTEMS**

The first numerical results obtained were for simulating the *CC3* piled raft system; later, as with these results, a prediction study was carried out to try to simulate the *CF3* defective system (implementing the same alterations made in the *CFI* Abaqus model). Figure 5.22 depicts the plotted curves obtained, the intact experimental, the intact numerical simulation and the prediction defective study. The intact numerical curve shows a good fit, and therefore the behavior represented by the parametric study should also be taken as good.

It should be emphasized that the elasticity modulus of the soil  $E_s$  was increased by 360% and the plasticity parameters were also altered (see Table 4.11). It was also observed during these simulations that varying these parameters of the soil changed its behavior considerably, yielding better numerical results. It can be assumed in principle that the big increase in  $E_s$  and the other modified values,  $c$  and  $\phi$ , was due to the greater rigidity of the foundation system itself; it is bigger, is made up of a greater number of piles and has a different layout at the experimental site.

However, the numerical results obtained from the *CF3* prediction defective study were unsatisfactory, when compared with the defective experimental curve measured, and according to the plotted results shown in Figure 5.23. For the parametric study, a horizontal displacement and ultimate load capacity of 10.48 mm and 145.45 kN respectively were computed; the experimental *CF3* foundation system measurements indicated a horizontal displacement of 31.85 mm and ultimate load capacity of 130 kN.

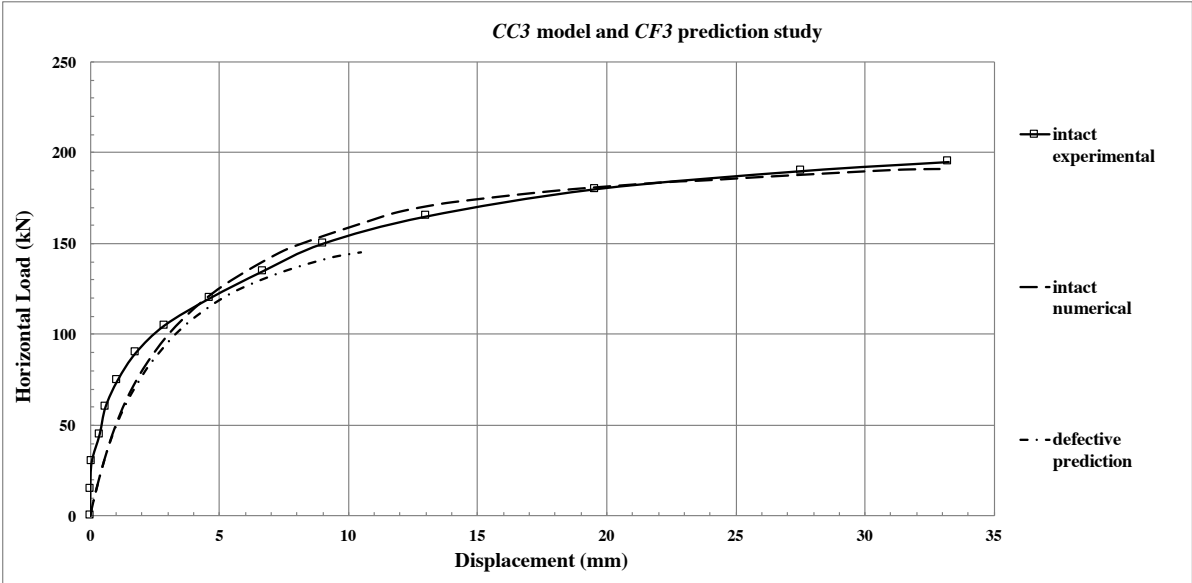


Figure 5.22. Plotted numerical results of the *CC3* intact model and *CF3* prediction study

The question then arises as to why it did not reach the *CF3* experimental curve or even come close to it, especially considering that these two foundation systems have the same size, geometry and quantity and quality of component materials; they also went through the same construction process and were even built at the same experimental site. An obvious conclusion is that the presence of a defective pile in the *CF3* foundation system resulted in the curves having such different behaviors (see Figure 5.23).

Then a numerical analysis was carried out for the *CF3* foundation system; good approximations were found that fitted well according to experimental curve, also depicted in Figure 5.23. During that numerical analysis, it was possible to acquire the sensibility to understand the differences between both foundation systems, seeing the need to change the material parameters, mainly geotechnical, until getting good numerical results. See Table 4.11

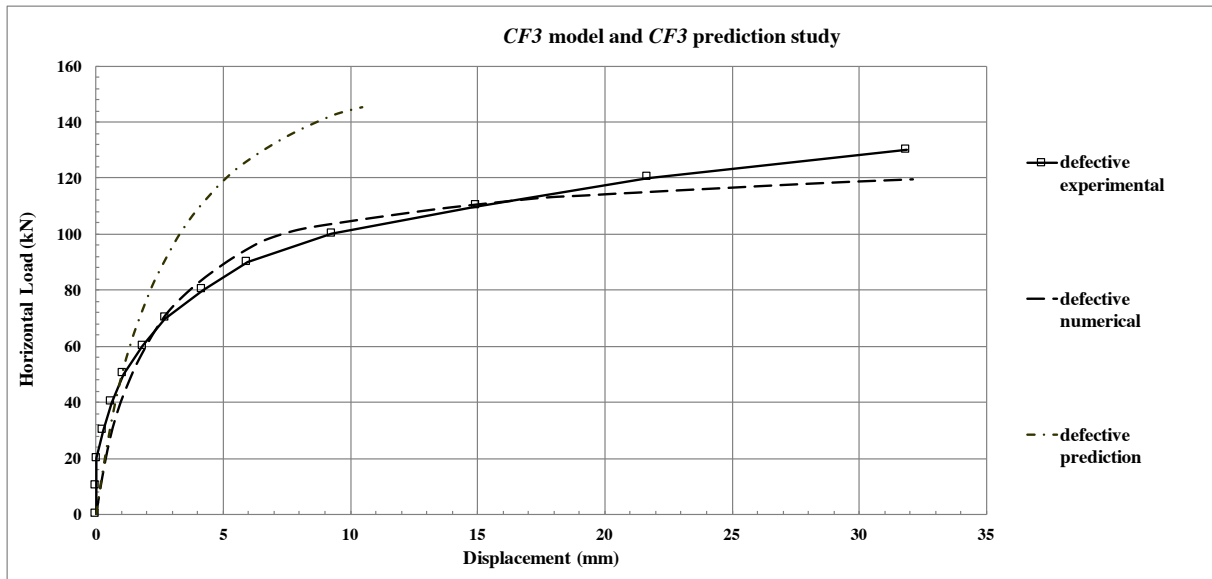


Figure 5.23. Plotted numerical results of *CF3* defective model.

Based on the above, it was possible to deduce that there were other factors that had some influence on those experimental performances that were not taken into account during the numerical simulations.

Indeed, one of those factors of greatest impact is the ignorance of the current stress state of the soil previous to lateral loading, especially if one considers that all piled raft systems here studied were submitted to vertical ultimate loading. Instead of that current stress state, the geostatic stress state of the soil was set as initial, prior to the horizontal loading during the numerical simulations.

Other influencing factors disregarded could be the heterogeneity of the soil, the rigidity contributions of other existent piled rafts built around the system tested, causing probably an increase in soil stiffness, and the current soil parameters after ending construction on all piled raft systems, among others.

In order to evaluate and check the influence of the damage on the behavior between these foundation systems, a control finite element was designed located at a depth of 2.0 m (3.0 m from the pile tip); Figure 5.24 displays these details. The purpose was to compare the horizontal displacements between both systems at the same soil depth, using the same control finite element previously chosen in each of the foundation systems.

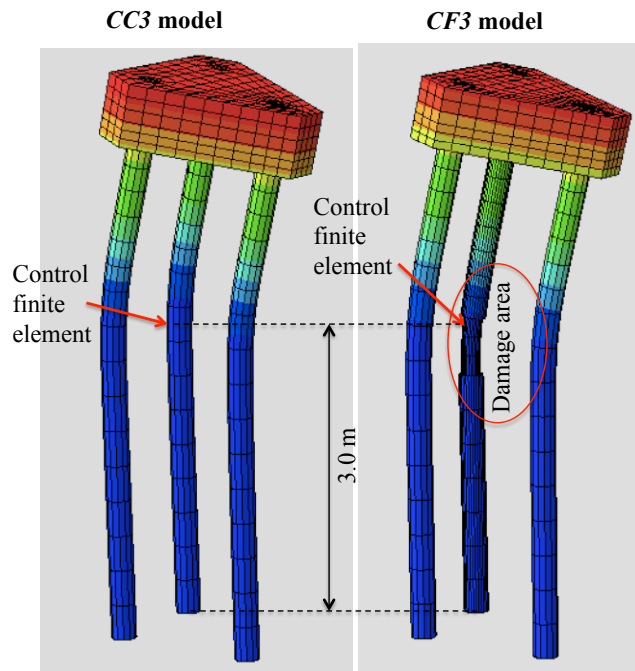


Figure 5.24. Piled rafts isolated at the final horizontal loading. Scale 15 times amplified.

The control finite elements are shown in Figure 5.25 and the horizontal numerical displacements in the direction of the loading  $y$  can be read for both systems. The numerical values were very small at the end of the lateral loading, indicated in the boxes in the same figure, around +0.445 mm for the intact pile and -1.18 mm for the defective pile, both measured at the center of each control finite element. The positive sign indicates displacement toward the passive zone, and the negative sign displacement toward the active zone.

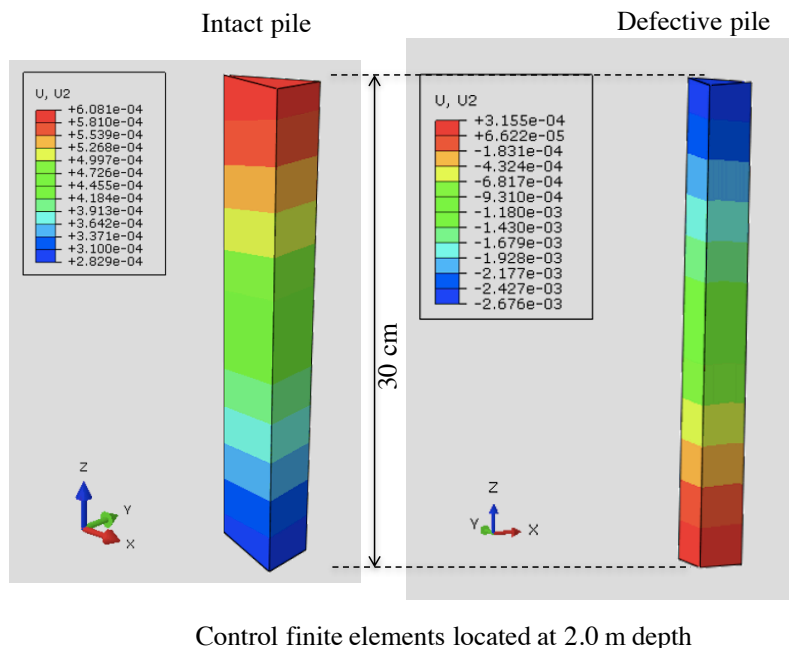


Figure 5.25. Control finite elements in each piled raft according to Figure 5.24

Comparing the horizontal displacement at that depth with the maximum horizontal displacement at the top (31.85 mm for the *CF3* foundation system), 3.7% of the maximum displacement under the horizontal load intensity that corresponds to that same depth was obtained. Therefore, it was deduced that the damage itself in that position in the piled raft had a minimum participation, so it can be essentially disregarded.

With regard to the graphical results, see Figure 5.26 and Figure 5.27, where some similarities can be seen in the *CC1* and *CF1* foundations systems, at the end of lateral loading. One of the most important observations is that damage placed at that depth in one of the piles does not have a direct participation in the behavior of the system.

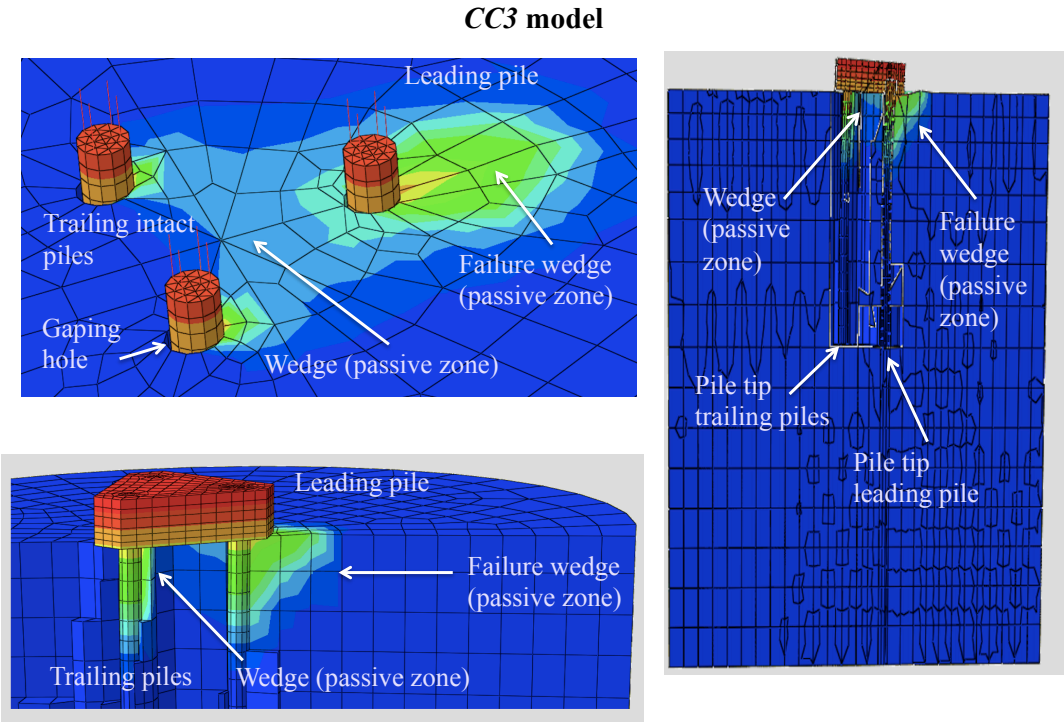


Figure 5.26. Graphical horizontal displacement results. Amplified 3 times.

It can also be seen in the graphical results that three passive wedges were formed in both piled raft systems, the largest formed by the leading pile and the smallest by the trailing piles. To improve the visual details of those figures, the graphical results were amplified three times. In the failure wedge the angle formed with respect to the ground surface was very close to  $\theta = 45 + \frac{\phi}{2}$  according to Mohr-Coulomb criterion, and for the trail wedge the angles were different compared to the failure.

Those figures also depict the gaping back hole formed in each of the concrete piles at the end of lateral loading. Finally, in a general way, both models graphically show that the contribution of the leading piles is larger than that of the trailing piles, as is also reported in the literature.

### CF3 model

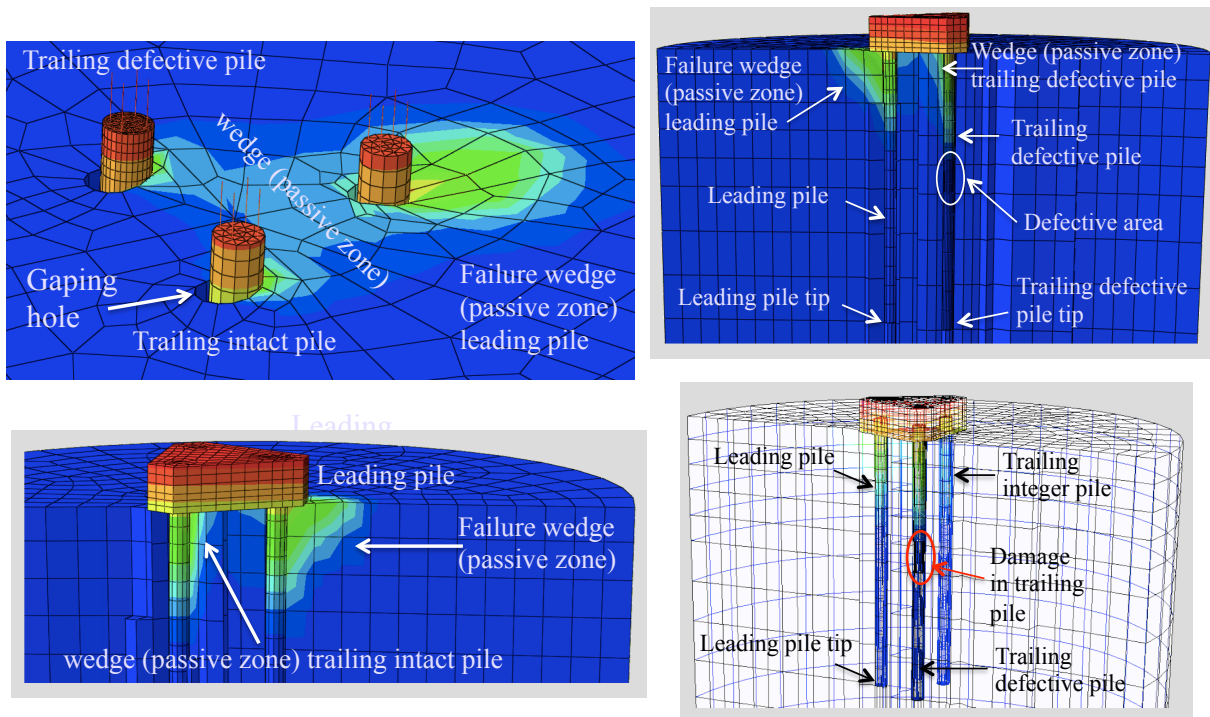


Figure 5.27. Graphical results of the horizontal displacements.

### 5.6.2 CC4 AND CF4 PILED RAFT SYSTEMS

For these piled raft systems, the same general numerical methodology was applied again, as earlier described in section 4.3.5, to model their behavior. Those piled raft foundation systems have a similarity with the foundation systems of three piles.

The first numerical analysis was achieved for the *CF4* foundation system; according to the numerical results obtained and plotted in Figure 5.28, it fitted well to the experimental curve when both were compared. However, in the elastic stretch it can be seen that there is no accurate fit, because the experimental curve practically does not show horizontal displacements under lower loadings (around 80 kN). Numerically, however, it is impossible to represent if Hook's law is considered. It means numerically that if there is stress there must

also be strain. As was mentioned for the *CC3* and *CF3* foundation systems, the stiffness of the *CF4* system itself must be larger because of its greater size and number of piles, and because of the layout at the experimental site.

Thus, it was necessary to increase the elasticity soil modulus until getting a better fit to the curve, around 500%, which was used for the elastic modulus of soil for this foundation system.

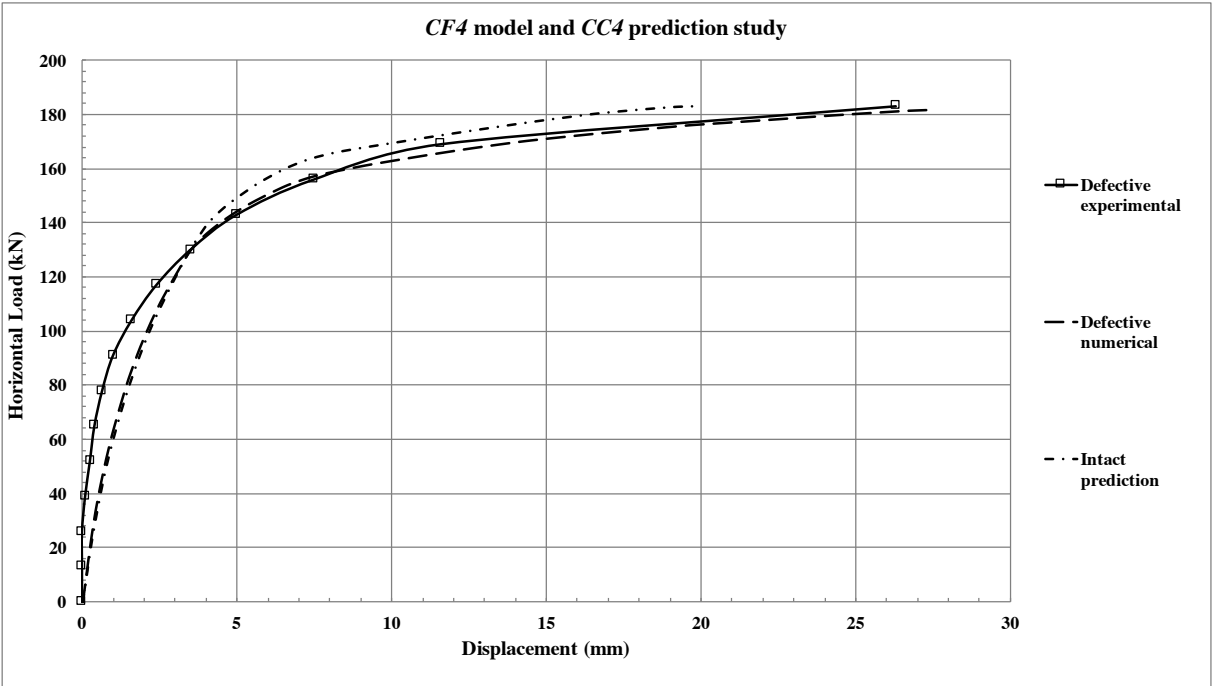


Figure 5.28. Numerical results plotted for the *CC4* intact and *CF4* defective foundation systems.

Later, as in the case of the *CF3* numerical model system, it was possible through parametric analysis to model the *CC4* foundation system; it meant that only the defective pile was replaced by an intact pile, placed in the same position as at the experimental site. The results are also plotted in Figure 5.28.

However, as for the three-pile system case, it was possible to verify its behavior by comparing the numerical results with both the experimental and numerical *CC4* intact piled raft systems.

Finally, by plotting those numerical results, it could be seen that the parametric curve does not fit to the experimental *CC4* foundation system. Therefore, the same reasons used to



explain the difference between the foundation systems with three piles are also valid for this comparison. See Figure 5.29. With regard to the graphical results, see Figure 5.30 and Figure 5.31, where it can be seen that some similarities formed as in all foundation systems previously studied here and already commented on.

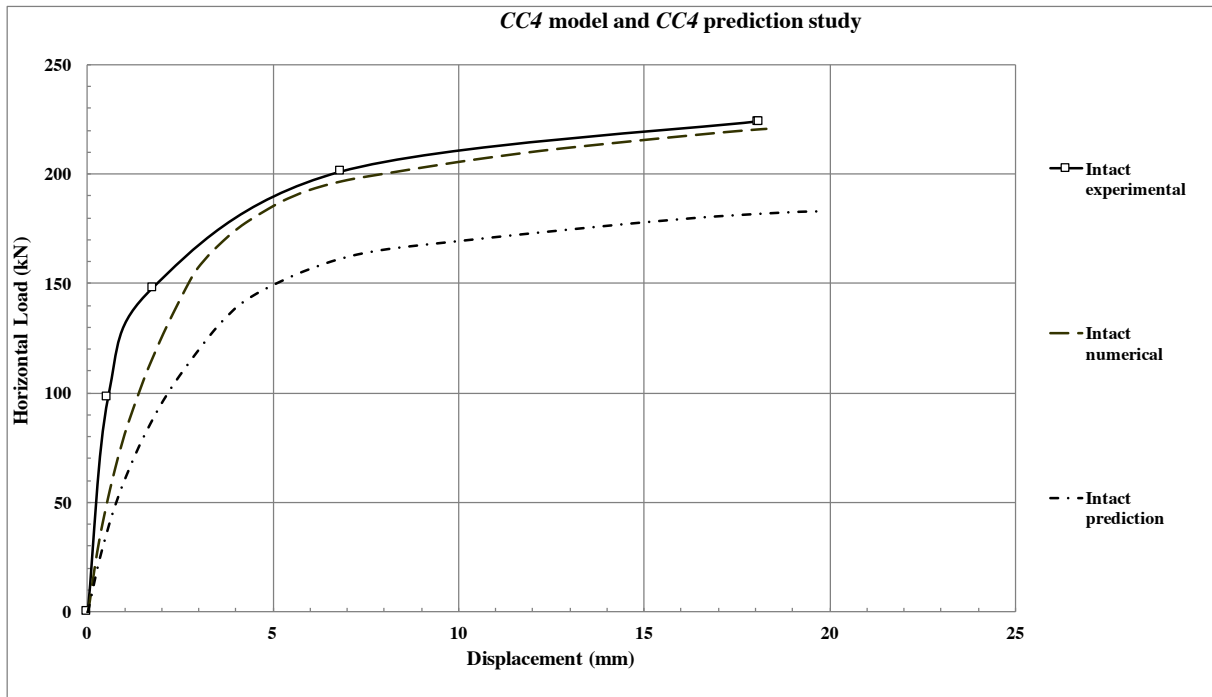


Figure 5.29. Numerical results plotted of the *CC4* intact model and *CC4* parametric study.

### *CC4* model

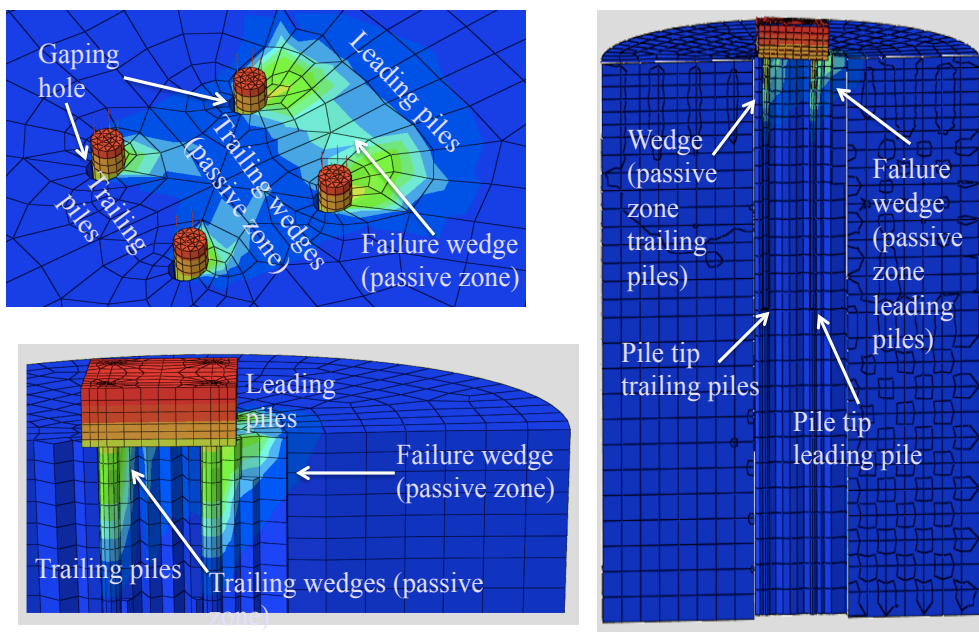


Figure 5.30. Graphical results of the horizontal displacements.

### CF4 model

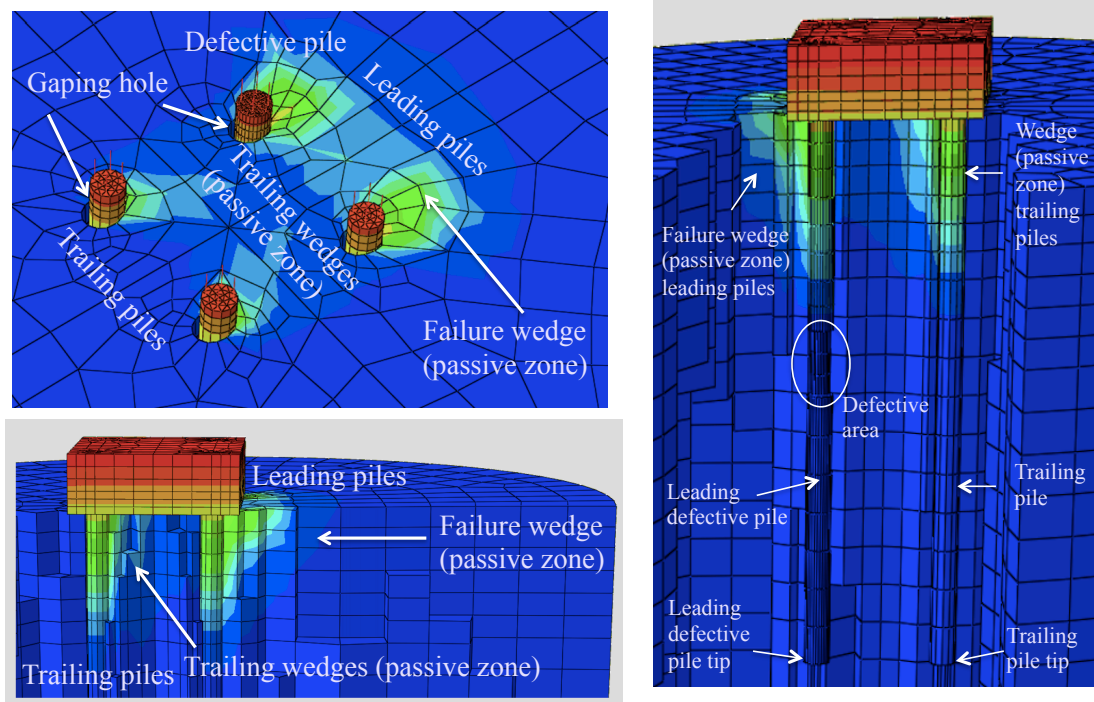


Figure 5.31. Graphical results of the horizontal displacements.

### 5.6.3 PREDICTION STUDIES

Based on the experimental observations and numerical experiences acquired during all analyses, especially between the *CC3* and *CF3*, as well as the *CC4* and *CF4* foundation systems, it would be interesting to evaluate the influence caused only by the defective pile, without considering the engagement of other factors disregarded and already discussed in section 5.6.1 of this chapter, meaning in the same way it was carried out between the *CC1* and *CF1* foundation systems (see section 5.3).

This evaluation could be achieved by comparing the *CC3* numerical model and *CF3* parametric study, as well as the *CF4* numerical model and *CC4* parametric study; however, although a defective pile is the only difference between them, there is a drawback in that they had the least damage influence according to their respective plotted results (see Figure 5.22, Figure 5.23 and Figure 5.28), when comparing the damage influence between the *CC1* numerical model and the *CF1* prediction study (see Figure 5.12).

Finally, it is possible in this comparison to observe the influence caused by the presence of a greater number of piles in the foundation systems.

## Discussion

Those piled raft systems composed of three and four piles were all measured structures that allowed, in the beginning, directly comparing the damage suffered by each of them, because all their features are almost the same, such as geometric shape, size dimensions, and quantity and quality of the materials; moreover, the same construction process was used for both and they were even built at the same experimental site.

Through a parametric study, the *CF3* and *CC4* foundation systems were simulated from the *CC3* and *CF4* numerical models respectively, only changing an intact pile for a defective one or vice versa, and keeping the same position they had at the experimental site. The plotted curve obtained from each of those specific studies did not fit when compared to the *CF3* and *CC4* experimental curves respectively, and indeed was completely different from them.

It could be said that the performance between those two similar systems (numerical vs parametric) is almost equal based on the plotted curves (see Figure 5.23 and Figure 5.28); therefore, the defective pile did not have a significant effect. In addition, the increase in the piles in the foundation system was reflected in turn by an increase in system rigidity, mainly through the modification of the elasticity modulus of soil (for example,  $E_s$  of the *CC3* system is lower than  $E_s$  of the *CF4* system).

Then a numerical simulation was carried out for the *CF3* and *CC4* foundation systems; it was through those separate numerical simulations conducted for each of these piled raft systems that several factors ended up not being taken into account by the Abaqus models.

Some of those missing factors are listed below; they were neither foreseen nor considered during the numerical simulations, but they might be somehow involved in the lateral loading performance at the experimental site:

- Soil anisotropy
- Loss of the original soil structure during drilling work and construction of the piled raft structures.
- Some details in the construction process between these concrete structures; for example, the physical final position of the rebar in the pile, the final diameter of

the concrete pile along the shaft, the contact between the pile and the soil along the shaft and the tip, among others.

- The physical conditions of the piled raft structures at the end of the vertical loading, which is impossible to check out because they are embedded into the soil.
- The current moisture of the material during the loading tests that would probably change some soil parameters, mainly at shallow depth where this phenomenon has its greatest influence. There were some rainy days even when some loading tests were performed.
- The rigidity influence by other piled raft systems located around the piled raft system studied.
- The interaction between some of the components of the piled rafts, such as the pile-raft, rebar-pile and rebar-raft interactions, was neglected.

It should be considered that all these missing factors are depicted intrinsically in all experimental  $p$ - $y$  curves obtained (see Figure 4.16), and it could be also thought that all of them were absorbed by the parameters of the materials assigned during the numerical work, mainly by the soil material, resulting in satisfactory numerical approximations.

Finally, the general tendency showed by all parametric studies carried out in this research work from a global view point, in an attempt to evaluate the effects caused by the presence of a defective pile, was that if the piled raft structure has more piles then the relative effects due to the defective pile decrease, although the bearing capacity of the foundation system increases.

It could also affirm that the damage at the current position placed on only one pile and at that specific depth, does not represent any problem locally, because the displacements and the stress state of the control elements did not show anything important to be concerned about.

All the factors listed above probably provide a little better understanding of the different behavior of those foundation systems at the experimental site, and of course their different numerical performance as well.

## **5.7 GEOTECHNICAL BEHAVIOR OF THE PILED RAFT SYSTEMS**

This section presents the behavior of each piled raft system (*CC3*, *CF3*, *CC4*, and *CF4*) separately, through the separate numerical analysis of the shaft and tip of each pile, and also the raft tilting of each system, in order to obtain a general idea of the distribution of the internal forces when the systems are subjected to lateral external forces.

For the case of tips and rafts, different loading stages were studied; for the pile shafts study only their performance under the work load were analyzed. Based on Table 4.6 (see section 4.3.1), the ultimate loads and the work loads were established and used to analyze each foundation system.

Finally, a comparison between the intact and defective systems was achieved, enabling the difference between them to be studied, discussed and graphically displayed.

### **5.7.1 UNIT BEARING PRESSURE AT PILE TIP**

#### *The CC3 and CF3 foundation systems*

To understand the global behavior of each system, the study began with a review of each pile tip under different loading stages less than the ultimate lateral load of one of those systems. To carry out this comparison, the *CF3* ultimate load was selected for analyzing both foundation systems. The reason for that is very simple: in the case of the *CC3* system, the corresponding ultimate load value does not touch the experimental curve of the *CF3* system, making it impossible to carry out this comparison study; see Table 4.6 and Figure 4.21 in section 4.3.1.

Thus, from the *CF3* ultimate horizontal loading applied, different partial loadings were calculated, so that 20%, 40%, 60%, 80% and 100% levels of this ultimate load were selected as loading stages, and the work load was also included as another loading stage.

Relating to the internal forces generated during the loading stages, firstly, for each pile of each system the internal vertical load  $P_i$  transmitted from the pile tip to the ground was obtained for each loading stage. Secondly, the maximum internal vertical load transmitted to

the ground  $P_{imax}$  from each pile tip of each system at the end of the *CF3* ultimate loading (100%) was obtained, meaning 122 kN according to Table 4.6.

Finally, the internal force of each loading stage divided by the maximum internal vertical load transmitted from the pile tip to the ground was normalized, meaning  $P_i / P_{imax}$ . Figure 5.32, Figure 5.33, Figure 5.34 and Figure 5.35 show the global behavior at each loading stage for each foundation system.

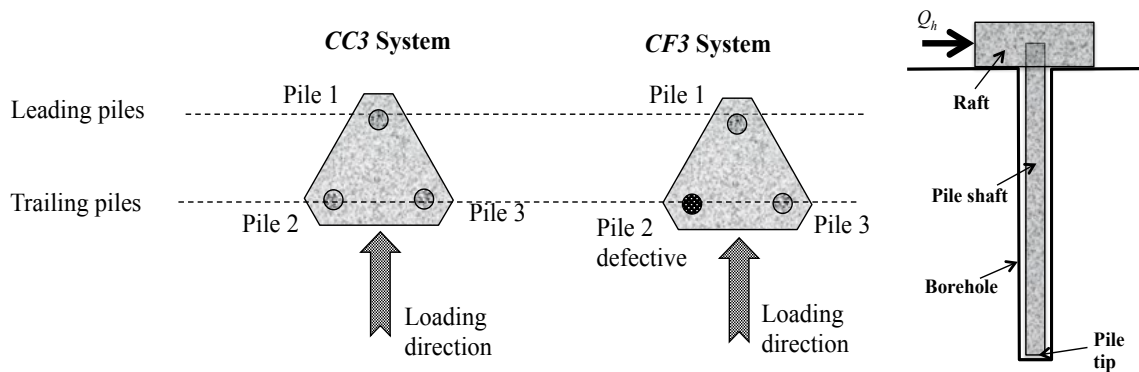


Figure 5.32. Sketch of the *CC3* and *CF3* foundation systems.

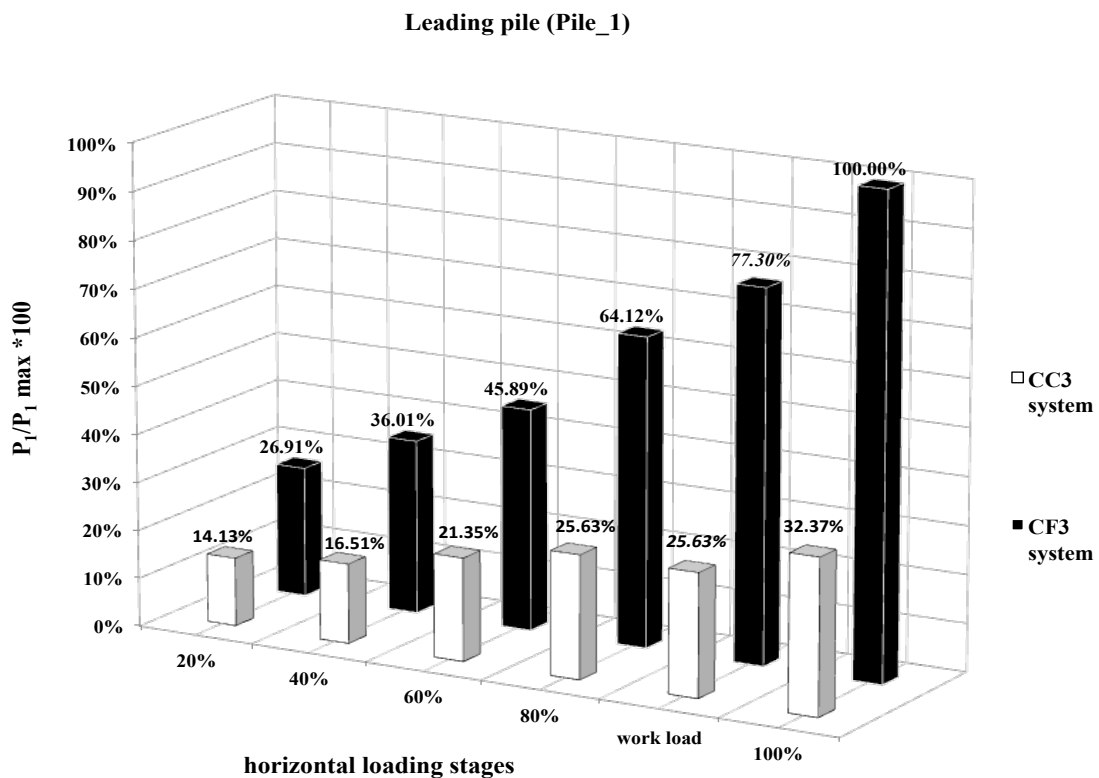


Figure 5.33. Pile 1 of the *CC3* and *CF3* foundation systems.

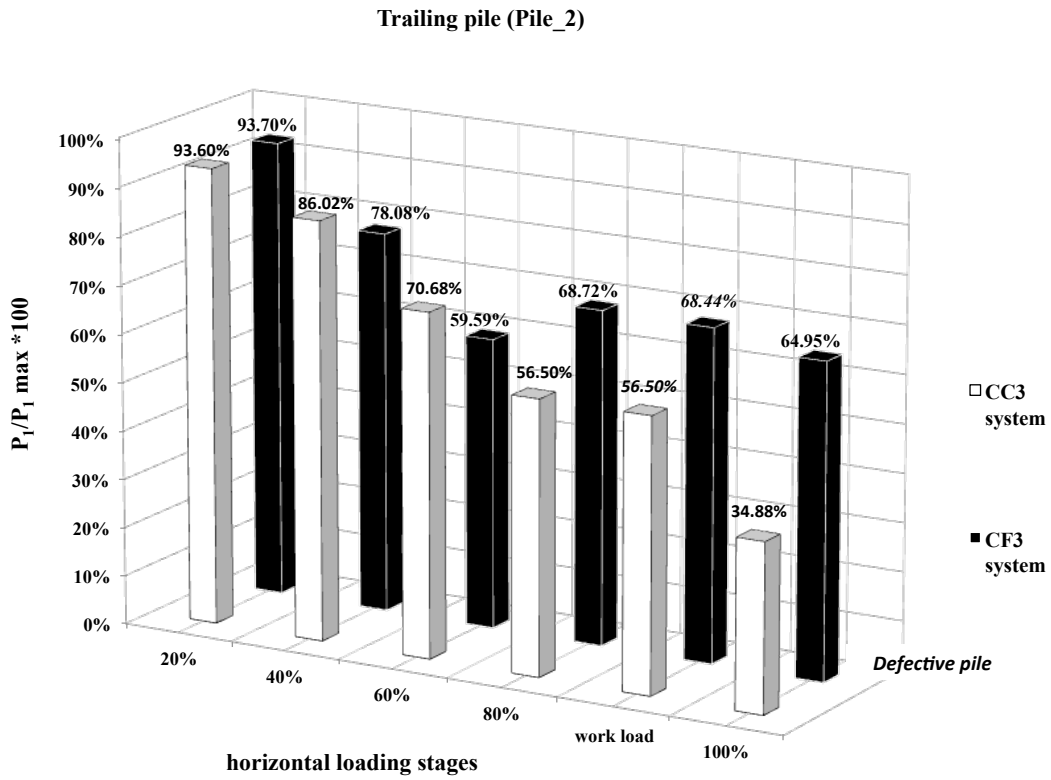


Figure 5.34 Pile 2 of the CC3 and CF3 foundation systems

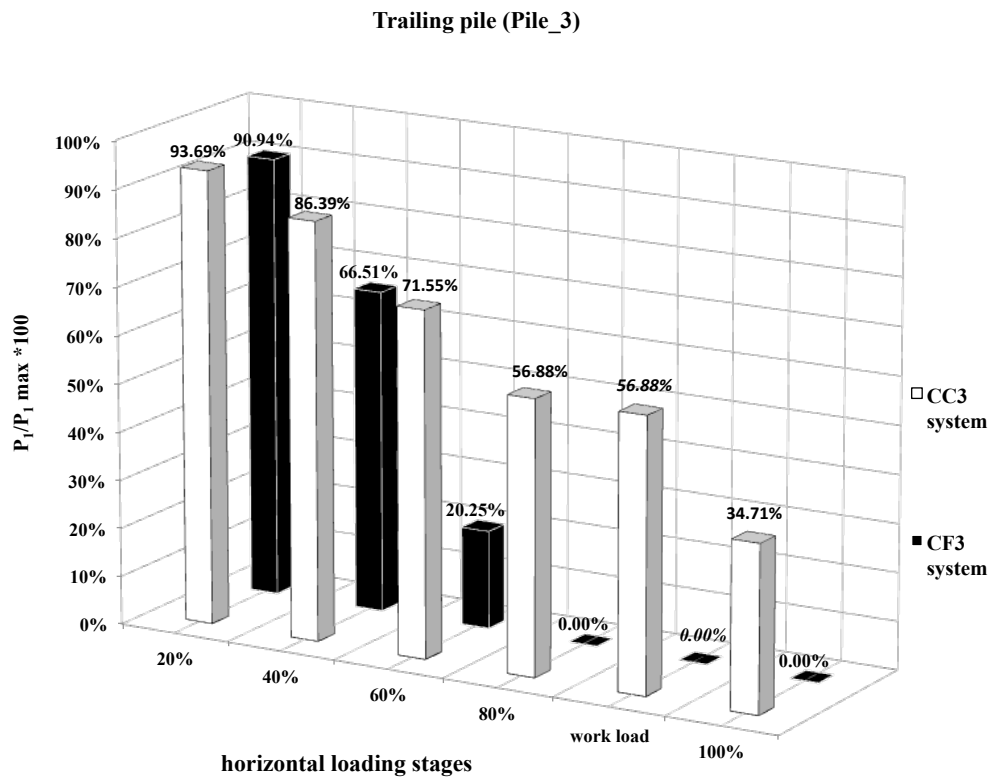


Figure 5.35. Pile 3 of the CC3 and CF3 foundation systems

Observing the figures above, the leading pile of both systems (pile 1) increases the vertical contact when the horizontal loading at the top of the raft is increasing; the leading pile of the defective system shows a greater vertical contact than the intact system (see Figure 5.33).

Concerning the trailing piles (2 and 3) of each foundation system, the opposite happens, meaning the vertical contact decreases when the horizontal loading at the top of the raft increases. When pile 2 of each system was compared, the defective pile shows a greater vertical contact than the intact pile (see Figure 5.34). Regarding pile 3 of each system, the pile of the intact system had vertical contact with the natural ground at all times; however, the same did not happen for the pile of the *CF3* defective system, which showed no further vertical contact with the natural ground as of the 80% loading stage (see Figure 5.35).

It should be noted that the defective pile 2 had more participation than the intact pile 2; therefore, a torsion effect was produced in the *CF3* foundation system due to the presence of the defective pile. As a result, the *CF3* system naturally compensates the horizontal load distribution over the other two pile components. In comparing the trailing piles of the intact system, it can be seen that their performance during all loading stages was very similar, almost equal (see Figure 5.34 and Figure 5.35).

It is important to mention that both 80% of the ultimate load (98 kN approximately) and the work load set (105 kN) for the *CF3* system are numerically very close; thus, it should be noted that in Figure 5.33, Figure 5.34 and Figure 5.35, for both foundation systems at those loading stages, the numerical values almost coincide according to Abaqus analysis.

Another comparison study was also carried out through the ultimate and work loads established by the criterion shown in Table 4.5 and under the work loads obtained by the criterion of allowable displacement (5% of the pile diameter) according to Table 4.6; the reason was to study through different optics the differences in tip behavior between those piled raft systems.

Therefore, it was possible to compare both failure criteria in the same graphic (see Figure 5.36 and Figure 5.37) to study the effect resulting from the presence of a defective pile.



The values of  $P_i$  and  $P_{imax}$  have already been defined in previous lines.

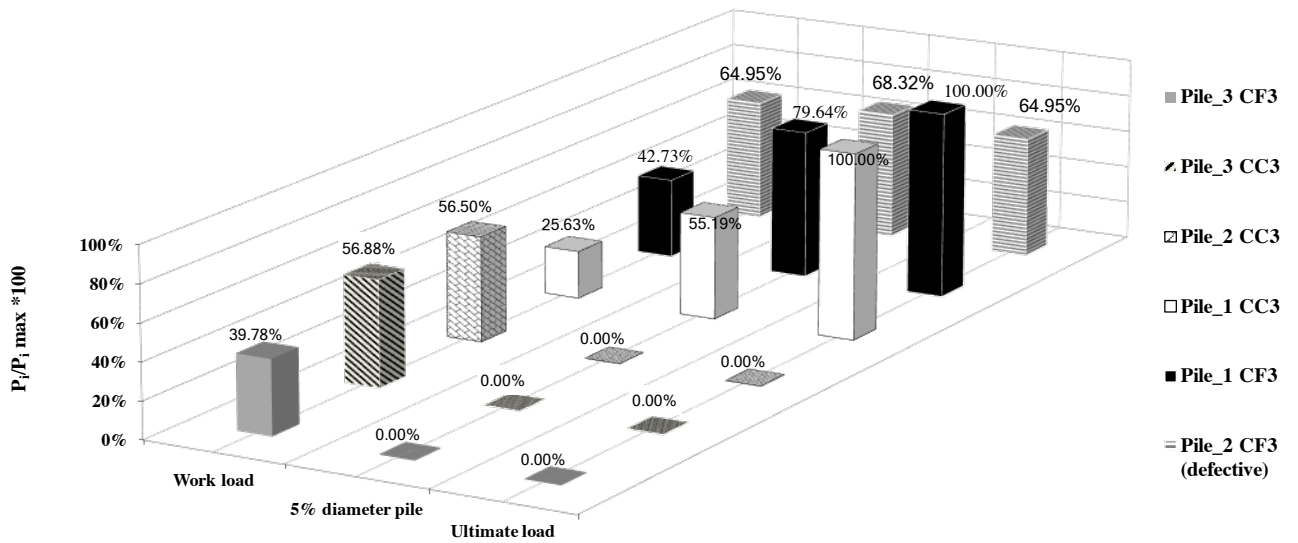


Figure 5.36. Evaluation of the effect of a defective pile for the *CC3* and *CF3* piled rafts through normalized loading.

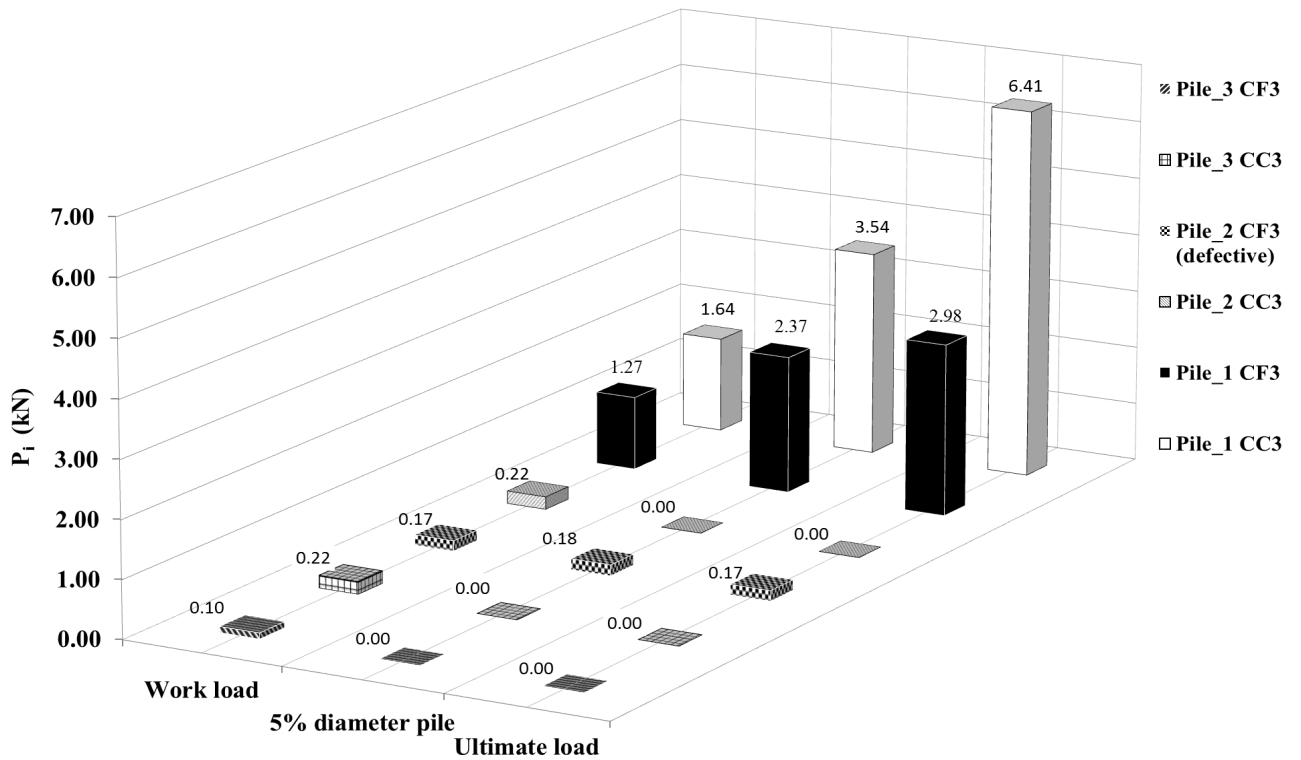


Figure 5.37. Evaluation of the effect of a defective pile for the *CC3* and *CF3* piled rafts through loading values.

*The CC4 and CF4 foundation systems*

Concerning the *CC4* and *CF4* systems, the same analysis of loading stages and normalization of the internal vertical loads as for the three-pile system was carried out; the only difference was the ultimate load and the work load used. For this comparative study, the loads were 180 kN and 170 kN respectively, both also shown in Table 4.6 (see section 4.3.1).

The reason why these loads were chosen is the same one previously given for the analysis of the *CF3* and *CC3* foundation systems, regarding the ultimate load calculated graphically. Figure 5.38, Figure 5.39, Figure 5.40, Figure 5.41 and Figure 5.42 show the global behavior at each loading stage for each foundation system.

Figure 5.39 and Figure 5.40 show that in the case of the leading piles of both systems (pile 1 and 2), overall the vertical contact increases when the horizontal loading at the top of the raft is also increased. The leading piles of the *CC4* intact system show similar performance, whereas those of the *CF4* defective system show a slight difference, because pile 1 supports greater loading than the defective pile 2.

Therefore, it is deduced that by increasing the number of piles in the system, the influence of the defective pile decreases, which is logical.

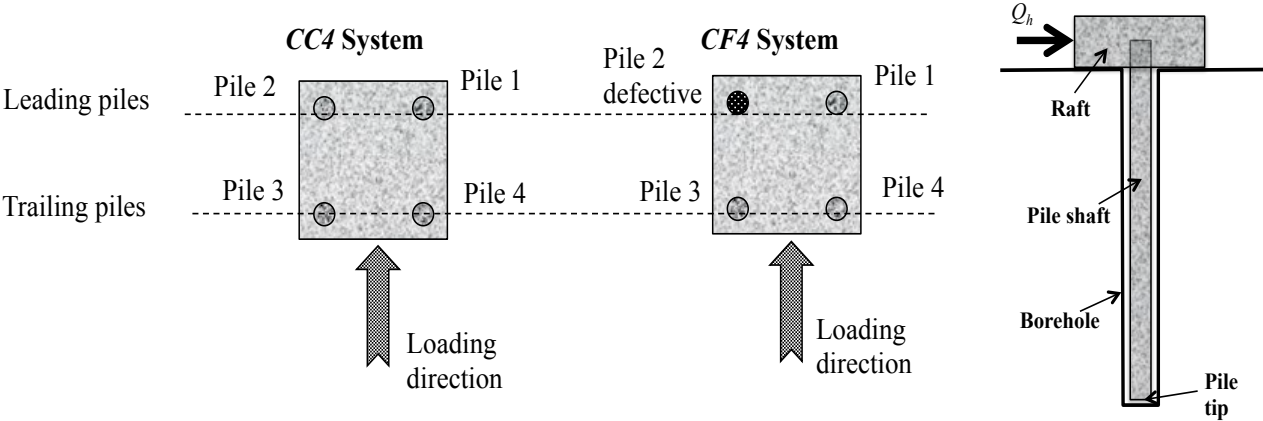


Figure 5.38. Sketch of the *CC4* and *CF4* foundation systems

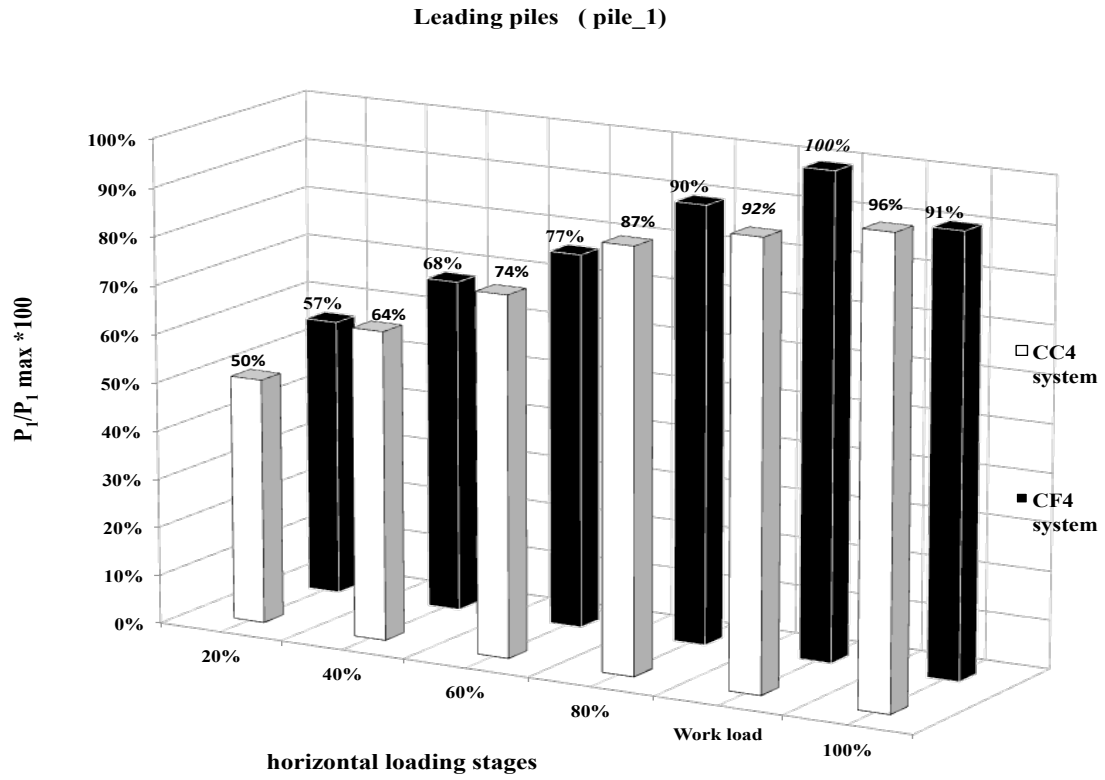


Figure 5.39. Pile 1 of the *CC4* and *CF4* foundation systems

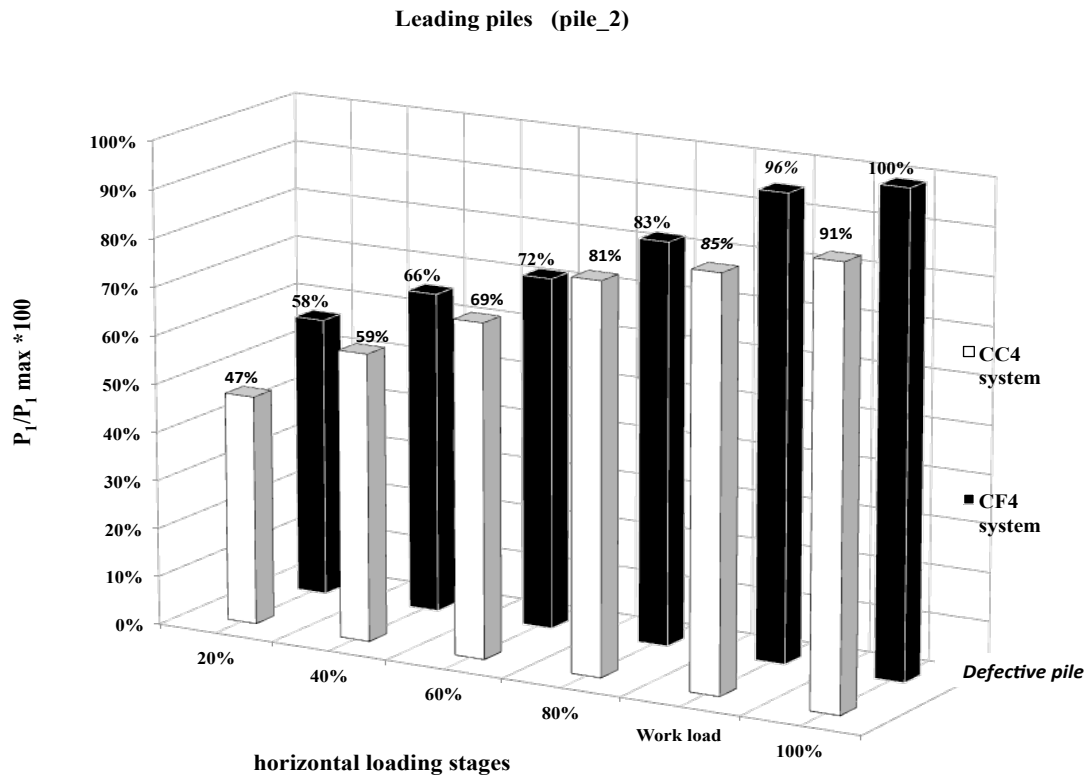


Figure 5.40. Pile 2 of the *CC4* and *CF4* foundation systems

Trailing piles (pile\_3)

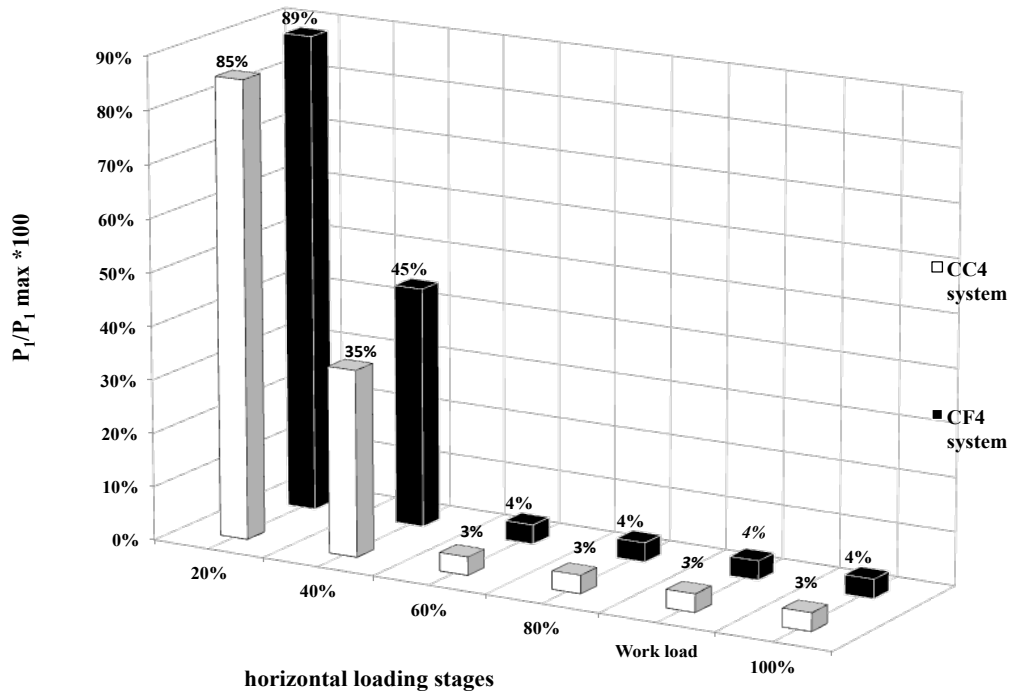


Figure 5.41. Pile 3 of the *CC4* and *CF4* foundation systems

Trailing piles (pile\_4)

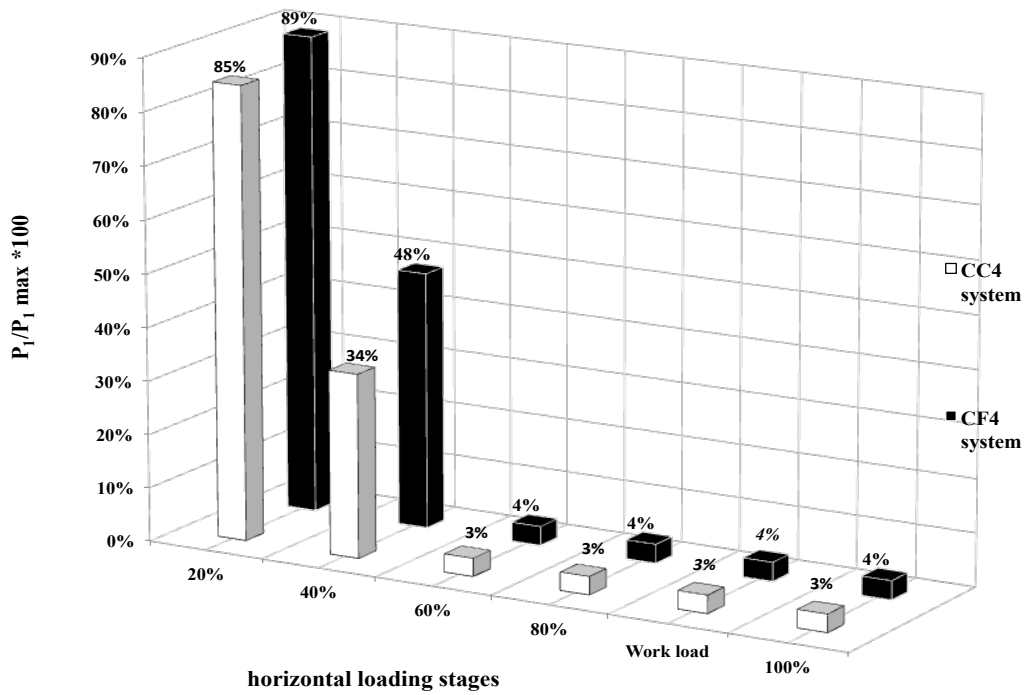


Figure 5.42. Pile 4 of the *CC4* and *CF4* foundation systems

Concerning the trailing piles of each system the opposite happens (piles 3 and 4), meaning the vertical contact decreases when the horizontal loading at the top of the raft increases. Their performances were very similar for both piles of each system; they even remained almost the same when comparing both piles between both systems. Attention should be drawn to the fact that from the 40% loading stage, the vertical contact decreased dramatically and remained constant thereafter in the following loading stages. All those details can be seen in Figure 5.41 and Figure 5.42.

Finally, it is possible to deduce that the number of piles and the geometric position of them, when comparing the *CF3* and *CF4* foundation systems, made the torsion effect decrease, because in three-pile system the distribution of the internal forces was uneven, whereas for the system with four piles the distribution was more even.

Also, the same analysis made for the three-piles systems (and the same reasons) was carried out to compare both failure criteria in the same graphic (see Figure 5.43 and Figure 5.44) to study the effect due to the presence of a defective pile in the systems with four piles.

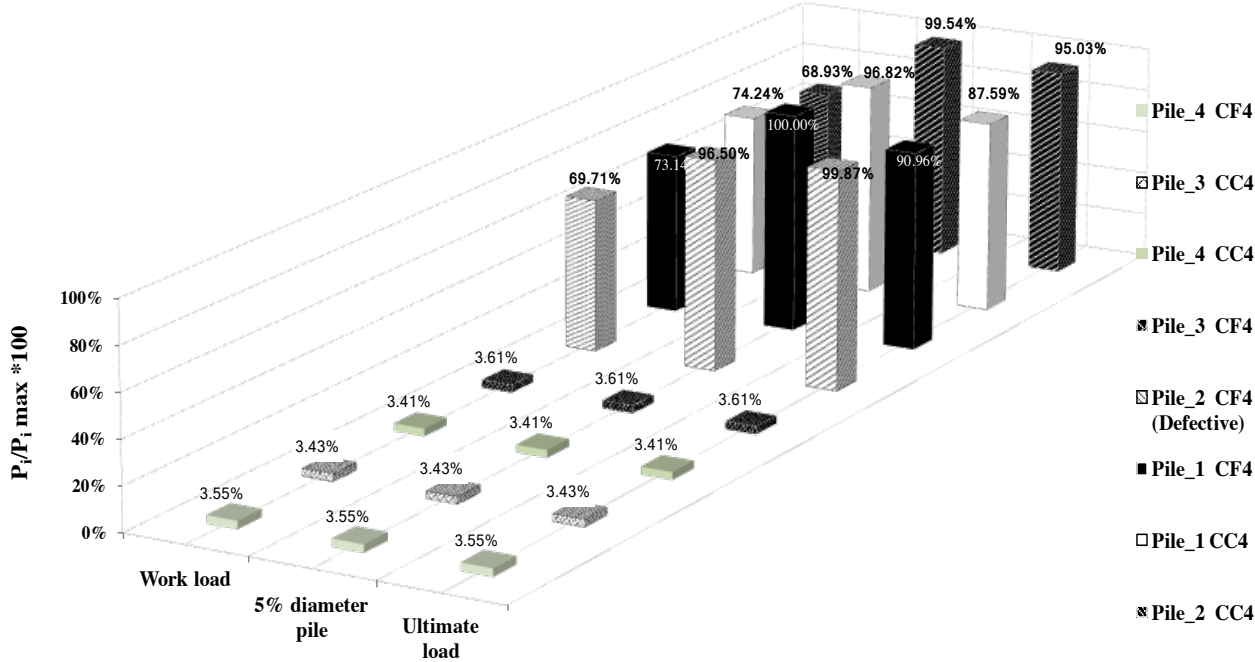


Figure 5.43. Evaluation of the effect of a defective pile for the *CC4* and *CF4* piled rafts through normalized loading.

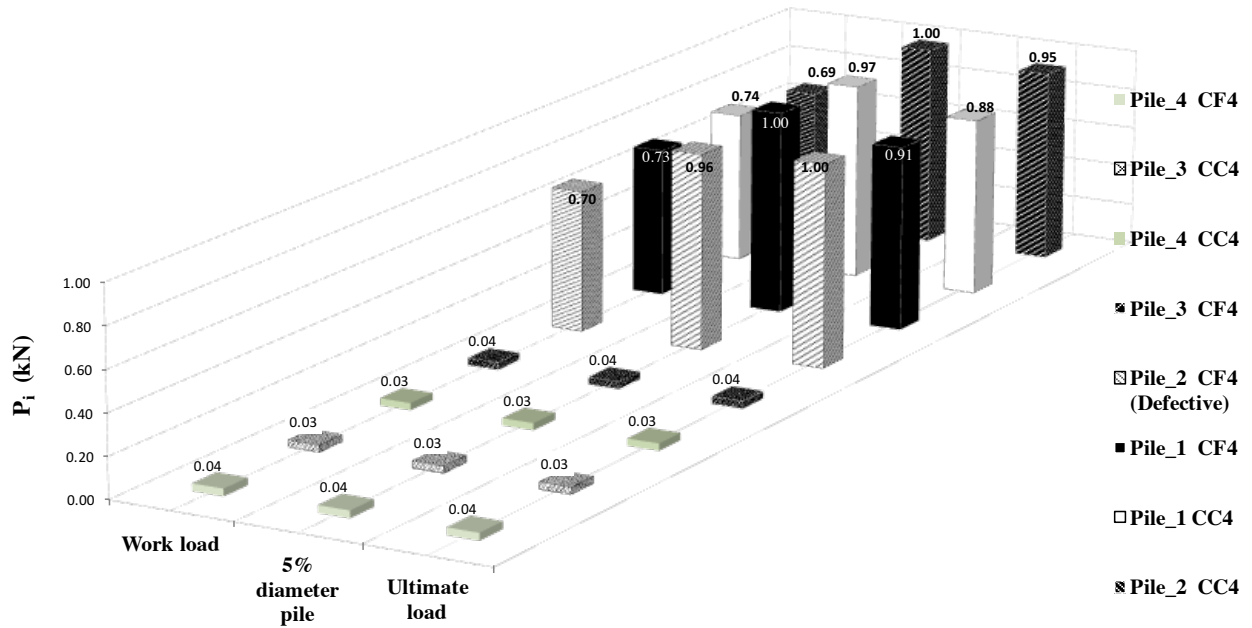


Figure 5.44. Evaluation of the effect of a defective pile for the *CC4* and *CF4* piled rafts through loading values.

## 5.7.2 RAFT TILTING

In the same way as the behavior of the tips subjected to different loading stages was studied, the raft behavior of each system was also studied; first, the variable tilting position of each raft was obtained through the angle  $\psi_i$ . Second, the angle obtained in each loading stage was normalized with respect to the maximum angle  $\psi_{max}$  developed at the end of the ultimate horizontal load applied, meaning  $(\psi_i / \psi_{max})$ . It should be recalled that the *CC3* and *CF3* systems were analyzed under the *CF3* ultimate load, and the *CC4* and *CF4* systems under the *CF4* ultimate load.

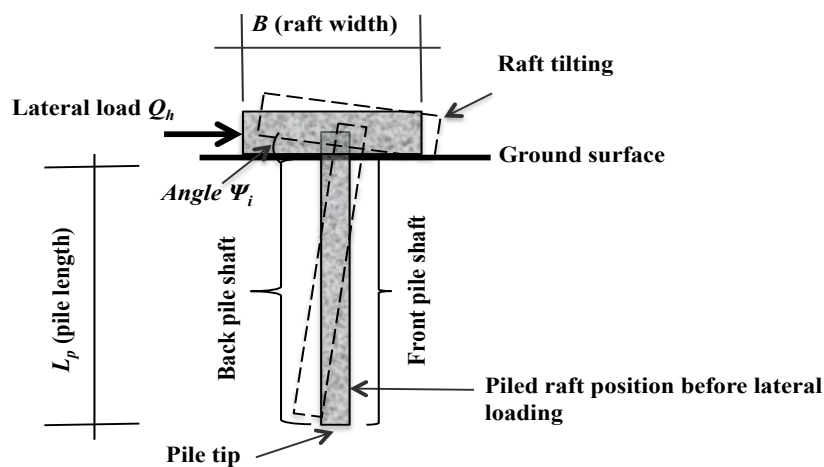


Figure 5.45. Sketch of the raft tilting

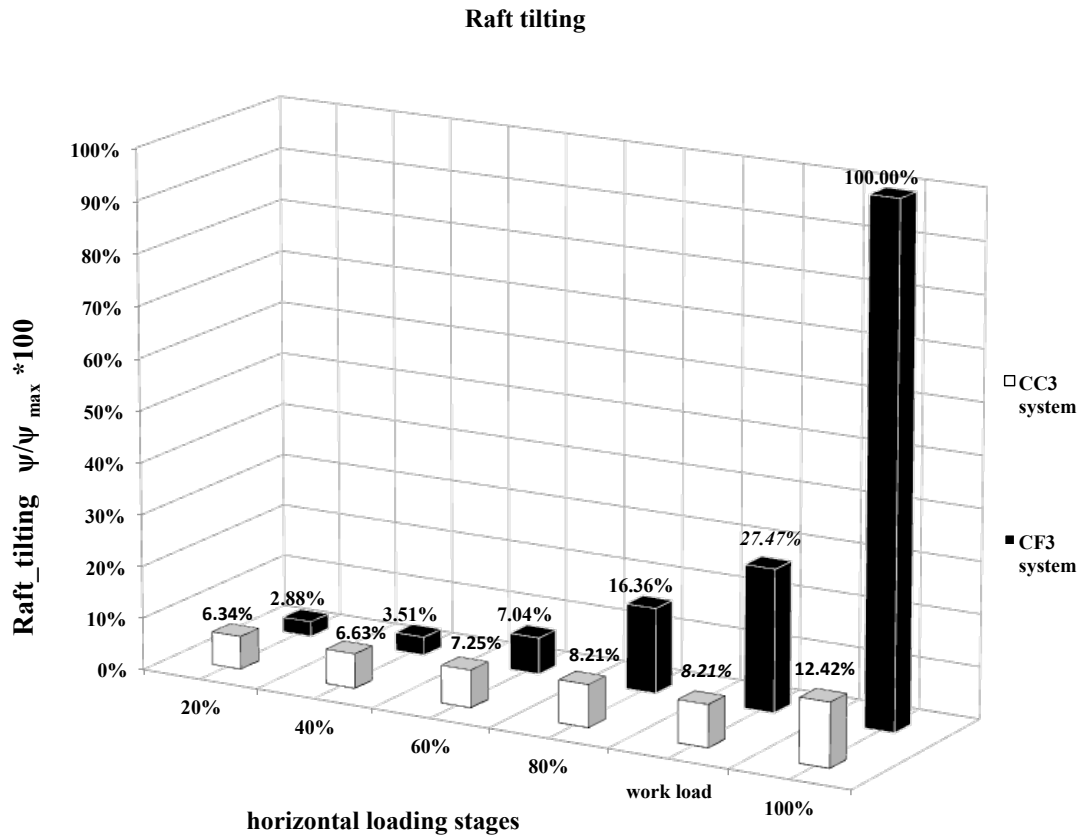


Figure 5.46. The raft tilting of the *CC3* and *CF3* foundation systems.

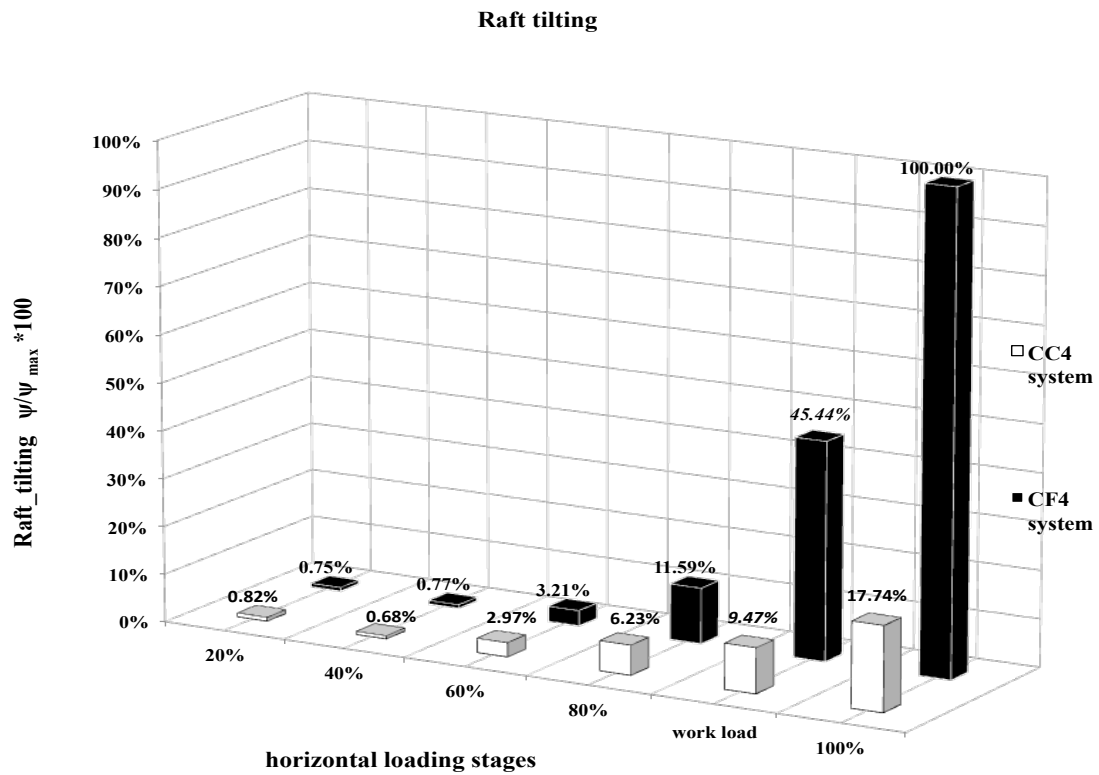


Figure 5.47. The raft tilting of the *CC4* and *CF4* foundation systems.

The behavior of the *CC3* and *CF3* rafts was found to be exactly the same as the leading pile tips in both the *CC3* and *CF3* systems (see Figure 5.33 and Figure 5.46). This was because the leading piles are the only components that receive all the compression internal force transmitted by the raft during the tilting.

Concerning the *CC4* and *CF4* rafts, it was found that the tilting under the same loading stages was almost equal until the 60% loading stage, but from the 80% loading stage it was uneven; thus, it can be deduced that the position of the defective pile as the leading pile in the *CF4* system causes the difference; therefore, by relating the performance between the pile tips (see Figure 5.39 and Figure 5.40) and the raft (see Figure 5.47), it is possible to understand the influence of the defective pile.

Therefore, it is verified that the geometric position of defective and intact piles, as well as the number of them, made the effect of tilting and torsion increase or decrease, when the systems with three and four piles were compared.

Another method used to analyze the tilting for these foundations systems was by means of the two criteria discussed at section 4.3.1(see Table 4.5 and Table 4.6). The two failure criteria were compared in the same graphic (see Figure 5.48 and Figure 5.49) to study the effect resulting from the presence of a defective pile in the systems with four piles.

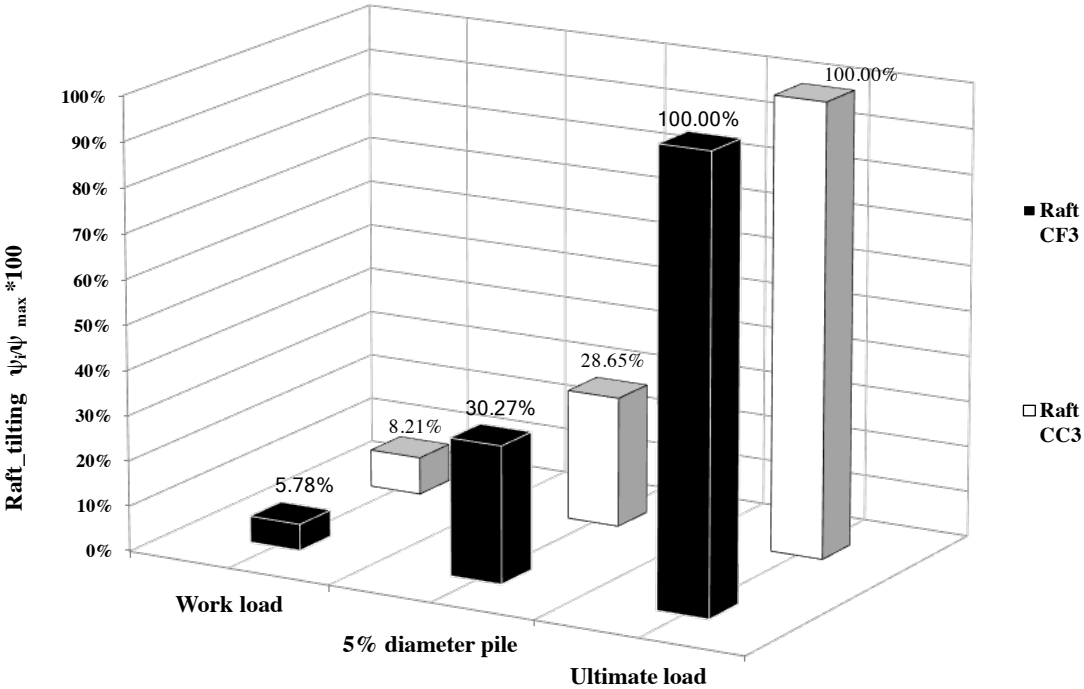


Figure 5.48. The raft tilting of the *CC3* and *CF3* foundation systems.



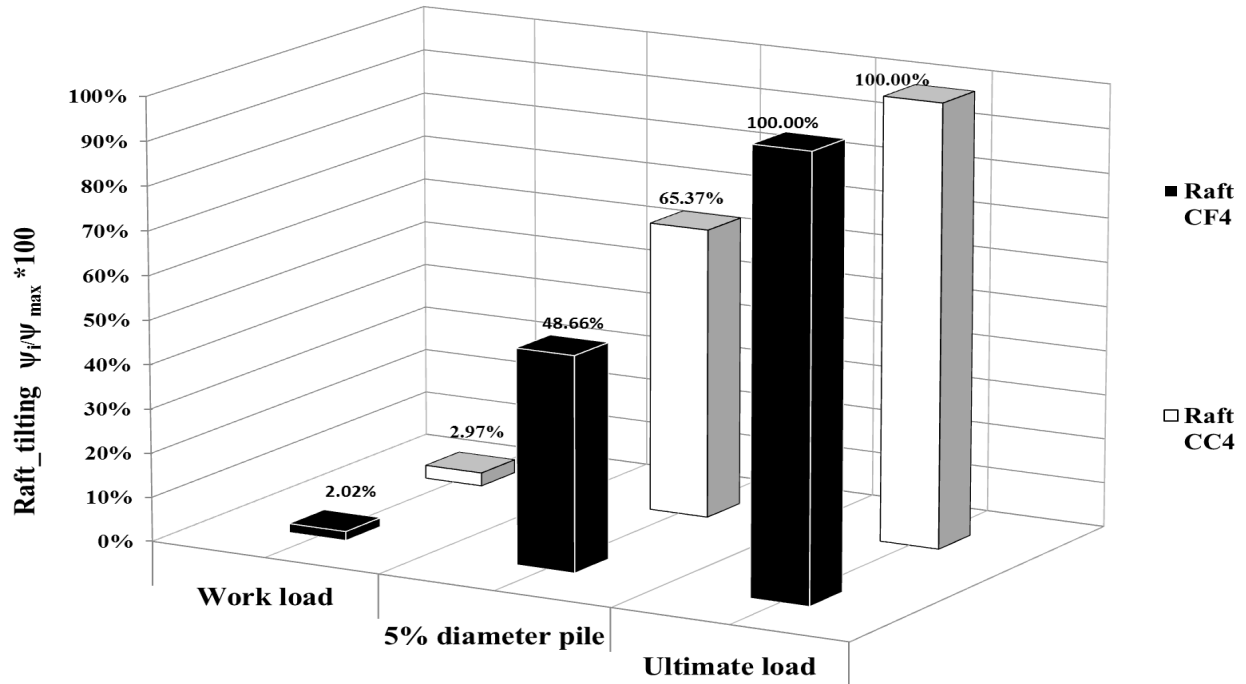


Figure 5.49. The raft tilting of the *CC4* and *CF4* foundation systems.

### 5.7.3 INTERACTION BETWEEN THE PILE SHAFT AND THE GROUND

To analyze the interaction behavior among the pile shaft faces, both front and back, and the vertical borehole wall, the work load was adopted as the only loading stage for all analyses. As in the previous studies and for reasons already given, the *CF3* work load was set to analyze both foundation systems with three piles, and the *CF4* work load was set to analyze both foundation systems with four piles.

The depths of interest to carry out those studies were set according to the nodes of the soil mesh along the pile shaft-soil contact length to obtain those interaction forces. The systems with three piles had the same soil mesh according to their Abaqus model; the same was true for the systems with four piles with respect to their Abaqus model.

#### *Horizontal subgrade force analysis*

The pile shaft-borehole wall interaction behavior was analyzed through the horizontal subgrade forces acting on both front and back walls of the borehole, at several depths of interest, along the vertical borehole (see Figure 5.50).

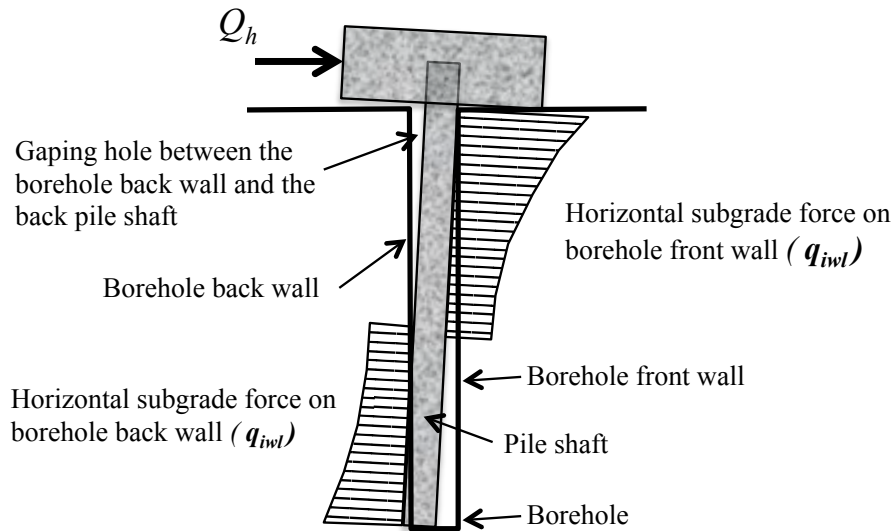


Figure 5.50. Sketch of the horizontal subgrade force transmitted by the pile shaft to the vertical borehole walls.

First, the horizontal subgrade force  $q_{iwl}$  transmitted from both pile faces to the vertical walls of the borehole at each depth of interest, for each pile, was obtained from the numerical results. Second, the maximum horizontal subgrade force  $q_{imaxwl}$  developed during the respective loading stage (*CF3* or *CF4* work loading) was obtained; finally, the horizontal subgrade forces were normalized, meaning  $q_{iwl} / q_{imaxwl}$  for front and back vertical walls respectively.

With respect to the signs, the positive sign means compression force in the same direction as the loading, whereas the negative means also compression force but in the opposite direction to the lateral loading, both generating passive forces. Figures 5.51 to 5.57 show the numeric analysis results for each pile of each foundation system.

According to the horizontal subgrade forces transmitted from the front pile face to the vertical front wall along the pile-soil contact length, it was observed that the greatest contact occurred at 1.0 m depth for all piles of both systems, thereafter decreasing with depth but always maintaining contact with the vertical front wall; with regard to the defective pile (see Figure 5.52), it can be seen that it had no contact between 1.5 to 2.5 m depth, where the defective section is located, but it had greater contact than all other piles of the *CF3* system between 3.0 to 4.5 m depth.

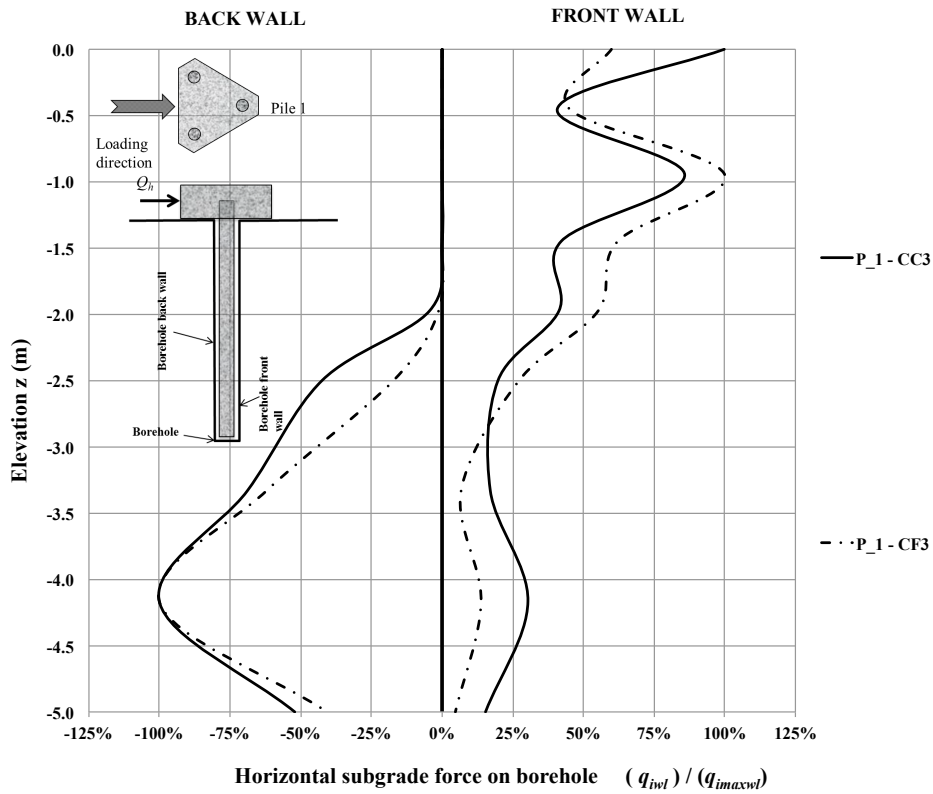


Figure 5.51. The horizontal subgrade force transmitted by pile 1 to the borehole vertical walls in both the CC3 and CF3 foundation systems.

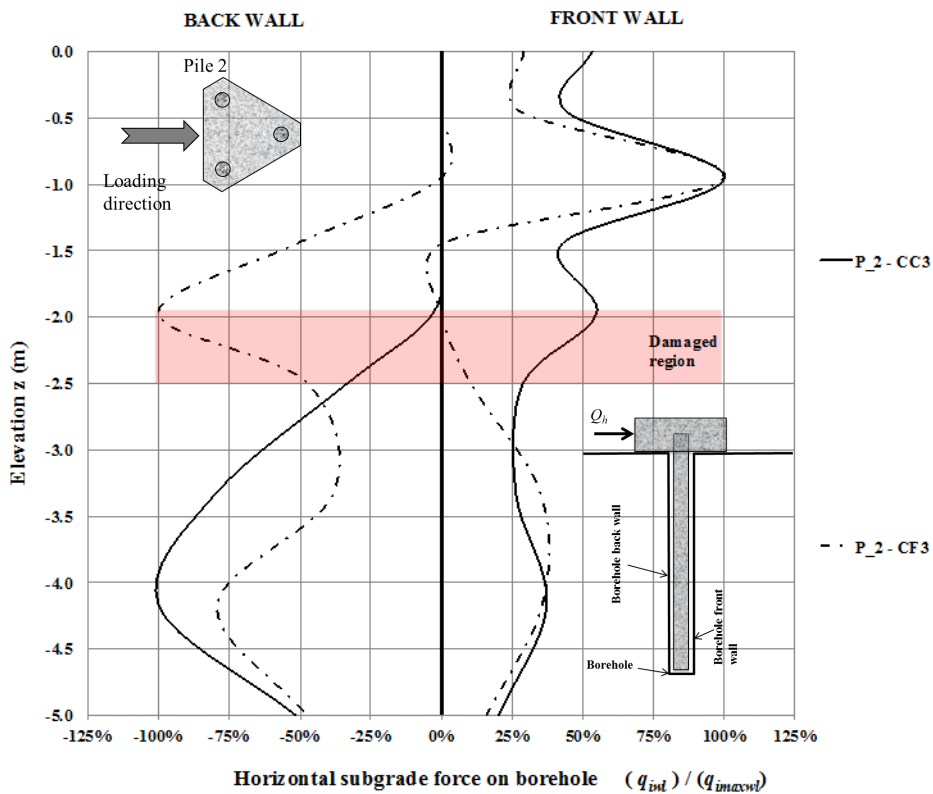


Figure 5.52. The horizontal subgrade force transmitted by pile 2 to the borehole vertical walls in both the CC3 and CF3 foundation systems.

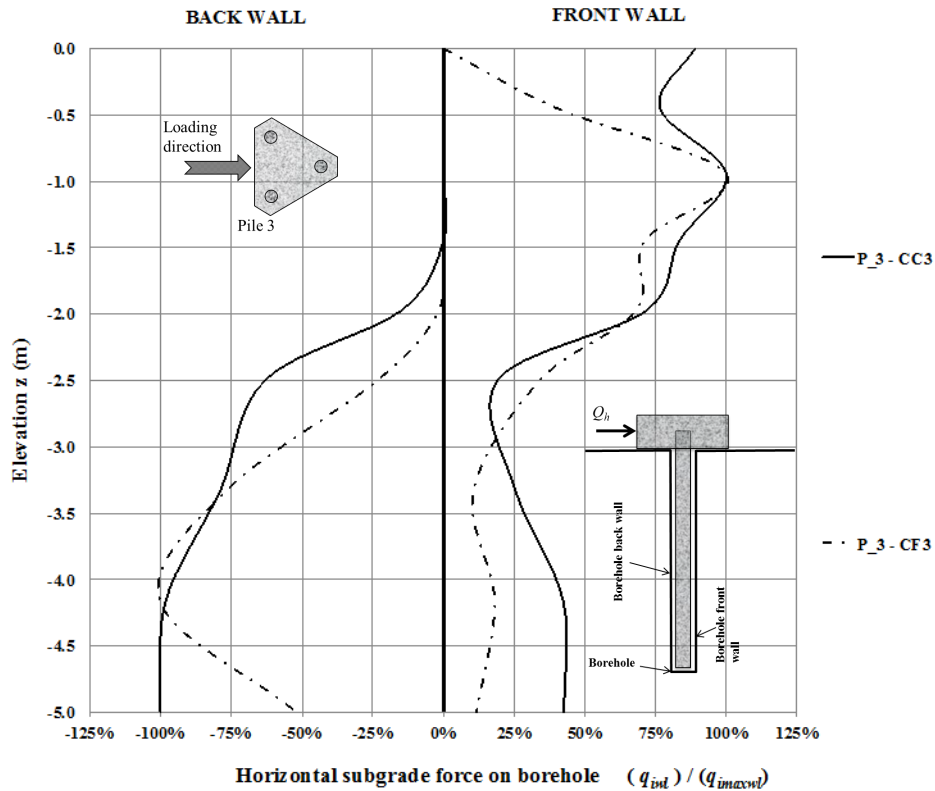


Figure 5.53. The horizontal subgrade force transmitted by pile 3 to the borehole vertical walls in both the *CC3* and *CF3* foundation systems.

On the other hand, referring to the forces transmitted from the back pile face to the vertical back wall along the pile-soil contact length, it was observed that the greatest contact occurs at 4.0 m depth for all piles of both systems. However, for the defective pile only, the greatest contact occurs at 2.0 m depth, exactly where the damage section is placed, and from this depth thereafter the contact begins to decrease. Finally, the gaping hole formation was observed, between 0.0 m and 1.80 m depth for all piles of both systems; hence, it is possible to assume that a plastic hinge is formed around this depth for each of them.

Concerning the horizontal subgrade forces transmitted from the front pile face to the vertical borehole front wall along the pile-soil contact length for the *CC4* and *CF4* systems, it was observed that the greatest contact was developed at 1.0 m depth in each pile of both systems, and decreased with depth. However, at 3.25 m depth the subgrade forces were reduced to zero for all piles until 4.0 m depth; from this depth until the bottom of the pile, low subgrade normal forces appeared, except for pile 1 of both systems.

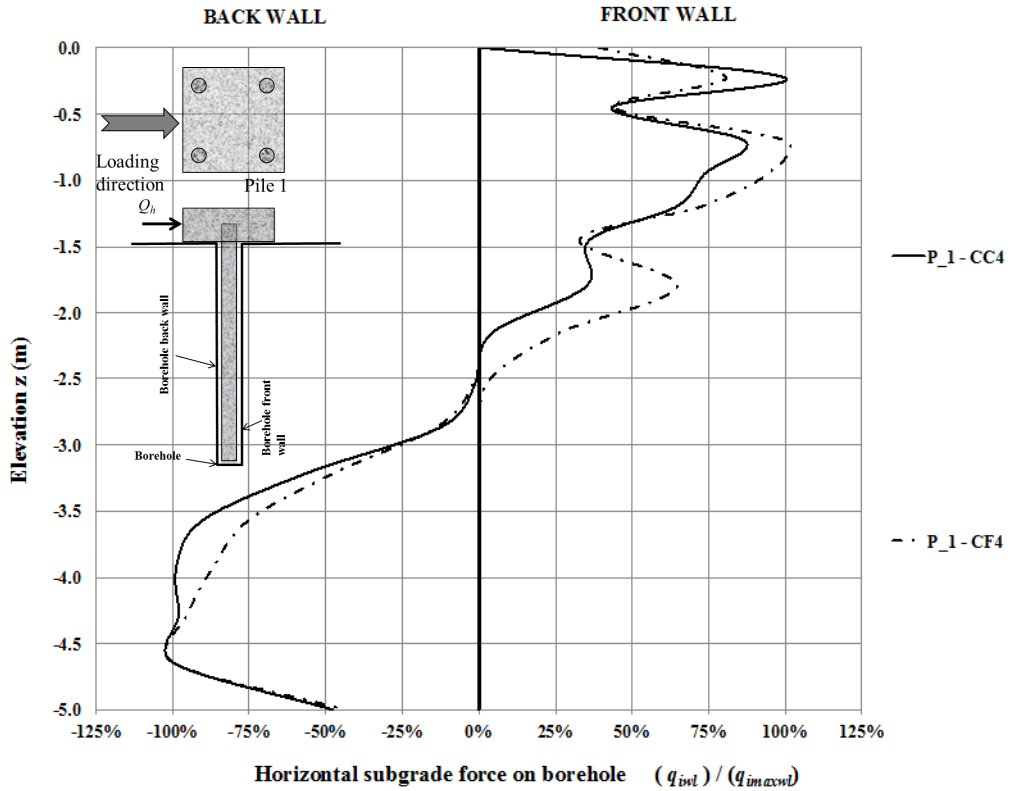


Figure 5.54. The horizontal subgrade force transmitted by pile 1 to the borehole vertical walls in both the CC4 and CF4 foundation systems.

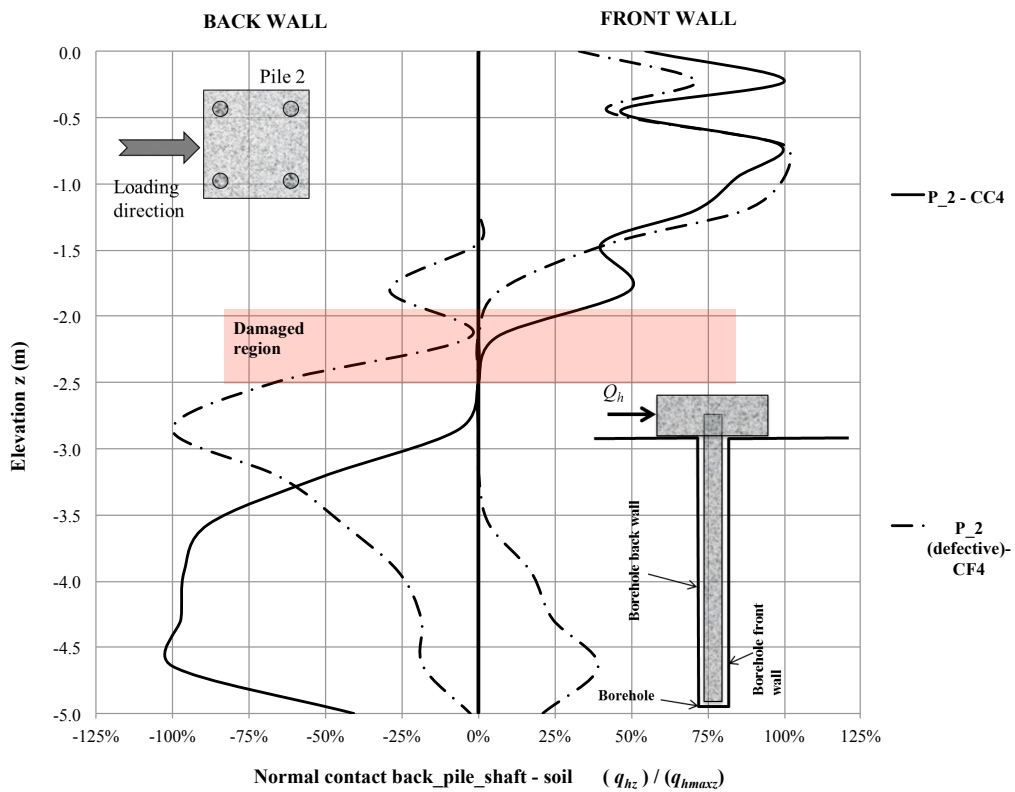


Figure 5.55. The horizontal subgrade force transmitted by pile 2 to the borehole vertical walls in both the CC4 and CF4 foundation systems.

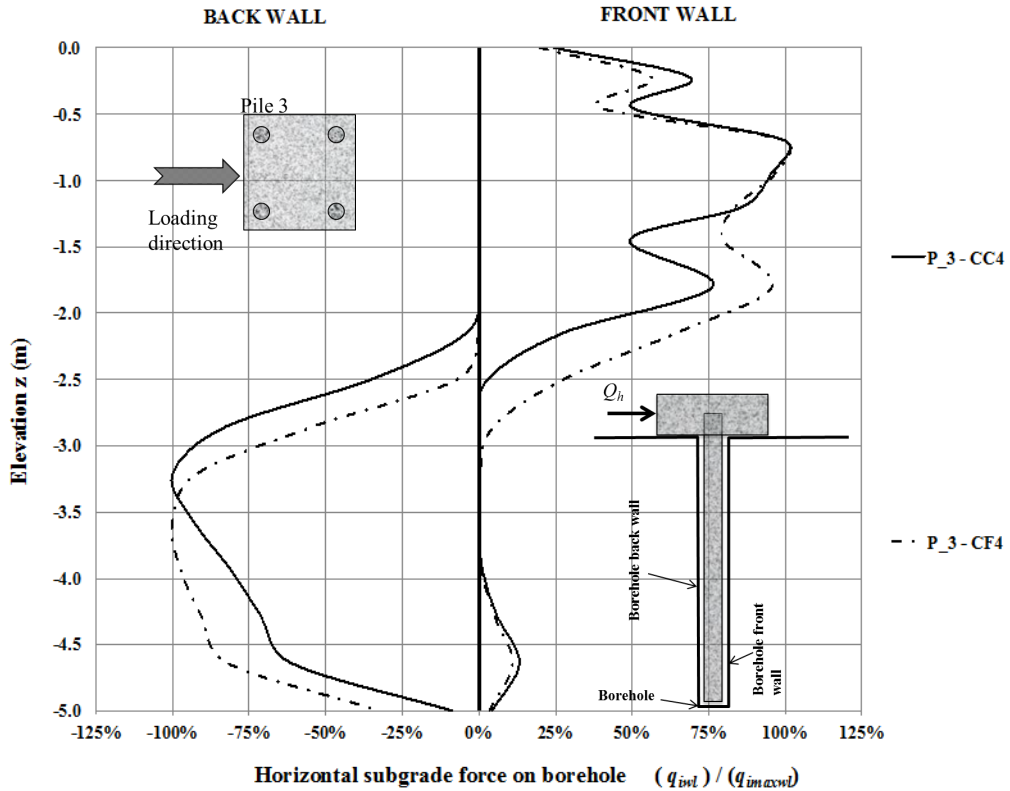


Figure 5.56. The horizontal subgrade force transmitted by pile 3 to the borehole vertical walls in both the CC4 and CF4 foundation systems.

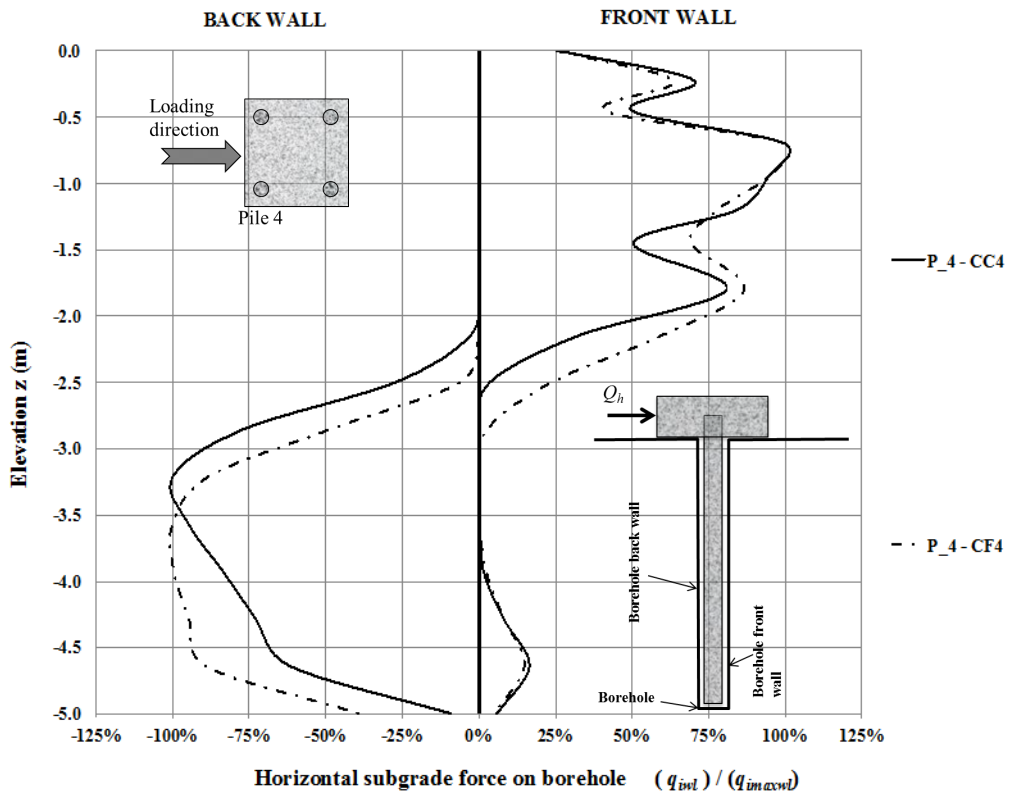


Figure 5.57. The horizontal subgrade force transmitted by pile 4 to the borehole vertical walls in both the CC4 and CF4 foundation systems.

Relating to the defective pile, it reflects its difference from all the others especially near the pile tip (see Figure 5.55).

On the other hand, referring to the horizontal subgrade forces transmitted from the back pile face to the vertical borehole back wall along the pile-soil contact length, it was observed that the greatest contacts occur between 3.5 m and 4.5 m depth for all piles of both systems, except the defective pile; it developed the largest contact at 2.80 m depth, thereafter decreasing with depth until reaching zero at the pile tip.

Finally, the formation of a gaping hole was observed between 0.0 m and almost 2.00 m depth, although the defective pile had low contact at 1.80 m depth; hence, it is possible to assume that a plastic hinge is formed around those depths.

#### *Lateral shear force analysis*

The interaction behavior between the pile shaft faces and the vertical borehole was analyzed through the lateral shear forces  $l_{sf}$  acting on both vertical walls of the borehole. The free body diagram of the borehole in Figure 5.58 shows the direction of acting forces over the vertical walls, taking the vertical borehole as reference during these analyses.

To carry out this analysis, first the lateral shear force acting under the work loading stage  $l_{sf_{wl}}$  was obtained at different depths of interest, which in turn depended on the nodes of the soil mesh according to the Abaqus models. Second, the maximum lateral shear force  $l_{sf_{maxwl}}$  developed during their respective work loading stages (*CF3* or *CF4* work loading) was obtained; finally, the lateral shear forces for all piles was normalized, meaning  $l_{sf_{wl}} / l_{sf_{maxwl}}$  for both front and back vertical walls.

From Figure 5.59 to Figure 5.72 the numeric analysis results for each pile of each foundation system are shown.

### Free body diagram

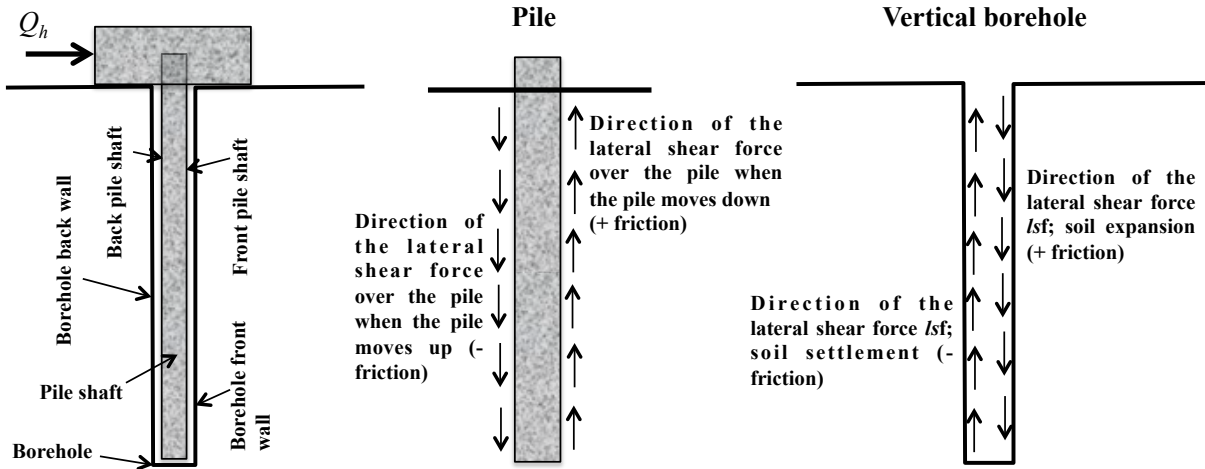


Figure 5.58. Sketch of the lateral shear forces transmitted by the pile shaft to the borehole vertical walls.

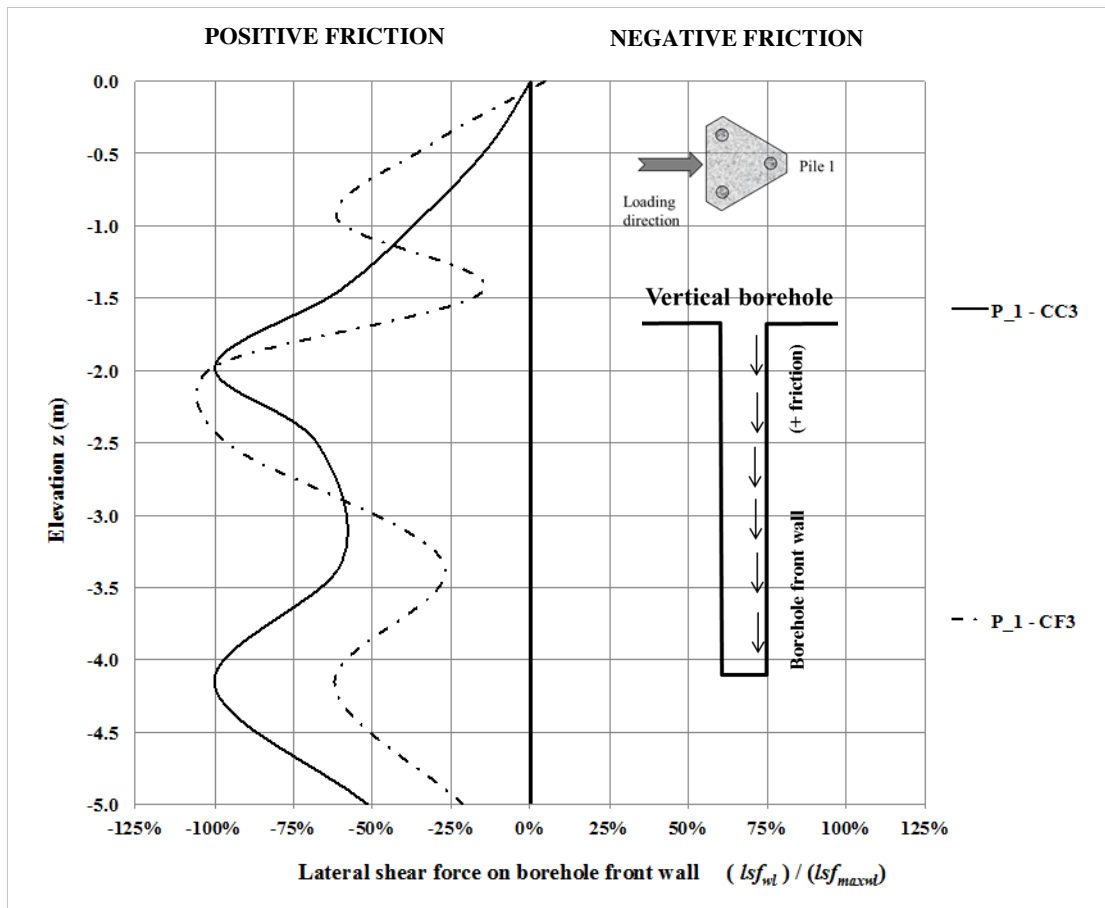


Figure 5.59. The lateral shear force transmitted by pile 1 to the front vertical wall in both the CC3 and CF3 foundation systems.



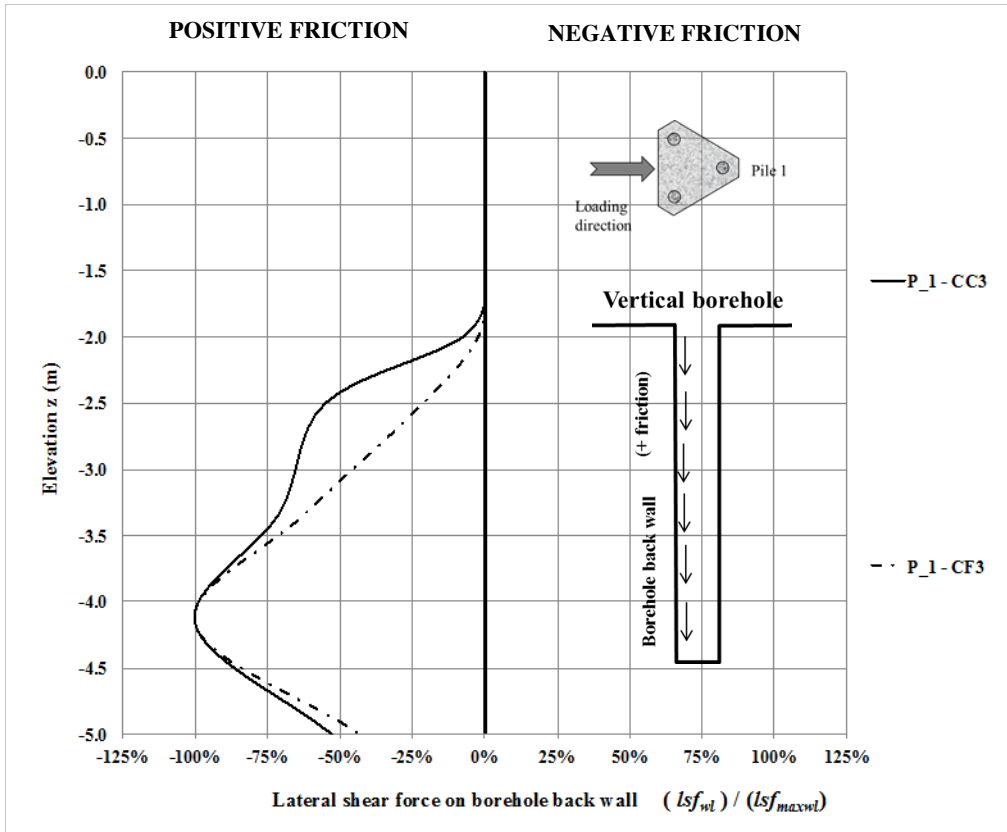


Figure 5.60. The lateral shear force transmitted by pile 1 to the back vertical wall in both the *CC3* and *CF3* foundation systems.

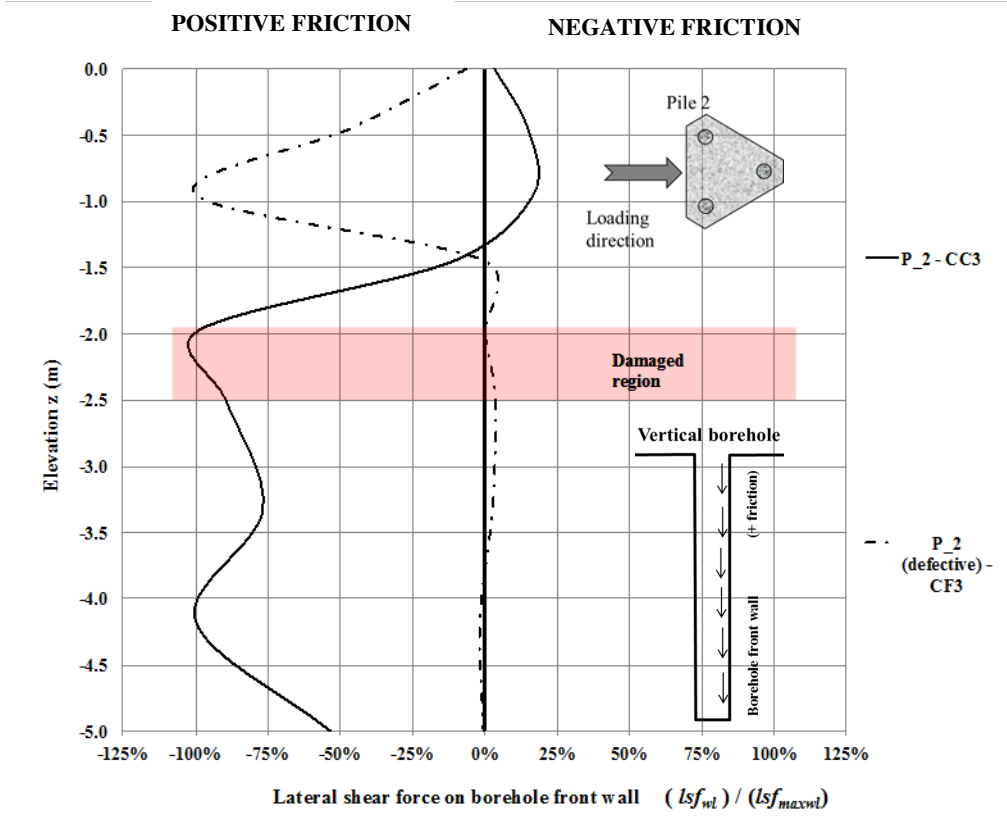


Figure 5.61. The lateral shear force transmitted by pile 2 to the front vertical wall in both the *CC3* and *CF3* foundation systems.

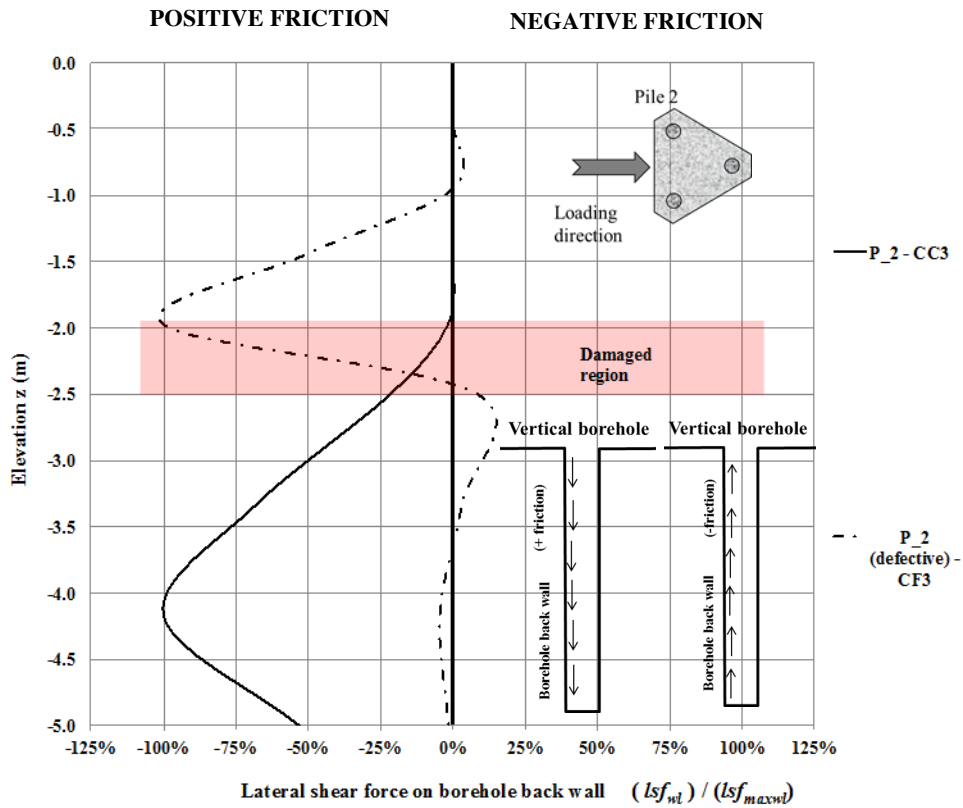


Figure 5.62. The lateral shear force transmitted by pile 2 to the back vertical wall in both the *CC3* and *CF3* foundation systems.

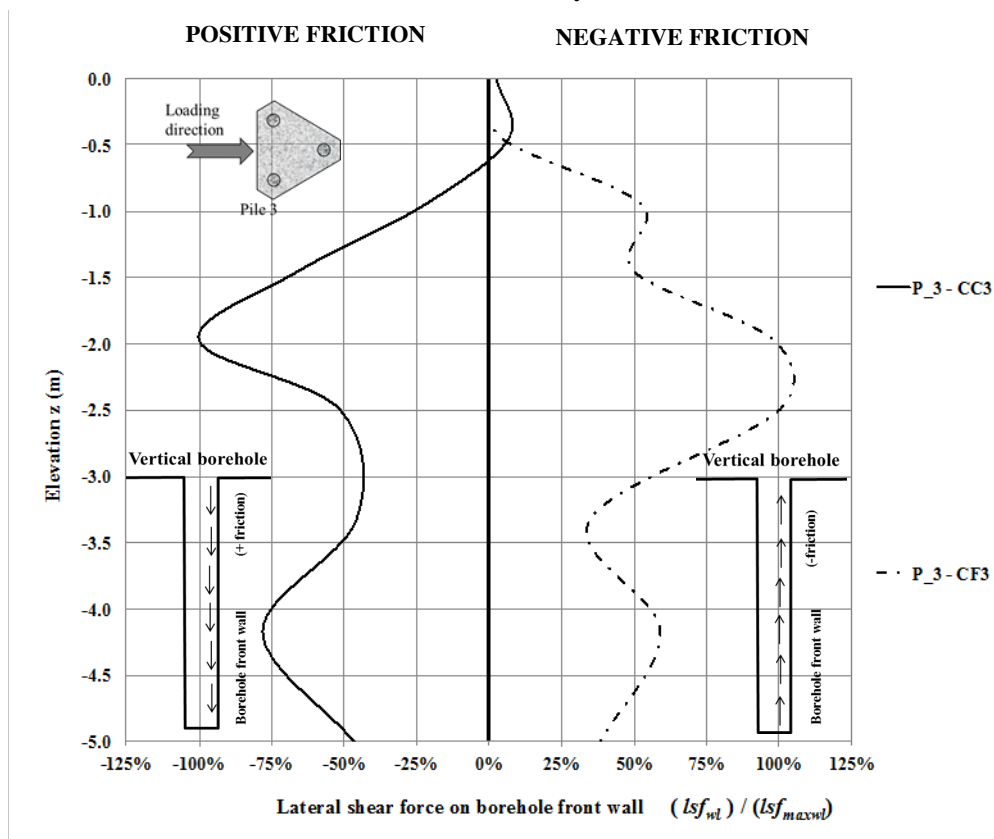


Figure 5.63. The lateral shear force transmitted by pile 3 to the front vertical wall in both the *CC3* and *CF3* foundation systems.

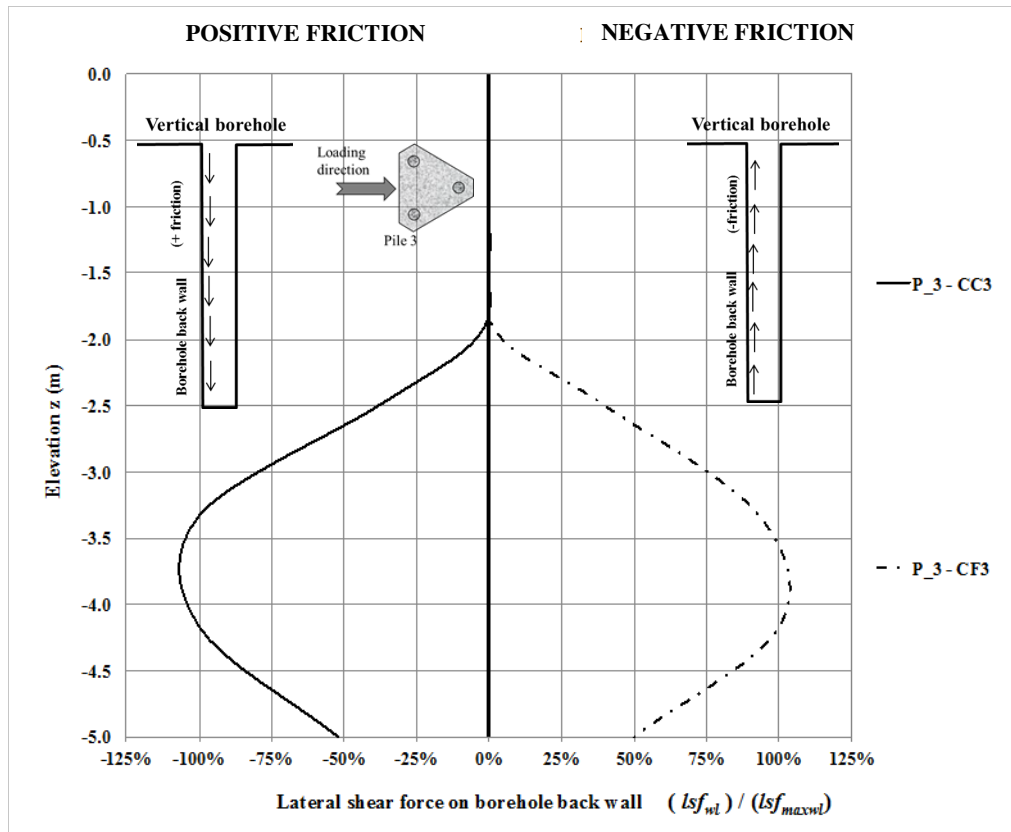


Figure 5.64. The lateral shear force transmitted by pile 3 to the back vertical wall in both the *CC3* and *CF3* foundation systems.

The behavior over the borehole front wall turned out to be both interesting and unexpected. In the two systems, pile I had a similar positive friction behavior, but for pile 2 there was a difference between the two systems: although both showed positive friction, the defective pile had low performance. Surprisingly, pile 3 behavior in the two systems was opposite in that while the *CC3* system pile had positive friction, the *CF3* system pile showed negative friction performance.

In relation to over the vertical borehole back wall, each pile of each system showed a similar performance in terms of the direction of lateral shear forces. However, a gaping hole formed between 0.0 and 2.0 m depth, because there was no contact between the pile and the borehole; therefore, a plastic hinge developed at more or less this depth.

The analyses confirm that the uneven distribution and direction of lateral forces produced a torsion effect, especially in the *CF3* system. Regarding the *CC3* system, it was possible to realize that the geometric arrangement of the piles had some influence due to the uneven performance of the trailing piles.

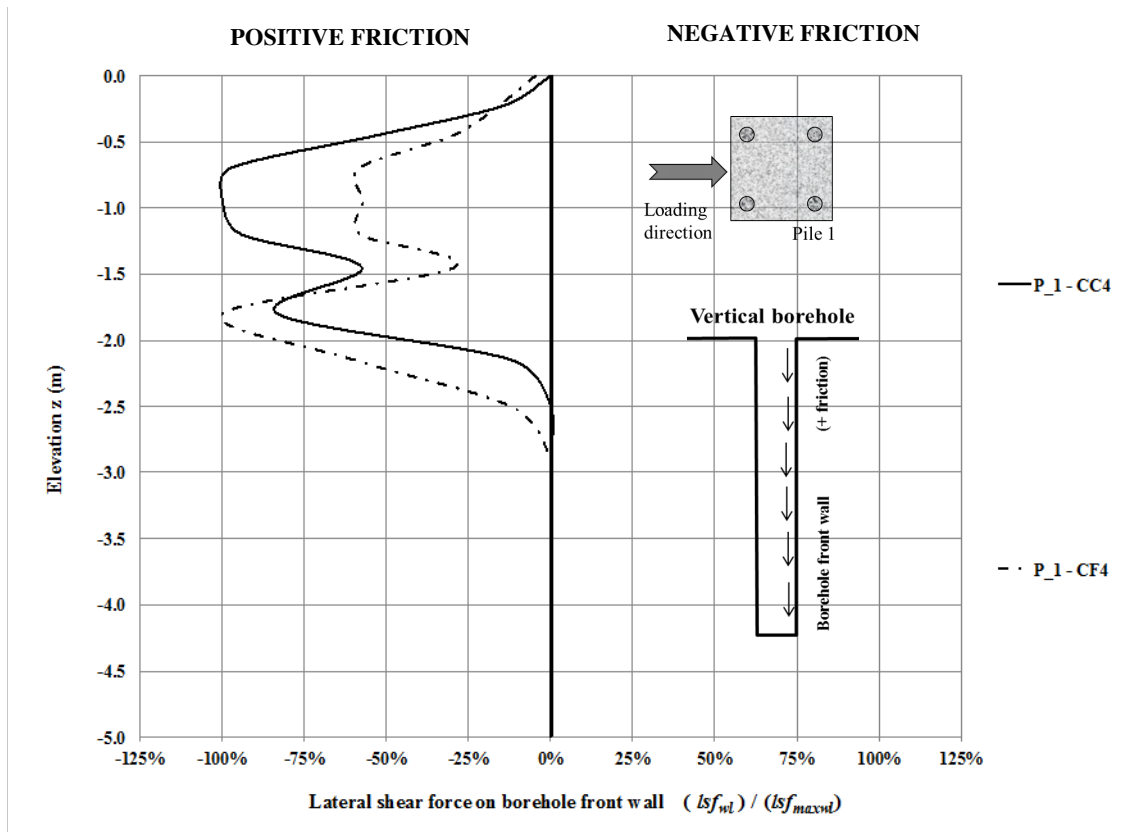


Figure 5.65. The lateral shear force transmitted by pile 1 to the front vertical wall in both the *CC4* and *CF4* foundation systems.

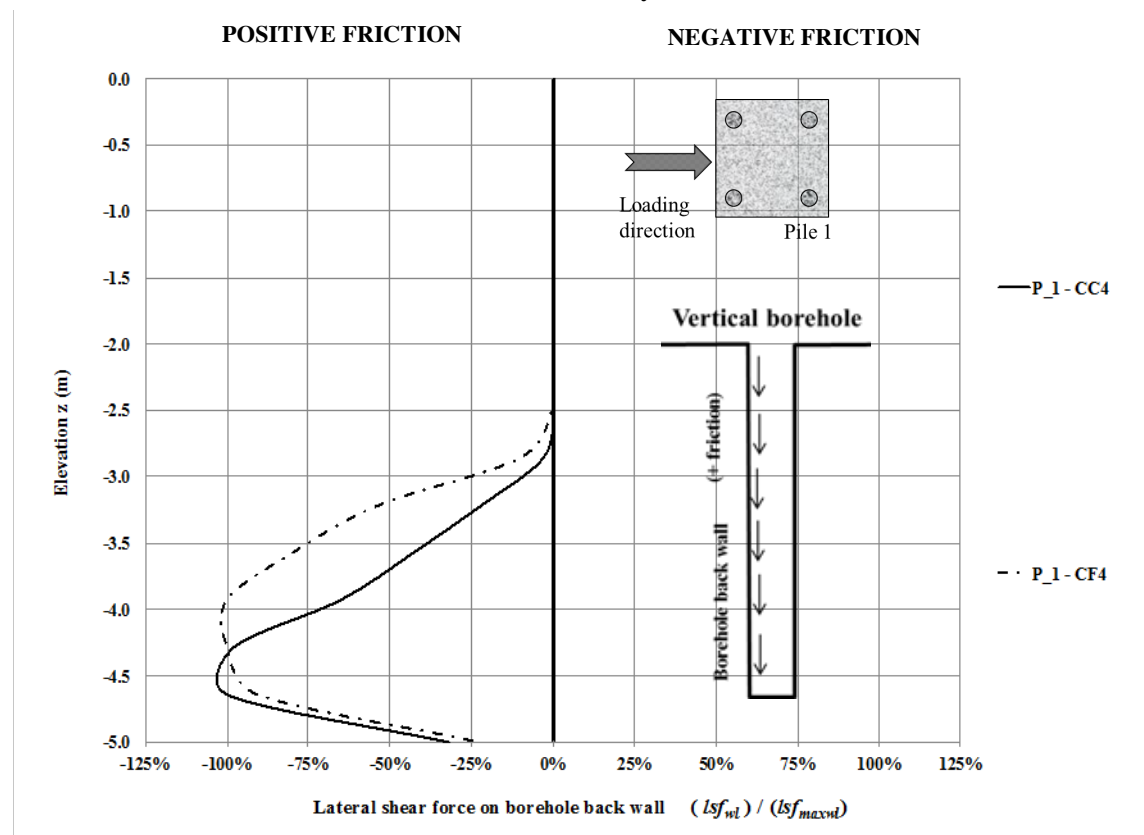


Figure 5.66. The lateral shear force transmitted by pile 1 to the back vertical wall in both the *CC4* and *CF4* foundation systems.

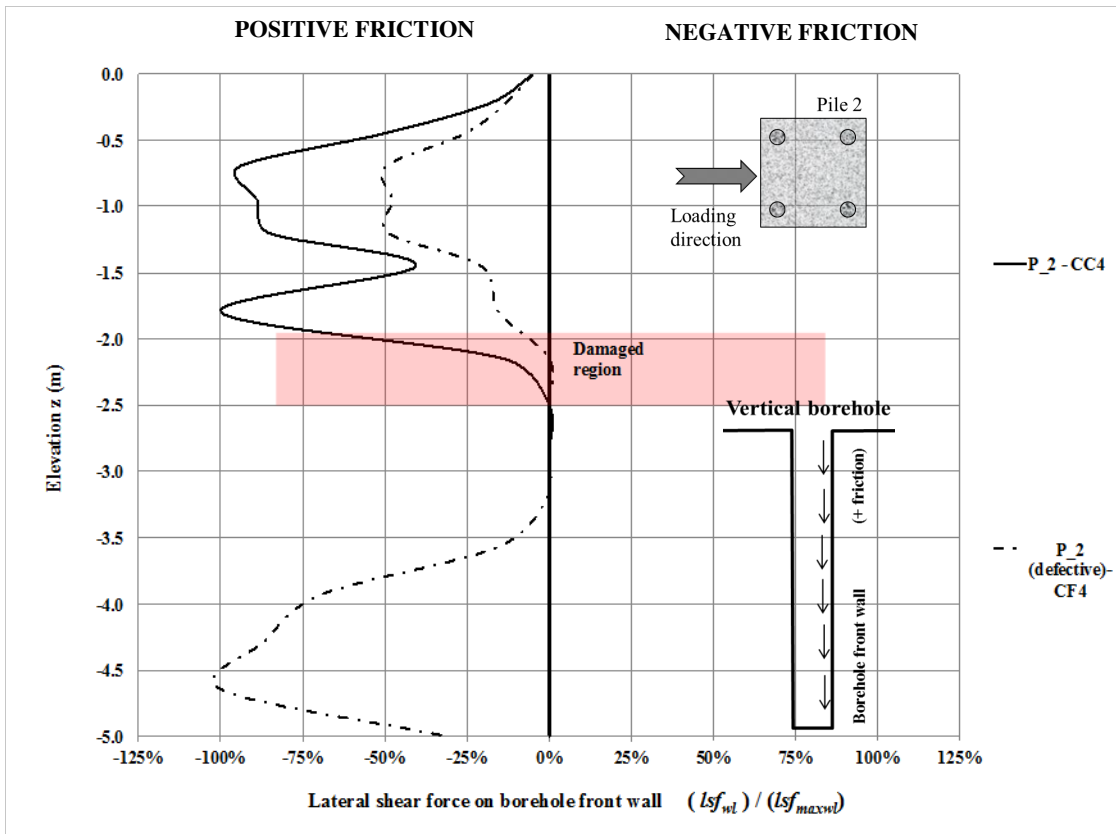


Figure 5.67. The lateral shear force transmitted by pile 2 to the front vertical wall in both the *CC4* and *CF4* foundation systems.

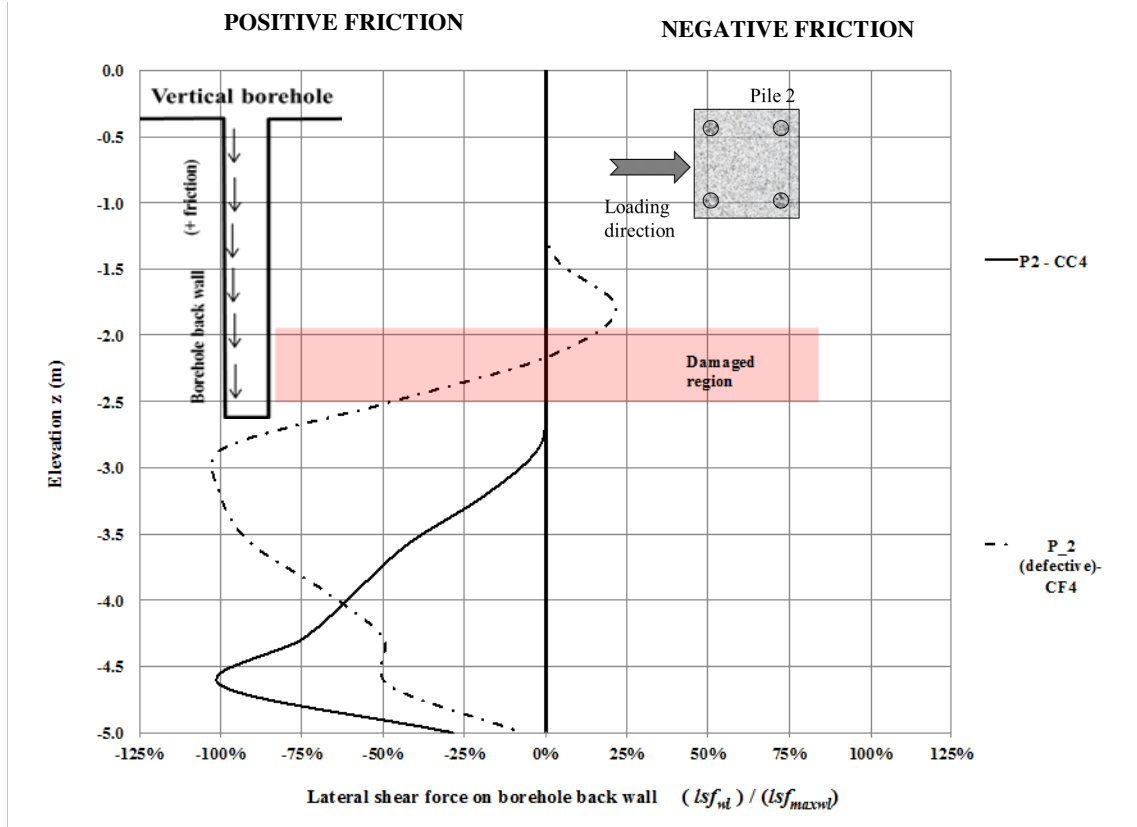


Figure 5.68. The lateral shear force transmitted by pile 2 to the back vertical wall in both the *CC4* and *CF4* foundation systems.

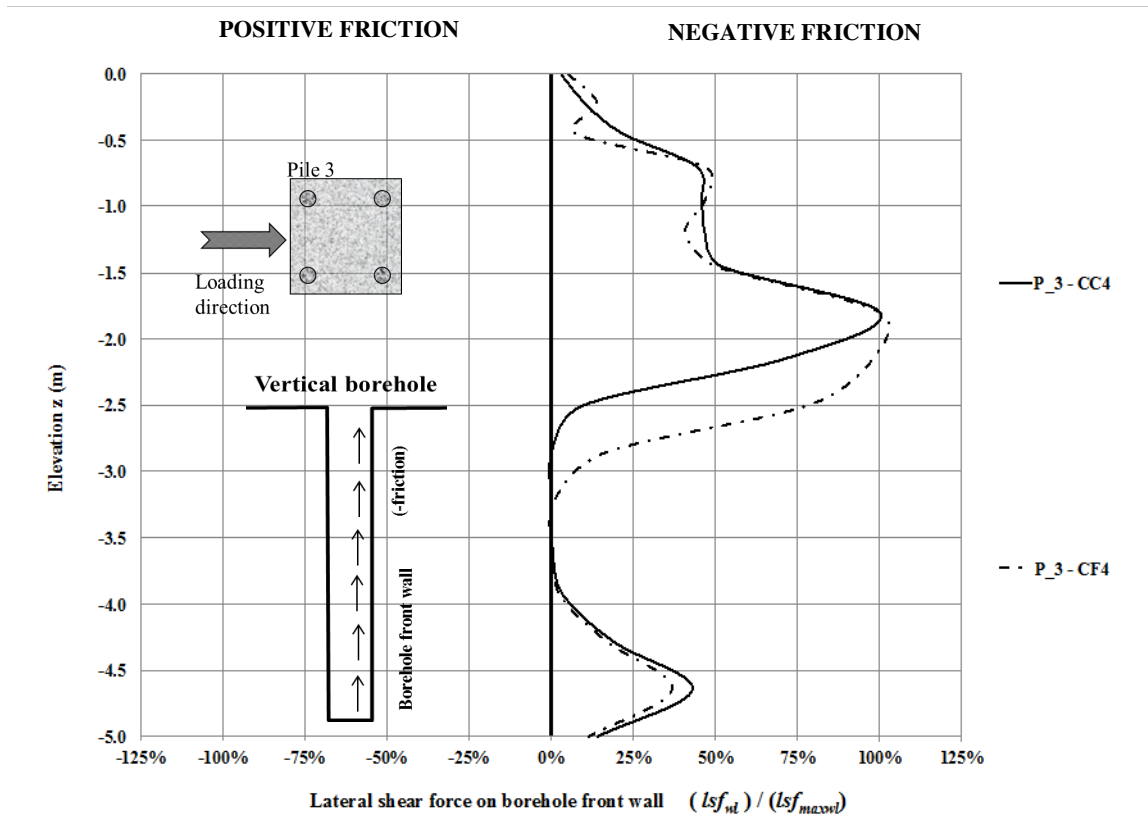


Figure 5.69. The lateral shear force transmitted by pile 3 to the front vertical wall in both the *CC4* and *CF4* foundation systems.

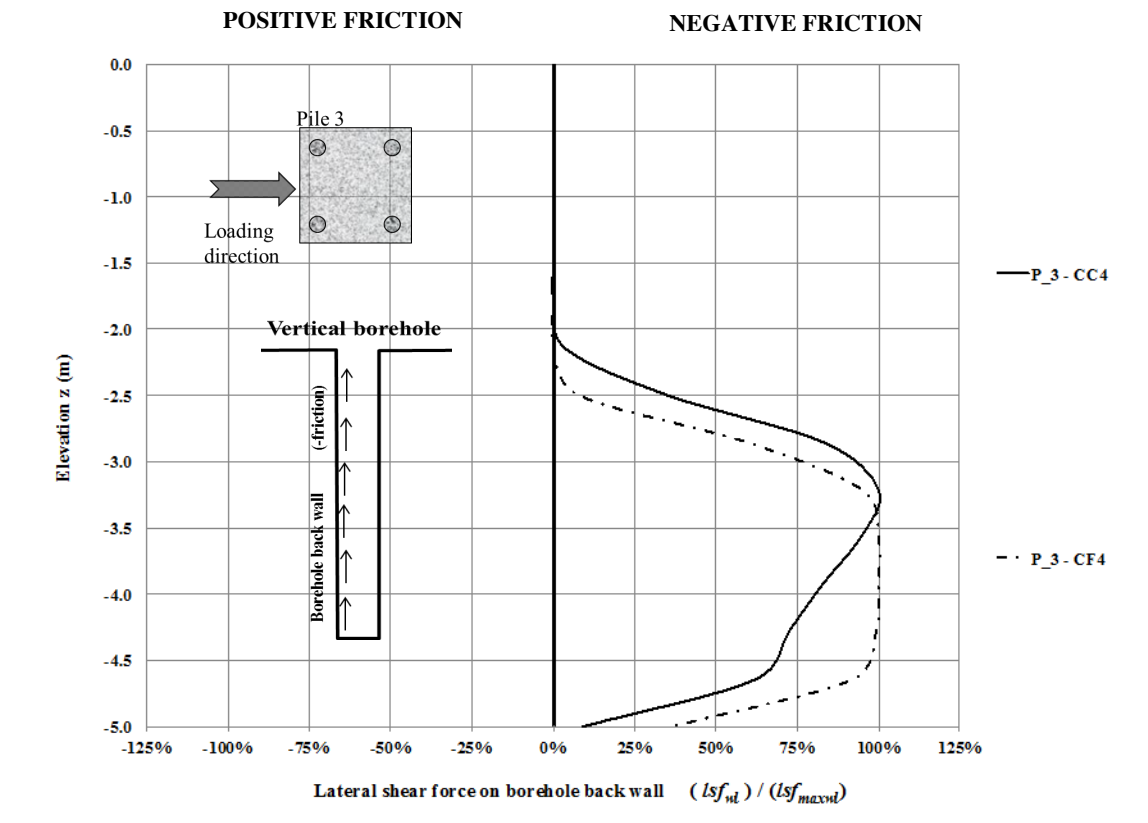


Figure 5.70. The lateral shear force transmitted by pile 3 to the back vertical wall in both the *CC4* and *CF4* foundation systems.

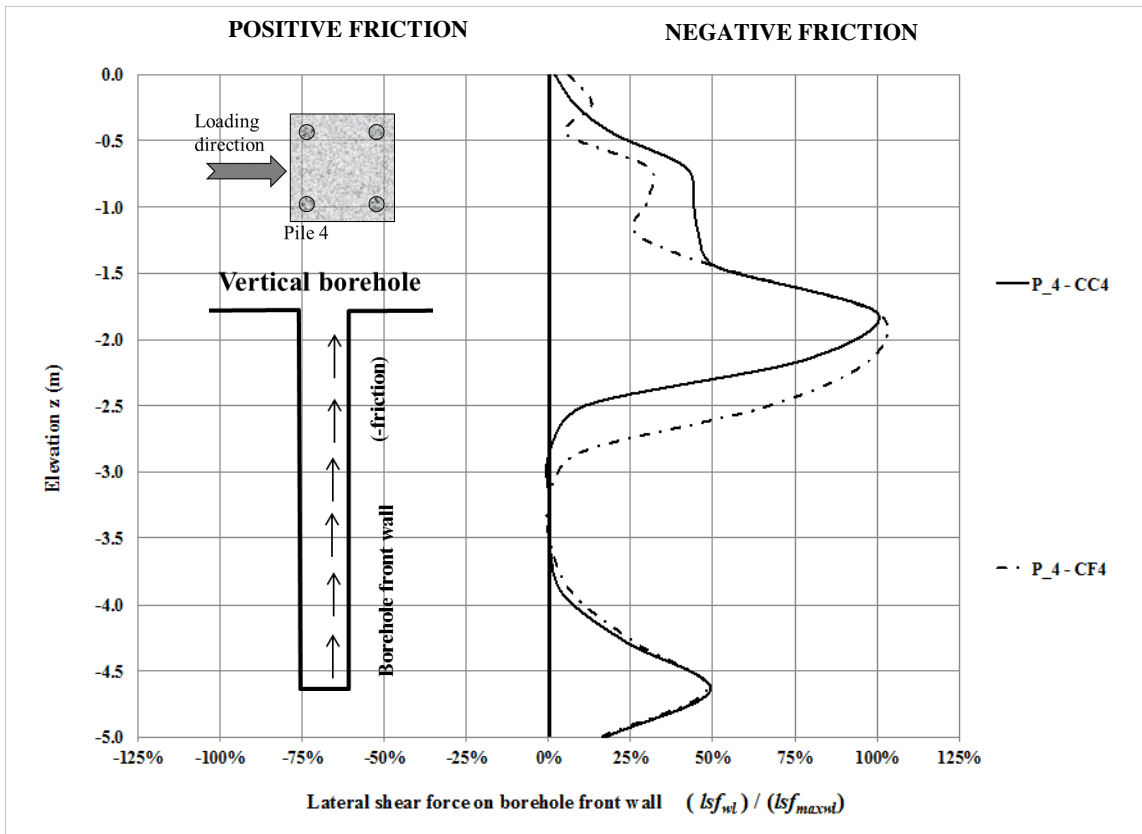


Figure 5.71. The lateral shear force transmitted by pile 4 to the front vertical wall in both the *CC4* and *CF4* foundation systems.

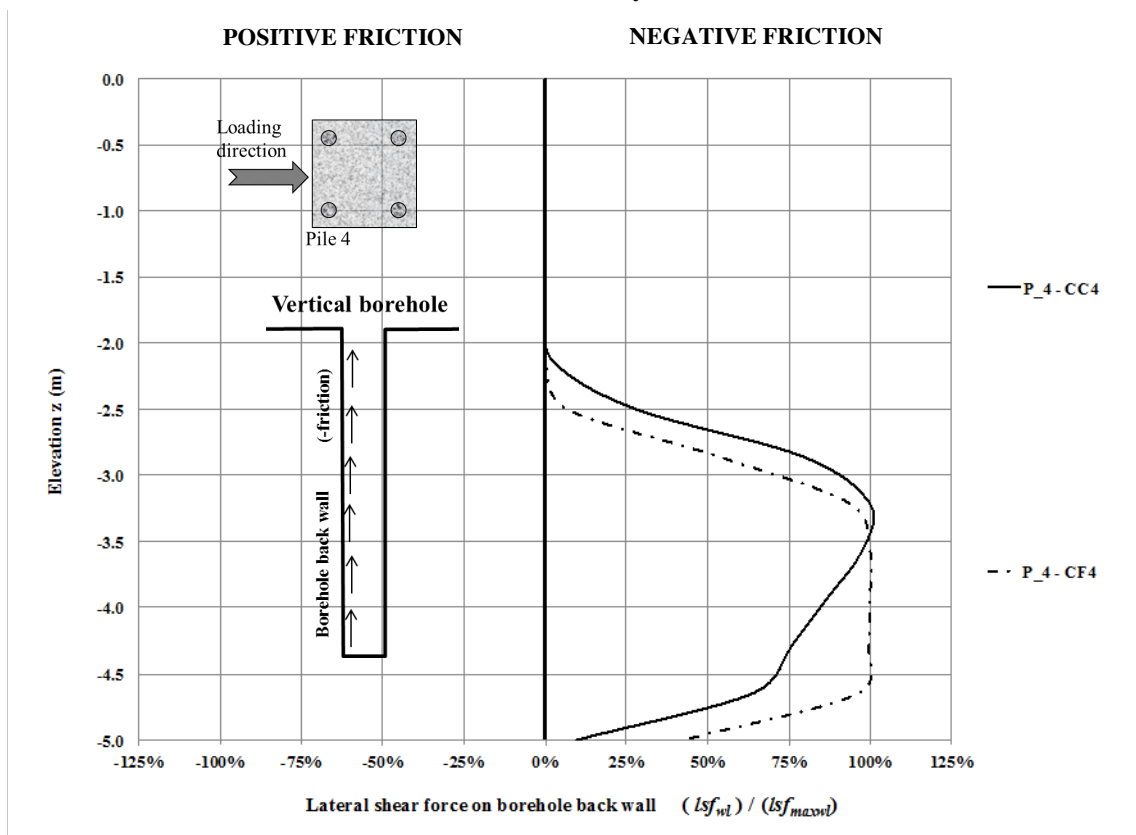


Figure 5.72. The lateral shear force transmitted by pile 4 to the back vertical wall in both the *CC4* and *CF4* foundation systems.

Regarding the behavior of the front pile shaft over the vertical borehole front wall, the leading piles (pile 1 and pile 2) showed a similar performance in terms of forces direction, both exhibiting positive friction; however, the defective pile had different performance especially down near the damaged region (see Figure 5.67). The trailing piles (pile 3 and pile 4) of both systems showed very similar negative friction performance.

With respect to the behavior of the back pile shaft over the vertical borehole back wall, the leading piles of both systems also developed positive friction, but the defective pile had a small performance difference, especially down near the damaged region (see Figure 5.68). The trailing piles of both systems showed very similar negative friction performance.

Also, a gaping hole formed between the back pile shaft face and the vertical borehole back wall, because there was no contact between 0.0 and practically 2.20 m depth; it should be noted that a plastic hinge developed at approximately the same depth.

The analyses confirm that the uneven distribution and direction of lateral forces produced a small torsion effect, especially in the *CF4* system. Regarding the *CC4* system, it was possible to realize that the geometric arrangement of the piles had some influence due to the uneven performance of the trailing piles when compared with the same foundation system.

### *Discussion*

It should be highlighted that the phenomenon of horizontal loading is very complex, due to the fact several interactions occur in different directions among all elements here studied, pile tip, raft tilting and pile shaft, at the same time. Therefore, it is not easy to capture the complete phenomenon in only one chart. Hence, it is necessary to consult other charts that show the element of interest involved simultaneously in other movements, in order to try to understand the overall behavior.

It is important to obtain that sensitivity of the whole movement. For example, over the pile shaft two movements happen at the same time; first, the shaft pushes against the vertical borehole walls in both positive and negative horizontal directions (subgrade normalized forces), meaning positive subgrade forces at the top of the pile and negative subgrade forces at its bottom (both passive forces). As a result, gaping holes appeared between the pile back



shaft and the vertical borehole back wall at the top of the piles. However, at the same time the leading pile tips increase their vertical contact forces, whereas the trailing piles decrease them. Simultaneously the piled raft begins to tilt, increasing its contact with the natural ground at the lead side and decreasing it at the rear side, until at a certain loading stage there was no more contact between the raft and the natural ground at this side. For the case of the systems with defective piles, tilting and twisting occurred.

Although it was difficult to compare the different foundation systems, due to their different geometrical features and soil properties, it was found that their limiting tolerable distortion value depends on the number of piles and their geometrical arrangement in the piled raft, and also the presence or absence of defective piles. However, in this sense the presence of a defective pile caused different degrees of impact: for the *CF3* system its influence was great, but for the *CF4* system it was less.

It should be emphasized that the numerical behavior exhibited under the loading work stage (lateral shear forces) gives a general idea of the behavior occurring during this loading stage only. In this regard, it is recommended to study the behavior of the complete phenomenon when the systems are subjected to other loading stages.

In general, the performance shown by all component parts of the piled raft follows some logical path based on the lateral loading, although some elements presented unexpected conduct, especially the defective piles. The foundation system should be studied as a whole entity with interacting forces because analyzing each of the components separately risks overlooking crucial details.

## 6 CONCLUSIONS AND FUTURE RESEARCH PROJECTS

A 3D study framework for simulating the behavior of different piled raft foundation systems was developed. These numerical works considered as base reference the results from the experimental full-scale lateral loading in each of the piled rafts tested, and the parameters of each of the material components of the complete system, meaning the concrete piled raft, the rebar and the soil dominium.

For the case of the soil, field trials and laboratory works were performed, while for the concrete and the steel materials the parameters used were those reported by previous research works during the earlier construction of the piled rafts at the experimental field.

Thirteen full-scale horizontal loading tests were carried out at the Campinas University experimental site. Only five of them were used to develop this thesis:

- A piled raft with an intact pile named the *CC1 foundation system* was loaded laterally, developing an ultimate bearing capacity of 45.50 kN and 40.04 mm horizontal displacement.
- A piled raft with three intact piles the *CC3 foundation system* was loaded laterally, developing an ultimate bearing capacity of 195.0 kN and 33.22 mm horizontal displacement.
- A piled raft with two intact piles and only one defective pile named the *CF3 foundation system* was loaded laterally, developing an ultimate bearing capacity of 130.0 kN and 31.85 mm horizontal displacement.
- A piled raft with four intact piles named the *CC4 foundation system* was loaded laterally, developing an ultimate bearing capacity of 224.0 kN and 18.07 mm horizontal displacement.
- A piled raft with three intact piles and only one defective pile named the *CF4 foundation system* was loaded laterally, developing an ultimate bearing capacity of 183.0 kN and 26.30 mm horizontal displacement.

Among all these experimental results plotted, in the piled rafts with three and four piles it was possible to evaluate the presence of the damage itself, because they apparently have the same features, meaning geometry, size, materials and quantity of all the components; moreover, they were built using the same construction process and at the same site. However, the experimental curves plotted showed a large difference with respect to the ultimate capacity horizontal bearing.

The significance of the damage was analyzed from two perspectives, taking into account the allowable displacement calculated through Terzaghi's criteria and from the work loads established as a half of the ultimate load; from those work loads, some safety factors were calculated for each criterion. It was hence determined that the presence of the damage was significant and therefore merits a more in-depth study.

It is important to emphasize that the full-scale lateral test load represents the actual behavior of the piled raft system at the site. The results were reliable and consistent when comparing among the five lateral test load performances at the experimental site. It is worth noting that without those full-scale tests, the results of the numerical Abaqus models would not have a reference to compare them, and thus, it would not be advisable to trust them.

It is also very important to mention that from the laboratory soil parameters reported in previous research works, all numerical analyses were achieved as first attempts. This is because, firstly, better numerical approximations were obtained as preliminary results than by using the field trial parameters, and secondly, because they were employed successfully in other numerical works previous to this research work.

The most significant conclusions of this thesis are as follows:

- Soil parameters had the largest influence on the behavior of the foundation systems simulated, especially the elasticity soil modulus  $E_s$  and the cohesion  $c$ ; the concrete and steel material had much less influence, but not much less importance.
- The large variability in suction and collapsibility in the soil from the experimental field caused considerable changes in the behavior of the piled rafts

studied. Thus, with little change in the natural moisture the bearing capacity underwent a sudden drop and the collapsibility produced large deformations in the soil dominium, especially at shallow depth, where the horizontal loading has the largest influence on behavior.

- The plasticity behavior consideration in the concrete material proved fundamental to numerically representing the experimental behavior.
- From a global point of view (considering the complete system), the loss of rigidity stiffness in the *CFI* system was the main reason it behaving differently than the *CCI* system. From a local point of view (considering only the defective section), the damage area showed a low performance according to its stress resistance and horizontal displacements.
- Through some prediction studies, the experimental *CF3* and *CC4* foundation systems were simulated from *CC3* and *CF4* numerical models respectively, only changing an intact pile for a defective one or vice versa, and keeping the same position they had at the experimental site. It was not possible to obtain satisfactory numerical approximations when compared to the respective experimental curves.
- The plotted curve obtained from each of those specific studies did not fit when compared to the respective *CF3* and *CC4* experimental curves, and indeed was completely different from it.
- Several factors, such as soil anisotropy, actual soil moisture, suction, current soil stress state, etc., were neither foreseen nor considered during the numerical simulations, but they might be somehow involved in the lateral loading performance.
- All those missing factors are depicted intrinsically in all experimental *p-y* curves obtained, and they were absorbed by the parameters of the materials assigned during the numerical work, mainly by the soil material, resulting in satisfactory numerical approximations.

- Regarding the functionality of the foundation system, its performance will depend on the ultimate and work load set by any criteria; this thesis found that under those set values the safety factor calculated is totally different.
- The presence of defective piles will generally lead to development of lateral deflection and rotation of the group, and induces additional moments in the piles.
- According to the ultimate and work loads established to carry out all behavioral analyses of the foundation systems, it would be necessary to reinforce the defective foundation system or to build a new one to improve its functionality.

## **6.1 FUTURE RESEARCH PROJECTS**

Some possible paths of interest that could be explored include the following:

- To carry out more parametric studies on these piled raft systems here simulated, changing loading direction, loading magnitude, position of the damage in the pile, and the position of the defective pile in the piled raft itself. It is also possible to change the geometric dimensions of the damage area, and the diameter and the length of the pile. Increasing the number of defective piles in the system could be another option.
- To allow for development and implementation of new analytical equations or design rules that may take into account some of the features observed in this thesis for defective and non-defective piled rafts.

## REFERENCES

- Abagnara, V. (2009). Modellazione e analisi di pali sotto carichi orizzontali. University of Naples.
- Abreu, J. (2014). Avaliação experimental do comportamento de grupos de fundação carregados lateralmente em solo poroso tropical. Universidade de Brasília.
- Almeida, M.A., Gonçalves, M.M. & Cardoso, T.S. (2011). Horizontal bearing capacity of piles in a lateritic soil. *J. Geotech. Geoenvironmental Eng.*, 137(1): 59–69.
- Basu, D., Salgado, R. & Prezzi, M. (2009). A continuum-based model for analysis of laterally loaded piles in layered soils. *Géotechnique*, 2: 127–140.
- Bergan, R., Pereira, V. & Cesar, N. (2015). Numerical experiments into piles in improved ground on the response to lateral loading. SEFE 8 Semin. Eng. fundações especiais e Geotec.,.
- Brinkgreve, R.B. (2005). Selection of soil models and parameters for geotechnical engineering application. ASCE, : 69–98.
- Broms, B. (1964). The lateral resistance of piles in cohesive soils. *J. Soil Mech. Found. Div.*, ASCE, 90: 27–63.
- Chandrasekaran, S.S., Boominathan, A. & Dodagoudar, G.R. (2010). Group interaction effects on laterally loaded piles in clay. *Geotech. Geoenvironmental Eng.*, : 573–581.
- Christan, P. & Kuster, R.F. (2015). Estudo da interação solo-estaca sob carregamento horizontal. *Soc. Port. Geotec.* 133, : 91–101.
- Comodromos, E.M., Papadopoulou, M.C. & Rentzeperis, I.K. (2009). Effect of cracking on the response of pile test under horizontal loading. *J. Geotech. Geoenvironmental Eng.*, 135(9): 1275–1284.
- Cordeiro, A.F.B. (2007). Avaliação numérica de reforço de grupo de estacas pela introdução de estacas adicionais. Universidade de Brasília.
- Freitas, N.O. (2013). Avaliação experimental e numérica de radiers estaqueados com estacas defeituosas em solo tropical do Brasil. Universidade de Brasília.
- Garcia, J.R. (2015). Análise experimental e numérica de radiers estaqueados executados em solo da região de Campinas/SP. Universidade Estadual de Campinas, Brasil.
- Gomes, A. (2013). Provas de carga estática com carregamento lateral. Universidade Federal do Rio Grande do Norte.
- Gon, F. (2011). Caracterização geotécnica através de ensaios de laboratório de um solo de diabásio da região de Campinas/SP. Universidade Estadual de Campinas, Brasil.

- Gonçalves, M.M., Belincanta, A. & Marques, J. (2001). Provas de carga horizontal em estacas escavadas a trado mecânico em solo colapsível da região de Londrina, estado do Paraná. *Maringá*, 23: 1579–1587.
- González, J. (2014). Estudo numérico do comportamento de estacas carregadas lateralmente. Universidade de Brasília.
- Guimarães, R.C. (2002). Análise das propriedades e comportamento de um perfil de solo laterítico aplicada ao estudo do desempenho de estacas escavadas. Universidade de Brasília, Brasília.
- Hansen, B.J. (1961). The ultimate resistance of rigid piles against transversal forces.
- Helwany, S. (2007). Applied soil mechanics with Abaqus applications. JOHN WILEY & SONS, INC.
- Janda, T., Cunha, R.P. Da, Kuklík, P. & Anjos, G.M. Dos. (2009). Three dimensional finite element analysis and back-analysis of cfa standard pile groups and piled rafts founded on tropical soil. *Soils and Rocks*, 32(1): 3–18.
- Kassouf, R. (2012). Análise de prova de carga em tubulão a céu aberto submetido a esforço horizontal em solo não saturado de diabásio da região de Campinas. Universidade Estadual de Campinas, Brasil.
- Katzenbach, R. & Schmitt, A. (2004). High-rise buildings in Germany soil-structure interaction of deep foundations. Fifth International Conference on Case Histories in Geotechnical Engineering, New York, NY, 0–8.
- Katzenbach, R., Schmitt, A. & Turek, J. (1998). Piled raft foundation - interaction between piles and raft.
- Kim, Y., Jeong, S. & Lee, S. (2011). Wedge failure analysis of soil resistance on laterally loaded piles in clay. *Geotech. Environmental Eng.*, : 678–693.
- Kong, L. & Zhang, L.M. (2004). Lateral or torsional failure modes in vertically loaded defective pile groups. *Geo-Support*, : 1–12.
- Lima, M.J. (2001). Avaliação de metodologias de projeto para estacas carregadas horizontalmente assentes em argila porosa colapsível. Universidade de Brasília.
- Matlock, H. & Reese, L.C. (1962). Generalized solutions for laterally loaded piles. *Trans. Am. Soc. Civ. Eng.*, 27: 1220–1247.
- Miranda Jr., G. (2006). Estacas submetidas a esforços horizontais em solos colapsíveis de São Paulo, nas condições naturais, melhorada e inundada. Campinas University.
- Miranda M., M. (2016). Análise do comportamento de estaca escavada de pequeno diâmetro submetida a carregamento horizontal em solo não saturado. Universidade Estadual de

Campinas.

- Mokwa, R.L. & Duncan, J.M. (2001). Investigation of the resistance of the pile caps and integral abutments to lateral loading. Virginia Polytechnique Institute and State University.
- Nath, U.K., Hazarika, P.J., Giri, V. & Tesfaye, A.M. (2011). Study of lateral resistance of pile cap using finite element analysis. *Int. J. Emerg. Trends Eng. Dev.*, 1: 15–31.
- Obrzud, R.F. (2010). On the use of the hardening soil small strain model in geotechnical practice. *Numer. Geotech. Struct.*,
- Papadopoulou, M.C. & Comodromos, E.M. (2012). Response evaluation of horizontally loaded pile groups in clayey soils. *Géotechnique*, 62(4): 329–339.
- Patil, J.D., Vasanvala, P.S. a & Solanki, P.C.H. (2013). A study on piled raft foundation: state of art. *Int. J. Eng. Res. Technol.*, 2(8): 1464–1470.
- Poulos, H.G. (1997). Behavior of pile groups with defective piles. 14th Int. Conf. Soil Mechanics Foundation Engineering, Hamburg, Germany, 871–876.
- Poulos, H.G. (1999). Pile defects - influence of foundation performance. 4th International Conference on Deep Foundation Praticice Incorporating Piletalk, Singapoure, 57–69.
- Poulos, H.G. (2001). Piled raft foundations: design and applications. *Géotechnique*, 51(2): 95–113.
- Poulos, H.G. & Davis, E.H. (1980). Pile foundation analysis and design.
- Qin, H. (2010). Response of pile foundations due to lateral force and soil movements. Griffith University.
- Randolph, M.F. (2003). Science and empiricism in pile foundation design. *Géotechnique*, 53(10): 847–875.
- Randolph, M.F. & Wroth, C.P. (1979). An analysis of the vertical deformation of pile groups. *Géotechnique*, 29(4): 423–439.
- Reese, L.C. (1977). Laterally loaded piles: program documentation. *J. Geotech. Eng. ASCE*, 103: 287–305.
- Reese, L.C. & Van Impe, W.F. (2001). Single piles and pile groups under lateral loading. London, UK.
- Ribeiro, L.C. (2010). Modelagem numérica do comportamento de fundações profundas submetidas a carregamento lateral. Universidade federal do Rio Grande do Sul.
- Rodriguez, T. (2013). Caracterização geotécnica de um solo de diabásio por meio de ensaios SPT e CPT. Universidade Estadual de Campinas, Brasil.
- Russo, G. & Viggiani, C. (2008). Piles under horizontal load: an overview. *Second BGA Int.*



Conf. Found., : 20.

- Scallet, M.M. (2011). Comportamento de estacas escavadas de pequeno diâmetro em solo laterítico e colapsível da região de Campinas / SP. Universidade Estadual de Campinas, Brasil.
- Sümer, Y. & Aktaş, M. (2015). Defining parameters for concrete damage plasticity model. *Chall. J. Struct. Mech.*, 1(3): 149–155.
- Ti, K.S., Gue, S.S., Bujang, B., Noorzaei, J. & Saleh, J. (2009). A review of basic soil constitutive models for geotechnical application. *Electron. J. Geotech. Eng.*, 14: 18.
- Xu, K.J. (2000). General analysis of pile foundations and application to defective piles. University of Sydney, Sydney, Australia.
- Zammataro, B.B. (2007). Comportamento de estacas tipo escavada e hélice contínua, submetidas a esforços horizontais. Universidade Estadual de Campinas, Brasil.
- Zhan, Y., Wang, H. & Liu, F. (2012). Modeling vertical bearing capacity of pile foundation by using abaqus. *Electron. J. Geotech. Eng.*, 17 M: 1855–1865.
- Zhang, H.H. (2000). Finite layer method analysis of piled raft foundations. University of Sydney.

# APPENDICES

## *A. Experimental results from full-scale loading tests.*

### **CC1 intact piled raft system**

Load (kN)	Displacement (mm)
0.00	0.00
3.50	0.16
7.00	0.41
10.50	0.87
14.00	1.35
17.50	1.96
21.00	3.03
24.50	4.36
28.00	6.44
31.50	8.87
35.00	12.79
38.50	18.86
42.00	26.66
45.50	40.04
13.14	39.93
6.76	39.21
3.80	37.67
0.00	32.81

### **CC3 intact piled raft system**

Load (kN)	Displacement (mm)
0.00	0.00
15.00	0.00
30.00	0.06
45.00	0.36
60.00	0.59
75.00	1.07
90.00	1.77
105.00	2.87
120.00	4.63
135.00	6.70
150.00	9.00
165.00	13.00
180.00	19.54
190.00	27.54
195.00	33.22
101.87	31.60
53.31	29.69
26.39	28.68
0.00	18.86

### **CC4 intact piled raft system**

Load (kN)	Displacement (mm)
0.00	0.00
98.00	0.55
148.00	1.75
201.00	6.81
224.00	18.07
223.00	18.11
162.00	17.00
68.00	14.00
0.00	7.25

### **CF3 defective piled raft system**

Load (kN)	Displacement (mm)
0.00	0.00
10.00	0.00
20.00	0.04
30.00	0.29
40.00	0.62
50.00	1.07
60.00	1.84
70.00	2.72
80.00	4.19
90.00	5.95
100.00	9.26
110.00	14.97
120.00	21.70
130.00	31.86

### **CF4 defective piled raft system**

Load (kN)	Displacement (mm)
0.00	0.00
13.00	0.00
26.00	0.00
39.00	0.10
52.00	0.26
65.00	0.40
78.00	0.65
91.00	1.00
104.00	1.60
117.00	2.40
130.00	3.50
143.00	5.00
156.00	7.50
169.00	11.60
183.00	26.30

## ***B. THEORETICAL ANALYSIS OF THE CCI PILED RAFT SYSTEM***

In the case of the *CCI* system, being the simplest of all those tested experimentally, the ultimate capacity load and ultimate displacement were estimated through classical theoretical methods of extrapolation; they were also obtained by other theoretical methods such as those of Matlock and Reese and Broms, as were other interesting parameters such as the reaction modulus  $n_h$ , the subgrade reaction modulus  $K$ , and the modulus of soil  $E_s$ . Finally, this particular piled raft system was evaluated to obtain the horizontal displacement through Winkler's approach.

### **MATLOCK AND REESE METHOD**

Matlock and Reese (1961) presented a method for calculating the total displacement of a pile under horizontal load  $Q_h$  and moment  $M_o$ , both acting at the top of the pile. The total displacement produced by each of those forces is expressed in the following equation:

$$y = y_{Q_h} + y_{M_o}$$

The general solution to find out the total displacement  $y$  to a certain depth  $z$  of a pile is expressed by the following equation:

$$y = \frac{Q_h \cdot T^3}{E_p \cdot I_p} \cdot C_p + \frac{M_o \cdot T^2}{E_p \cdot I_p} \cdot C_m$$
$$T = \left( \frac{E_p \cdot I_p}{n_h} \right)^{\frac{1}{5}}$$

Where:

$E_p I_p$  - bending stiffness or flexural rigidity

$T$  - Relative rigidity factor

$C_p$  and  $C_m$  - Non-dimensional coefficients for displacements due to lateral force and moment.

$n_h$  - Reaction modulus

Since there is no moment  $M_o$  at the top due to the restriction imposed by the raft (see Figure 4.10), then the total displacement  $y$  (equation 4.4) will be equal to  $y_{Q_h}$ , and substituting equation 4.6 into 4.5 results in:

$$y_{Q_h} = \frac{Q_h \cdot C_p}{E_p \cdot I_p} \cdot \frac{(E_p \cdot I_p)^{\frac{3}{5}}}{(n_h)^{\frac{3}{5}}}$$

from above equation  $n_h$ :

$$n_h = \left[ \frac{Q_h \cdot C_p}{y_{Q_h} \cdot (E_p \cdot I_p)^{\frac{2}{5}}} \right]^{\frac{5}{3}}$$

**Error! Reference source not found.** shows the calculations for each displacement  $y$  read from each increment of horizontal loading  $Q_h$  of the full-scale test load. These values are displayed in the shaded columns. According to the work load of 35 kN for the *CCI* system (see Table 4.6), the value of 5.26 MN/m<sup>3</sup> (bold and italic letters) was adopted as the reaction modulus  $n_h$ ; from this value the other parameters, namely subgrade reaction modulus  $K$  and relative rigidity factor  $T$ , were computed.

Table 6.1. Matlock and Reese method

$$\begin{array}{ll} E_p I_p = & 9.50 \text{ MNm}^2 \\ \Phi_p = & 0.25 \text{ m} \\ L = & 5.00 \text{ m} \end{array} \qquad \begin{array}{ll} z = & 0.00 \text{ m} \\ C_p = & 2.44 \\ (C_p)^{(5/3)} = & 4.41 \end{array}$$

$Q_h$ (kN)	$y$ (mm)	$n_h$ (MN/m <sup>3</sup> )	$K$ (MN/m <sup>2</sup> )	$T$ (m)	$L/T$	REMARKS
0.00	0.00	-----	-----	-----	-----	
3.50	0.16	168.11	42.03	0.56	8.88	
7.00	0.41	111.23	27.81	0.61	8.18	
10.50	0.87	62.39	15.60	0.69	7.29	
14.00	1.35	48.46	12.11	0.72	6.93	
17.50	1.96	37.76	9.44	0.76	6.59	
21.00	3.03	24.75	6.19	0.83	6.06	
24.50	4.36	17.45	4.36	0.89	5.65	
28.00	6.44	11.38	2.84	0.96	5.18	
31.50	8.87	8.12	2.03	1.03	4.85	
<b>35.00</b>	<b>12.79</b>	<b>5.26</b>	<b>1.32</b>	<b>1.13</b>	<b>4.44</b>	<b>L/T &gt; 4 (LONG PILE)</b>
38.50	18.86	3.23	0.81	1.24	4.03	
42.00	26.66	2.10	0.52	1.35	3.70	
45.50	40.04	1.22	0.30	1.51	3.31	

## BROMS' METHOD

The Broms' method establishes that the collapse of the structure should not happen, even in the most adverse conditions, and that the horizontal displacements under working

loads should not be too large so as not to compromise the functioning of the foundation system.

The horizontal displacement for a pile restrained at the top, placed inside non-cohesive soil, with a rate of  $L/T > 4$  could be computed as:

$$y = \frac{0.93 \cdot Q_H}{n_H^{\frac{3}{5}} \cdot (E_p \cdot I_p)^{2/5}} \quad (4.9)$$

Through this equation it was possible to compute the reaction modulus  $n_h$  according to the full-scale horizontal loading; Table 6.2 displays the calculation of reaction modulus  $n_h$ , the subgrade reaction modulus  $K$ , and the relative rigidity factor  $T$ . The  $n_h$  computed under the work load (35 kN) corresponds to 1.06 MN/m<sup>3</sup>.

Figure 6.1 shows the variation in the reaction modulus  $n_h$  subjected to the full-scale test load for the *CCI* piled raft system, by both methods mentioned above.

Table 6.2. Broms' Method

Brom's Method					
$Q_h$ (kN)	$y$ (mm)	$N_h$ (MN/m <sup>3</sup> )	$K$ (MN/m <sup>2</sup> )	$T$ (m)	$L/T$
0.00	0.00	-----	-----	-----	-----
3.50	0.16	33.80	8.45	0.78	6.4447
7.00	0.41	22.36	5.59	0.84	5.9337
10.50	0.87	12.54	3.14	0.95	5.2858
14.00	1.35	9.74	2.44	0.99	5.0252
17.50	1.96	7.59	1.90	1.05	4.7806
21.00	3.03	4.98	1.24	1.14	4.3935
24.50	4.36	3.51	0.88	1.22	4.0968
28.00	6.44	2.29	0.57	1.33	3.7611
31.50	8.87	1.63	0.41	1.42	3.5158
<b>35.00</b>	<b>12.79</b>	<b>1.06</b>	<b>0.26</b>	<b>1.55</b>	<b>3.22</b>
38.50	18.86	0.65	0.16	1.71	2.9232
42.00	26.66	0.42	0.11	1.86	2.6813
45.50	40.04	0.24	0.06	2.08	2.4047

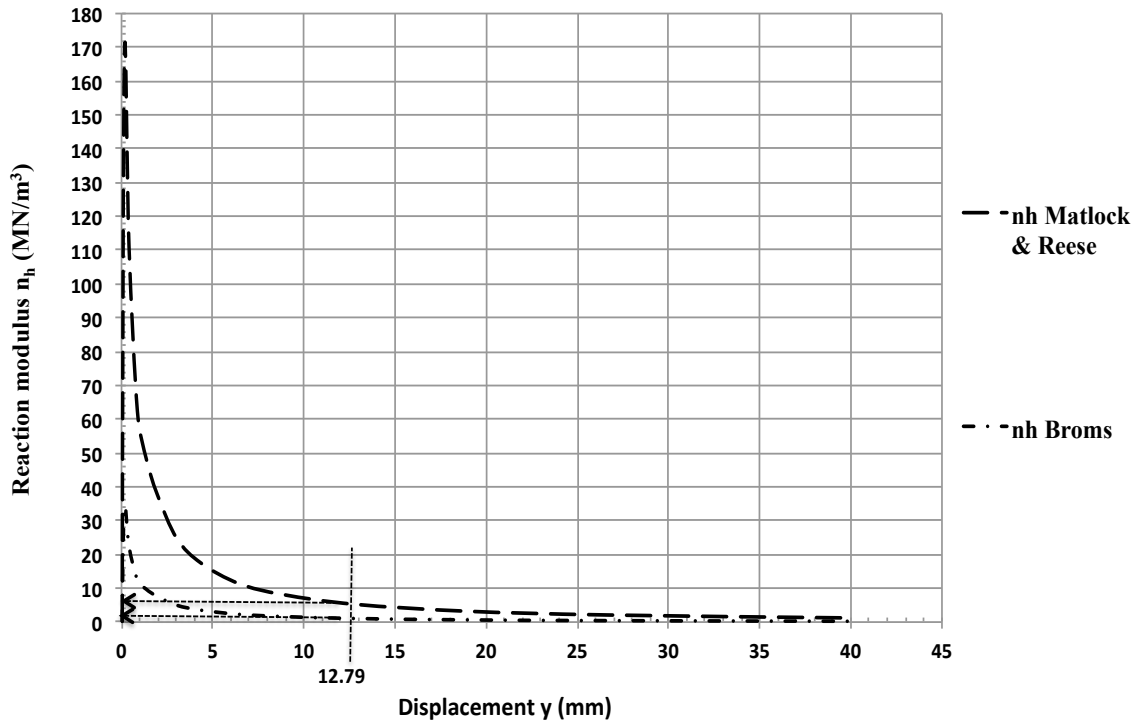


Figure 6.1. Variation in the reaction modulus subjected to the full-scale load test of the *CCI* piled raft system.

## EMPIRICAL PARAMETERS FROM *SPT* FIELD TEST

Four standard penetration tests (*SPT*) were performed at the experimental site by Rodriguez (2013). Those field works were conducted in accordance with NBR 8464/2001. Table 6.3 shows the results based on the *SPT* field test (see also chart in Figure 4.2).

Using the mean  $N_{SPT}$  results, it is possible by empirical correlations to obtain some geotechnical parameters of practical use, such as the reaction modulus  $n_h$ , the subgrade reaction modulus  $K$ , the elastic modulus soil  $E_s$  and the friction angle  $\Phi$ .

The friction angle values displayed in the last two columns of Table 6.3 belong to De Mello (1971) and Décourt (1991); the empirical expressions are available and explained by Rodriguez (2013).

The following are the correlations used in the table:

*Reaction modulus  $n_h$  [kN/m<sup>3</sup>] (clay soils), Fleury (2014):*

$$n_h = 3,000[N_{SPT}] \quad (4.10)$$

Subgrade reaction modulus  $K$  [MPa], Fleury (2014):

$$K = 0.0003 \cdot n_h \quad (4.11)$$

Modulus of elasticity of the soil  $E_s$  [MPa] (clay soils), Fleury (2014):

$$E_s = 1.098564 \cdot [N_{SPT}] \quad (4.12)$$

Table 6.3. Results of the SPT field works

Depth (m)	SPT RESULTS			GEOTECHNICAL PARAMETERS				
	Geological profile	$N_{SPT}$ mean	$n_h$ (kN/m <sup>3</sup> )	$n_h$ (MN/m <sup>3</sup> )	$K$ (MPa)	$E_s$ (MPa)	$\phi$ (°) [1]	$\phi$ (°) [2]
1.00	Silty-clay very soft, red color, colluvial	2.30	6,900	6.90	2.07	2.53	38	32
2.00		2.60	7,800	7.80	2.34	2.86	36	32
3.00		3.70	11,100	11.10	3.33	4.06	36	33
4.00		3.60	10,800	10.80	3.24	3.95	34	31
5.00	Silty sand, low compact material, brown color, colluvial	5.00	15,000	15.00	4.50	5.49	35	33
6.00		6.00	18,000	18.00	5.40	6.59	36	34
7.00		5.10	15,300	15.30	4.59	5.60	33	31
8.00		4.60	13,800	13.80	4.14	5.05	32	31
9.00		6.80	20,400	20.40	6.12	7.47	32	31
10.00	Silty sand-clay medium compact material, red color	10.00	30,000	30.00	9.00	10.99	32	31
11.00		21.00	63,000	63.00	18.90	23.07	32	31
12.00		23.00	69,000	69.00	20.70	25.27	32	31
13.00		-----	-----	-----	-----	-----	-----	-----
14.00		-----	-----	-----	-----	-----	-----	-----

[1] De Mello (1971)

[2] Décourt (1991)

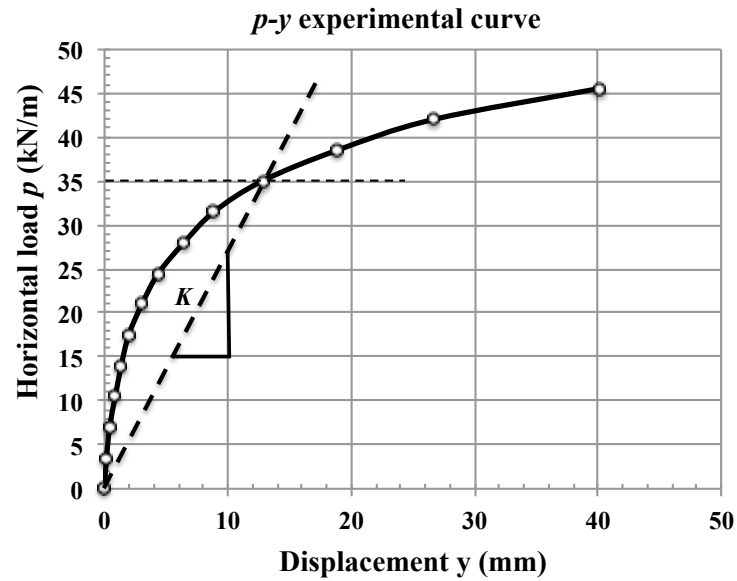
The table above shows the variation in modulus  $n_h$  with soil depth; therefore, only the first layer's  $n_h$  value was adopted, due to the proximity at the top of the pile where the lateral load was applied. Therefore, it was possible to compare this experimental value with those theoretically obtained through Matlock and Reese and Broms methods previously.

Thus, through the  $n_h$  of 6.90 MN/m<sup>3</sup>, the work load of 35 kN and the 0.25 m pile diameter, the horizontal displacement was computed using the equation (2.1)  $n_h = \frac{\sigma_y}{y}$ , resulting in:  $y = 20$  mm.

Table 6.4 shows those numerical results. As from the equations (2.2)  $\sigma_y \cdot \phi_p = n_h \cdot \phi_p \cdot y$  and (2.3)  $p = -K \cdot y$  it was possible to compute the subgrade reaction modulus  $K$ . The  $p$ - $y$  experimental curve of the CCI piled raft system depicted in the figure of the same table is a simple reference to show the modulus  $K$ .

Table 6.4 Comparison of the modulus  $n_h$ .

Method	$Q_h$ (kN) (work load)	$y$ (mm)	$n_h$ (MN/m <sup>3</sup> )	$K$ (MN/m <sup>2</sup> )
Matlock and Reese	35.00	12.79	5.26	1.32
Broms	35.00	12.79	1.06	0.27
SPT	35.00	20.00	6.90	2.07



From the reaction modulus  $n_h$  or the subgrade reaction modulus  $K$ , it is possible to calculate the modulus of elasticity of the soil  $E_s$ , and with this last value an attempt was made to use it as an initial input parameter in subsequent numerical simulations.



### ***C. Winkler's approach***

From equation (2.7) mentioned in chapter 2, it is possible to re-write that general solution as (Bowles, 1997):

$$y = \frac{Q_H \cdot \beta}{K} \cdot \frac{(F\xi + F\psi)}{\sinh^2(\lambda) - \sin^2(\lambda)}$$

where:

$$F\xi = 2 \cdot \cosh(Y) \cos(Y) \cdot [\sinh(\lambda) \cos(A) \cosh(B) - \sin(\lambda) \cosh(A) \cos(B)]$$

$$F\psi = [\cosh(Y) \sin(Y) + \sinh(Y) \cos(Y)] \cdot (F\zeta + F\delta)$$

$$F\zeta = \sinh(\delta) [\sin(A) \cosh(B) - \cos(A) \sinh(B)]$$

$$F\delta = \sin(\delta) [\sinh(A) \cos(B) - \cosh(A) \sin(B)]$$

$$\beta = \sqrt[4]{\frac{K}{4 \cdot E_p \cdot I_p}} \text{ (equation 2.8); and } Y, A, B \text{ and } \lambda \text{ are boundary conditions.}$$

Evaluating all these equations considering as input data the *SPT-E* values gives (as an example):

$K = 2.07 \text{ MPa}$  (see Table 6.3);  $E_p I_p = 9.5 \text{ MN m}^2$ ;  $\beta = 0.483 \text{ m}^{-1}$ ;  $A=B=Y=0$  (at top of the pile);  $\lambda = 2.45$  (Fleury, 2014).

The calculation found for the horizontal displacement is:  $y = 11 \text{ mm}$ .